UNIVERSITÀ DEGLI STUDI DI PALERMO

DIPARTIMENTO DI INGEGNERIA

Dottorato di Ricerca in Ingegneria Civile, Ambientale, dei Materiali

Indirizzo: Infrastrutture Viarie

S.S.D. ICAR 04

Surface and mechanistic properties of recycled bituminous mixtures

IL COORDINATORE

Chiar.ma Prof.ssa Ing. Antonina PIRROTTA

IL CANDIDATO

Ing. Armando ASTOLFI

IL TUTOR

Chiar.mo Prof. Ing. Filippo Giammaria PRATICÒ

CICLO XXXI
Triennio 2015/2018

to my Family...
my greatest gift.

Acknowledgements/Ringraziamenti

Con questa tesi si conclude il mio percorso di dottorato. Tre anni molto intensi e ricchi di esperienze indimenticabili.

È stato un percorso che mi ha permesso di crescere, di fare nuove conoscenze e di arricchire notevolmente il mio bagaglio culturale e personale.

Un traguardo importante che poche persone riescono a raggiungere nella vita e che, allo stesso tempo, restituisce alla mia famiglia la giusta ricompensa per gli innumerevoli sacrifici compiuti nel supportarmi e nello starmi sempre accanto.

È a loro… la mia famiglia… che dedico questo mio percorso.

Questa esperienza mi ha permesso si viaggiare e di conoscere da vicino città e culture diverse.

Ricordo il periodo trascorso a Palermo, arricchito non soltanto dall'ambiente universitario che ho avuto modo di frequentare, ma da tutto ciò che fa di questa città un luogo meraviglioso ed affascinante.

L'esperienza nel Regno Unito, che ha rappresentato un periodo della mia vita che conserverò gelosamente tra i miei ricordi. Nottingham ed i tanti luoghi visitati mi hanno regalato immagini stupende di un paese bello ed entusiasmente.

Qui ho avuto il piacere e la fortuna di incontrare persone provenienti da ogni angolo del pianeta e di condividere con loro un pezzo della mia strada. Grazie a loro ho potuto apprendere il lato migliore di diverse culture che spero di rivivere presto.

Un grazie molto sentito, infine, va anche a tutti coloro che mi hanno seguito e guidato in questi tre anni di ricerca sviluppata tra Reggio Calabria, Palermo e Nottingham.

Ad maiora semper…

Ing. Armando Astolfi

Declaration

The research described in this thesis was conducted between November 2015 and October 2018 at:

- University of Palermo (Italy);
- Mediterranea University of Reggio Calabria (Italy);
- Nottingham Transportation Engineering Centre (NTEC), University of Nottingham (United Kingdom).

I declare that the work is my own and has not been submitted for a degree at another University.

Summary

List of Figures

List of Tables

Executive summary

Problem

Often, when the characteristics of a bituminous mixture are analised, there are major differences between in-lab and in-situ results. This is due to the fact that the procedures and techniques implemented during the design phase (in lab) may be different from those used on site. Then, is very important to be able to predict the main properties of a mixture particularly when innovative materials are used. For example, when crumb rubber is used, phisical and volumetric properties of mixes may change over time, in particular due to the swelling phenomenon that it alters different properties of the mixture (e.g., viscosity). This study aims to investigate the main aspects of road pavement design in order to improve the performance of innovative mixes.

Objectives and scopes

The main objectives of this thesis are:

- Ob. 1 – To set up models for the prediction of surface characteristics of conventional and innovative road pavements.
- Ob. 2 – To design innovative bituminous mixtures with crumb rubber.
- Ob. 3 – To analyse the consequences related to Life Cycle Cost Analysis deriving from the application of different pavement design methods.

Description

This thesis intends to investigate the superficial and mechanical properties of conventional and innovative road pavements. The thesis contains a collection of experiments related to: i) laboratory-based study of the surface properties of road pavement; ii) laboratory-based study of the mechanical properties of road pavement and; iii) determination of expected life and pay adjustment.

Conclusions

The main conclusions of this thesis are:

- Macro- and microtexture test can be explained and predicted based on simple physical and geometric models. In lab- measures can be related to the corresponding measures on real pavements.
- The variation of viscosity over time is linked to the swelling process of the rubber. The order of components in the asphalt plant does not have significant effects on viscosity.

- Short-time oven aging (STOA) and interrupted compaction process entail a worse compaction of mixes.
- CRT2 mixes are usually easier to compact and are the most resistant to permanent deformation.
- STOA effects are more evident than interrupted compaction effects in terms of compactability, workability, stiffness and rutting.
- Rubberised mixes are easier to compact, when STOA process is applied. They have higher stiffness and a better resistance to permanent deformation.
- Regard to the variables under investigation (e.g., AV), AASHTO, KenPave, MnPAVE and, M-EPDG have a similar trend in terms of expected lives.

1 Introduction

The increasing global sensitivity, which aims at reducing the environmental impact, is leading the scientific research to the use of eco-compatible materials, even in the field of transportation infrastructures.
Different opportunities to recycling may be detected in the road infrastructure sector. Infact, it is possible to reuse:

- road construction materials, for example:
    - RAS - Recycled Asphalt Shingles (Ghabchi et al. 2016);
    - RAP - Reclaimed Asphalt Pavement (Basueny et al. 2016; Pradyumna, Mittal, and Jain 2013);
- other types of materials, for example:
    - recycled aggregates (Ossa, García, and Botero 2016; Bocci, Cerni, and Colagrande 2016);
    - industrial waste made during the steel production process (Maghool et al. 2017);
    - crumb rubber (Behl, Kumar, and Sharma 2013; Pettinari et al. 2013; Dondi et al. 2014);
    - sugar cane (Zainudin et al. 2016).

The use of these materials allows to reduce the negative effects resulting from the use of hot mix asphalt and, at the same time, the recycling of waste material. This entails a significant reduction in the quantity of waste going to disposal.
When deviating from standard paving solutions, it is necessary to verify that the use of supplementary components or the adoption of different processing conditions do not lead for construction workers to an increase of the risk associated to fume exposure (Zanetti et al. 2016; Santagata et al. 2013).
In the specific case of bituminous materials containing crumb rubber from end-of-life tyres, Zanetti et al. (2014, 2015, 2016) show that that emissions coming from asphalt rubber materials lead to toxic and carcinogenic risks for construction workers which are comparable to those of standard paving mixtures containing neat bitumen or polymer-modified binders.

In light of the above, the reuse of end of life tyres (ELT) represents one of the most interesting cases of recovery (a Ecopneus 2013).

The disposal of ELT is one of the biggest environmental problems in the world. This is due to the fact that: i) it is a not biodegradable waste; ii) it's being produced in large amounts.

The disposal of ELT is regulated by a series of European and national regulations.

The main European regulations currently in force are:

- Directive 2008/98/EC of the European Parliament and of the Council of 19 November 2008 on waste and repealing certain Directives.
- Council Directive 1999/31/EC of 26 April 1999 on the landfill of waste.

Instead, the main Italian regulations currently in force are:

- D.M. 31 agosto 2013 n.101, art.11 – "Semplificazione e razionalizzazione del sistema di controllo della tracciabilità dei rifiuti".
- D.M. 7 marzo 2012 n. 44 – "Decreto di nomina del Tavolo Permanente di Consultazione sulla gestione degli pneumatici a fine vita - PFU".
- D.M. Ambiente 20 gennaio 2012 – "Parametri tecnici relativi alla gestione degli pneumatici fuori uso".
- D.M. 11 aprile 2011 n. 82 – "Regolamento per la gestione degli pneumatici fuori uso (PFU) ai sensi dell'articolo 228 del DLgs 3 aprile 2006 n.152 e successive modificazioni e integrazioni, recante disposizioni in materia ambientale".
- D.M. 18 febbraio 2011 n.52 – "Regolamento recante istituzione del sistema di controllo della tracciabilità dei rifiuti, ai sensi dell'articolo 189 del decreto legislativo 3 aprile 2006, n. 152 e dell'articolo 14-bis del decreto-legge 1° luglio 2009, n. 78, convertito, con modificazioni, dalla legge 3 agosto 2009, n. 102".
- D.Lgs 3 aprile 2006 n. 152 – "Parte IV - Norme in materia di gestione dei rifiuti e di bonifica dei siti inquinanti".
- D.Lgs 13 gennaio 2003 n. 36 – "Attuazione della direttiva 1999/31/Ce relativa alle discariche di rifiuti".
- D.M. Ambiente 9 gennaio 2003 – "Esclusione dei pneumatici ricostruibili dall'elenco di rifiuti non pericolosi".

In order to quantify the scale of the problem, it is important to provide a general overview of state of the art. Note that, a detailed and updated analysis of the quantity of used and/or end of life tyres (ELTs) it is difficult to determine

This is due to the fact that, in some countries, there is no requirement to provide information on the quantity of such material (L'Italia del riciclo 2015).

In this context, in Europe, about 3.42 million tonnes per year of used tyres and end of life tyres are produced. The 60% of these is produced in Germany, United Kingdom, France, Italy and Spain (ETRMA 2014).

This material consists in (ETRMA 2014):

- 19% are used tires. They are suitable for reuse and/or reconstruction.
- 81% is end of life tyres (ELTs). They are considered as waste and are used as follows:
    - 37% is intended for energy recovery.
    - 39% is intended for material recovery.
    - 5% is intended for landfill.

In turn, ELTs intended for energy recovery are used as (ETRMA 2014):

- fuel, in cement production plants (about 91%).
- material, in plants for the production of thermal or electrical energy (about 9%).

Instead, ELTs intended for material recovery are used for (ETRMA 2014):

- the production of rubber granules and powders (88%).
- the recovery into infrastructure works (12%).

In Italy, over 473000 tonnes of end of life tyres are produced in 2016. A large part of these have been exported in other countries (e.g., Czech Republic, Germany and Slovenia; ISPRA 2018).

Analyzing the data related to the management of ELTs (ISPRA 2018), it is possible to note that (Figure 1.1):

- The 79.8% of ELTs was intended for material recovery.
- The 7.3% of ELTs was intended for energy recovery.
- The 12.6% of ELTs was remained in storage at end of the year. This quantity was subsequently intended for recovery.
- Small quantities of ELTs were destined for other kind of recovery (in particular, 375 tonnes were incinerated, 112 tonnes were intended for other forms of disposal and, 171 tonnes were intended for landfills).

Collection and recovery data of ELTs at regional level were also published by TEKNECO (2015).

At the top of the ranking there is Lombardia (with 96170 tonnes per year), followed by Campania (82394 tonnes per year), Lazio (79357 tonnes per year) and Sicily (77836 tonnes per year).

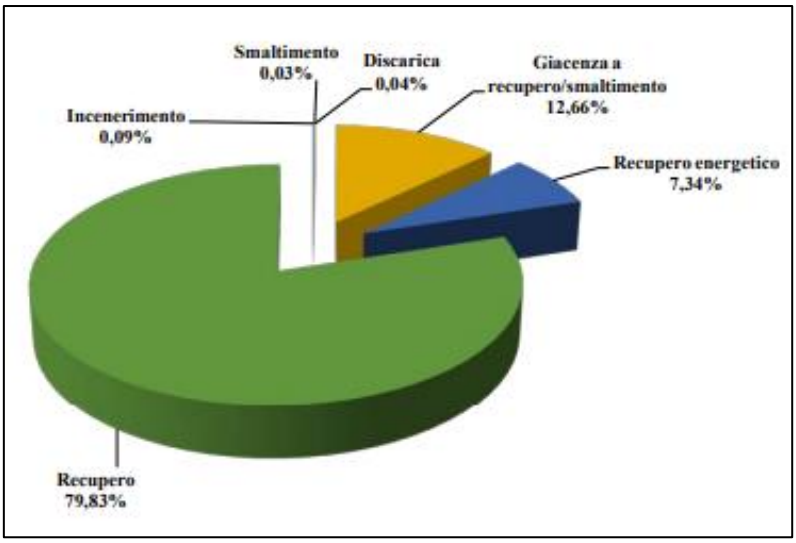

Figure 1.1: – Management of ELTs related to the year 2016, Italy (source: ISPRA 2018)

The technical and physical properties of tyre rubber are particularly appreciated for the manufacturing of Ecopneus (2012, 2013, 2016):

- modified bituminous mixes;
- play areas flooring (e.g., astroturf surfaces, athletics track, anti-trauma flooring);
- building materials (e.g., soundproofing material, material for heat insulation);
- urban furnishings;
- civil engineering works (e.g., soundproofing barriers, anti-erosion barriers, coastal protection);
- anti-vibration material in railway field.

The use of rubber powder in civil engineering applications is supported (with some exceptions) by several literature studies (Chang and Gronwald 2016; Feraldi et al. 2013; Clauzade 2010; J. Sousa, Way, and Carlson 2001):

- Chang et al, 2016: “The study found that retreading tires for reuse was the best option. However, since that is not always a practical or long-term solution the study found that either using the scrap tires to create crumb rubber or for the purpose of civil engineering applications would be the optimal solutions.”
- Feraldi et al., 2013: “The results in both methodological approaches indicate that the material recycling scenario provides greater impact reductions than the energy recovery scenario in terms of the examined environmental impact potentials: energy demand, iron ore consumption, global warming potential, acidification, eutrophication, smog formation, and respiratory effects. The

additional impact reductions from material recycling are significant, and the establishment of new infrastructure required for a shift to material recycling incurs relatively insignificant burdens."

- Clauzade C., 2010: "The hierarchy of recovery methods brought into doubt: The Life Cost Analysis shows that the environmental assessment of material recycling methods is not systematically better than that of energy recovery ones. End use applications must be assessed on a case-by-case basis."
- Sousa et al., 2001: "Besides the potential energy savings gained by using granulated tire rubber as a modifier to asphalt pavement, it should be noted that this process can substantially improve the highway assets maintained by our communities."

The recycled rubber can be incorporated into asphalt mixtures by two different processes (Farina et al. 2017; Gibreil and Feng 2017; Koba, Skotnicki, and Szydlo 2012): "wet process" and "dry process".

However, these processes require the transformation of ELTs into granular form, before their use (a Ecopneus 2013; Dondi et al. 2014).

The first process consists in the modified of bitumen with crumb rubber (S. Li, Harris, and Wells 2016; Xie and Shen 2016; Babalghaith, Alsoliman, and Al-Suhaibani 2016; González et al. 2010, 2012; Hung et al. 2014; Junan Shen et al. 2009).

The crumb rubber is blended with the bitumen for a period of time (about 60 minutes) at elevated temperature (160 °C to 180°C) before introducing it into the aggregate.

The advantages of this technique are the increase of the properties and performance of bitumen (Ibrahim et al. 2013; Santagata et al. 2012).

The interaction between crumb rubber and bitumen leads to an increase in the viscosity of the matrix and imparts enhancement to the engineering characteristics of the product (A. T. Subhy 2016).

The properties of modified bitumen with crumb rubber vary significantly with the interaction process, and the extent of this interaction also depends on a number of variables such as blending temperature, blending time, type and amount of mechanical mixing, crumb rubber type, size, content and specific surface area of the crumb rubber, extender oil and the type of bitumen. However, there are some shortcomings. They are the phase separation and the construction challenges due to the high viscosity of the binder (A. T. Subhy 2016).

Asphalt-rubber pavement could be considered a more cost-effective option than a conventional pavement when the long-term performance is taken into account (Jung, Kaloush, and Way 2002).

The second process is called "dry process". In this technology, the recycled crumb rubber is added to the aggregate before blending with the bitumen (Sangiorgi et al. 2017; Bai, Yang, and Zeng 2016; M. A. Yazdi, J. Yang, L. Yihui 2015; López-Moro et al. 2013; Zhang 2012; Kubo 2011; Youssf, Mills, and Hassanli 2016; Hesami, Salehi Hikouei, and Emadi 2016; Shu and Huang 2014).

The percentage of crumb rubber usually used is from 1 to 3% of total weight of the mixture, or, roughly as 15 to 35% by the weight of the binder (A. T. Subhy 2016).

There are two types of dry process technology used in the industry: i) PlusRide and; ii) Generic dry process.

The first was developed in the United States by modifying a gap-graded mixture. The modification is achieved by replacement of up to 3% of aggregate by a coarse granulated crumb rubber (A. T. Subhy 2016).

The second, instead, is known as the "TAK" system. In this process, both coarse and fine rubber are added to the dense graded mixture by a percentage up to 3% of total mixture mass.

The philosophy behind the Generic dry process is to allow a greater binder modification by the fine rubber, while the coarse particles act as a flexible replacement to the aggregate that improves the elastic properties of the mixture (A. T. Subhy 2016).

Although dry process requires the use of larger quantities of rubber with minimal or no modification of the asphalt plant, its use is not very widespread because of the inconsistency in field performance (Rahman 2004).

One of the most important aspects is about the bitumen-rubber interaction. It causes swelling of the rubber particles when they are inside the bituminous mix (Farouk et al. 2017).

Bitumen and rubber interact together at high temperature. This entails a variation of the physical properties of both binder and rubber.

Basically, the interaction process between rubber particles and bitumen can be divided into two simultaneous mechanisms: i) swelling phenomenon and; ii) devulcanisation/depolymerisation (A. T. Subhy 2016).

Devulcanisation consist in the cleavage of cross-linking sulphur–sulphur or carbon–sulphur bonds that are formed by the vulcanization process during tyre production.

Depolymerisation, instead, consist in the cleavage of polymer chain bonds.

Devulcanisation and depolymerisation cause a reduction in the molecular weight of the rubber and they are sometimes considered a chemical reaction (Abdelrahman and Carpenter 1999).

Referring to Heitzman studies (1992), the rubber particles are first swollen by absorbing the aromatic oil available in the bitumen to a degree depending on the type of bitumen and the structure of the polymer.

This can lead to an increase in the rubber particle size and at the same time a reduction in the oily fraction forming a gel-like matrix. That could lead to an increase in the viscosity of the matrix up to a factor of 10 (Heitzman 1992).

Moreover, bitumen-rubber interaction can be influenced by the presence of impurities on the rubber surface. For this reasons, different types of rubber treatment have been proposed (Xiaowei et al. 2017; Zhu 2016; Su et al. 2015; Yu et al. 2011; Segre and Joekes 2000; Zanetti et al. 2015; Shu and Huang 2014).

Different studies show the comparison of the two processes ("wet" and "dry"). Strengths and weaknesses have been analysed (J. Shen, Xie, and Li 2014; Koba, Skotnicki, and Szydlo 2012).
Finally, it is well known that rubberised bituminous mixes have different advantages in terms of performance (Pereira and Oliveira 2010). In more detail:

- higher expected life (Antunes et al. 2005; J. Shen, Xie, and Li 2014);
- lower maintenance costs (Altieb et al. 2016; Antunes et al. 2005);
- lower traffic noise (quieter road surfaces, Sodupe-Ortega et al. 2016; Ecopneus 2012).

Another important aspect concerns the analysis of the surface characteristics of road surfaces.
Surface characteristics are one of the main aspects related to road safety and represents one of the main problems that affect society, in terms of costs and human lives.
The rolling resistance of tyres depends on the micro and macro structure of the road surface (Cantisani et al. 2016; C. Huang and Mei 2011). It greatly reduces it value in the case of wet surfaces (Kogbara et al. 2016; Zhao, Qiu, and Zhang 2016; Woodward et al. 2016; Araujo, Bessa, and Castelo Branco 2015).
Friction and surface texture of road pavement affect the state of play of the transportation infrastructure (Postorino and Praticò 2012).
Also, they interact with the volumetric properties of a mixture (Pratico' and Moro 2011); they change over time (Iuele 2016; S. Li, Harris, and Wells 2016; Pratico' and Casciano 2015; Pratico' and Vaiana 2012; Pratico', Ammendola, and Moro 2010) and they depend by a number of factors, including the production process, the compaction and the mix design (Pratico' 2017).
What has just been said is heightened when mixes contain crumb rubber. Rubberised mixes undergo unavoidable modifications due to the interaction of rubber and of the other components of the mix.
Therefore, in-lab analyzes are essenzial in order to understand the consequences in terms of safety and road adherence.
The mechanical characteristics of a road pavement play an important role in the study of rubberized mixtures. For each layer different performance characteristics are requested, based on: i) type of layer and; ii) task to fulfil.
The surface layer is stressed by important horizontal actions while the vertical actions, imposed by the transiting loads, mainly determine compressive and flexural stresses, which progressively reduce with depth (Coni 2010).
These properties can be obtained by acting directly on the components that make up a bituminous mixture (e.g., aggregate, bitumen and, crumb rubber).
One of the parameters that allows you to control the evolution of these properties is the dynamic module that characterizes each mixture.

The dynamic modulus is one of the most important parameter of pavement desing. It affects the expected life, the quality level and the acceptance / rejection procedures of each single layer (Bianchi 2009; Clyne et al. 2003).

2 Objectives and experimental program

The objectives of this thesis are the following:

- **Ob. 1 – To set up models for the prediction of surface characteristics of conventional and innovative road pavements:**
    - Ob. 1.1 - To study the main aspects of the road surface characteristics.
    - Ob. 1.2 - To analyse the measurement methods and their classification.
    - Ob. 1.3 - To suggest a new and simplified laboratory approach to assess the pavement surface (micro- and macrotexture measurements) at the design stage on samples or small slabs, in the laboratory.
- **Ob. 2 – To design innovative bituminous mixtures with crumb rubber:**
    - Ob. 2.1 - Micro-component affinity, MASTIC (bitumen-rubber-filler)
        - Ob. 2.1.1 - Order of components in the asphalt plant: to study the variation of viscosity related to mixing sequence.
        - Ob. 2.1.2 - Swelling phenomenon: to study the variation of viscosity related to different types of rubber (CRT2, CRT1 and, CRN) and different mix design (PA – Porous Asphalt and SMA10 – Stone Mastic Asphalt).
    - Ob. 2.2 - Mixture compaction effects
        - Ob. 2.2.1 - Effect of different laboratory short-term oven aging (STOA) on compactability and workability of dry rubberised asphalt mixture
    - Ob. 2.3 - Macro-component affinity (MIXTURE) and performance related test
        - Ob. 2.3.1 - Effect of different laboratory short-term oven aging (STOA) on stiffness of dry rubberised asphalt mixture: to study the stiffness using the ITSM test (Indirect Tensile Stiffness Modulus).
        - Ob. 2.3.2 - Effect of different laboratory short-term oven aging (STOA) on rutting of dry rubberised asphalt mixture: to study the rutting phenomenon using the RLAT test (Repeated Load Axial Test).

- **Ob. 3 – To analyse the consequences related to Life Cycle Cost Analysis deriving from the application of different pavement design methods:**
    - Ob. 3.1 - To analyse of main design models and inputs assessing.
    - Ob. 3.2 - To derive the expected life of road pavement when the main variables under investigation (e.g., Air Voids) change.
    - Ob. 3.3 - To derive the pay adjustment as a function of the expected life.

In the pursuit of the objectives of this thesis, an experimental plan has been developed. It consists of the following tasks (Figure 2.1):

- **Task 1 – Study of the literature (UNIRC – University of Reggio Calabria).**
  This task focused on the research of materials and innovative solutions (e.g., use of crumb rubber) to apply in the road infrastructure sector.
- **Task 2 – Design of experiments (UNIRC – University of Reggio Calabria and NTEC – Nottingham Transportation Engineering Centre).**
  This task focused on the study of use of rubber powder in road mixtures. The corresponding techniques of use, performances, advantages and disadvantages have been analysed. Also, the main input parameters of a pavement design have been assessed. For this section experiments have been set up.
- **Task 3 – Surface characteristics of conventional and innovative road pavements (UNIRC).**
  This task focused on the study of surface characteristics of conventional and innovative road pavements. A new laboratory approach to assess the micro- and macrotexture was provided. For this section experiments have been set up.
- **Task 4. Mastic properties: experiments and analyses (NTEC).**
  This task focused on the study of the aspects related to the mechanical characteristics of conventional and innovative road pavements (using rubber powder). An analysis of the properties of mastics (bitumen-filler-rubber), mixing sequence and, swelling phenomenon has been developed. For this section experiments have been set up.
- **Task 5 Mixture compaction: experiments and analyses (UNIRC and NTEC).**
  This task focused on the study of the effect of different laboratory short-term oven aging (STOA) on compactability and workability of dry rubberised asphalt mixture. An interrupted compaction process has been developed and its effects on compactability and workability have been studied. For this section experiments have been set up.
- **Task 6 Mixture performance: experiments and analyses (NTEC).**

This task focused on the study of the effect of different laboratory short-term oven aging (STOA) and interrupted compaction process on stiffness and rutting of dry rubberised asphalt mixture. For this section experiments have been set up.

- **Task 7 Expected life & Pay adjustment: analyses and simulations (UNIRC).**

  This task focused on the study of the modelling of the pavement aimed at the study of expected life and pay adjustment.

- **Task 8 Interrupted compaction: experiments and analyses (UNIRC).**

  This task focused on the study of the interrupted compaction process. An in-depth analysis of compaction process has been developed and its effects on compactability and workability have been studied. For this section experiments have been set up.

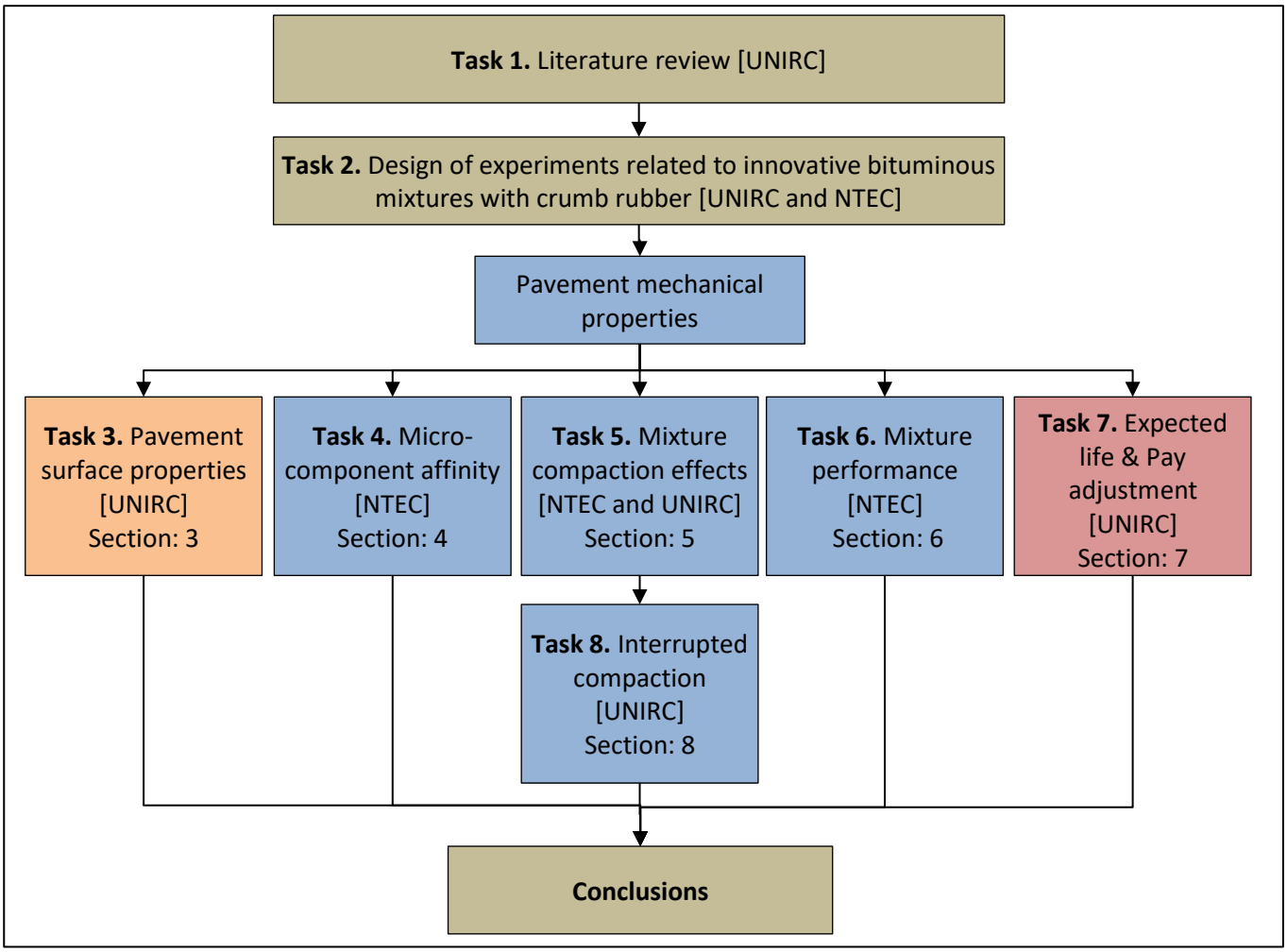

Figure 2.1: Tasks and sections

Symbols. UNIRC: Mediterranean University of Reggio Calabria (IT); NTEC: Nottingham Transportation Engineering Centre, University of Nottingham (UK).

In Table 2.1 the thesis outline is reported.

Table 2.1: Thesis outline

Chapter	Description
Executive summary	In the first section, the executive summary is reported.
Chapter 1	An overview and general background information about the reasons underpinning of this study is included in this chapter.
Chapter 2	This chapter includes a detailed description of the objectives of the thesis. Furthermore, the experimental plan of the thesis is described.
Chapter 3	This chapter aims at setting up and validating simple methods for assessing surface texture and skid resistance based on core/sample measurements. Experiments were carried out and predictive relationships were set up to explain and predict results. Experiments carried out have involved conventional and rubberised mixes.
Chapter 4	In this chapter, a brief description of materials and the mix design methods is presented. All attention focused on the micro-component affinity of mastic (bitumen, rubber and filler). The order of components in the asphalt plant and the swelling phenomenon have been analysed. In the pursuit of the objectives of this study, the viscosity in real time test was carried out.
Chapter 5	In this chapter, the manufacture of samples using different crumb rubber is described. This chapter also investigates the effect of different laboratory short-term oven aging (STOA) and compaction process on compactability and workability of dry rubberised asphalt mixture. Compactability and workability were evaluated through different parameters as: i) air void content (AV); ii) locking point; iii) compaction slope; iv) number of gyrations corresponding to 92% of G_{mm}; v) percentage of maximum theoretical specific gravity at N_{ini}.
Chapter 6	This chapter investigates the performance of different mixes manifactured in the sections above. The effect of different laboratory short-term oven aging (STOA) and compaction process on stiffness and rutting were analysed. The stiffness study of each samples was carried out using the ITSM test (Indirect Tensile Stiffness Modulus). The rutting resistance of asphalt mixtures was investigated using the Repeated Load Axial Test (RLAT).
Chapter 7	The analysis of the consequences related to Life Cycle Cost Analysis deriving from the application of different road pavement design methods was carried out in this chapter. In more detail, this section includes: i) analysis of main design models; ii) assessment of input and output of each design models; iii) derivation of expected life and pay adjustment of road pavements.
Chapter 8	In this section, a more in-depth investigation of interrupted compaction process is reported.
Chapter 9	In this section, the main conclusions are reported.
Chapter 10	In this section, all references of the study were reported.
Chapter 11	This section includes the annexes related to the study of compactability and workability of dry rubberised asphalt mixture. It contains the densification curves of each sample investigated.

Chapter 12	This section includes the annexes related to the study of rutting of dry rubberised asphalt mixture. It contains the curves recorded during the RLAT test. They are classified based on mix disign (PA or SMA10) and type of rubber used (CRT1, CRT2, CRN or control).

3 Surface characteristics of conventional and innovative road pavements[1]

3.1 Introduction

Pavement texture is a continuum which includes different scales, as a function of the wavelength: micro, macro, mega-texture and unevenness (Snyder 2007; C. Huang and Mei 2011; Andersen et al. 2015; Dunford 2013; Cantisani et al. 2016).

Micro-texture refers to wavelengths, λ, lower than 0.5mm and peak-to-peak amplitudes, A, in the range 10^3mm-0.5mm. Macrotexture refers to λ=0.5-50mm and A=0.1mm-20mm.

Macrotexture can be assessed through laser-based methods (ASTM-E1845 2015; ISO-13473:1 2013; ASTM-E2157 2015; ISO-13473:2 2002; ISO-13473:3 2002), sand-patch-like methods (EN-13036:1 2010; ASTM-E965 2006; CNR-B.U.-94 1983; Colorado-Procedure:77-09 2009; Colorado-Procedure:77-14 2014), or other extrinsic methods (ASTM-E2380/E2380M 2015). Methods above differ based on a number of parameters: the "material-method" used to "fill" the texture (sand, glass beads, or laser, see M in Table 3.1 Table 3.1Table 3.1), the number of points on the surface investigated (1 to 10, see P in Table 3.1), and the number of diameters measured *per* point (2-4, see D in Table 3.1) (ASTM-E965 2006).

The mean texture depth (MTD, EN-13036:1 2010) pertains to the macrotexture domain. It usually ranges from 0.3 mm to 0.7 mm for Dense-Graded Friction Courses (DGFC) and from 1 mm to 6 mm for porous asphalt concretes (PA) and it requires a surface diameter that is usually between 50 mm and 300 mm (ANAS 2009).

Micro-texture pertains to the roughness of the surface of the exposed aggregate chips that can be felt by one's fingertips. It interacts with the tire rubber on a molecular scale and provide adhesion (one out of the two key mechanisms of tire-pavement friction, cf. Kogbara et al. 2016).

[1] This section mainly refers to the papers Praticò and Astolfi, 2017 and Praticò, Noto and Astolfi, 2017 (see References)

Research shows that the evolution of the asperity-peak curvature of micro-texture follows that of the surface friction coefficient (Nataadmadja et al. 2015).

Table 3.1: Macrotexture methods.

Standard	M; V	D	P	L-S
EN 13036-1	S; 25	2	≥4	8k-300k mm2
ASTM E 965	S; 25	2	≥4	8k-300k mm2
CNR 94/83	S; 25	2	10	19k-700k mm^2
CP 77-14	GB; 20	4	2	4k-150k mm^2
ASTM E 1845	L	NA	10 (*)	1k mm
ISO 13473-1	L	NA	10 (**)	1k mm
ASTM E 2157	L	NA	1 (***)	1k mm

Symbols. M: material; V: volume in kmm^3; S: sand; GB: glass beads; D: number of diameters; P: number of point of the surface investigated; L-S: length or area of the surface which is investigated; NA: not present; L: laser; (*): "A minimum requirement shall be ten evenly spaced profiles of 100 mm in length for each 100 m of the test section". (**): "10 evenly distributed profiles per 100 m test section, each profile being at least 100 mm long; (***): "the profile is […] divided into eight segments for analysis", "the sensor is attached to the arm at a radius of 142 mm".

Micro-texture values are indirectly estimated in terms of pendulum test value (termed PTV in the standard EN and termed BPN in ASTM and CNR standards), using low speed friction measurement devices such as the British Portable Tester (Meegoda and Gao 2015; Wambold and Henry 1995). PVT values usually have to be greater than 45-65 (based on pavement type and road relevance), with measurements baselines which are about 125 mm (EN-13036:4 2011; CNR-B.U.-105 1985). Furthermore, surface texture affects friction, in terms of both macrotexture and micro-texture (Meegoda and Gao 2015; Balmer 1979; Ergun, Iyinam, and Iyinam 2005; Jackson, Choubane, and Holzschuher 2007; Khasawneh and Liang 2008).

Pavement micro- and macrotexture are a vital requirement of a pavement because they impact road safety, (Kogbara et al. 2016; Zhao, Qiu, and Zhang 2016; Chu, Fwa, and Tan 2016; Woodward et al. 2016; Araujo, Bessa, and Castelo Branco 2015; Snyder 2007; Noyce et al. 2005; Sandberg 1998) and greatly affect the state of play of the transportation infrastructure (Postorino and Praticò 2012). It turns out that the design of pavement texture at an early stage, in the laboratory, is crucial because of many reasons: i) concurrent requirements have to be satisfied: volumetric properties (Pratico' and Moro 2011), "premium" properties (Biligiri 2016), variations over time (Kogbara et al. 2016; Pratico', Ammendola, and Moro 2010; Pratico' and Vaiana 2012; Pratico' and Casciano 2015), and production requirements (Pratico' 2017); ii) the ability of laboratory specimens to reproduce real pavements may be sometimes controversial (cf. Georgiou and Loizos 2014; Goodman, Hassan, and AbdElHalim 2006; Boscaino et al. 2009) and methods and studies are needed to link field and laboratory results; iii) laboratory experiments enforce scientific control by testing hypotheses in the artificial and highly controlled setting of a laboratory and imply considerable savings. Unfortunately,

MTD and PTV measurements require extended surface areas and this hinders from having MTD and PTV estimates based on laboratory samples.

Understanding and deriving relationships between MTD (/PTV) tests carried out on samples and on real pavements is crucial: 1) to assess if mixes with identical volumetrics and components may have surface properties which are significantly different based on on-site vs. in-lab compaction (Iuele 2016; F.G. Praticò and Vaiana 2013); 2) given the above, to help carry out a realistic design of surface characteristics during the so-called prequalification of the mix friction course. This research gap calls for research and investigation.

This section wants to provide a theoretical and practical framework to carry out micro- and macrotexture measurements at the design stage, on samples or small slabs, in the laboratory (see Figure 3.1).

In more detail: i) standardized measurements were carried out on several friction courses according to the sand patch method (EN-13036:1 2010) and to the British Pendulum Method (EN-13036:4 2011); ii) both dense-graded and open-graded friction courses were considered; iii) in-lab and on-site tests were carried out; iv) the tests were both modelled. Algorithms were set up and finally applied to explain results and predict further developments.

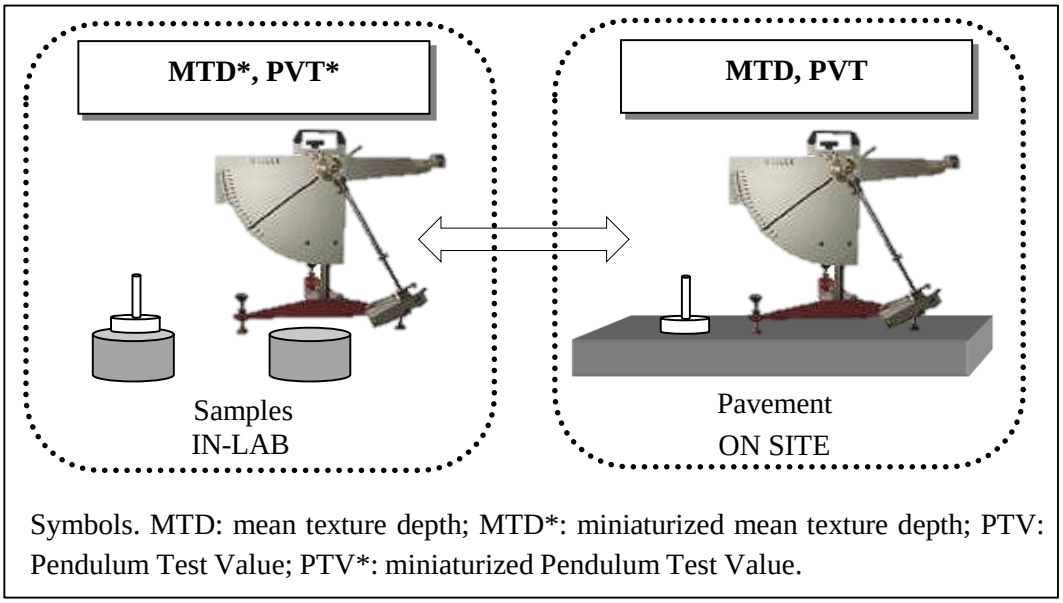

Symbols. MTD: mean texture depth; MTD*: miniaturized mean texture depth; PTV: Pendulum Test Value; PTV*: miniaturized Pendulum Test Value.

Figure 3.1: Graphical diagram of the experimental design (Praticò and Astolfi, 2017; Praticò, Noto and Astolfi, 2017)

Table 3.2 refers to the approximate range of variation of the mean texture depth (MTD, ASTM-E965 2006). Friction or microtexture-related measurements have baselines which are longer than 125 mm (PVT: 125.4 ± 1.6 mm for test on flat surfaces, see EN-13036:4 2011 and CNR-B.U.-105 1985) and this hinders from having results based on cores (about 100 mm) or/and small in-lab compacted samples.

Table 3.2: MTD: Range of variation of MTD.

	LSL (MTD)		max (MTD	
	mm	References	mm	References
DGFC	0.4	(1)	0.7	(2)
	0.3	(3)	3.0	(4)
PA	1.0	(1)	11.8	(2)
SMA	0.5	(1)	4.4	(5)
	0.7	(3)	2.9	(2)
PCC	1.1	(4)	2.5	(4)

Symbols. LSL (MTD): lower specification limit (MTD); max (MTD): max value of MTD; DGFC: dense-graded friction courses; PA: porous asphalt concrete; SMA: splittmastix; PCC: Portland Cement Concrete. (1): (ANAS 2009); (2): (Fisco 2009); (3): (Government of South Australia 2016); (4): (Sarsam and Al Shareef 2015); (5): (Woodward et al. 2016).

For sand-patch-like methods, they need a surface diameter usually between 50 and 300 mm (ANAS 2009).

On the other hand, having an in-lab assessment of surface properties would make it possible to speed up studies with a limited budget before full scale implementation.

To this end, note that Woodward et al. (2016) used a non-standard version of the volumetric patch test to determine the macrotexture of a 150 mm diameter test specimen surface. The modified test was based on EN-13036:1 (2010) in order to derive the amount of sand required to fill the top surface texture of a 150mm diameter test specimen. The volume used was obtained from the difference between the standard volume and the excess volume, measured after the spread the material.

Ramírez et al. (2015) focused on the development of new laboratory equipment for measuring the accelerated polishing of asphalt mixes, while Fisco (2009) and Flintsch et al. (2007) dealt with different macrotexture measurement methods and their relationships. Relationships between laser-based and sand-patch methods and indicators were proposed by (Filippo G. Praticò and Vaiana 2015; Pratico', Vaiana, and Iuele 2015).

In more detail, note that the standard CNR-B.U.-94 (1983) requires 10 points of the surface to be investigated, while EN-13036:1 (2010) and ASTM-E965 (2006) require that the "same operator should per-form at least four, randomly-spaced measurements of average macrotexture depth on a given test pavement surface type".

As mentioned above, skid resistance and *MTD* vary over time (Figure 3.2 and Figure 3.3, where y-axes refer to PVT and MTD, %, and x-axes refer to time or traffic).

The curves of both indicators are usually non-monotonic (Iuele 2016; S. Li, Harris, and Wells 2016; Vaiana et al. 2012; Do et al. 2013; Roque, Ravanshad, and Lopp 2013; R. M. Larson et al. 2008). Skid resistance may undergo a slight early increase (positive gradient). Afterwards, curves generally have a negative gradient. In contrast, curves representing macrotexture may have a negative gradient followed by a positive gradient.

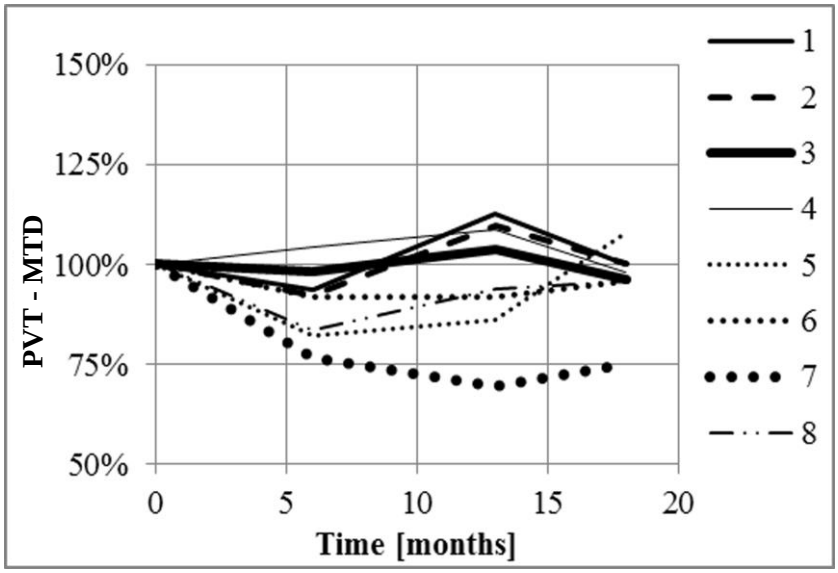

Figure 3.2: Variation over time of BPN and MTD (based on Iuele 2016, Source: Praticò, Noto and Astolfi, 2017)

Symbols. PVT: Pendulum Test Value; MTD: Mean Texture Depth; DGFC: dense grade friction course; 1: variation of PVT for DGFC composed of 85% limestone and 15% basalt; 2: variation of PVT for DGFC composed of 70% limestone and 30% basalt; 3: variation of PVT for DGFC composed of 82% limestone and 8% expanded clay; 4: variation of PVT for DGFC composed of 100% limestone; 5: variation of MTD for DGFC composed of 85% limestone and 15% basalt; 6: variation of MTD for DGFC composed of 70% limestone and 30% basalt; 7: variation of MTD for DGFC composed of 82% limestone and 8% expanded clay; 8: variation of MTD for DGFC composed of 100% limestone.

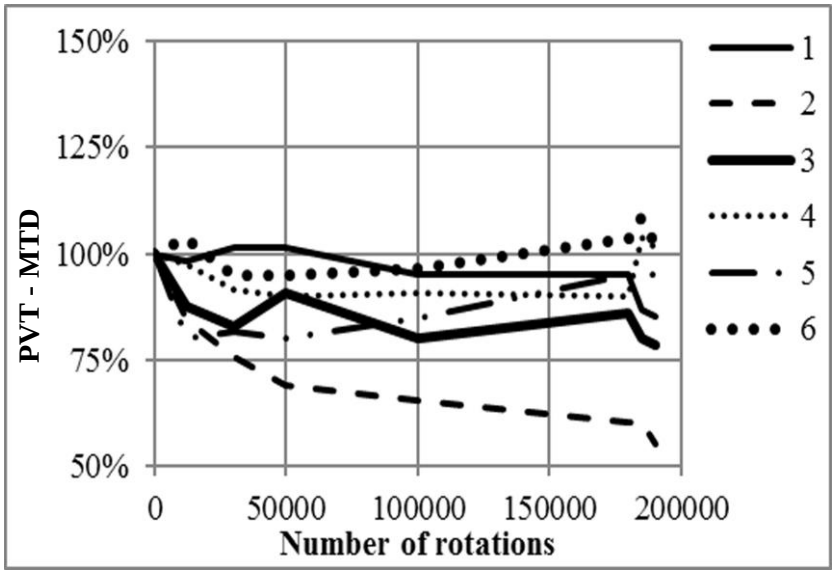

Figure 3.3: Variation over time of BPN and MTD (based on Do et al. 2013, Source: Praticò, Noto and Astolfi, 2017).

Symbols. PVT: Pendulum Test Value; MTD: Mean Tex-ture Depth; 1: variation of PVT for road surface with maximum aggregate size =10 mm; 2: variation of PVT for road surface with maximum aggregate size =14 mm; 3: variation of PVT for road surface with maximum aggregate size =6 mm; 4: variation of MTD for road surface with maximum aggregate size =10 mm; 5: variation of MTD for road surface with maximum aggregate size =14 mm; 6: variation of MTD for road surface with maximum aggregate size =6 mm.

3.2 Experiments

In task 1, in the aim of gathering practical information and data about the potential of the two tests to be used in the laboratory, experiments were carried out on pavements and on cores extracted.
Six reference friction courses were considered: three dense-graded friction courses (DGFC), herein termed DG1-DG3, and three porous asphalt concretes (PA), herein termed PA1-PA3.
On average, for DGFCs, specific gravity was 2.32 and asphalt binder content was 5.1% (by weight of mix), while for PAs, specific gravity was 2.11 and asphalt binder content was 5.0% (by weight of mix).
Two types of indicators were derived: Mean Texture Depth (MTD, EN-13036:1 2010) and Pendulum Test Value (PVT, EN-13036:4 2011).
The volume used to measure MTD and the length of the contact path were the ones set up in the concerned standards (EN-13036:1 2010 and EN-13036:4 2011) and the ones needed in order to make it possible to perform them on samples, in the laboratory.

3.2.1 Macrotexture

For macrotexture, note that a volume of 25000 mm^3 is required by the traditional, current methods (Snyder 2007; ASTM-E965 2006; CNR-B.U.-94 1983; EN-13036:1 2010), while a smaller volume (4500 mm^3, Praticò, Noto, and Astolfi 2017) is required by the diameter of Marshall (EN-12697:30 2012) or gyratory specimens (EN-12697:31 2014).
By referring to the miniaturization of the MTD test, it appears relevant to observe that when sample, sand patch, and spreading tool are considered: the sample diameter varies from “infinity” (pavement), to about 100 mm (Marshall specimen), while the spreading tool has a constant diameter of 63.5 mm, and the sand patch diameter varies based on mix type, compaction and volume (see Figure 3.4 - Figure 3.5 - Figure 3.6).
After the preliminary tests, in which different volumes were considered (cf. Figure 3.7-A), two volumes were considered: 25000 mm^3 (as per the abovementioned standard) and 4500 mm^3 (miniaturised test).

Figure 3.4: Miniaturised MTD (Marshall sample, V= 4500 mm^3, Praticò, Noto and Astolfi, 2017)

Figure 3.5: Miniaturised MTD (Giratory sample, V= 4500 mm^3, Praticò, Noto and Astolfi, 2017)

Figure 3.6: MTD ("pavement" sample, current method with V= 25000 mm^3, Praticò, Noto and Astolfi, 2017)

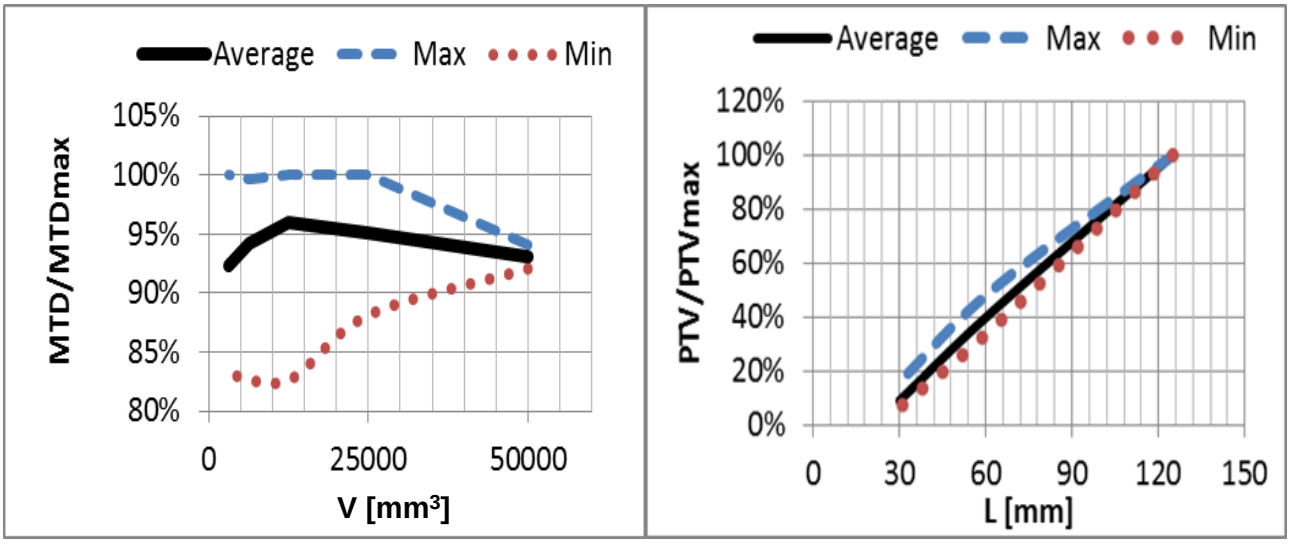

Figure 3.7: Preliminary tests performed (example: left/A: MTD as a percentage of the maximum value; right/B: PTV).

Source: Praticò and Astolfi, 2017.
Symbols. PVT: Pendulum Test Value; MTD: Mean Tex-ture Depth; V: volume of sand [mm³]; L: Slide length [mm].

Figure 3.8 summarises the rationale behind the miniaturization of the current method. Note that:

- Curve 1 refers to the current specifications (V= 25000 mm³).
- Curve 2 refers to the proposed specification (V= 4500 mm³).
- DM stands for the diameter of Marshall samples, while DGC refers to the gyratory compactor (where the diameter is 6 inches, corresponding to about 150 mm).
- Boxes illustrate to approximate range of variation of MTD (mean texture depth, x-axis) and D (sand patch diameter, y-axis) for the given type of mixture (e.g., SMA): the more open the mixture, the lower the diameter D.

In each point of each surface (e.g., point B of surface DG1), multiple repetitions of the MTD measurement were carried-out (up to 31, Table 3.3).

For V=4500 mm³, note that each measurement was followed by compressed air jet blasting in order to clean the surface and that this procedure is not usually required because both CNR and EN-ASTM standards do not require to repeat the measurement in the same point of the surface (see Figure 3.9).

Table 3.3 illustrates the averages obtained for the six pavements under analysis. Values in the range 0.5 mm to 1.9 mm were obtained for DGFCs.

On the contrary, values between 1.6 mm and 2.9 mm were obtained for PAs (see Figure 3.10). Note that the standard deviation ranged from 0.01 mm to 0.22 mm for DGFCs, while it ranged from 0.00 mm to 0.10 mm for PAs (see Figure 3.11).

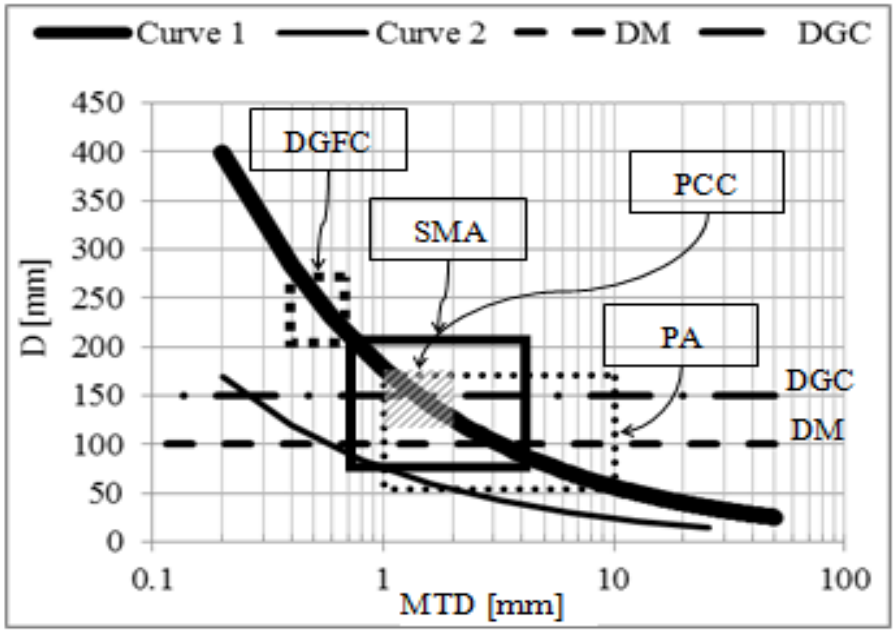

Figure 3.8: Rationale behind the miniaturised MTD (Praticò, Noto and Astolfi, 2017)

Symbols. DM: diameter of Marshall samples; DGC: diameter of the Giratory Compactor samples; DGFC: dense-graded fric-tion courses; PA: porous asphalt concretes; SMA: splittmastix asphalt; PCC: Portland Cement Concrete.

Figure 3.9: Cleaning of the pavement between two successive tests on the same point of the surface (Praticò, Noto and Astolfi, 2017).

Symbols. OGFC: Open Graded Friction Course.

Note that DG1 differs from DG2 and DG3 and this may be due to the fact that DG1 corresponds to a dense-grade friction course that is older than DG2 and DG3. This partly complies with Iuele 2016 and Do et al. 2013

(see Figure 3.2 and Figure 3.3) and refers to the fact that surface texture deterioration is greater than for the other two types of surface.

Many factors, including aggregate properties, binder properties, aggregate-binder combination, road geometry, traffic, weather, rainfall, and environmental conditions can be responsible for this (Iuele 2016; Do et al. 2013; S. Li, Harris, and Wells 2016; Vaiana et al. 2012; Roque, Ravanshad, and Lopp 2013; R. M. Larson et al. 2008). Table 3.3 also illustrates the coefficients of variation (CV, ratio of standard deviation to mean) for each mix (with V= 4500 mm^3 and V= 25000 mm^3).

DGFCs have CVs lower than 14%, while PAs have CVs lower than 4% (see Figure 3.12). It is possible to observe that:

- the higher the volume is, the higher the MTD becomes;
- the standard deviation decreases when the volume used increases from 4500 mm^3 to 25000 mm^3;
- the coefficient of variation (CV) decreases when the volume increases.

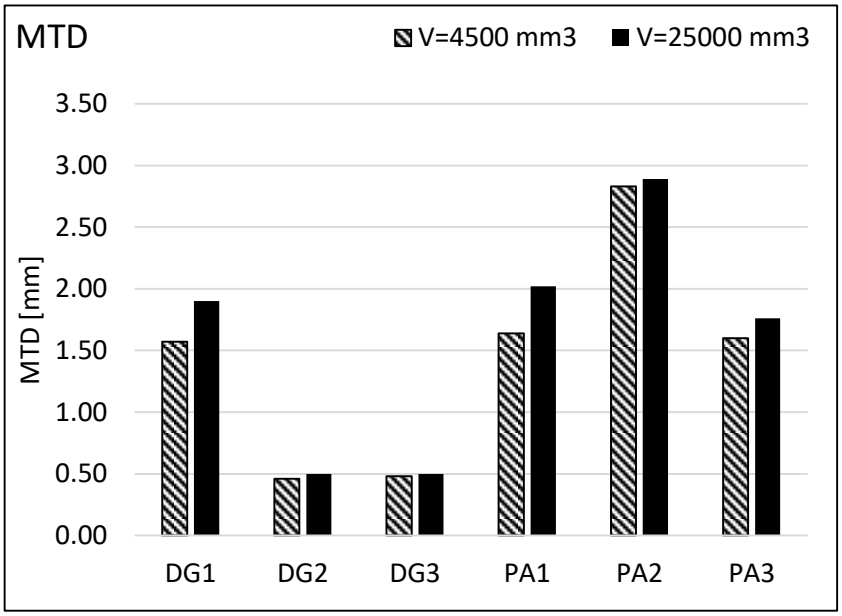

Figure 3.10: Averages obtained for the six pavements under analysis (MTD).

Symbols. MTD: Mean Texture Depth; V: Volume of sand; DG1-DG3: Dense-graded friction courses; PA1-PA3: Porous asphalt concretes.

R_{MTD} is the ratio $MTD_{25}/MTD_{4.5}$, i.e., the ratio between the value of MTD obtained when using a volume of 25000 mm^3 or 4500 mm^3. By referring to $R_{MTD}= MTD_{25}/MTD_{4.5}$ (Table 3.3), note that this ratio ranges from 103% to 121% for the dense-graded friction courses considered, while it ranges from 102% to 123% for porous asphalt concretes.

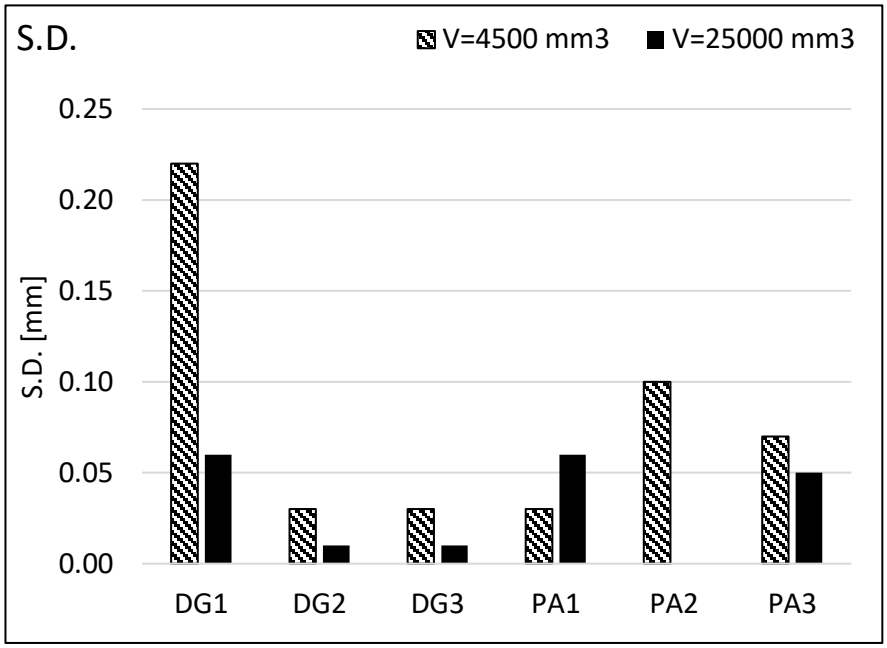

Figure 3.11: Standard deviations obtained for the six pavements under analysis (MTD).

Symbols. S.D.: Standard Deviation; V: Volume of sand; DG1-DG3: Dense-graded friction courses; PA1-PA3: Porous asphalt concretes.

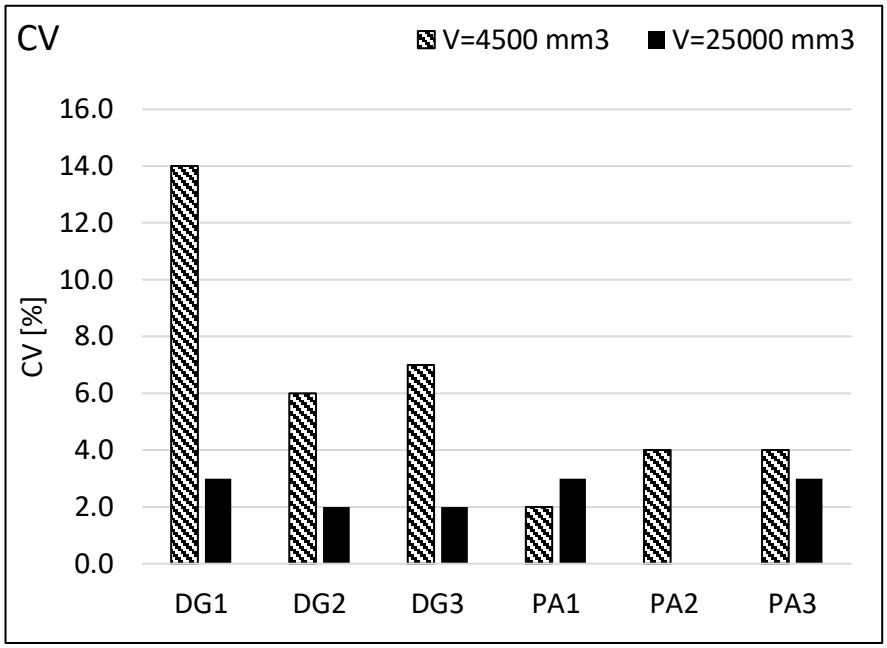

Figure 3.12: Coefficient of variation obtained for the six pavements under analysis (MTD).

Symbols. CV: Coefficient of Variation; V: Volume of sand; DG1-DG3: Dense-graded friction courses; PA1-PA3: Porous asphalt concretes.

It is noted that high values of MTD (e.g. PA2) may be linked to sand percolation into the interconnected pores "under the surface", which may imply higher variances for MTD and R_{MTD} and non-linearities in MPD-MTD relationship (Filippo G. Praticò and Vaiana 2015).

Table 3.3: MTD values obtained according to the EN 13036-1.

Sample	DG1		DG2		DG3		PA1		PA2		PA3	
V	25000	4500	25000	4500	25000	4500	25000	4500	25000	4500	25000	4500
MTD	1.90	1.57	0.50	0.46	0.50	0.48	2.02	1.64	2.89	2.83	1.76	1.60
R_{MTD}	-	1.21	-	1.09	-	1.03	-	1.23	-	1.02	-	1.10
$1/R_{MTD}$	-	0.83	-	0.91	-	0.97	-	0.81	-	0.98	-	0.91
S.D.	0.06	0.22	0.01	0.03	0.01	0.03	0.06	0.03	0.00	0.10	0.05	0.07
CV	3%	14%	2%	6%	2%	7%	3%	2%	0%	4%	3%	4%

Symbols. V: Volume of sand [mm^3]; MTD: Mean Texture Depth, mm (EN-13036:1 2010); R_{MTD}: ratio $MTD_{25}/MTD_{4.5}$; MTD_{25}: Mean Texture Depth corresponding to V=25000 mm^3; $MTD_{4.5}$: Mean Texture Depth corresponding to V=4500 mm^3; S.D.: Standard Deviation [mm]; CV: Coefficient of Variation [%]; DG1-DG3: dense-graded friction courses; PA1-PA3: porous asphalt concretes.

3.2.2 Skid resistance

For skid resistance, preliminary tests were carried out in order to explore for different slide lengths (cf. Figure 3.7-B).

For both PTV and MTD, note that the smaller the lengths/surfaces are, the higher the variability is. Table 3.4 refers the results (PTV) obtained for dense-graded mixtures (DG1-DG3) and porous asphalt concretes (PA1-PA3), when using the slide length as per standard (L=125 mm) or reducing it in the pursuit of miniaturization (L=62.5 mm).

Each result (e.g., PTV=76) refers to a given sample and is the average of 6 values. In turn, each of these six values is the average of 5 "swings".

In summarising, each result derives from 30 "swings". The coefficient of variation (CV, %) is derived starting from the standard deviation and the average (PTV).

1/R refers to the ratio $PTV_{62.5}/PTV_{125}$ (same mixture, e.g., DG2). Note that $PTV_{125}/PTV_{62.5}$ ranges from 1.99 to 2.77 (all the samples) and its average is 2.40. In contrast, $PTV_{125}/PTV_{62.5}$ ranges from 1.99 to 2.22 and its average is 2.14 for porous concretes (PAs), while $PTV_{125}/PTV_{62.5}$ ranges from 2.48 to 2.77 and its average is 2.66 for dense-graded friction courses (DGs).

Note that: i) PTV ranges from 59 to 76 for DGs and from 59 to 61 for PAs (L=125mm); ii) If the contact path is halved then the results obtained decrease and the standard deviation increase; iii) R_{PVT} ranges from 1.9 to 2.2 for DGs and from 2.4 to 2.7 for Pas; iv) $1/R_{PTV}$ ranges from 36 to 50%.

Table 3.4: PTV values obtained according to EN 13036-4.

Sample	DG1		DG2		DG3		PA1		PA2		PA3	
L	125.0	62.5	125.0	62.5	125.0	62.5	125.0	62.5	125.0	62.5	125.0	62.5
PTV	76	34	59	29	64	29	59	21	59	24	61	22
CFT	-3	-2	-2	-2	-2	-2	-2	-2	-2	-2	-2	-2
R_{PVT}	-	2.20	-	1.99	-	2.22	-	2.77	-	2.48	-	2.74
$1/R_{PVT}$	-	0.45	-	0.50	-	0.45	-	0.36	-	0.40	-	0.37
S.D.	1.53	1.11	1.09	1.23	1.00	0.72	1.27	1.16	1.12	0.84	2.06	0.76
CV	2%	3%	2%	4%	2%	2%	2%	5%	2%	3%	3%	3%

Symbols. L: Slide length [mm]; PTV: Pendulum Test Value (EN-13036:4 2011); RPVT: ratio PTV125/PTV62.5; PTV125: Pendulum Test Value corresponding to L=125 mm; PTV62.5: Pendulum Test Value corresponding to L=62.5 mm; S.D.: Standard Deviation; CV: Coefficient of Variation [%]; DG1-DG3: dense-graded friction courses; PA1-PA3: porous asphalt concretes; CFT correction factor for temperature.

3.3 Modelling, calibration, and validation

In order to explain the rationale behind the results obtained, attention was focused on modelling both tests. In both cases, analyses were carried out to simulate what happens when small surfaces are used, in the aim of providing insights and explanations.

3.3.1 MTD modelling

As is well known, *MTD* is the ratio between a given volume, *V* (e.g. V_{25}= 25000 mm^3 or $V_{4.5}$= 4500 mm^3), and the corresponding area ($\pi D^2_{25}/4$ or $\pi D^2_{4.5}/4$, respectively):

$$MTD = \frac{4 \cdot V}{\pi \cdot D^2} \qquad \text{(Eq. 1)}$$

Where *D* (e.g., D_{25}) is the diameter of sand patch. If *R* is the ratio between MTD_{25} (volume=25000 mm^3) and $MTD_{4.5}$ (volume=4500 mm^3), for the diameters of sand patch, $D_{4.5}$ and D_{25}, it follows:

$$\frac{D_{25}^2}{25} = \frac{1}{R}\frac{D_{4.5}^2}{4.5} \quad \text{(Eq. 2)}$$

Under the hypothesis that R>1, it follows:

$$\frac{D_{25}^2}{25} < \frac{D_{4.5}^2}{4.5} \quad \text{(Eq. 3)}$$

By referring to the reasons for having such a relationship (as observed in the experiments), different hypotheses might be formulated, among which the following: i) Results are affected by spreading procedure and by the ratio D_{ST}/D_V, where D_{ST} is the diameter of the spreading tool (63.5mm), while D_V is the diameter of the sand patch for the given volume (V); ii) when smaller quantities of sands are investigated, for the relationship between *MTD* (dependent variable) and the volume of sand used (V, independent variable), there are local domains of V in which the first derivative changes sign.

In order to provide explanations, let us model surface texture in terms of spherical holes on a flat surface (see Figure 3.13).

Let us suppose that the volume of each hole is:

$$V_H = \frac{2\pi \cdot r^3}{3} \quad \text{(Eq. 4)}$$

Where V_H (mm^3) is the volume of the given hole and r (mm) is the radius of the semi-sphere. Let us suppose that the distance (centre to centre) between two adjacent spheres is $k \cdot r$ on both the x-axis and the y-axis ($k \geq 2$). For $D >> 2r$, the number of semi-spheres is approximately given by:

$$N \cong \left(\frac{(D - 2 \cdot r)}{k \cdot r \cdot \sqrt{2}} + 1 \right)^2 \quad \text{(Eq. 5)}$$

Consequently, it results approximately that:

for $\frac{(D-2\cdot r)}{k\cdot r\cdot\sqrt{2}}\geq 1$ $$MTD\cong\left[\frac{(D-2\cdot r)}{k\cdot r\cdot\sqrt{2}}+1\right]^2\cdot\frac{\frac{2}{3}\pi\cdot r^3}{\frac{\pi D^2}{4}}+0.2\ \text{[mm]}$$ (Eq. 6)

and

for $\frac{(D-2\cdot r)}{k\cdot r\cdot\sqrt{2}}<1$ $$MTD\cong 0.2\ \text{[mm]}$$ (Eq. 7)

when *D* approaches infinity, then it results:

$$\lim_{D\to\infty}(MTD)\cong\frac{4\cdot r}{3k^2}+0.2$$ (Eq. 8)

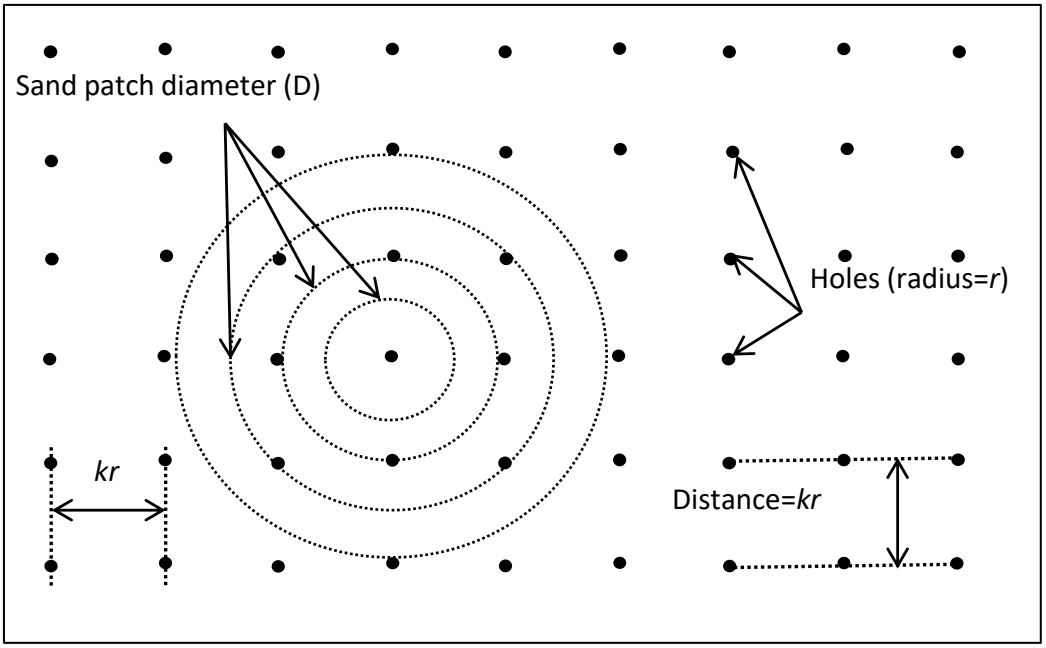

Figure 3.13: Modelling sand patch test in an ideal surface (Praticò and Astolfi, 2017)

Based on the algorithms herein set up (equations 5-8) it follows that:

- the lowest value depends on sand diameter (0.2mm);
- the highest value depends on hole geometry;
- the higher *D* becomes, the lower the variability of *MTD* is (cf. Figure 3.14-A). The asymptotic value depends on the geometric model.

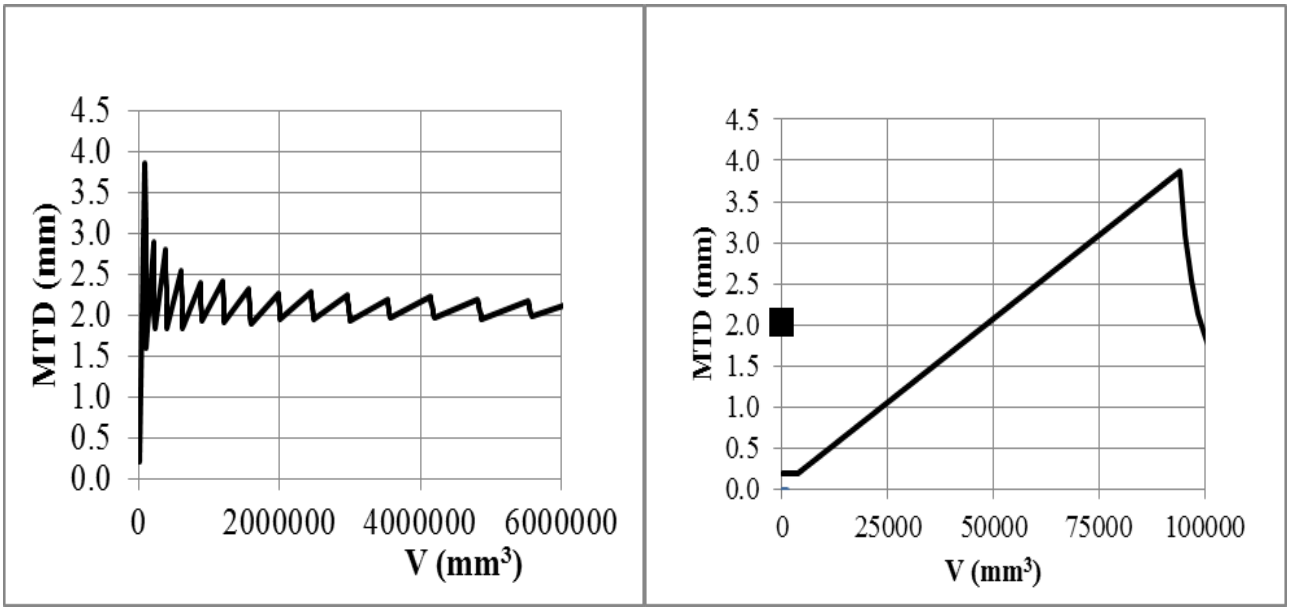

Figure 3.14: MTD predicted through the model (Praticò and Astolfi, 2017)

Symbols. MTD: Mean Texture Depth; V: volume of sand [mm³].

The rationale behind Eq.6 is that *MTD* is given by 0.2 mm (i.e., sand diameter) plus 1, 9, 25 times the volume of a semi-sphere divided by the overall surface area covered. The multiplier is in square brackets.

Figure 3.14 refers to how *MTD* (*y*-axis, Eq.6) varies based on the volume of sand (*x*-axis).

It appears evident that the model confirms that there are contexts in which the first derivative may be positive and, *vice versa*, there are situations in which the first derivative may be negative.

Model predictions (see Figure 3.14) confirm that the first derivative undergoes different values (positive and negative), due to the fact that sand can be spread over sags, crests, or flat surfaces.

For the number of repetitions, note that based on the dependence of the standard deviation of the mean (SDOM) on the number of repetitions, for a volume of 4500 mm^3, 4 repetitions are needed in order to have a standard deviation-to-average ratio of 2% (as per EN and ASTM standards).

Table 3.5 summarises the main characteristics of the proposed method for the miniaturization of *MTD* test.

By referring to test repeatability and reproducibility (CV% s.o. and CV% d.o., respectively, cf. Table 3.5), it appears noteworthy to highlight that in ASTM-E965 2006 and EN-13036:1 2010 it is reported that “The standard deviation of the site-to-site measurements may be as large as 27 % of the average texture depth”, where site “defines a randomly selected location within a nominally homogeneous pavement section”. In contrast, fixed-site CV is about 1-2%.

Table 3.5: Characteristics of the proposed method.

Standard	CNR BU 94/83	EN 13036-1	ASTM E 965	Proposed
Points	5 + 5	4	4	1
Diameters	2	2	2	2
Distribution	2A	Random	Random	COS
CV% s.o.	N.A.	1% (*)	1% (*)	2%
CV% d.o.	N.A.	2% (*)	2% (*)	2%
Repetitions	1	1	1	4
Cleaning	N.A.	N.A.	N.A.	CA

Symbols. (*): Macrotexture depth of 0.5 to 1.2 mm; N.A.: not available; s.o.: same operator; d.o.: different operator; Points: number of points for the given surface; Diameters: number of diameters per point; Distribution: distribution of points on the surface; CV%: Precision in terms of coefficient of variation in percentage; Repetitions: number of repetitions in the same point; 2A: two alignments (quasi-deterministic); CV%: coefficient of variation in percentage. CA: compressed air. COS: centre of specimen (F.G. Praticò, Noto, and Astolfi 2017).

3.3.2 PTV modelling

As is well known, following da Vinci observations, Amontons' laws states that the ratio of the friction force to the loading force (friction coefficient) does not depend on the loading force or the apparent contact area. When an object begins to slide, it is often considered that a shear force greater than the maximum static friction force is needed.

This notwithstanding, according to Otsuki and Matsukawa (2013), precursors appear as local slips at the interface under shear forces quite below before the maximum static friction force, and this force corresponds to the onset of bulk sliding. According to Tuononen (2016), the onset of the frictional sliding (i.e., when the phenomenon commences) depends on the state of the surfaces between the two sliding materials. In more detail, Tuononen (2016) focuses on rubber–glass contact under dry and lubricated conditions and obtained different curves. For rubber on dry glass, the force curve over time undergoes a smooth transition from the static situation (friction coefficient zero) to sliding (friction coefficient quasi-constant), without any identifiable peak value, and with no precursors of sliding. For rubber on wet glass, the force curve over time shows a clear peak value (which would traditionally be the static friction coefficient), involved phenomena are more complex, and after the peak a quasi-constant value is approached (over time).

Based on theory and based on preliminary experiments, an equation in which the sliding force varies over space according to a three-step model is formulated in this paper. In order to derive information about the expected variation of PTV when different lengths of contact path are considered, let us consider that the pendulum motion starts from a given height (h_1) and ends at a given height (h_F), due to two main classes of energy losses (Figure 3.15): i) friction losses (W) in the contact path between pavement/core and the

pendulum rubber shoe (slider assembly), based on friction coefficient (μ), on reference orthogonal force (F_{ort}) and on contact length (*L=A+B+(L-A-B)*); ii) friction losses in the hinge of the device, which refer to h_{piv} (see below) and *h** (zero reading below the horizontal, Hallas and Hunwin 2009; Kim and Kim 2008; Inturri 2012).

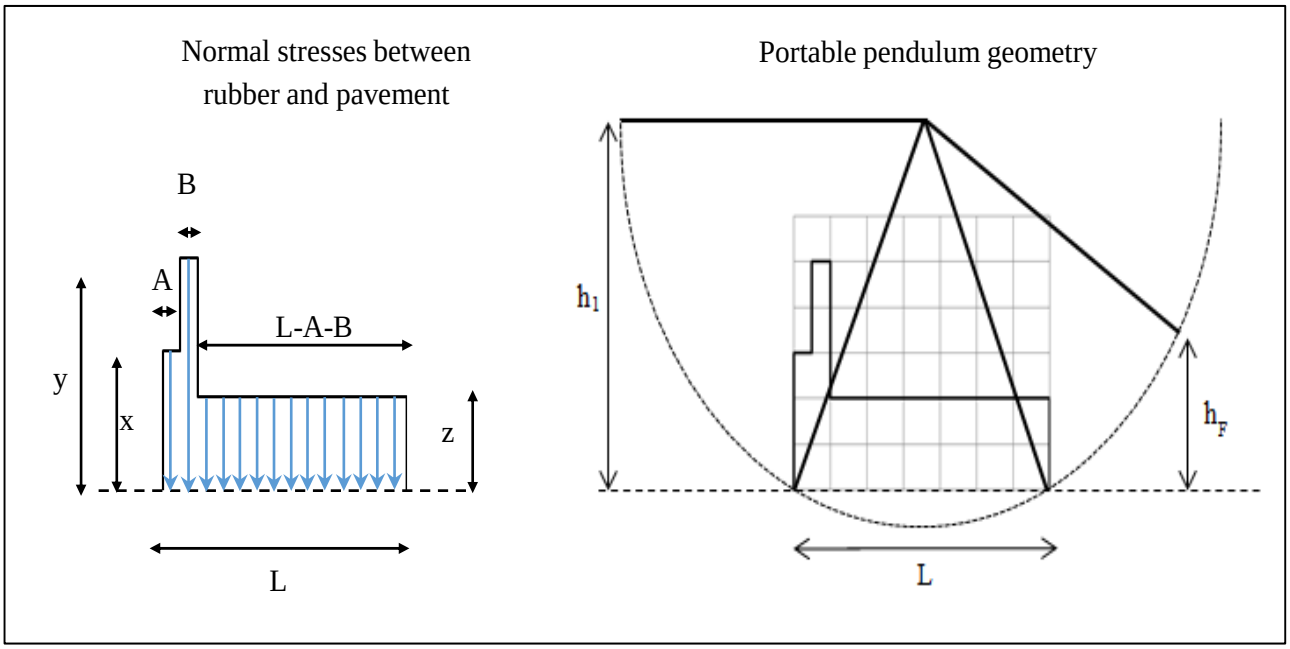

Figure 3.15: PTV stress distribution (left) and test geometry (right).

Source: Praticò and Astolfi, 2017; Praticò, Noto and Astolfi, 2017.

The main algorithms herein set up are summarised in Equations 9 to 14.

The relationship between PTV_{ob125} (*PTV* observed, L=125 mm) and the friction coefficient is as follows:

$$\mu = \frac{PTV_{ob12.5}}{100} \qquad \text{(Eq. 9)}$$

Three stretches (*A*, *B*, *L-A-B*) in the contact path *L* are supposed to exist, with a contact force which undergoes corresponding changes (x F_{ort} in A, y F_{ort} in B, z F_{ort} afterwards):

$$W = F_{ort} \cdot \mu \cdot \left[Ax + By + (L - A - B)z\right] \qquad \text{(Eq. 10)}$$

The final height (no friction at hinge) is as follows:

$$h_2 = \frac{1}{mg}\left[(\frac{1}{2} m \cdot 2h_1 \cdot g) - W \right] \quad \text{(Eq. 11)}$$

where $m \cong 1.5 \pm 0.03$ kg (EN-13036:4 2011), $g = 9.81 m/s^2$, $h_1 \approx 0.512$m, $F_{ort} \approx 22.5$N.

The final height results:

$$h_F = h_2 - h_{piv} = h_2 - \frac{h_2}{h_1} h^* \quad \text{(Eq. 12)}$$

where $h^* = 0.01016$m.

Based on the as-built characteristics of the British Pendulum, the relationship between the final height (h_F) and the value of *PTV* is here estimated as follows:

$$PTV_e = -0.7013 \cdot h_F + 352.06 \quad \text{(Eq. 13)}$$

Overall, based on tests, the calibration of the proposed model is carried out through the following error function (objective function):

$$\Phi = \sum (PTV_e - PTV_{ob})^2 \quad \text{(Eq. 14)}$$

where PTV_{ob} is the value observed, while PTV_e is the value estimated through the equation above.

3.3.3 Calibration and validation

PTV model calibration was carried out based on equations above. Based on results it is possible to observe that, for the cases under analysis: i) on average there are three different steps/phases in rubber vs. pavement sliding.

In the first phase (length A<15mm) there is a force which is less than 1% of the reference force set up un the standard (22.5N).

In the second phase (length B<0.3mm), there may be an increase of the reciprocal, orthogonal force. This supplementary phase (B), if existing, accounts for less than 1cm of sliding path.

In the third phase (*L-A-B*), which corresponds to almost the entire sliding length (*L*), the force is close to 100% of the reference force; ii) overall an average error of 1-3 *PTV* points was obtained, as a function of the minimization process chosen; iii) F_{ort} resulted to range from 17 to 23 N; iv) in all the optimizations attempts, $PTV_{62.5}/PTV_{125}$ resulted close to 44%.

In summarising, based on modelling it appears that the results obtained and the relationship between contact length and results are well explained by the physical model set up herein.

By referring to the number of repetitions and to the precision of the proposed and miniaturised method (see Table 3.6), note that: i) the EN-13036:4 (2011) states that the precision is 1 PTV, uncorrected for temperature and on a fine-textured, plane surface.

At the same time, it mentions that coarse textured or very smooth surfaces will reduce the precision and it warns about porous surfaces on which the test may give erroneous results.

Furthermore, the same standard states that (Note 2) the use of the temperature correction will reduce the precision of the test and that (10.3) the number of samples necessary to obtain the PTV of an area will be dependent upon the variability of the surface; ii) experiments prove that the miniaturised method has a standard deviation which is close to 1 PTV (0.7 for the tests under investigation); iii) the EN precision in terms of standard deviation corresponds to a precision in terms of coefficient of variation of about 1.6 %; iv) based on the above, it is suggested to perform at least six tests (each test consisting of five swings) for dense-graded friction courses and at least nine tests (each test consisting of five swings) for porous asphalt concretes. These repetitions (e.g., 1·6·5 for DGFCs) make the standard deviation of the miniaturised test consistent with the one of the EN standard for both DGFCs and PAs.

Based on the above, Table 3.6 summarises the characteristics of the proposed method.

Table 3.6: Characteristics of the proposed method (PTV-BPN).

Standard	ASTM E 303	EN 13036-4	CNR 105/85	Proposed
Points	4-5	≥3	5·3	1
Measures *per* point	1	1	1	6-9 (*)
Swings *per* point	>4	5	5	5
Distribution of points	N.A.	Random	3A	COS
S.D.	1-1.2 BPN unit	1 PTV	1.2 BPN unit	1 PTV

Symbols. 3A: three alignments (quasi-deterministic) in areas more stressed by traffic; COS: centre of specimen; S.D.: Standard Deviation; N.A.: not available; (*): 6·5 swings for DGFCs, 9·5 swings for PAs.

Figure 3.16 summarizes model validation. Validation data were independently measured from the calibration data.

Figure 3.16-A (left) focuses on *MTD*. Note that *R*-square is 0.93 while the residual scatter plot shows no systematic patterns apparent. This indicates that the model fits the data well. Figure 3.16-B (right) refers to *PVT*. This plot shows that there is only random scatter in the relationship between the observed *PTV* and the order in which the data were collected. Note that in this case the *R*-square is only 0.4. This fact may be due to the high standard deviation of PAs and calls for further study and research.

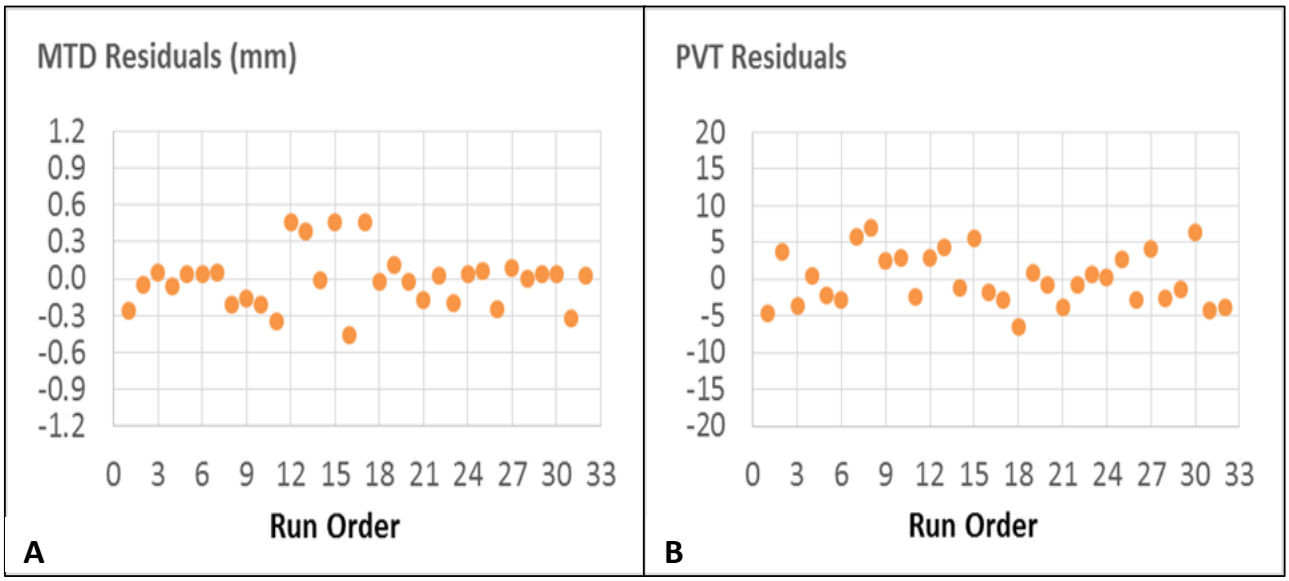

Figure 3.16: Run sequence plot for the residuals (MTD: Figure 3.16-A; PTV: Figure 3.16-B; Praticò and Astolfi, 2017).

3.4 Conclusions

Based on the results shown above, it may be observed that for macrotexture:

- 4500 mm^3 are appropriate for Marshall/Giratory specimens and for different types of mixes, included DGFCs and PAs.
- The miniaturised MTD (V=4500 mm^3) is approximately 10% less than the one obtained according to in-situ tests (for both PAs and DGFCs). This implies that the results should be consequently corrected (R=1.02-1.23).
- Four measurements are needed in order to have a σ/MTD ratio complying with the one stated in the ASTM-EN standards.
- Due to the small quantity of sand and to the complexity of surface texture, modelling explains that MTD measurements are affected by the volume of sand used.

At the same time, for skid resistance:

- A contact path of 62.5 mm is appropriate for Marshall/Giratory specimens of different types of mixes, including DGFCs and PAs.
- The value of PTV which is obtained when using a length of 62.5 mm is approximately 58% less than the one obtained according to in-situ tests (for both PAs and DGFCs). This implies that the results should be consequently corrected (R=1.99-2.77).
- Based on the dispersion indicators obtained, 6-9 measures per point are needed in order to have a precision complying with the one stated in the ASTM E 303 and in the EN 13036-4.
- Test model set up and calibrated explains that lower contact paths correspond to lower PTVs and quantifies the difference with a fair precision (44% *versus* 42%, on average).

Based on the above, it seems possible to point out that this study makes several contributions to the literature. First, it adds to the relatively small amount of research that examines whether macrotexture and pendulum test can be explained and predicted based on simple physical and geometric models.
Second, the results of this research help provide a better understanding of the importance and the criticalities of assessing macro- and micro-texture at an early stage and on small samples.
Whereas previous research provides evidence that small samples may provide valuable information about texture, this study reveals that such measures can be related to the corresponding measures on real pavements.

4 CR-added bituminous mixtures - Mastic properties: experiments and analyses[2]

4.1 Introduction

Millions of scrap tyres are generated each year across the world. In the UK alone, around 30 million are produced each year (Y. Huang, Bird, and Heidrich 2007; S.J. Lee et al. 2007; Rahman 2004). These scrap tyres pose a serious landfilling problem because of their large size and they are a non-biodegradable waste. The environmental impacts of the used tyres have driven research towards recycling them into the different construction applications as a sustainable practice for protecting the environment and also for enhancing the mechanical properties of materials (F.G. Praticò et al. 2016).

The bituminous materials constitute the main elements of a flexible pavement. Thus, involving the recycled tyre rubber into the bituminous materials would open a large market for scrap tyres because much higher quantity of recycled tyres can be used in the pavement industry (Davide Lo Presti 2013; A. Subhy, Lo Presti, and Airey 2015). Additionally, this approach has been broadly recognised to improve the performance characteristics and increase the service life of pavements in comparison to conventional materials (Ruth and Roque 1995; Cao 2007; Chiu and Lu 2007; Paje et al. 2010; Wang et al. 2012; A. Subhy, Lo Presti, and Airey 2015).

The introduction of rubber particles into road asphalt mixtures are generally accomplished via two process: the wet and the dry. In the wet process, the ground rubber particles are blended with the bitumen and the modified binder is then mixed with aggregates; while in the dry process, the crumb rubber is added directly in the asphalt mixer.

[2] This section mainly refers to the papers Astolfi et al., 2019 (see references).

Although larger quantities of recycled tyre rubber are consumed in mixtures produced using the dry process and with minimal or no modification required in asphalt plant, the inconsistency in field performance makes the dry process not widely used and increasingly being abandoned (Rahman 2004). In fact, in the dry process, the interaction between the bitumen and the rubber particles is hard to control and the CR particles keep swelling during hauling and possibly also after paving operations, often causing instability to the volumetric properties of the matrix which in turns could provoke stripping and premature cracking on the surfacing.
In this paper the interaction between bitumen, rubber and, filler during the production of mastic was investigated. The main objectives of the study are:

1. Reproducing a realistic methodology to allow real-time monitoring of apparent viscosity of different bitumen/filler/rubber systems (mastics) within a timeframe that could consider mixing, hauling and paving operations (5 hours).
2. Investigating the swelling process of the rubberised mastics of asphalt mixtures for surface courses, namely a Porous Asphalt (PA) and Stone Matrix Asphalt (SMA).
3. Evaluating the effect of two different pre-treatment of rubber particles and comparing it with the swelling extent of more conventional ambient rubber.

4.2 Materials and methods

4.2.1 Bitumen

A pen grade 50/70 bitumen was used in this study. Several tests such as the penetration test, softening point test, viscosity test and elastic recovery test were carried out to characterize the properties of the bitumen. The physical properties of the bitumen are shown in Table 4.1.

Table 4.1: Physical properties of bitumen 50/70 used in this study.

Property	Unit	Standard	Results (*)
Specific gravity (@25°C)	[g/cm^3]	(EN-ISO-3838 2004)	1.051
Penetration (100 g, 5 s, 25°C)	[0.1mm]	(EN-1426 2015)	61
Softening point (@ 25°C)	[°C]	(EN-1427 2015)	48.4
Viscosity			
(@ 60°C)			167
(@ 135°C)	[Pa·s]	(EN-13302 2003)	0.34
(@ 160°C)			0.12
(@ 180°C)			0.06
Fragility temperature (Fraas method)	[°C]	(EN-12593 2015)	-10
Elastic recovery (@ 25°C)	[%]	(EN-13398 2017)	6

Note. (*): test carried out by NTEC - Nottingham Transportation Engineering Centre.

4.2.2 Crumb rubber and filler

Three different types of rubber were used in this study: an ambient crumb rubber la-belled as CRN, two pre-treated rubber particles la-belled in this study as CRT1 and CRT2.

The physical properties of rubbers are presented in Table 4.2.

Table 4.2: Properties of crumb rubber particles.

Rubber type	Property	Unit	Result
CRT1	Typology	[-]	Powder
	Specific gravity	[g/cm^3]	1.15 ± 0.04
	Colour	[-]	Black
	Particles morphology	[-]	Irregular
	Grinding method	[-]	Mechanical griding
	Source	[-]	Trunk and car
	Average diameter	[mm]	<0.6
	Flash point	[°C]	246
	Solubility	[-]	Slight (0.1 – 1.0%)
	Chemical stability	[-]	Stable
	Characteristic	[-]	Chemical additive (polymer)
	Composition	[-]	Crumb rubber (99.1%)
CRT2	Typology	[-]	Powder
	Specific gravity	[g/cm^3]	1.031 ± 0.03
	Colour	[-]	Black/Grey with Brownish color grenules
	Particles morphology	[-]	Irregular
	Grinding method	[-]	Mechanical griding
	Source	[-]	Trunk and car
	Average diameter	[mm]	<0.6
	Flash point	[°C]	>300
	Solubility	[-]	Insoluble in water
	Chemical stability	[-]	Incompatible with strong oxidizing
	Characteristic	[-]	Pre-digested
	Composition	[-]	Natural mineral (<40%) - bitumen (<30%) - crumb rubber (<75%)
CRN	Typology	[-]	Powder and fine granulate
	Specific gravity	[g/cm^3]	1.10 - 1.20
	Colour	[-]	Black
	Particles morphology	[-]	Irregular
	Grinding method	[-]	Mechanical griding
	Source	[-]	Rubber granulate from waste Tyres
	Average diameter	[mm]	<0.6
	Flash point	[°C]	N/A
	Solubility	[-]	Insoluble in water, partially soluble in acetone
	Chemical stability	[-]	Stable under recommended storage conditions
	Characteristic	[-]	normal rubber
	Composition	[-]	Passenger car tyre tread recyclates

Symbols. N.A.: not available.

All three rubbers have the same typology (powder), morphology (irregular), grinding method (mechanical grinding), source (trunk and car rubber), size (average diameter < 0.6mm), but different characteristics:

- CRT2 is a pre-digested rubber. It is composed of plain soft bitumen, fine crumb rubber, and an Activated Mineral Binder Stabilizer (AMBS) at optimized proportions (J. S. Sousa 2015; SILENT RUBBER PAVE 2017). CRT2 is produced by a short- time hot blending and activation in a specially designed process to form a dried granulated activated rubber. It can be added to any type of Hot Mix Asphalt (HMA) – Dense, Open Graded, Gapgraded and, SMA (J. S. Sousa 2015).
- CRT1 is a rubber with a chemical additive. It is a chemically engineered, dry crumb rubber designed for use in asphalt mix production. It can be added like a fine aggregate during mix production. The rubber is designed to improve both the cracking and rutting resistance of asphalt mixes, thus extending pavement life in the most challenging use environments. This product can reduce or eliminate the need for binder modification (with polymers or rubber), it can reduce or eliminate the need for warm mix additives and/or compaction aids, it will reduce or eliminate binder drain-down in SMA and other mix designs, and it can reduce or eliminate the need for various anti-stripping additives. This product permits the creation of a cost-effective asphalt modification process at the asphalt producer's site, and it reduces the life-cycle cost of asphalt pavements in a wide range of environments employing a wide range of mix designs.
- CRN is normal rubber obtained through mechanical grinding at ambient temperatures.

Finally, the filler used in this study consisted of limestone. Its specific gravity is equal to 2.72 g/cm^3.

4.2.3 Experimental design

4.2.3.1 Experimental parameters and objectives

A study of the real-time viscosity was developed. The main parameters of the experimentation are summarized in Table 4.3. Two different bitumen/filler/rubber ratios were considered in this study. These ratios were selected to mimic two common asphalt mixtures, i.e. Stone Mastic Asphalt (SMA) and Porous Asphalt (PA). It should be mentioned that SMA tends to have higher bitumen and filler content in comparison to PA.

The rubber content used in this study is equal to 1% (by weight, referred to the mixture) for both PA and SMA10 mixes. This content corresponds to 16.95% (by bitumen weight) for PA mix and 15.15% (by bitumen weight) for SMA10 mix.

Is important to observe that, when crumb rubber is added like a fine aggregate during mix production, the rubber grains are coated with binder during the mixing process. Moreover, the filler content used was 6% for PA and 10% for SMA 10.

Figure 4.1 shows a graphical diagram of the experimental design adopted in this study. The viscosity measurements of mastic are complex due to the suspension of rigid spheres (filler and rubber) in the matrix which may hinder from obtaining representative measurements using the standard spindle.

Therefore, the effect of using different spindle was investigated in order to obtain representative viscosity measurements for the system.

Table 4.3: Main parameters of experimentation.

Parameter	Type/Quantity
Bitumen type (penetration grade)	50-70
T_{mix} [°C]	180
t_{mix} [min]	300
Filler type	Limestone
Rubber type	CRT1 / CRT2 / CRN
Mix design	PA / SMA 10
PA mix, Porous Asphalt ANAS	
Rubber content [%, by bitumen weight]	16.95
Rubber content [%, by weight referred to total blend, bitumen+rubber]	14.49
B/F/R (ratio bitumen/filler/rubber)	1/0.95/0.17
SMA 10 mix	
Rubber content [%, by bitumen weight]	15.15
Rubber content [%, by weight referred to total blend, bitumen+rubber]	13.16
B/F/R (ratio bitumen/filler/rubber)	1/1.4/0.15
Laboratory tool	Brookfield viscometer with a modified Dual Helical Ribbon (DHR)
Speed of mixing [rpm]	100
Test	Viscosity in real-time
Viscosity readings	every 1 min (for the first 30 min), every 3 min (for the next 30 min) and, every 10 min (for the next 240 min)
Replicates	2 or 3

Symbols. T_{mix}: mixing temperature [°C]; t_{mix}: mixing time [min]; CRT1: CRT1 rubber; CRT2: CRT2 rubber; CRN: CRN rubber; PA: Porous Asphalt; SMA 10: Stone Mastic Asphalt with an upper sieve size of the aggregate of 10 mm; B: bitumen 50-70; F: filler; R: rubber.

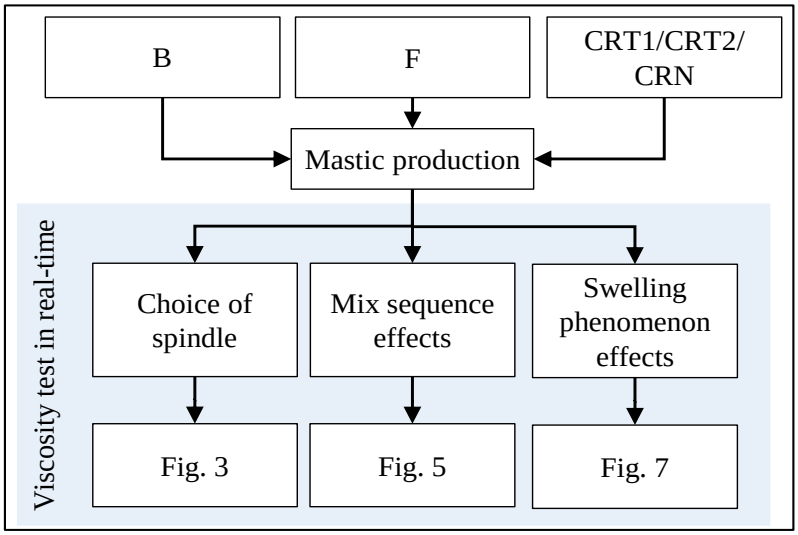

Figure 4.1: Graphical diagram of the experimental design (Astolfi et al., 2019)

Symbols. B: bitumen 50-70; F: filler; CRT1: CRT1 rubber; CRT2: CRT2; CRN: CRN rubber.

4.2.3.2 Apparent viscosity measurements

In the pursuit of the objectives of this study related to the micro-component affinity of mastic, the viscosity in real time test was carried out.

One of the most important aspect to observe is the rubber-bitumen interaction that, at different temperatures, implies an increase in the blend viscosity. The rotational viscosity is one of the physical parameters that can be monitored during the modification process.

Due to the different constituent materials of mastic (bitumen, rubber and filler), the rigid spheres need to be kept uniformly distributed within the blend during the test.

Therefore, a dual helical ribbon (DHR), improving the tool developed in previous studies and applications (D. Lo Presti, Giancontieri, and Hargreaves 2017; A. Subhy, Lo Presti, and Airey 2015), was used to adapt the Brookfield rotational viscometer as low shear mixing device. This allowed obtaining:

i) homogeneous mixing during testing;

ii) an accurate control of the temperature;

iii) a real-time monitoring of the system apparent viscosity and;

iv) a methodology for quality-control of the swelling process of rubberised mastics.

This system offers the opportunity of understanding what is physically occurring during a blending process by monitoring the key parameter, rotational viscosity (D. Lo Presti 2011).

Figure 4.2 shows the tools used to measure the viscosity in real time test. These bespoke impellers have been developed within another research and might be available upon request to the corresponding author.

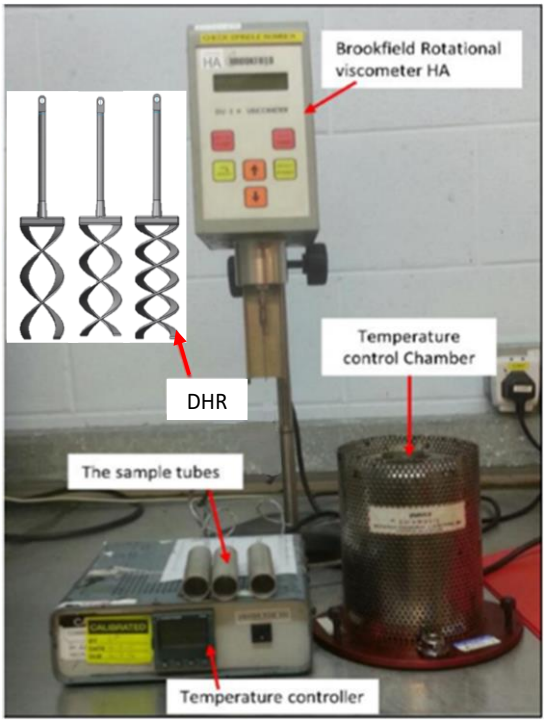

Figure 4.2: Tools used to viscosity in real time test (Astolfi et al., 2019)

Figure 4.3 shows the results of the viscosity over time for a mastic manufactured using bitumen, filler and CRT2 rubber at bitumen/filler/rubber of 1.00/0.95/0.17. All tests have been carried out at the temperature of 180°C.

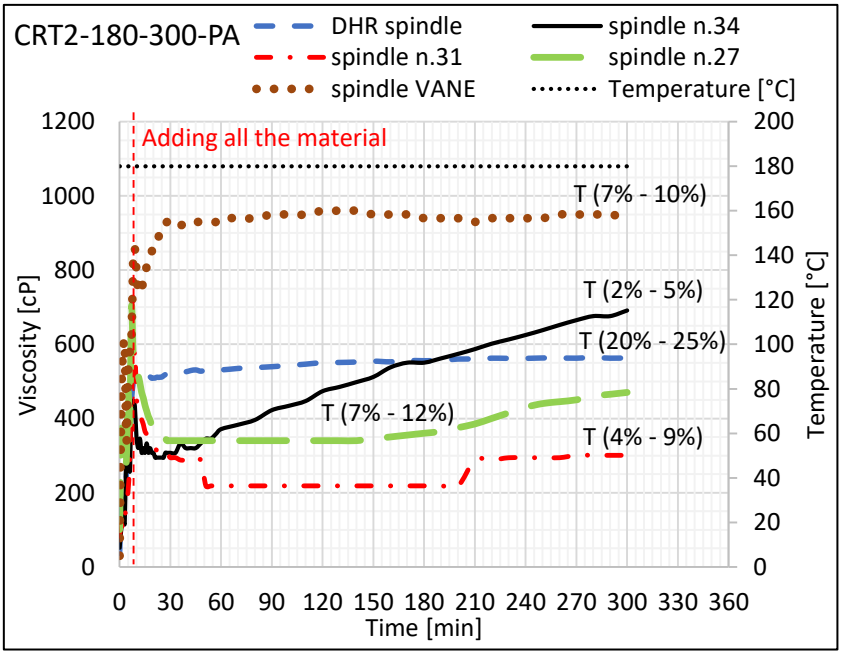

Figure 4.3: Viscosity over time for CRT2-180-300-PA sample using different impeller (Astolfi et al., 2019).

Symbols. T: torque, [%].

It is possible to note that a fundamental role is played by the impeller type used during the test. The standard impellers used for the viscosity test are not suitable for this purpose.

It can be observed that the standard impeller (i.e. spindle n.27) exhibited fluctuating viscosity trends during the test with corresponding values of torque varying between 4% and 12%. The trend of the DHR impeller is more constant than others with measured torque values varies between 20% and 25% while in the case of traditional impeller, the torque and viscosity results are not within the recommended rage of Brookfield.

The DHR impeller has been implemented by researchers of Nottingham Transportation Engineering Centre (NTEC).

This new set of impellers allows obtaining more realistic viscosity measurements of multiphase systems.

The main features of this impellers are: i) strong axial pumping able to enhance mixing capacity of the impeller; ii) suitable for complex systems made of flu-ids also with suspended particles; iii) able to provide stable readings while avoiding particle settling even at low rotational speed; iv) tested with several materials from different fields such as civil engineering, food science, etc.; v) versatile range capability (3-piece spindle set).

The use of untraditional impellers implicates a different way to derive the viscosity values. In fact, in the case of traditional impeller, the torque and viscosity results are output of the Brookfild tool.

For the DHR impeller, instead, the torque is an output of Brookfild tool and the viscosity is obtained from the following equation:

$$\eta = TK \cdot SMC \cdot T \cdot \frac{100}{RPM} \qquad \text{(Eq. 15)}$$

where η is the viscosity [cP], *TK* is the viscometer torque constant (for LV Brookfield is equal to 0.09373; for HA Brookfield is equal to 2), *SMC* is the spindle multiplier constant (for DHR1=12.5, for DHR2=11.5 and, for DHR3=9.5), *T* is the torque [%] and, *RPM* is the rotation speed [rpm].

To analyse the swelling phenomenon, different parameters are evaluated: i) swelling rate (increasing viscosity with time); ii) swelling extent/maturation time (time to reach maximum viscosity); iii) peak viscosity; iv) maximum swelling and; v) final viscosity; vi) viscosity plateau; vii) viscosity plateau time, as defined in (A. Subhy, Lo Presti, and Airey 2015).

The swelling rate is defined by as the rate of viscosity gain with respect to time and determined by taking the arithmetic average of tangents ($\partial v/\partial t$) of the viscosity progression curve from the point of adding all the rubber up to the peak viscosity. The swelling extent (or maturation time) is defined as the time to reach maximum viscosity from the point of adding all the rubber up to the peak viscosity. The peak viscosity is the

maximum value of viscosity measured during the test. The maximum swelling represents the relative increase in viscosity and is calculated using the following equation:

$$s_{\max} = \max swelling = \frac{v_p - v_i}{v_i} \quad \text{(Eq. 16)}$$

where v_p is the peak viscosity, v_i is the initial viscosity corresponding to the time when all the rubber has been added. The viscosity plateau was fixed at the point when viscosity does not increase by more than 3.5% within a 30-minute period and the viscosity plateau time is the corresponding time. Finally, the final viscosity is the value of viscosity measured at the end of test (@300 min).

4.2.3.3 Manufacture of rubberised mastics

Table 4.5 shows the composition of the mastic used in this study. In more details, for each sample, components (bitumen, filler and, rubber, by weight and by volume), type of rubber used, time of mixing and, temperature of mixing are defined. The different samples were labelled in such a way to give information about the processing conditions and materials. For example, the code of “CRT2-180-300-PA" means, CRT2 rubber at processing temperature of 180°C, mixing time of 300 minutes and PA mix. The following protocol was used for each blend:

1. About 200g of bitumen 50/70 (contained in a tin) have been heated at 160°C in an oven for 45 minutes. Then, the fluid test samples have been stirred and transferred into separate Brookfield viscometer tubes (see the correct weight in Table 4.4). The sample tubes have been then placed in a sealed container to protect them against any unwanted oxidation and then left to cool down to room temperature.
2. Each of the sample tubes have been then placed into the preheated temperature control Chamber of the Brookfield viscometer (preheated to the selected mixing temperature, 180°C) and given 15-20 minutes to obtain equilibrium temperature throughout the sample.
3. After that, the preheated DHR (modified dual helical ribbon) has been lowered into the bitumen sample into the tube and the impeller was rotated at a constant speed of 100 rpm. Viscosity has been constantly monitored throughout the mixing time, with starting point being the moment when the impeller starts rotating.
4. The designed filler or rubber quantities were added gradually, depending on the mixing sequence as shown in Figure 4.4, i.e., a&b (bitumen-filler-rubber) or c&d (bitumen-rubber-filler). All the filler has

been fed into the sample viscometer tube within 6 minutes while all the rubber has been fed into the sample viscometer tube within 2 minutes.

5. At least two replicates of each blend have been produced and the average values have been reported.
6. The viscosity readings from the Brookfield viscometer have been recorded every minute for the first 30 minutes, every three minutes for the next 30 minutes and, then every ten minutes for the next 240 minutes.

Figure 4.4 shows the timeline of the mixing for the two mixing sequence used in this study ("a&b" and "c&d"). The viscosity test starts when all the mastic component has been fed into the tube. For all the samples, this moment corresponds to eighth minute from the start of the mixing.

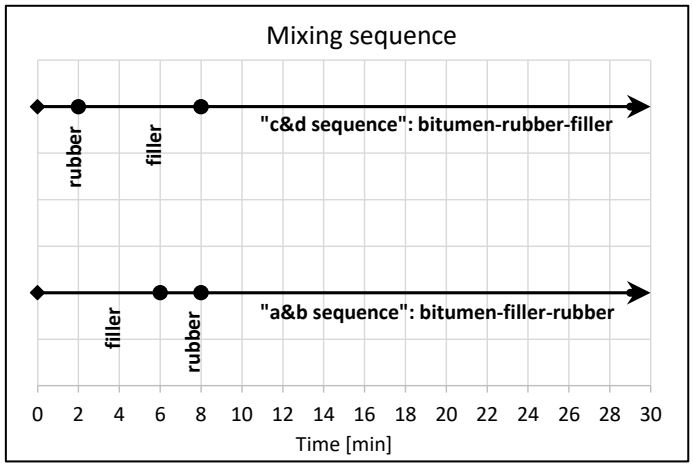

Figure 4.4: Mixing sequence (Astolfi et al., 2019)

Table 4.4: Sample composition of experimentation.

Label	T_{mix} [°C]	t_{mix} [min]	B [g]	Filler [g]	CRT2 [g]	CRT1 [g]	CRN [g]	R/B [%]	R/(B+R) [%]
CRT2-180-300-PA	180	300	8.00	7.84	1.21	-	-	16.95	14.49
CRT1-180-300-PA	180	300	8.00	7.84	-	1.21	-	16.95	14.49
CRN-180-300-PA	180	300	8.00	7.84	-	-	1.21	16.95	14.49
CRT2-180-300-SMA10	180	300	7.20	10.08	1.09	-	-	15.15	13.16
CRT1-180-300-SMA10	180	300	7.20	10.08	-	1.09	-	15.15	13.16
CRN-180-300-SMA10	180	300	7.20	10.08	-	-	1.09	15.15	13.16

Symbols. T_{mix}: mixing temperature [°C]; t_{mix}: mixing time [min]; B: pure bitumen 50/70; CRT2: CRT2 rubber; CRT1: CRT1 rubber; CRN: CRN rubber; R: rubber; R/B: ratio of rubber and bitumen content [%]; R/(B+R): ratio of rubber and total blend, bitumen + rubber; PA: Porous Asphalt; SMA10: Stone Mastic Asphalt with an upper sieve size of the aggregate of 10 mm.

4.3 Results and discussions

4.3.1 Repeatability

Figure 4.5 shows the viscosity variation over time for each sample. Each curve represents the average of two replicates and the respective coefficient of variation is also reported.

The coefficient of variation (CV) is a standardized measure of dispersion of a probability or frequency distribution. For each sample, CV is often lower than 8.0%.

For CRT2 rubber, mixing sequence ("a&b" and "c&d") does not have significant effects on viscosity development.

The variability of the average trend is similar to the variability of the single trend ("a&b" and "c&d"). In the absence of a specific standard related to the viscosity in real time, it is important to understand the quality of the results obtained in this study. For this reason, the coefficient of variation and the viscosity standard test are reported in Table 4.5 and Table 4.6.

Note that the standards in Table 4.5 and Table 4.6 are not referred to the viscosity in real time.

They are reported here only to derive a possible quality level to compare with the results obtained in this study.

The repeatability of viscosity test is different in order to the standard used (EN, AASHTO or ASTM).

In this case, the variability of each test (CV) is lower than AASHTO limit (7.3%). Only in one case (CRN-180-300-PAa&b) the CV obtained (8.0%) is higher than the standard limit.

Table 4.5: Reference values and statistical analysis related to study of mixing sequence.

	Reference	T [%]	Final viscosity @300 min [cP]	Repeatability or CV [%]	Reproducibility
Standard	EN 13302:2010	-	-	5% (*)	15% (*)
	AASHTO T316-04	-	-	7.3%	21.1%
	ASTM D 4402-02	10-98	-	3.5%	14.5%
Test	CRT2-180-300-PAa&b	20-25	564	4.5%	-
	CRT2-180-300-PAc&d	21-24	562	2.0%	-
	CRT1-180-300-PAa&b	15-43	988	4.2%	-
	CRT1-180-300-PAc&d	25-36	826	2.9%	-
	CRN-180-300-PAa&b	40-88	1761	8.0%	-
	CRN-180-300-PAc&d	19-77	2008	2.0%	-

Symbols. T: torque range measured; CV: coefficient of variation; (*): only one case in twenty.

Table 4.6: Reference values and statistical analysis related to study of rubber and mix type.

	Reference	T [%]	Final viscosity @300 min [cP]	Repeatability or CV [%]	Reproducibility
Standard	EN 13302:2010	-	-	5% (*)	15% (*)
	AASHTO T316-04	-	-	7.3%	21.1%
	ASTM D 4402-02	10-98	-	3.5%	14.5%
Test	CRT2-180-300-PA	20-25	563	3.9%	-
	CRT1-180-300-PA	15-43	907	10.7%	-
	CRN-180-300-PA	19-88	1884	7.8%	-
	CRT2-180-300-SMA10	28-30	1460	12.7%	-
	CRT1-180-300-SMA10	23-39	1958	2.4%	-
	CRN-180-300-SMA10	32-83	4168	2.7%	-

Symbols. T: torque range; CV: coefficient of variation; (*): only one case in twenty.

Table 4.7: Swelling process parameters related to study of rubber and mix type.

Samples	Component ratio (B/F/R)	v_i [cP]	v_{Peak} [cP]	t_{Peak} [min]	SR [cP/min]	v_f @300 min [cP]	S_{max} [%]	$v_{Plateau}$ [cP]	$t_{Plateau}$ [min]
CRT2-180-300-PA	1.00/0.95/0.17	500	564	272	0.6	563	12.8	533	49
CRT1-180-300-PA	1.00/0.95/0.17	523	907	292	6.3	907	73.5	812	52
CRN-180-300-PA	1.00/0.95/0.17	759	1888	272	13.3	1884	148.8	1806	142
CRT2-180-300-SMA	1.00/1.40/0.15	1371	1553	8	7.7	1460	691.1	1490	31
CRT1-180-300-SMA	1.00/1.40/0.15	1410	1958	298	12.9	1958	751.1	1880	40
CRN-180-300-SMA	1.00/1.40/0.15	1985	4168	298	31.8	4168	1415.5	3868	132

Symbols. v_i: initial viscosity, [cP]; v_{Peak}: peak viscosity, [cP]; t_{Peak}: peak time, [min]; v_f: final viscosity, value of viscosity @300 min, [cP]; $v_{Plateau}$: viscosity plateau, [cP]; $t_{Plateau}$: viscosity plateau time, [min], SR: swelling rate, [cP/min]; S_{max}: maximum swelling, [%].

The reason could be that the torque measured during the test, has assumed values of about 70-88%.

Figure 4.6 shows the variation of CV (coefficient of variation) and σ (standard deviation) as a function of the measured torque.

For the a&b sequence, note that higher and lower values of torque (T>75% and T<25%) correspond to higher values of σ and CV, then to a greater variability of the results.

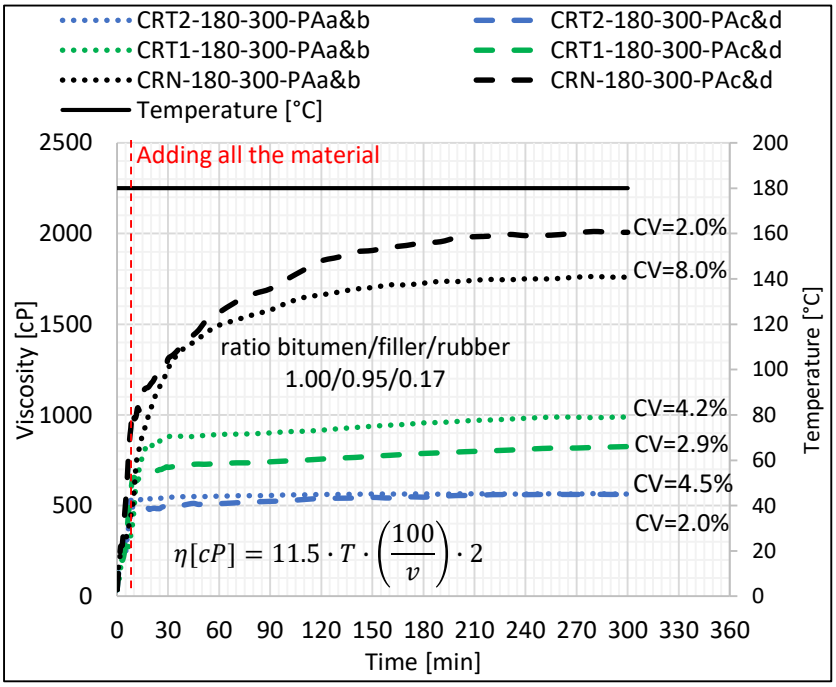

Figure 4.5: Viscosity variation over time and mixing sequence effects (Astolfi et al., 2019)

Symbols. a&b: sample with production sequence bitumen-filler-rubber; c&d: sample with production sequence bitumen-rubber-filler; $CV = \frac{\sum_{i=1}^{N} CV_i}{N} = \frac{\sum_{i=1}^{N}\left(\frac{\sigma_i}{\mu_i}\right)}{N}$*, coefficient of variation; σ: standard deviation; μ: average; i: i-th value; N: number of values; η: viscosity, [cP]; v: speed, [rpm]; T: torque, [%].*

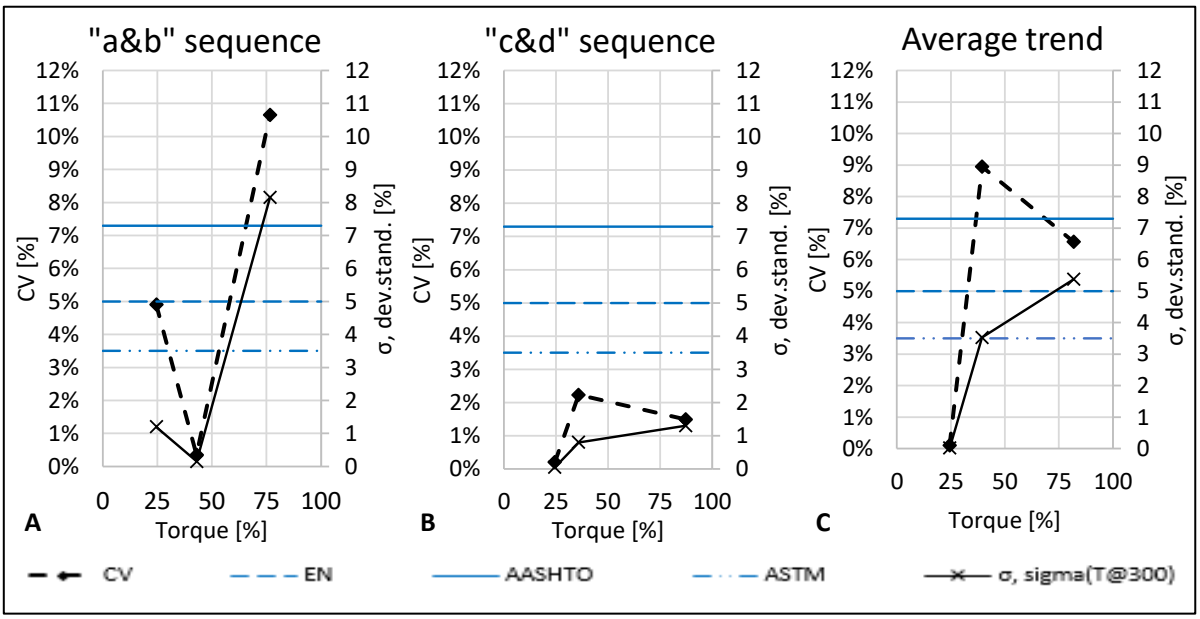

Figure 4.6: CV and σ variation vs. torque (Astolfi et al., 2019)

Symbols. a&b: sample with production sequence bitumen-filler-rubber; c&d: sample with production sequence bitumen-rubber-filler; $CV = \frac{\sum_{i=1}^{N} CV_i}{N} = \frac{\sum_{i=1}^{N}\left(\frac{\sigma_i}{\mu_i}\right)}{N}$*, coefficient of variation; σ: standard deviation; EN: (EN-13302 2003); AASHTO: (AASHTO T316 2013); ASTM: (ASTM-D4402/D4402M 2015).*

4.3.2 Monitoring the swelling process of mastics

Figure 4.7 and Figure 4.8 show the viscosity variation over time for both PA and SMA10 samples with different types of rubber particles. Each curve represents the average of two replicates and the respective coefficient of variation is reported. The main parameters related to the viscosity monitoring are reported in Table 4.7.

The viscosity variation over time is attributed only to the swelling process of the rubber, because the other involved material is the filler. Filler influences the viscosity of mastic but remains constant over time (see "control PA" in Figure 4.7 and "control SMA10" in Figure 4.8).

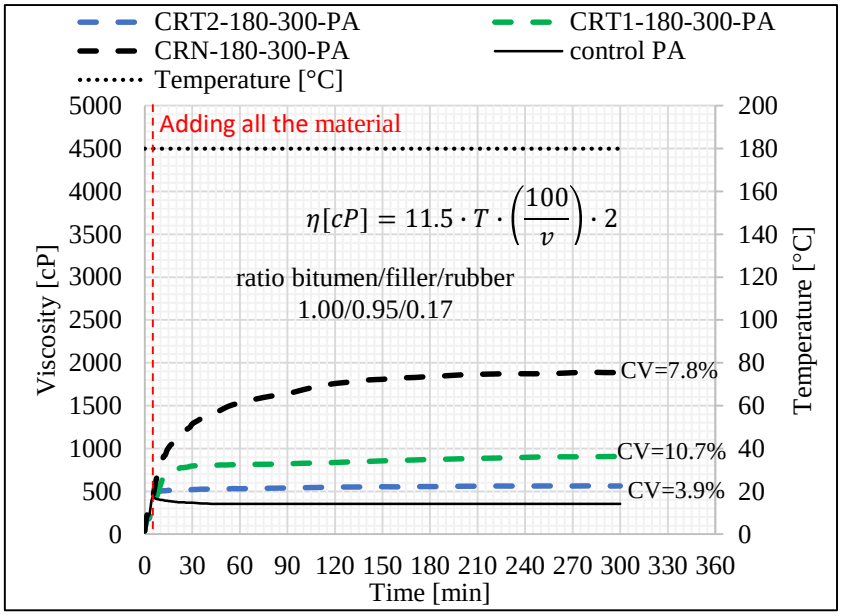

Figure 4.7: Viscosity variation over time – rubber type effects (Porous Asphalt, Astolfi et al., 2019)

Symbols. $CV = \frac{\sum_{i=1}^{N} CV_i}{N} = \frac{\sum_{i=1}^{N}\left(\frac{\sigma_i}{\mu_i}\right)}{N}$*, coefficient of variation; η: viscosity, [cP]; v: speed, [rpm]; T: torque, [%].*

From Figure 4.7 and Table 4.7 that related to PA, it is possible to note the following:

- The CRT2 rubber presents the lowest value of viscosity (563 cP @300 minutes) and, at the same time, a constant trend (SR=0.6 cP/min).
- The CRT1 rubber presents a similar behaviour to CRT2 rubber, but it has a viscosity value (@300 minutes) of 907 cP and a swelling rate (SR) of 6.3 cP/min.
- The CRN rubber, instead, over the 300 minutes, presents an upward trend with a final viscosity (@300 minutes) of 1884 cP and a SR of 13.3 cP/min.

Based on Figure 4.8 and Table 4.7, related to SMA, it is possible to note the following:

- The CRT2 rubber presents the lowest value of viscosity (1460 cP @300 minutes) and a constant trend (SR=7.7 cP/min).
- The CRT1 rubber presents a similar behaviour to CRT2 rubber but, it has a viscosity value (@300 minutes) of 1958 cP and a swelling rate (SR) of 12.9 cP/min.
- The CRN rubber, instead, over the 300 minutes, presents an upward trend with a final viscosity (@300 minutes) of 4168 cP and a SR of 31.8 cP/min.

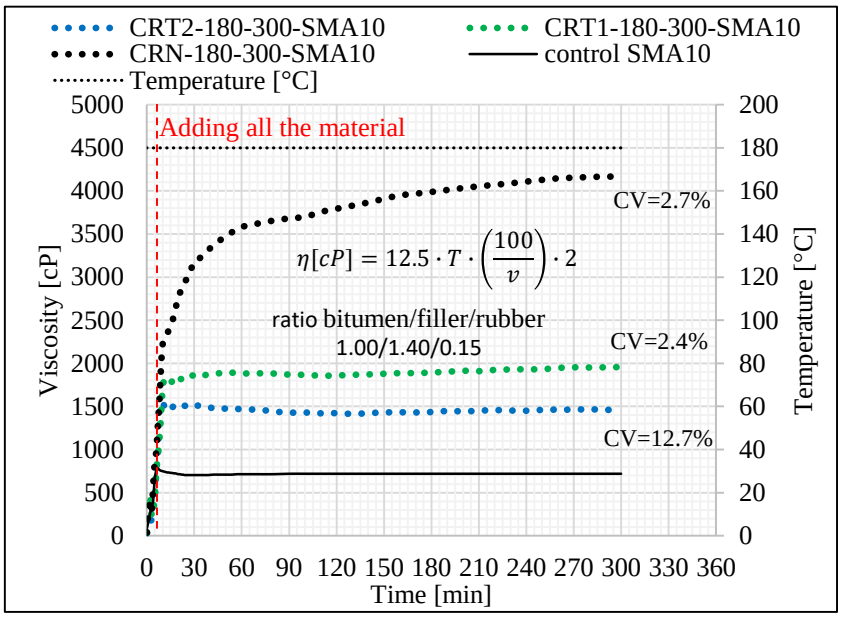

Figure 4.8: Viscosity variation over time – rubber type effects (SMA10, Astolfi et al., 2019)

Symbols. $CV = \frac{\sum_{i=1}^{N} CV_i}{N} = \frac{\sum_{i=1}^{N} \left(\frac{\sigma_i}{\mu_i}\right)}{N}$*, coefficient of variation; η: viscosity, [cP]; v: speed, [rpm]; T: torque, [%].*

A similar trend was observed for SMA samples and PA samples. However, the values of viscosity of SMA samples were higher than the ones of PA.

The higher viscosity is an obvious consequence of the different content of materials (bitumen, rubber and filler). In fact, the SMA mastic contains higher filler than PA mastic, i.e. the ratio of bitumen/filler was 1/1.4 for SMA compared to 1/0.95 for PA.

In terms of viscosity plateau, note that an increase of filler content of 47% (from PA mix to SMA mix) corresponds to an increase of viscosity of 180% for CRT2, 132% for CRT1 and, 114% for CRN.

For both PA and SMA, the lowest viscosity was obtained using CRT2 rubber while the highest viscosity was obtained using CRN rubber, i.e. η(CRT2) < η(CRT1) < η(CRN).

The results also show that the blend with CRT2 rubber has a trend almost constant over time and the effect of swelling process is negligible. In fact, CRT2 rubber presents the lowest viscosity plateau time and the lowest final viscosity.

During the test, the viscosity of the blend varies with rubber type and bitumen-filler-rubber ratios. In more details, when considering the variation between the initial viscosity (@8 minutes) and the final viscosity (@300 minutes), it is possible to note that there is an increase of 12.5% (from 500 cP to 566 cP) for PA mixes with CRT2; an increase of 6.5% (from 1371 cP to 1460 cP) for SMA mixes with CRT2; an increase of 73.5% (from 523 cP to 907 cP) for PA mixes with CRT1; an increase of 38.8% (from 1410 cP to 1958 cP) for SMA mixes with CRT1; an increase of 148.3% (from 759 cP to 1884 cP) for PA mixes with CRN and; an increase of 109.9% (from 1985 cP to 4168 cP) for SMA mixes with CRN.

In summary:

- The CRT2 rubber presents a constant trend over time with the lowest plateau time (49 minutes for PA and 31 minutes for SMA), the lowest viscosity plateau (533 cP for PA and 1490 cP for SMA) and a variation of viscosity, from start to end of the test, of 12.5% for PA and 6.5% for SMA.
- The CRT1 rubber presents an almost constant trend over time with a plateau time of 52 minutes for PA and 40 minutes for SMA, a viscosity plateau of 812cP for PA and 1880 cP for SMA and, a variation of viscosity of 73.5% for PA and 38.8% for SMA.
- The CRN rubber, instead, tends to keep swelling over time with the highest plateau time (142 minutes for PA and 132 minutes for SMA), the highest viscosity plateau (1806 cP for PA and 3868 cP for SMA) and a variation of viscosity, from start to end of the test, of 148.3% for PA and 109.9% for SMA.

4.4 Conclusions

A quality-control procedure for rubberised asphalt mastic produced through the dry process was defined to investigate the interaction between several CRs and bitumen during mixing, hauling and paving operations. For this purpose, mastics of two surface asphalt mixtures have been evaluated (PA and SMA10), together with three different types of CR including ambient and pre-treated particles (CRT1, CRT2 and, CRN).

The main property investigated has been the monitoring of the viscosity over time.

The study was carried out adapting a Brookfield rotational viscometer as a low shear mixer and a new set of impellers developed at the Nottingham Transportation Engineering Centre (NTEC).

In this way, it has been possible to have: i) a homogeneous blend during all test; ii) an accurate control of the temperature; iii) a constantly monitoring the viscosity of the binder and; iv) a control of the modification process.

The main conclusions are the following:

- Quality control of rubberised mastics during mixing, hauling and paving operations is possible via a reliable laboratory-based real-time monitoring of the swelling process by means of apparent viscosity measurements.
- A fundamental role is played by the impeller type used during the viscosity test. Standard impellers are not suitable for this purpose. The DHR impeller allows obtaining more realistic viscosity measurements of multiphase systems.
- Comparing the bitumen-filler-rubber sequence with the bitumen-rubber-filler sequence, does not seem to have significant effects on viscosity property even after 5 hours: 0.20% for CRT2, 16.41% for CRT1 and, 14.04% for CRN.
- The SMA mastics have a similar behaviour of PA mastics, but higher viscosity values. This is due to a higher filler content. In both cases, the lowest viscosity was obtained using CRT2 rubber and the highest viscosity is obtained using CRN rubber, $\eta(CRT2) < \eta(CRT1) < \eta(CRN)$.
- The variation of viscosity over time is linked to the swelling process of the rubber.
- Constant swelling of the ambient CR was recorded over the 5 hours, while the specifically pre-treated rubber particles allows a significant mitigation of the mastic swelling phenomena which in all cases ceased slightly after the mixing operations (below 30 mins).
- CRT2 rubber showed a constant trend over time with the lowest viscosity plateau (533 cP for PA and 1490 cP for SMA10) and the lowest variation of viscosity (12.5% for PA and 6.5% for SMA10).
- CRT1 rubber showed an almost constant trend over time with a viscosity plateau of 812cP for PA and 1880 cP for SMA10 and, a variation of viscosity of 73.5% for PA and 38.8% for SMA10.
- CRN rubber, instead, showed a not constant trend over time with the highest plateau time (142 minutes for PA and 132 minutes for SMA10), the highest viscosity plateau (1806 cP for PA and 3868 cP for SMA10) and the highest variation of viscosity (148.3% for PA and 109.9% for SMA10).

5 CR-added bituminous mixtures - compaction: experiments and analyses

5.1 Introduction

This section deals with the study of compaction effects of dry rubberised asphalt mixture. In more detail, the effects of different laboratory short-term oven aging (STOA) and compaction process on compactability and workability are analysed.

This study has an important role when innovative materials (e.g., rubber), effects of which are time- and temperature dependent, are used (how it has been seen in the preceding section).

Consequently, all mixes have been short-term aged by placing the loose mix in a flat pan in a forced draft oven.

After aging, mixes have been compacted and, at a later time, their compactability and workability have been evaluated.

Finally, this section contains a detailed description of the mix design characteristics and the manufacture of samples.

5.2 Experimental design

In Table 5.1 and Figure 5.1 the main parameters and the plan of the study are summarised.

In this study the compaction of bituminous mixes has been analysed using the Superpave Gyratory Compactor (SGC).

Note that two different compaction procedures were applied: i) “standard procedure” (GC1) and, ii) “interrupted procedure”.

Table 5.1: Main parameters of the study.

Parameter	Type/Quantity
Bitumen type (penetration grade)	50-70
T_{mix} [°C]	180
t_{mix} [s]	210
Mix design	PA / SMA10
Rubber type	CRT2 / CRT1 / CRN
Rubber content [%, by weight referred to total mix]	1
Crumb rubber particles size [mm]	< 0.6
STOA - short-term oven aging	
STOA Time [min]	60 / 240
STOA temperature [°C]	135 / 180
Compaction type	Superpave Gyratory Compaction
N_{ini}	10 *for PA* 8 *for SMA10*
N_{des}	50 *for PA* 100 *for SMA10*
N_{max}	130 *for PA (a, b)* 160 *for SMA10 (c, d, e)*
Compaction process	Standard (GC1) / Interrupted (GC2)
v [rpm]	30
ϕ [°]	1.25 *(a, b)*
T_{GC} [°C]	160±5
d [mm]	100
F [N]	4700
compaction pressure [kPa]	600 *(f)*

Symbols. T_{mix}: mixing temperature [°C]; t_{mix}: mixing time [s]; PA: Porous Asphalt; SMA10: Stone Mastic Asphalt with an upper sieve size of the aggregate of 10 mm; CRT2: CRT2 rubber; CRT1: Asphalt plus rubber; CRN: CRN rubber; STOA: short-term oven aging; N_{max}: maximum number of gyrations; GC1: Gyratory compaction with standard procedure; GC2: Gyratory compaction with interrupted procedure; v: speed of rotation [rpm]; φ: angle of gyration [°]; T_{GC}: gyratory compactor temperature [°C]; d: specimen diameter [mm]; F: force [N]; a: (ANAS 2008); b: (ANAS 2009); c: (AASHTO 2001); d: (Cominsky et al. 1994); e: (EN-12697:10 2017); f: (EN-12697:31 2014).

GC1 is the same procedure indicated by EN-12697:31 (2014), with a rotation speed of 30 rpm.

GC2, instead, is a modified procedure. It was adopted to simulate a slower compaction process that it is supposed to occur in field.

Because of the fact that it was not possible to properly set up the machine in terms of speed rotation during the compaction process, different interruptions were manually imposed to obtain GC2.

In more detail, the compaction was stopped for 60 seconds after each 10 gyrations.

For each mix (PA and SMA10), type of rubber (CRT2, CRT1, CRN and control), process of aging (STOA1, STOA2 and STOA3) and compaction procedure (GC1 and GC2) two samples were manufactured. Each sample had a diameter of 100 mm and a height of 110 mm. After manufacturing, each sample was cut in four parts along the height.

In particular, the first part had a thickness of 5 mm, the second and third part had a thickness of 50 mm and, the last part had a thickness of 5 mm.

Only the second and the third part were used for the study, while the first (top) and the last (bottom) were removed.

This step was necessary to obtain four samples (two for each original samples) for each case investigated and to be undergo a next test.

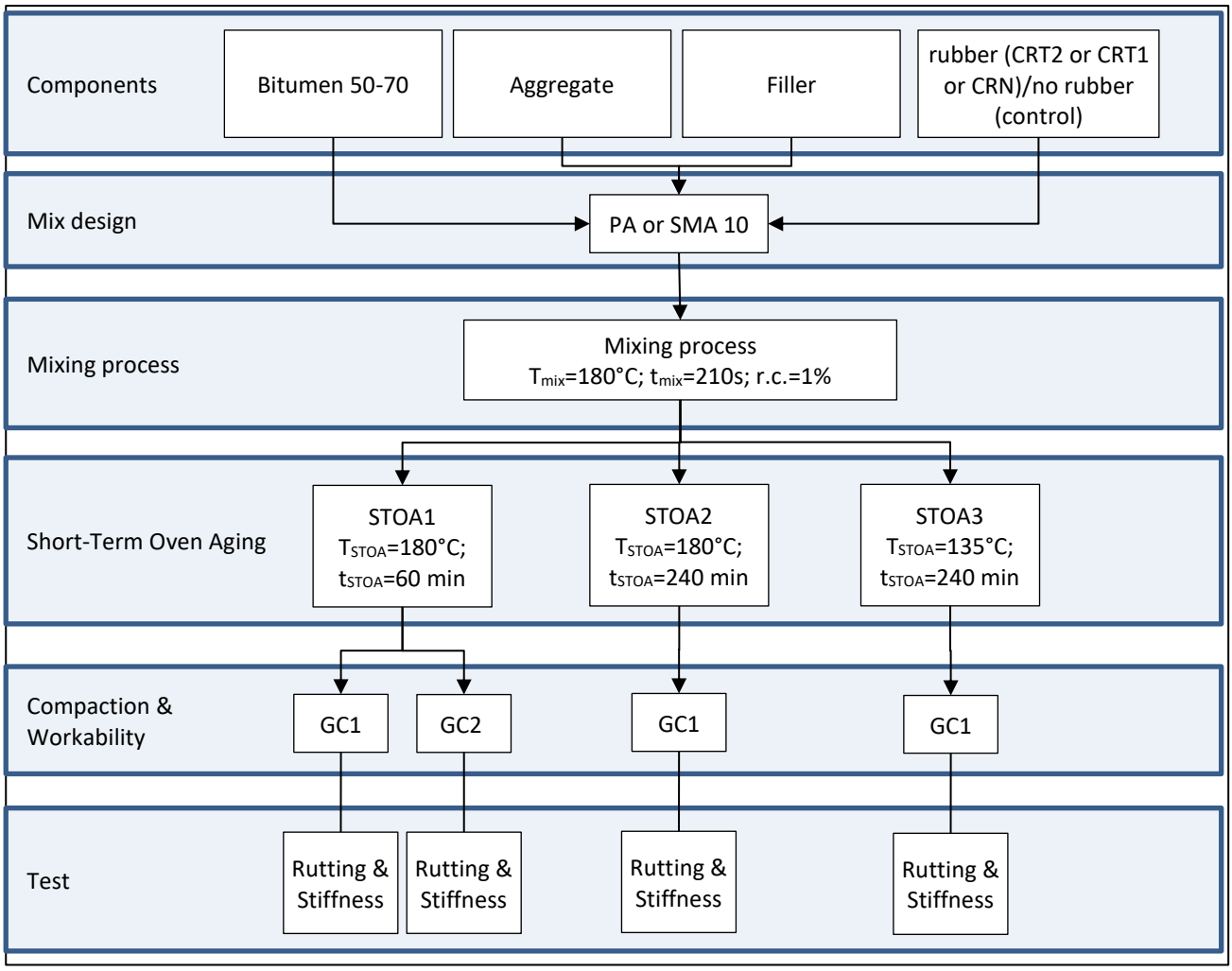

Figure 5.1: Experimental plan.

Symbols. T_{mix}: mixing temperature [°C]; t_{mix}: mixing time [s]; r.c.: rubber content [%, by weight referred to total mix]; PA: Porous Asphalt; SMA10: Stone Mastic Asphalt with an upper sieve size of the aggregate of 10 mm; STOA1: short-time oven aged (@180°C for 60 minutes); STOA2: short-time oven aged (@180°C for 240 minutes); STOA3: short-time oven aged (@135°C for 240 minutes); T_{STOA}: short-time aging temperature [°C]; t_{STOA}: short-time aging time [min]; GC1: Gyratory compaction with standard procedure; GC2: Gyratory compaction with interrupted procedure; CRT2: CRT2 rubber; CRT1: Asphalt plus; CRN: CRN rubber.

Figure 5.2 shows the timeline of the manufacturing of the samples, from mixing to performance-related tests.

The samples production includes the following steps: i) mixing of all materials; ii) ageing loose mix; iii) compacting the mix and; iv) testing the samples.

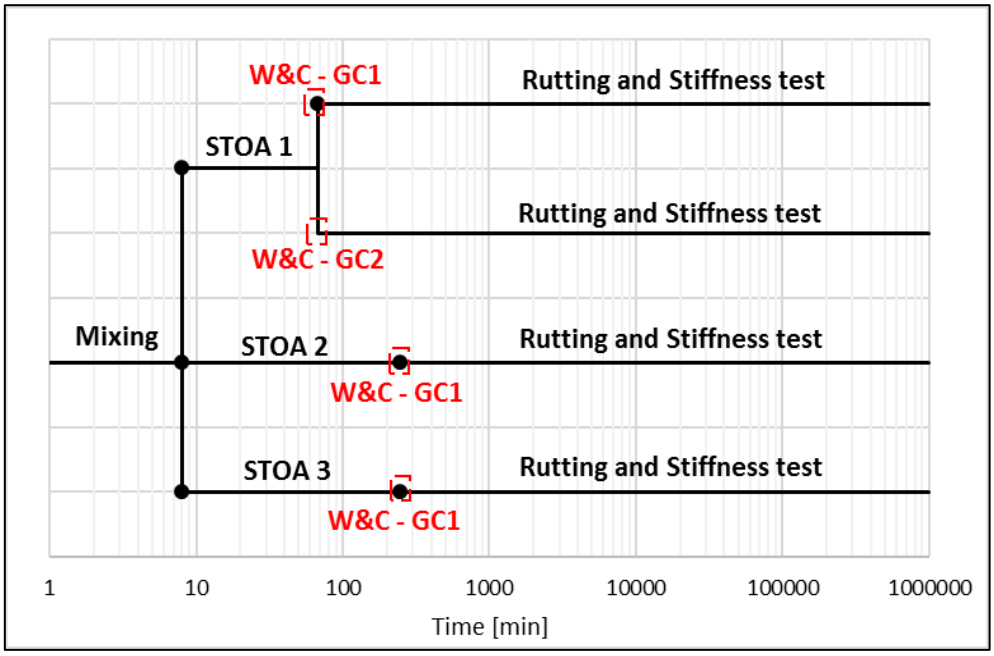

Figure 5.2: Manufacturing and test sequence.

Symbols. Mixing: mixing process; STOA 1: short-time oven aged (@180°C for 60 minutes); STOA 2: short-time oven aged (@180°C for 240 minutes); STOA 3: short-time oven aged (@135°C for 240 minutes); W&C: workability and compaction process; GC1: Gyratory compaction with standard procedure; GC2: Gyratory compaction with interrupted procedure.

In Figure 5.2 the symbols STOA1, STOA2, and STOA3 refers to short-time oven aged process. Instead, W&C refers to workability and compaction process.

These two processes are the main goals of this section. They are described in more detail below.

5.3 Mix design characteristics

As already indicated in the previous section, in this study two different types of mixes were used.

The first one is called PA (Porous Asphalt, ANAS 2008, 2009a); the second one, instead, is called SMA10 (Stone Mastic Asphalt with an upper sieve size of the aggregate of 10 mm, (EN-13108:5 2016). Each mix has the same mineral skeleton and the same rubber content (1% by weight of the mixture), but a different type of rubber (CRT2, CRT1 and, CRN). The rubber content was chosen by the authors based on (CTI project 2017).

The corresponding rubber content, by volume of the mixture, varies in the range 1.66% to 1.85% for PA and in the range 1.99% to 2.22% for SMA10.

The final gradation of each mixture was obtained by combining the individual material gradations.

After that, the blend gradation was compared with the specification requirements for the appropriate sieves.

The coarse and fine aggregate fractions, used in this study, consisted of Granite aggregate obtained from Bardon Hill (UK). On the contrary, the filler used was limestone.

Filler, rubber, and bitumen are the same materials that have been defined previously (Section 3).

The specific gravity of the materials used for the manufacturing of the mixtures is reported in Table 5.2.

Table 5.2: Specific gravity of mixture components.

Component	Type	Specific gravity [g/cm^3]
Coarse aggregate	Granite	2.81
Fine aggregate	Granite	2.82
Filler	Limestone	2.72
	CRT2	1.03
Crumb rubber	CRT1	1.15
	CRN	1.15
Bitumen	50-70	1.05 (*)

Note. (*): test carried out by NTEC - Nottingham Transportation Engineering Centre.

In order to balance binder content and rubber and manage mix voids, additional binder should be added to the mix design, when crumb rubber is used. For this reason, a specific relationship was used to determine the bitumen content. It consists to add an extra bitumen content, 0.4%, for each one percent of rubber added.

According to (Asphalt Plus 2017) this mix adjustment is going to keep mix voids under control and will provide sufficient binder for the crumb rubber.

In Table 5.3 the bitumen percentages as a function of rubber content are reported.

Table 5.3: Rubber and bitumen content of Phase 2

Mix type	Symbol	Reference mixture		CRT2 mixture		CRT1 mixture		CRN mixture	
		Content [%]	R/B [%]	Content [%]	R/B [%]	Content [%]	R/B [%]	Content [%]	R/B [%]
PA	R [%]	0.0 (a)	0	1.0	10	1.0	17	1.0	17
	B [%]	5.5 (a)		5.9		5.9		5.9	
SMA10	R [%]	0.0 (b)	0	1.0	9	1.0	15	1.0	15
	B [%]	6.2 (b)		6.6		6.6		6.6	

Symbols. PA: Porous Asphalt, ANAS; SMA10: Stone Mastic Asphalt with an upper sieve size of the aggregate of 10 mm; R: rubber content [%]; B: bitumen content (by total mix) [%]; CRT2: CRT2 rubber; CRT1: CRT1 rubber; CRN: CRN rubber; R/B: rubber-bitumen ratio; a: (ANAS 2008, 2009); b: (EN-13108:5 2016).

Note that, for CRT2-mixes, the same quantity of additive was added (17% or 15%). Anyhow, the rubber-to-bitumen ratio, R/B, is 10%, which is lower than the one obtained for the remaining rubberised mixes (CRT1-mixes and CRN-mixes).

This is due to the fact that CRT2 is composed by rubber (60%), bitumen and a third component similar to a filler (see Section 3).

Consequently, in relation to the quantity of each component, the real R/B ratio is 10% for PA and 9% for SMA10.

5.3.1 Porous Asphalt (PA)

In Table 5.4, the main characteristics of PA (Porous Asphalt, ANAS 2008, 2009a) are reported.

Table 5.4: Porous Asphalt characteristics

Characteristic	Limits of standard (a)		Theoretical reference mix	Real reference mix
	LL	UL		
Grading				
sieve 20 mm (passing, %)	100	100	100.0	**100.0**
sieve 14 mm (passing, %)	90	100	95.0	**90.7**
sieve 8 mm (passing, %)	12	35	23.5	**29.0**
sieve 4 mm (passing, %)	7	18	12.5	**11.9**
sieve 2 mm (passing, %)	6	12	9.0	**9.2**
sieve 0.5 mm (passing, %)	5	11	8.0	**7.2**
sieve 0.25 mm (passing, %)	5	10	7.5	**6.8**
sieve 0.063 mm (passing, %)	4	8	6.0	**6.2**
Bitumen type (penetration range)	modify bitumen (hard)		50-70	**50-70**
B [%]	4.8	5.8	5.5	**5.9**
R [%]	-	-	-	**1.0 (*)**
AV [%]	16	27	22.0	**22.0**

Symbols. LL: lower limit; UL: upper limit; Tol: tolerance; R: rubber content [%, by weight referred to total mix]; B: bitumen content (by total mix) [%]; AV: air voids content [%]; a: (ANAS 2008, 2009); (*): it corresponds to 1.85% (by volume) when CRT2 is used and 1.66% (by volume) when CRT1 or CRN is used.

In Figure 5.3 the PA gradation curve, used in this study, is reported. In particular, it is possible to distinguish:

- Upper- and lower limit curve (blue lines, ANAS 2008, 2009a).
- Tolerances (black points, ANAS 2008, 2009a).
- Theoretical reference curve (black line, selected by author).
- Combined aggregate curve (red line).

Theoretical reference curve has been obtained considering the middle values of standard limits. Instead, combined gradation curve has been obtained by mathematical combination of the individual materials gradation.

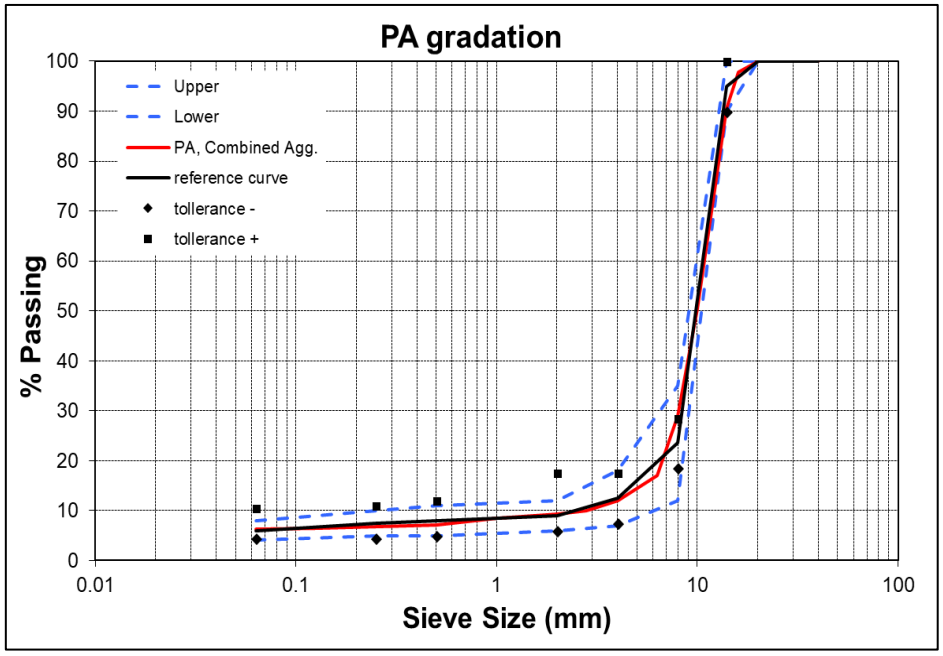

Figure 5.3: PA gradations according to (ANAS 2008, 2009)**.**

5.3.2 Stone Mastic Asphalt (SMA10)

In Table 5.5, the main characteristics of SMA10 (Stone Mastic Asphalt with an upper sieve size of the aggregate of 10 mm, (EN-13108:5 2016) are reported.

Table 5.5: Stone Mastic Asphalt (SMA10) characteristics.

Characteristic	Limits of standard (a)		Theoretical reference mix	Real reference mix
	LL	UL		
Grading				
sieve 20 mm (passing, %)	100	100	100.0	**100.0**
sieve 14 mm (passing, %)	100	100	100.0	**98.8**
sieve 10 mm (passing, %)	90	100	93.0	**92.4**
sieve 2 mm (passing, %)	15	35	24.0	**29.1**
sieve 0.063 mm (passing, %)	5	13	10.0	**11.3**
Bitumen type (penetration range)	-	-	50-70	**50-70**
B [%]	4.6	7.6	6.2	**6.6**
R [%]	-	-	-	**1.0 (*)**
AV [%]	1.5	5	4.0	**4.0**

Symbols. LL: lower limit; UL: upper limit; Tol: tolerance; R: rubber content [%, by weight referred to total mix]; B: bitumen content (by total mix) [%]; AV: air voids content [%]; a: (EN-13108:5 2016); (*): it corresponds to 2.22% (by volume) when CRT2 is used and 1.99% (by volume) when CRT1 or CRN is used.

In Figure 5.4 the SMA10 gradation curve, used in this study, is reported. In particular, it is possible to distinguish:

- Upper- and lower limit curve (blue lines, EN-13108:5 2016).
- Theoretical reference curve (black line, selected by author).
- Combined aggregate curve (red line).

Theoretical reference curve has been obtained considering the middle values of standard limits. Instead, combined gradation curve has been obtained by mathematical combination of the individual materials gradation.

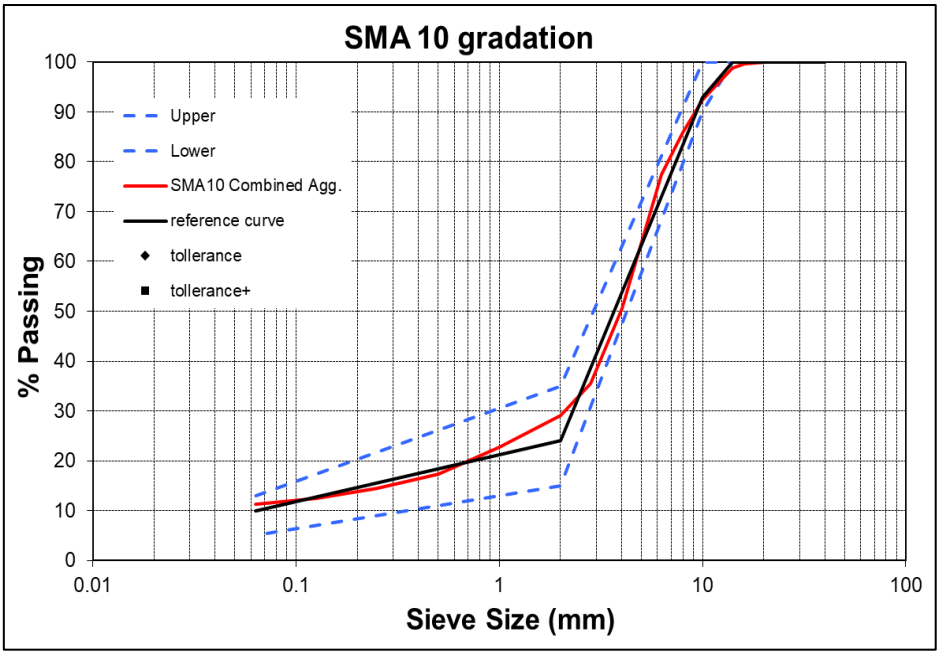

Figure 5.4: SMA10 gradations according to EN-13108:5 (2016).

5.3.3 Samples manufacturing

In this paragraph the samples manufacturing was analysed.

The logic behind was to define an in-lab procedure to simulate, in the best way, the real field procedure.

For this reason, the following protocol has been developed for samples manufacturing:

1. Pre-heat virgin aggregates and bitumen. To distribute heat uniformly, the aggregate was pre-heated at least 8 hours at 180°C (Figure 5.5-A) while the bitumen 3 hours at 170°C (Figure 5.5-B).
2. Insert the aggregates (@ 180°C) in the mixer (Figure 5.5-C).
3. Insert the filler (@ 180°C) in the mixer (Figure 5.5-C).

4. Insert the rubber (@ room temperature) in the mixer (Figure 5.5-C).
5. Mix aggregate, filler and, rubber for 90 seconds using a mechanical mixer (white mixing, @ 180°C, Figure 5.5-D).
6. Insert the bitumen (@ 170°C) in the mixer (Figure 5.5-E).
7. Mix aggregate, filler, rubber and, bitumen for 120 seconds using a mechanical mixer (black mixing, @ 180°C, Figure 5.5-F).
8. Put the loose mix in a flat pan and insert it in the oven (STOA1 or STOA2 or STOA3, Figure 5.5-G).
9. After STOA process, compact the mix with Superpave gyratory compactor (GC1 or GC2, Figure 5.5-H). Allow the samples to cool and extrude it (after extrusion, the bituminous mixture is ready for use in a test procedure as required, Figure 5.5-I).

Often, after the mix step, the loose mix must be transported from the plant to the field.
Generally, this step (that can be called "transport") is very difficult to control because it depends on different factors:

- characteristics of the plant (if the plant has a high hourly production, the mix is temporary stored in silos before to the transport);
- distance between plant and site;
- type of truck used (e.g., traditional truck, trucks equipped with tarps needed to keep the material from cooling, etc.);
- temperature of air (it depends of the geographic area).

This step plays a very important role when innovative materials (e.g., rubber), which are time- and temperature dependent, are used.
For this reason, after mixing, all specimens have been short-term aged by placing the loose mix in a flat pan in a forced draft oven.
Three different short-time oven aged (STOA) have been used: i) STOA1 (@180°C for 60 minute); ii) STOA2 (@180°C for 240 minutes) and; iii) STOA 3 (@135°C for 240 minutes, AASTHO R 30).
At the end of the short-term aged, the mixes followed different compaction processes:

- standard procedure (GC1);
- interrupted procedure (GC2).

Figure 5.5: Steps of samples manufacturing.

Before to compaction, the loose mix have been brought within the compaction temperature range 150°C to 170°C and, finally, compacted.

After the compaction process, all samples have been cut to obtain samples with a diameter of 100 mm and a height of 50 mm.

The different samples were labelled in such a way to give information about the processing conditions and materials. The logic is the following: rubber type-STOA type-gyratory compaction type-mix type.

For example, the code of “CRT2-STOA1-GC1-PA" means, hot mix asphalt with CRT2 rubber at STOA type 1 (temperature of 180°C for 60 minutes), gyratory compaction type 1 (standard procedure) and PA mix.

5.3.4 Laboratory compaction (Superpave Gyratory Compactor)

One of the most important aspect of the Superpave mix design method is the use of the gyratory compactor to simulate field compaction.

The Superpave gyratory compactor was developed to improve the ability to compact samples and to simulate actual filed particle orientation (Roberts, Kandhal, et al. 1996).

It is an effective tool to ensure that engineering properties of laboratory compacted specimens are equivalent to those of the in-place paving mix (Cominsky et al. 1994).

A different opinion, instead, has been formulated by (Zaumanis, Poulikakos, and Partl 2018) which, in his studies, affirmed that gyratory compactor is a poor measure of workability because it is not sensitive to temperature, a factor that highly influences workability in field (Anderson R.M., Turner P.A., Peterson R.L. 2002; Hurley and Prowell 2005).

In addition, the lateral confinement does not replicate the semi-infinite field situation during compaction.

However, the gyratory compactor is capable of central laboratory and field control operations and permits real-time determination of specific gravity and air voids content during compaction (Cominsky et al. 1994).

For this reasons, the gyratory compactor has been used in this study (EN-12697:31 2014; ASTM-D6925 2015; AASHTO-T312 2015; Tex-241-F 2015).

During the compaction process, the height of the specimen is continually monitored. In this way, knowing the initial weight of the mix, the volume of the mould, and the measured height, the density can be continually monitored.

Figure 5.6 shows the schema of Superpave Gyratory Compactor.

The gyratory compactor produces cylindrical specimens through a combination of vertical consolidation pressure and gyratory kneading effort (Cominsky et al. 1994).

The Superpave gyratory compactor establishes three compaction parameters (Pavement-Interactive 2018; Douries 2004):

- N_{ini} – Number of gyrations used as a measure of mixture compactability during construction. It is a small number of gyrations that simulates mixture behaviour during breakdown rolling.
- N_{desing} – This is the design number of gyrations required to produce a sample with the same density as that expected in the field **after the indicated amount of traffic at the end of a 20-year design life** (Khosla and Ayyala 2013; Speight 2016).
- N_{max} – The number of gyrations required to produce a laboratory density that should never be exceeded in the field. If the air voids at N_{max} are too low, then the field mixture may compact too much under traffic resulting in excessively low air voids and potential rutting. It is a large number of gyrations that simulates mixture behaviour in an extreme stress situation.

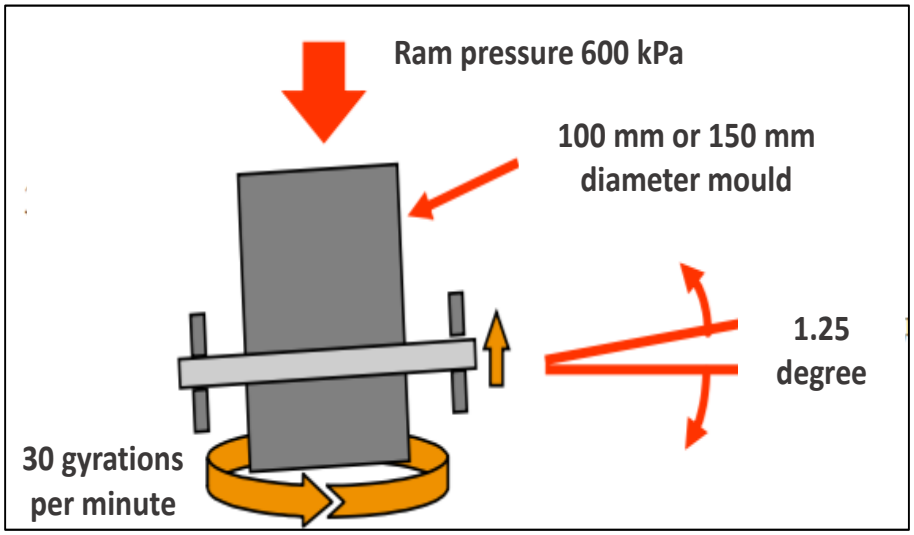

Figure 5.6: Superpave Gyratory Compactor schema.

Typically, samples are compacted to N_{design} to establish the optimum asphalt binder content. The additional samples, instead, are compacted to N_{max} as a check.

Usually, the N_{design} is determined from the traffic level expected on the pavement and the design 7-day maximum air temperature for the pavement site.

In this study, to determine the number of gyrations, two different approaches were used.

For PA mixes, the number of gyrations has been determined using the "Capitolato ANAS" (ANAS 2008, 2009). In this case, it is a function of mix type and bitumen type.

For SMA10 mixes, instead, the number of gyrations has been determined using:

- "Superpave Mix Design Manual for New Construction and Overlays" (Cominsky et al. 1994);
- "AASHTO Provisional Standards" (AASHTO 2001).

In this case, the traffic level on the pavement and the design 7-day maximum air temperature for the pavement site had been supposed.

In Table 5.6 the corresponding numbers of gyrations are reported.

Table 5.6: Number of gyrations of mixes design.

Mix	N_{ini}	N_{des}	N_{max}	Reference
PA	10	50	130	(ANAS 2008, 2009)
SMA10	8	100	160	(AASHTO 2001)

Symbols. PA: Porous Asphalt, ANAS; SMA10: Stone Mastic Asphalt with an upper sieve size of the aggregate of 10 mm; N_{ini}: initial number of gyrations; N_{des}: design number of gyrations; N_{max}: maximum number of gyrations.

Each specimen has been compacted to the maximum number of gyrations, with data collected during the compaction process, as indicated by (ANAS 2008, 2009) and Cominsky et al. (1994).

5.4 Short-time oven aged (STOA)

During the construction process of a road pavement, one of the most important aspect is to control the changes in the mixture properties in the lab.
One way is to condition the laboratory mixtures in such a way as to simulate the aging that happens during construction.
The aging phenomena is extremely complex because of numerous factors influencing the rate of aging (Abdullah et al. 2013) and represents one of the most important characteristics of asphalt materials.
STOA (short-term oven aging) is designed to simulate the aging of mixes during the production stage of HMA (from the end of mixing, in the plant, until the laydown and compaction phases, in the field).
During these steps loss of volatile fractions such as oils in the asphalt binders play a significant role in oxidizing the binders (Kumbargeria and Biligiri 2016; Petersen 2009).
The result of asphalt aging is the hardening of asphalt binders and the increasing of the viscosity, both in application and service phases (Lesueur 2009; Kumbargeria and Biligiri 2016).
This process contributes significantly to the deterioration of paving surfaces (Bell et al. 1994).
Infact, the main effects of age hardening are (Vallerga 1981):

- load-bearing capacity and permanent deformation resistance may increase due to the pavement becoming stiffer;
- it can result in the formation of cracks in the pavement due to reduced pavement flexibility.

The recommended laboratory procedure for STOA is to put the loose mix in a tray (immediately after mixing) to a uniform depth and to heat it in a forced draft oven for 4 hours at a temperature of 135 °C (Kliewer, Bell, and Sosnovske 1995; Soon Jae Lee, Amirkhanian, and Kim 2009; Cominsky et al. 1994).
After that, the mix is brought to the appropriate compaction temperature and the specimen compacted (Cominsky et al. 1994).
The short-term conditioning for the mixture mechanical property testing procedure applies to laboratory-prepared, loose mix only (AASHTO-R30 2002).
In addition to the standard procedure (AASHTO-R30 2002, here called STOA3) other two aging process were set up (STOA 1 and STOA2).
All aging conditions used in this study are listed above (STOA1, STOA2 and STOA3).

5.5 Compactability and Workability

The compactability of a bituminous mix consists in the relationship between its density or void content and the compaction energy applied to it (EN-12697:10 2017). It represents the ability of an asphalt mixture to be compacted. Then, the results of compactability test serve to supplement the results of mixture design.

There are three test methods that can be used to characterize the compactability (EN-12697:10 2017): i) impact (Marshall) compactor; ii) gyratory compactor; iii) vibratory compactor.

In this study, as mentioned before, the gyratory compactor was used. Consequently, the compaction energy is characterized by the number of gyrations.

In Table 5.7, the main laboratory parameters to evaluate the compactability of the mixes are reported.

In Figure 5.7 and Figure 5.8 the indicators above are explained.

Figure 5.7 shows: i) the number of gyrations corresponding to 92% of Gmm; ii) the percentage of the maximum theoretical specific gravity at the initial number of gyrations and; iii) the compaction energy index (CEI).

In Figure 5.8, instead, it is possible to note the representation of: i) locking point; ii) compaction densification index (CDI) and; iii) traffic densification index (TDI).

In light of this, is important to understand how the parameters above can provide information on the ease or difficulty to compact a mixture.

The number of gyrations corresponding to 92% of G_{mm} (N@92%G_{mm}) is one of the easier parameters to use to assess the compactability of a HMA. Higher values of N@92%G_{mm} are associated to mixes that need more compaction energy.

The %G_{mm}@N_{ini} parameter (percentage of the maximum theoretical specific gravity at the initial number of gyrations) is suggest by Superpave mix procedure. Mixtures that compact too quickly (the air voids at N_{ini} are too low) may be tender during construction and unstable when they are subjected to traffic (Leiva and West 2008; Roberts, Kandhal, et al. 1996).

The compaction energy index represents the work applied by the roller to compact the mixture to the required density during construction. Then, mixtures with lower values of CEI are easier to compact (Bahia et al. 1998).

The compaction densification index (CDI) is a parameter related to compactability of asphalt mixtures, instead, the traffic densification index (TDI) is a parameter related to the mixture's stability under traffic loading.

According to Al-shamsi and Louary (2006), higher values of CDI are associated with mixtures that are difficult to compact and higher values of TDI are supposed to be indicative of better mixtures stability.

Table 5.7: Main parameters to evaluate the compactability.

Parameter	Definition	Impact
$N@92\%G_{mm}$	Number of gyrations corresponding to 92% of G_{mm} (Leiva and West 2008).	Higher values are associated to mixes that need more compaction energy.
$\%G_{mm}@N_{ini}$	Percentage of the maximum theoretical specific gravity at the initial number of gyrations (Leiva and West 2008).	Mixtures with N_{ini} too low may be tender during construction and unstable when they are subjected to traffic.
CEI (Compaction Energy Index)	The area beneath the compaction curve from the eighth gyration to 92% of Gmm (Bahia et al. 1998).	Lower values of CEI correspond to mixtures easier to compact.
CDI (Compaction Densification Index)	The area under the SGC densification curve from N=1 to the locking point (Al-shamsi and Louary 2006).	Higher values of CDI are associated with mixtures that are difficult to compact.
TDI (Traffic Densification Index)	The area under SGC densification curve from the SGC locking point to at 90% Gmm or the end of compaction, whichever comes first (Al-shamsi and Louary 2006).	Higher values of TDI are supposed to be indicative of better mixtures stability.
Compaction slope	The slope of the best-fit line between the percentage of the maximum theoretical density and log N (Leiva and West 2008).	Higher values of are associated to mixtures with higher shear stiffness and lower permanent shear strain.
Locking point	Number of gyrations after which the rate of change in height is equal to or less than 0.05mm for three consecutive rotations (Al-shamsi and Louary 2006).	Higher locking point corresponds to higher compaction energy.
Gyratory ratio	Ratio of the number of gyrations required to achieve 2 percent voids and 5 percent voids (Al-shamsi and Louary 2006; Mallick 1999).	Mixes with a gyratory ratio less than 4 may be considered unstable.

With regard to compaction slopes, higher values of this index are associated to mixtures with higher shear stiffness and lower permanent shear strain (Vavrik and Carpenter 1998).

The locking point data provide information about the energy needed to compact a mixture. Higher compaction energy is equal to higher locking point (Al-shamsi and Louary 2006).

Is important to note that, generally, locking points are lower than the design number of gyrations recommended by the Superpave system.

Gyratory ratio is suitable for characterizing HMA. A gyratory ratio of 4 can be used to differentiate between stable and unstable mixes and, further, mixes with a gyratory ratio less than 4 may be considered unstable (Al-shamsi and Louary 2006; Mallick 1999).

Workability is used to describe the ease with which asphalt can be mixed, placed, worked by hand and compacted (Gudimettla, Cooley, and Brown 2003).

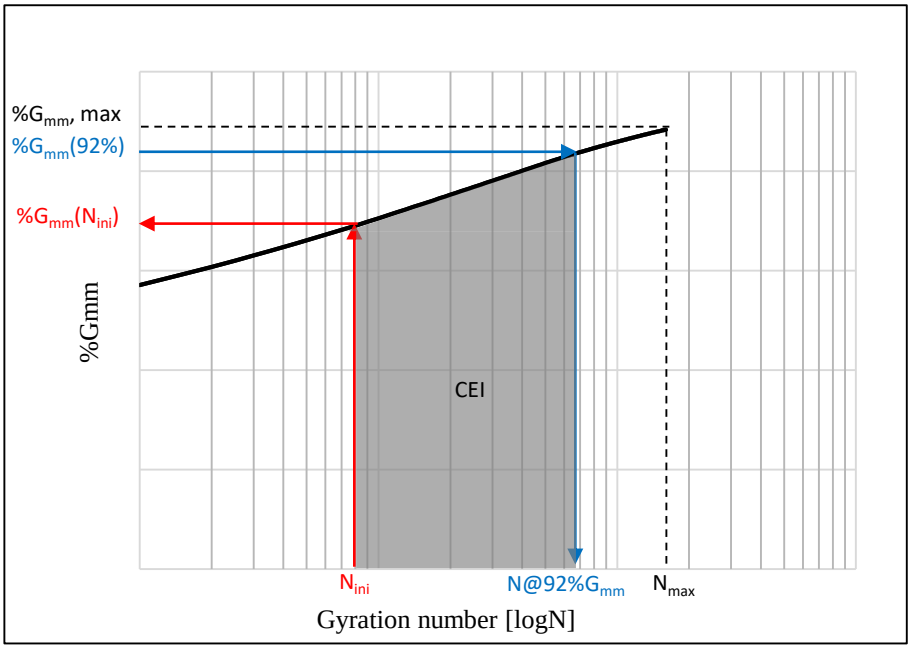

Figure 5.7: Representation of compaction parameters (N@92%G_{mm}; %G_{mm}@N_{ini} and; CEI).

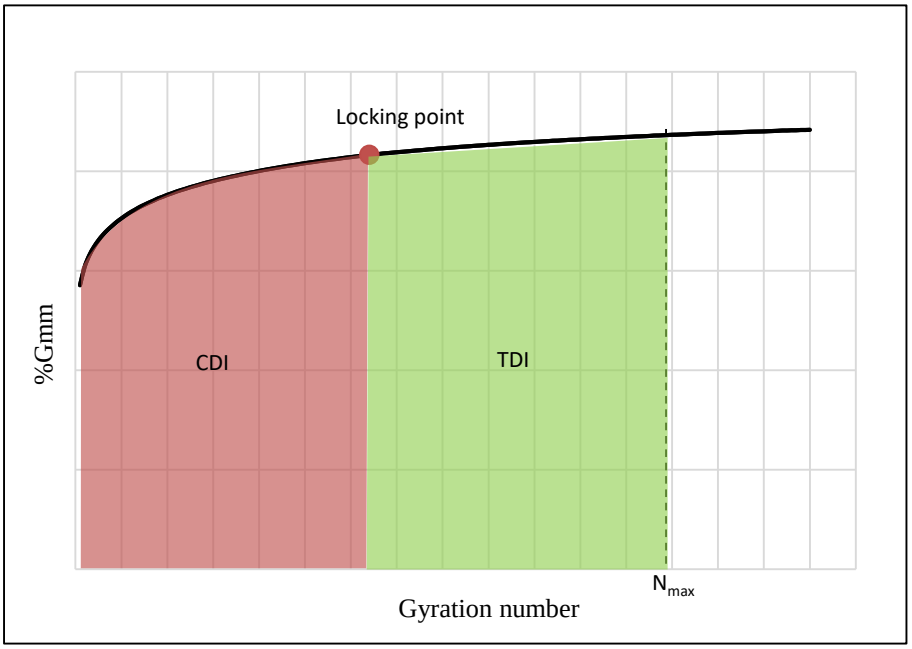

Figure 5.8: Representation of compaction parameters (locking point; CDI and; TDI).

Workability is related to the final air voids content in the compacted mixture, as less workable mixtures will be densified to a lesser degree by application of constant compaction effort (Zaumanis, Poulikakos, and Partl 2018). It depends on different factors, including bitumen type, bitumen content, aggregate properties, modifiers, and temperature of the mixtures (Marvillet and Bougalt 1979).

It is important to note that no laboratory test method has been widely recognized for characterization of workability (Zaumanis, Poulikakos, and Partl 2018).

Based on the literature, the workability is derived by the same parameters needed for the compactability assessment (Leiva and West 2008; Bahia et al. 1998).

However, some criticisms were expressed by (Anderson R.M., Turner P.A., Peterson R.L. 2002) and (Hurley and Prowell 2005). They consider the gyratory compactor a poor measure of workability because it is not sensitive to temperature, a factor that highly influences workability in field.

Furthermore, methods and instruments to measure the workability of HMA are also available in literature. They are developed case by case (Marvillet and Bougalt 1979).

A fundamental role is attributed to binder viscosity. Infact, to determine the compaction and mixing temperatures the binder viscosity charts are used. The workability of HMA decreases when modified binders are used. This is due to the fact that the modifiers tend to increase the viscosity of binders.

The consequence is that the compaction can be more difficult with modified binders than unmodified binders. Therefore, if the properties of a mix are kept constant, the workability of HMA is basically a function of binder properties at a given temperature (Gudimettla, Cooley, and Brown 2003).

In addition to the air void content, the slope of the densification curve is a parameter that represents the workability of the mix. Higher value of slope corresponds to mixes that are more workable (Wellner et al. 2015).

5.6 Results

To define the effects of different laboratory short-term oven aging (STOA) on compactability and workability, the following parameters have been analysed:

- Densification curves
- Air void content (AV)
- Locking point
- $\%G_{mm}@N_{ini}$
- $N@92\%G_{mm}$
- Compaction Slope

The locking point of the mix and the slope are strongly correlated and as these parameters increase the compactability of the mixture decrease. Mixes with higher values of slope and locking point are difficult to compact in the lab (Leiva-Villacorta 2007).

Compaction slope and number of gyrations to reach the locking point of the mixture are related to resistance to permanent deformation.

5.6.1 Densification curves

The compaction curve (or densification curve) was recorded during the compaction process for each specimen. It was obtained by the number of gyrations and the height of specimen.
The continually monitoring of the specimen height has allowed to derive the percentage of theoretical maximum specific gravity (%G_{mm}).
The densification curves, as a function of %G_{mm} and number of gyrations, had been reported in ANNEX 1.

5.6.2 Air void content (AV)

Percent air voids were calculated using G_{mm} (theoretical maximum specific gravity of the mixes) and G_{mb} (bulk specific gravity of the mixture) based on the following equation:

$$AV(\%) = \frac{G_{mm} - G_{mb}}{G_{mm}} \cdot 100 = \left(1 - \frac{G_{mb}}{G_{mm}}\right) \cdot 100 \qquad \text{(Eq. 17)}$$

The theoretical maximum specific gravity of the mixes (G_{mm}) was determined through the following equation at the design stage:

$$G_{mm} = \frac{100}{\sum_i \frac{P_i}{G_i}} \qquad \text{(Eq. 18)}$$

where P_i is the percentage in mix of each component (e.g., filler; the sum of P_i is 100) and G_i is the density of each component (e.g., rubber). Bulk specific gravity (G_{mb}) was calculated considering the weight (W) and the volume (V) of each sample after the cut stage (see Eq. 5).

$$G_{mb} = \frac{W}{V} \qquad \text{(Eq. 19)}$$

Equation 19 refers to a dimensional G_{mb}. *W* was derived by sample weighing and; *V* was estimated by determining diameter and specimen thickness (EN-12697:29 2002).

For air voids analysis, Table 5.8 summarises the following parameters:

- Theoretical maximum specific gravity of each mix design.
- Air voids content of each case investigated.
- Air void variation related to:
  - Interrupted compaction effect: air void variations between STOA1-GC1 and STOA1-GC2.
  - Aging time effect: air void variations between STOA1-GC1 and STOA2-GC1.
  - Aging temperature effect: air void variations between STOA3-GC1 and STOA2-GC1.

Table 5.8: Air void content

	G_{mm} [Kg/m³]	AV				ΔAV		
		STOA1-GC1	STOA1-GC2	STOA2-GC1	STOA3-GC1	Interrupted compaction effect	Aging time effect	Aging temperature effect
PA-control	2558	23.50	27.05	28.30	26.49	15%	20%	7%
PA-CRT2	2521	24.48	23.03	25.41	24.06	-6%	4%	6%
PA-CRT1	2527	25.12	-	23.69	25.08	-	-6%	-6%
PA-CRN	2527	23.90	23.00	24.70	24.10	-4%	3%	2%
SMA10-control	2530	6.50	6.70	7.80	6.50	3%	20%	20%
SMA10-CRT2	2494	3.50	3.80	5.50	3.10	9%	57%	77%
SMA10-CRT1	2500	5.06	-	7.11	5.95	-	41%	19%
SMA10-CRN	2500	4.70	5.20	6.90	6.40	11%	47%	8%

Symbols. G_{mm}: theoretical maximum specific gravity of the mixes; AV: Air void content; ΔAV: Air void content variation; STOA1: short-time oven aged (@180°C for 60 minutes); STOA2: short-time oven aged (@180°C for 240 minutes); STOA3: short-time oven aged (@135°C for 240 minutes); GC1: Gyratory compaction with standard procedure; GC2: Gyratory compaction with interrupted procedure (stops of 60 seconds); PA: Porous Asphalt; SMA10: Stone Mastic Asphalt with an upper sieve size of the aggregate of 10 mm; control: sample without rubber; CRT1: sample with CRT1 rubber; CRT2: sample with CRT2 rubber; CRN: sample with CRN rubber.
Note: Air void content refers to N_{max} (maximum number of gyrations).

In Table 5.9, a quantitative trend of air void content is represented. The symbol + means that there is an increase of air void variation of less than 10%; the symbol ++ means that there is an increase of air void variation of more than 10%; the symbol - means that there is a decrease of air void variation of less than 10%; the symbol - - means that there is a decrease of air void variation of more than 10% and; the symbol = means that the air void variation is not significant (less than 2% in absolute value).

Table 5.9: Air void content trend

AV	Interrupted compaction	Aging time (from 60 min to 240 min)	Aging temperature (from 135°C to 180°C)
PA – control	++	++	+
PA – CRT2	-	+	+
PA – CRT1	N.A.	=	=
PA – CRN	-	+	=
SMA10 – control	+	++	++
SMA10 – CRT2	+	++	++
SMA10 – CRT1	N.A.	++	++
SMA10 – CRN	++	++	+

Symbols. PA: Porous Asphalt; SMA10: Stone Mastic Asphalt with an upper sieve size of the aggregate of 10 mm; control: sample without rubber; CRT1: sample with CRT1 rubber; CRT2: sample with CRT2 rubber; CRN: sample with CRN rubber; +: increase < 10%; ++: increase ≥ 10%; -: decrease < 10%; - -: decrease ≥ 10%; =: unvaried (variations less than 2% in absolute value); N.A.: not available.

In the light of the results obtained, the air voids study has shown that:

- The effects of different laboratory short-term oven aging (STOA) methods, in terms of air void variation, are more evident in SMA10 samples than in PA samples.
- The air void variations of SMA10 mixes are generally higher than PA mixes (from 3% to 77% for SMA10 and from -6% to 20% for a PA).
- The effects of short-term oven aging methods (aging time and aging temperature effects) are more evident than the ones due to the interrupted compaction. In the first case the air voids variations are in the range -6% to 77%; in the second case they are in the range -6% to 15%.
- Mixes exposed to STOA1 tend to have the lowest air void contents. Instead, mixes exposed to STOA2 have the highest air void contents.
- Aging time is the main parameter that influence the air void variations.
- Higher aging temperatures are associated to higher air void contents. The corresponding increase is less than 7% for PA and in the range 8-77% for SMA10.
- For SMA10 samples, higher air void variations correspond to rubberised mixtures. Instead, for PA samples, they correspond to mixtures without rubber.
- Further studies and investigations are needed to assess the real effect of the interrupted compaction.

Figure 5.9 and Figure 5.10 highlight the air void content of PA and SMA10 samples.

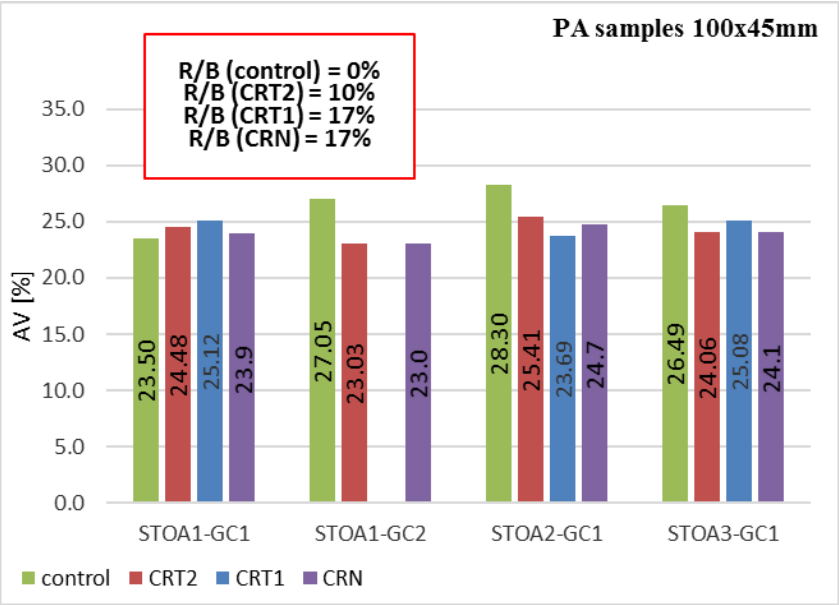

Figure 5.9: AV content for PA

Symbols. R: rubber; B: bitumen; R/B: rubber-bitumen ratio; STOA1: short-time oven aged (@180°C for 60 minutes); STOA2: short-time oven aged (@180°C for 240 minutes); STOA3: short-time oven aged (@135°C for 240 minutes); GC1: Gyratory compaction with standard procedure; GC2: Gyratory compaction with interrupted procedure (stops of 60 seconds); PA: Porous Asphalt; control: sample without rubber; CRT1: sample with CRT1 rubber; CRT2: sample with CRT2 rubber; CRN: sample with CRN rubber.

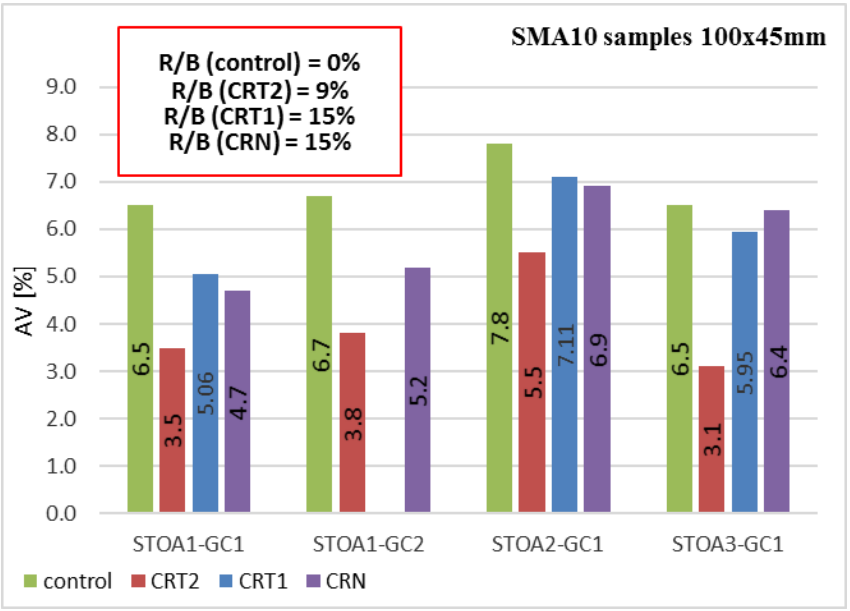

Figure 5.10: AV content for SMA10

Symbols. R: rubber; B: bitumen; R/B: rubber-bitumen ratio; STOA1: short-time oven aged (@180°C for 60 minutes); STOA2: short-time oven aged (@180°C for 240 minutes); STOA3: short-time oven aged (@135°C for 240 minutes); GC1: Gyratory compaction with standard procedure; GC2: Gyratory compaction with interrupted procedure (stops of 60 seconds); SMA10: Stone Mastic Asphalt with an upper sieve size of the aggregate of 10 mm; control: sample without rubber; CRT1: sample with CRT1 rubber; CRT2: sample with CRT2 rubber; CRN: sample with CRN rubber.

Based on the results obtained, it is possible to observe that:

- Air void content of samples without rubber is usually higher than the air void content of samples with rubber. This aspect needs further investigation.
- For SMA10 mixes, samples with CRT2 have the lowest voids content. Note that CRT2 is composed by rubber, bitumen and, filler. In this case, the real ratio rubber/bitumen is 9%.
- For PA mixes, the different type of rubber (CRT2, CRT1 and, CRN) seems does not have significant effects on the voids content.

Figure 5.11 and Figure 5.12 are focused on interrupted compaction effects.

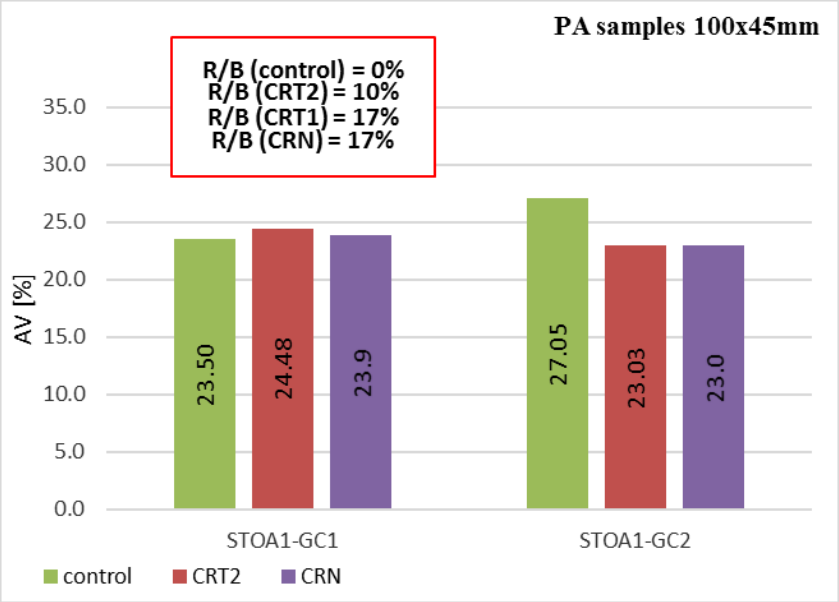

Figure 5.11: Interrupted compaction effect on AV content for PA

Symbols. R: rubber; B: bitumen; R/B: rubber-bitumen ratio; STOA1: short-time oven aged (@180°C for 60 minutes); STOA2: short-time oven aged (@180°C for 240 minutes); STOA3: short-time oven aged (@135°C for 240 minutes); GC1: Gyratory compaction with standard procedure; GC2: Gyratory compaction with interrupted procedure (stops of 60 seconds); PA: Porous Asphalt; control: sample without rubber; CRT2: sample with CRT2 rubber; CRN: sample with CRN rubber.

In this case, it is possible to note that:

- Samples made with interrupted compaction present a different behaviour in terms of air void content.
- PA samples seems to have a decrease of air void content for mixes with rubber (-6% for CRT2 and, -4% for CRN) and an increase of air void content for mixes without rubber (+15% for control).

- Instead, SMA10 samples always present an increase in the air void content (+3% for control, +9% for CRT2 and, +11% for CRN).
- PAs and SMAs give different insights. Results call for further investigations because of the many variables involved.

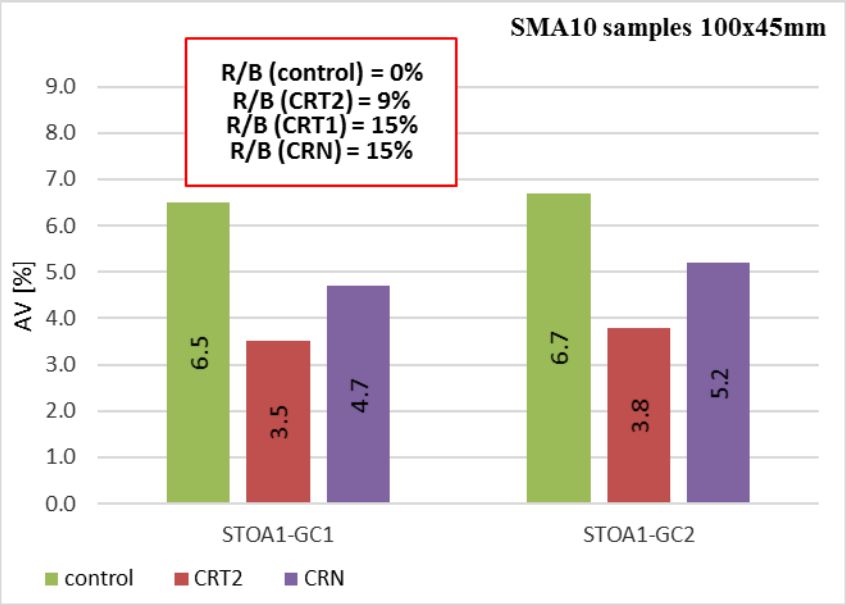

Figure 5.12: Interrupted compaction effect on AV content for SMA10

Symbols. R: rubber; B: bitumen; R/B: rubber-bitumen ratio; STOA1: short-time oven aged (@180°C for 60 minutes); STOA2: short-time oven aged (@180°C for 240 minutes); STOA3: short-time oven aged (@135°C for 240 minutes); GC1: Gyratory compaction with standard procedure; GC2: Gyratory compaction with interrupted procedure (stops of 60 seconds); SMA10: Stone Mastic Asphalt with an upper sieve size of the aggregate of 10 mm; control: sample without rubber; CRT2: sample with CRT2 rubber; CRN: sample with CRN rubber;

Figure 5.13 and Figure 5.14 are referred to aging time effects.

The increase of aging time (from 60 minutes to 240 minutes) causes a general increase in the voids content. This entails that the compaction of mixes aged for 240 minutes is worse than the compaction of mixes aged for 60 minutes (for the same aging temperature).

The air voids variation is different for PA and SMA10 samples. In the first case, un-rubberised mixes have higher variations than rubberised mixes (+20% for control, +4% for CRT2, -6% for CRT1 and, +3% for CRN).

In the second case, rubberised mixes have higher variations than un-rubberised mixes (+20% for control, +57% for CRT2, +41% for CRT1 and, +47% for CRN).

Finally, for PA samples it is possible to note that:

- Samples with CRT1 rubber seem to present a decrease of air void content (-6%).
- Air void variations of samples made with rubber (CRT2, CRT1 and CRN) are less than 10%.

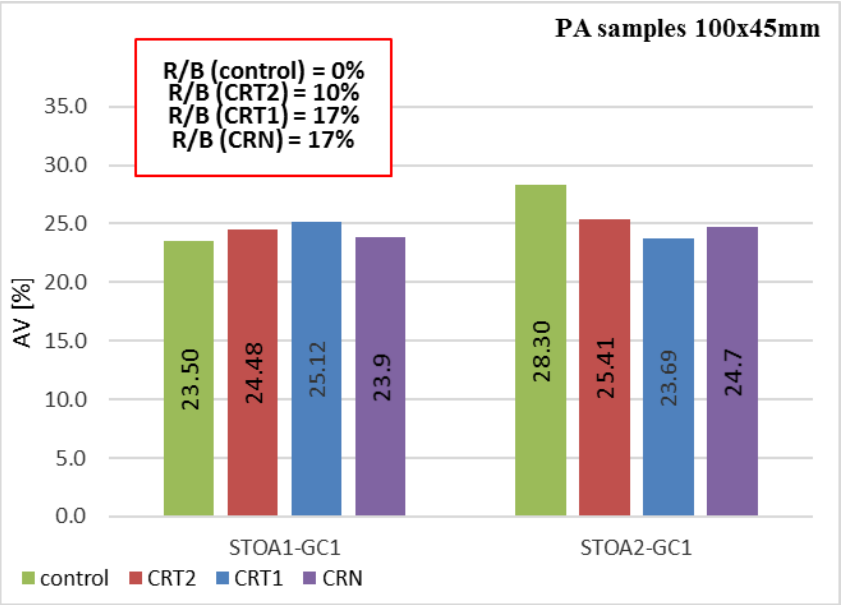

Figure 5.13: Aging time effect on AV content for PA

Symbols. R: rubber; B: bitumen; R/B: rubber-bitumen ratio; STOA1: short-time oven aged (@180°C for 60 minutes); STOA2: short-time oven aged (@180°C for 240 minutes); STOA3: short-time oven aged (@135°C for 240 minutes); GC1: Gyratory compaction with standard procedure; GC2: Gyratory compaction with interrupted procedure (stops of 60 seconds); PA: Porous Asphalt; control: sample without rubber; CRT1: sample with CRT1 rubber; CRT2: sample with CRT2 rubber; CRN: sample with CRN rubber.

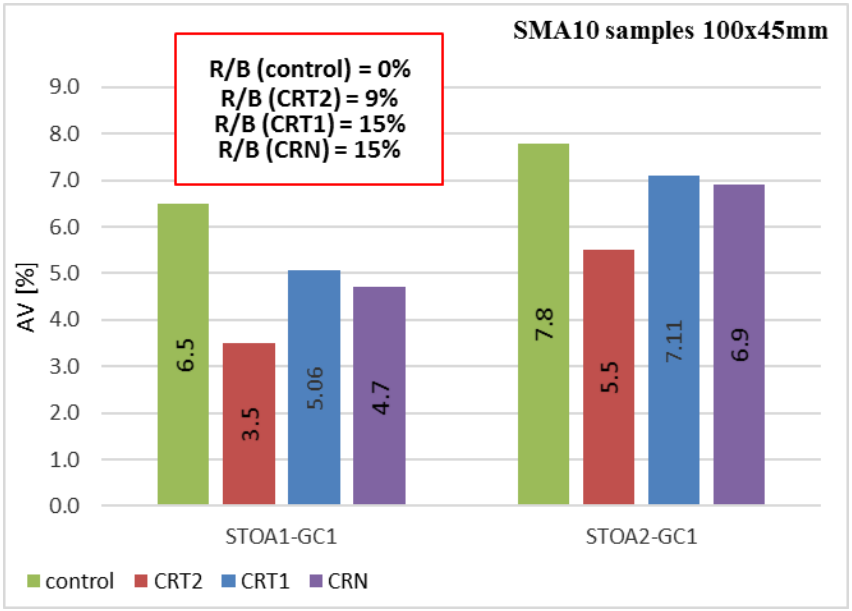

Figure 5.14: Aging time effect on AV content for SMA10

Symbols. R: rubber; B: bitumen; R/B: rubber-bitumen ratio; STOA1: short-time oven aged (@180°C for 60 minutes); STOA2: short-time oven aged (@180°C for 240 minutes); STOA3: short-time oven aged (@135°C for 240 minutes); GC1: Gyratory compaction with standard procedure; GC2: Gyratory compaction with interrupted procedure (stops of 60 seconds); SMA10: Stone Mastic Asphalt with an upper sieve size of the aggregate of 10 mm; control: sample without rubber; CRT1: sample with CRT1 rubber; CRT2: sample with CRT2 rubber; CRN: sample with CRN rubber.

Finally, Figure 5.15 and Figure 5.16 are referred to aging temperature effects.

It is easy to note that the increase of aging temperature (from 135°C to 180°C) causes a general increase in the voids content (from -6% to +7% for PA and from +8% to +77% for SMA10).

This entails that the compaction of mixes aged at 180°C is worse than the compaction of mixes aged at 135°C (for the same aging time).

Moreover, for PA mixes, it is possible to note that:

- Air void variations of all samples are less than 10%.
- Samples with CRT1 rubber seem to present a decrease of air void content (-6%).

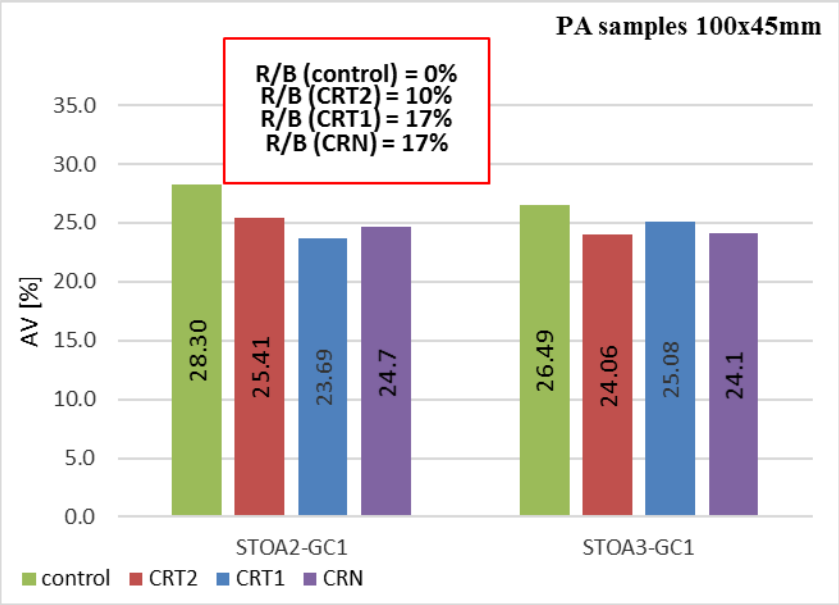

Figure 5.15: Aging temperature effect on AV content for PA

Symbols. R: rubber; B: bitumen; R/B: rubber-bitumen ratio; STOA1: short-time oven aged (@180°C for 60 minutes); STOA2: short-time oven aged (@180°C for 240 minutes); STOA3: short-time oven aged (@135°C for 240 minutes); GC1: Gyratory compaction with standard procedure; GC2: Gyratory compaction with interrupted procedure (stops of 60 seconds); PA: Porous Asphalt; control: sample without rubber; CRT1: sample with CRT1 rubber; CRT2: sample with CRT2 rubber; CRN: sample with CRN rubber.

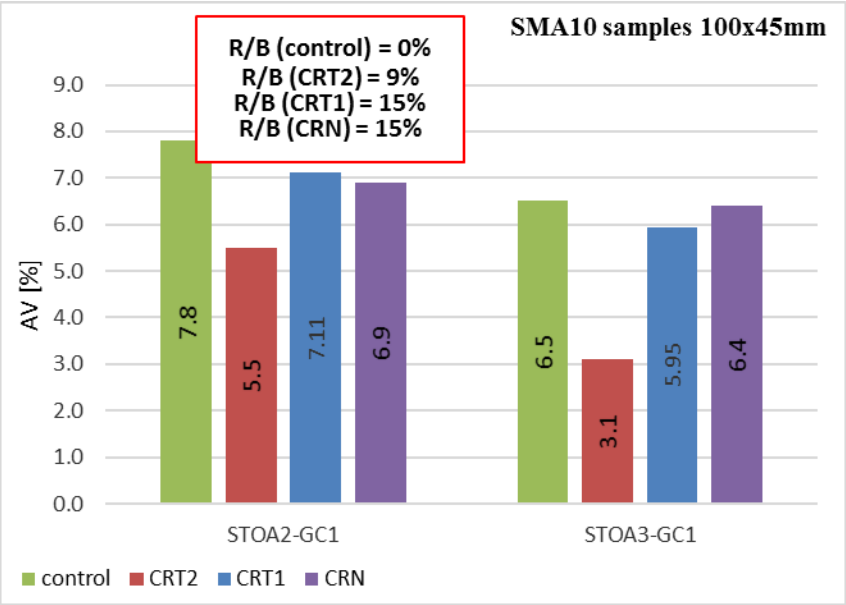

Figure 5.16: Aging temperature effect on AV content for SMA10

Symbols. R: rubber; B: bitumen; R/B: rubber-bitumen ratio; STOA1: short-time oven aged (@180°C for 60 minutes); STOA2: short-time oven aged (@180°C for 240 minutes); STOA3: short-time oven aged (@135°C for 240 minutes); GC1: Gyratory compaction with standard procedure; GC2: Gyratory compaction with interrupted procedure (stops of 60 seconds); SMA10: Stone Mastic Asphalt with an upper sieve size of the aggregate of 10 mm; control: sample without rubber; CRT1: sample with CRT1 rubber; CRT2: sample with CRT2 rubber; CRN: sample with CRN rubber.

5.6.3 Locking point

Locking point is one of the main laboratory compactability parameters. It can be used to represent the applied energy to reach a level of compaction in the SGC (Superpave Gyratory Compactor).

Locking point is defined as the number of gyrations after which the rate of change in height is equal to or less than 0.05 mm for three consecutive rotations (Al-shamsi and Louary 2006).

The data obtained by Leiva-Villacorta (2007) suggest that mixes with higher value of locking point and compaction slope are difficult to compact in the lab.

Mixes that require more energy to compact (higher Locking point) are considered long lasting, stable and more resistance to failure and deformation (Dessouky and Diaz 2015).

For Locking point analysis, Table 5.10 summarises the following parameters:

- Locking point value of each case investigated;
- Locking point variation related to:
  - Interrupted compaction effect: Locking point variations between STOA1-GC1 and STOA1-GC2.
  - Aging time effect: Locking point variations between STOA1-GC1 and STOA2-GC1.
  - Aging temperature effect: Locking point variations between STOA3-GC1 and STOA2-GC1.

Table 5.10: Locking point

	Locking point value				Locking point variation		
	STOA1-GC1	STOA1-GC2	STOA2-GC1	STOA3-GC1	Interrupted compaction effect	Aging time effect	Aging temperature effect
PA-control	47	59	57	51	26%	21%	12%
PA-CRT2	61	55	61	62	-10%	0%	-2%
PA-CRT1	54	-	58	55	-	7%	5%
PA-CRN	41	41	55	54	0%	34%	2%
SMA10-control	52	55	78	72	6%	50%	8%
SMA10-CRT2	57	55	64	66	-4%	12%	-3%
SMA10-CRT1	59	-	64	61	-	8%	5%
SMA10-CRN	52	55	65	63	6%	25%	3%

Symbols. STOA1: short-time oven aged (@180°C for 60 minutes); STOA2: short-time oven aged (@180°C for 240 minutes); STOA3: short-time oven aged (@135°C for 240 minutes); GC1: Gyratory compaction with standard procedure; GC2: Gyratory compaction with interrupted procedure (stops of 60 seconds); PA: Porous Asphalt; SMA10: Stone Mastic Asphalt with an upper sieve size of the aggregate of 10 mm; control: sample without rubber; CRT1: sample with CRT1 rubber; CRT2: sample with CRT2 rubber; CRN: sample with CRN rubber.

In Figure 5.17, a graphical representation of the locking point is reported. It is referred to the PA-STOA1-GC1 cases.

In Table 5.10, each locking point value is obtained by the average of two value (see Figure 5.18): i) locking point of "a&b densification curve" (first repetition) and; ii) locking point of "c&d densification curve" (second repetition).

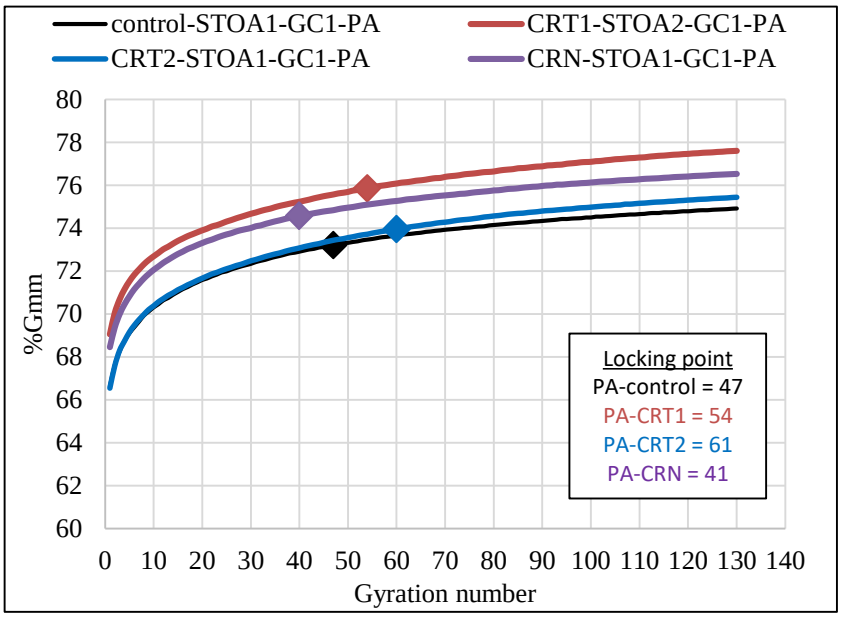

Figure 5.17: Graphical representation of locking point for PA-STOA1-GC1 cases.

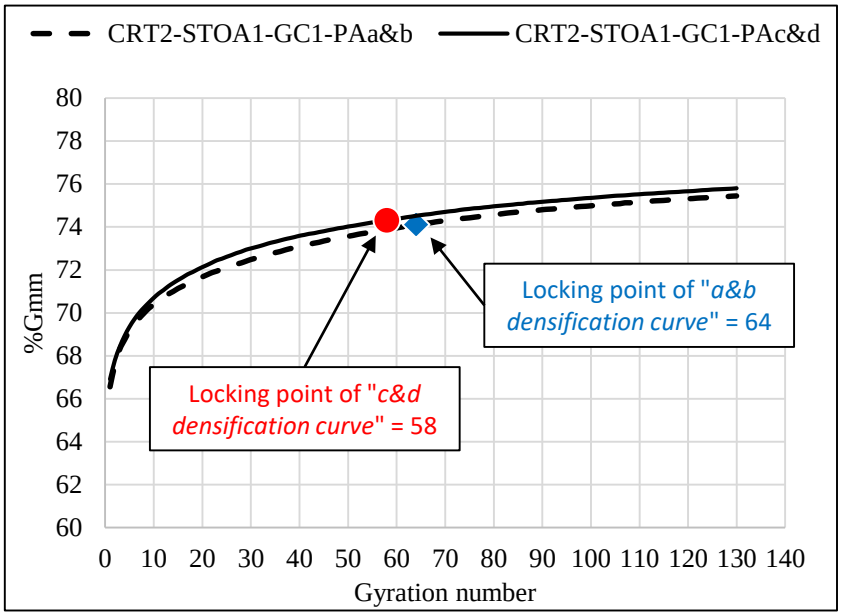

Figure 5.18: Graphical representation of locking point for CRT2-STOA1-GC1-PA.

Table 5.10 shows the effects of short-term oven aging and interrupted compaction process on locking point. It is possible to observe that:

- SMA10 mixes have a Locking point higher than the one of PA mixes. It can be seen that SMA10 mixtures resulted in Locking points in the range of 52-78 while PA mixtures have a locking point in the range of 41-62. This means that higher compaction energy is needed to compact SMA10 mixtures.
- Mixes exposed to STOA1 tend to have lower locking points while mixes exposed to STOA2 usually tend to have higher locking points. This shows that the locking point is affected by the aging process. A heavier aging process entails an increase of the oxidation rate of mixes. Therefore, binder of STOA2 mixes is stiffer than binder of STOA1 mixes and thus is expected to be less compactable than STOA1 mixes.
- Aging time implies the highest variations of locking point. It is the main parameter that influences the locking point variations.
- Higher aging temperature are associated with higher locking point, but the corresponding increase is less than 12%.
- Higher locking point variations are associated to mixtures without rubber (control).
- For rubberised mixtures, interrupted compaction process tends to have no significant effects on locking point. Instead, in the cases of control mixtures (without rubber) there is a significant increase of locking point (26% for PA and 6% for SMA10).

In Table 5.11, a quantitative trend of locking point variation is represented. The symbol + means that there is an increase of locking point variation less than 10%; the symbol ++ means that there is an increase of locking point variation more than 10%; the symbol - means that there is a decrease of locking point variation less than 10%; the symbol -- means that there is a decrease of locking point variation more than 10% and; the symbol = means that the locking point variation is not significant (less than 2% in absolute value).

Table 5.11: Locking point trend

Locking point	Interrupted compaction	Aging time (from 60 min to 240 min)	Aging temperature (from 135°C to 180°C)
PA – control	++	++	++
PA – CRT2	--	=	=
PA – CRT1	N.A.	+	+
PA – CRN	=	++	=
SMA10 – control	+	++	+
SMA10 – CRT2	-	++	-
SMA10 – CRT1	N.A.	+	+
SMA10 – CRN	+	++	+

Symbols. PA: Porous Asphalt; SMA10: Stone Mastic Asphalt with an upper sieve size of the aggregate of 10 mm; control: sample without rubber; CRT1: sample with CRT1 rubber; CRT2: sample with CRT2 rubber; CRN: sample with CRN rubber; +: increase < 10%; ++: increase ≥ 10%; -: decrease < 10%; - -: decrease ≥ 10%; =: unvaried (variations less than 2% in absolute value); N.A.: not available.

5.6.4 Slope

Another important parameter to evaluate the compactability and workability of a mixture is the slope of densification curve (compaction slope).

It is defined as the slope of the best-fit line between the percentage of the maximum theoretical density and log N (Leiva-Villacorta 2007).

Compaction slope and Locking point of the mixture are strongly correlate and are related to resistance to permanent deformation. When these parameters increase the compactability of the mixture decreases (Leiva-Villacorta 2007).

Moreover, mixtures with higher compaction slopes tend to have higher shear stiffness and lower permanent shear strain (Leiva and West 2008).

In Table 5.12 the compaction slope of each case is reported.

Table 5.12: Compaction slope

	Compaction slope			
	STOA1-GC1	STOA1-GC2	STOA2-GC1	STOA3-GC1
PA-control	1.56	1.85	1.80	1.77
PA-CRT2	1.96	1.94	2.01	1.90
PA-CRT1	2.06	-	2.01	1.82
PA-CRN	1.59	1.68	1.84	1.94
SMA10-control	1.94	2.53	3.06	2.76
SMA10-CRT2	2.55	2.52	2.60	2.76
SMA10-CRT1	2.66	-	3.07	2.94
SMA10-CRN	2.65	2.61	2.74	2.88

Symbols. STOA1: short-time oven aged (@180°C for 60 minutes); STOA2: short-time oven aged (@180°C for 240 minutes); STOA3: short-time oven aged (@135°C for 240 minutes); GC1: Gyratory compaction with standard procedure; GC2: Gyratory compaction with interrupted procedure (stops of 60 seconds); PA: Porous Asphalt; SMA10: Stone Mastic Asphalt with an upper sieve size of the aggregate of 10 mm; control: sample without rubber; CRT1: sample with CRT1 rubber; CRT2: sample with CRT2 rubber; CRN: sample with CRN rubber.

Figure 5.19 shows an example of densification curves from which the compaction slope has been derived. Also, in the same figure, the respective locking point is reported.

Note that, in Table 5.12, for each case analised, the average of the two compaction slopes is reported ("a&b densification curve" and "c&d densification curve").

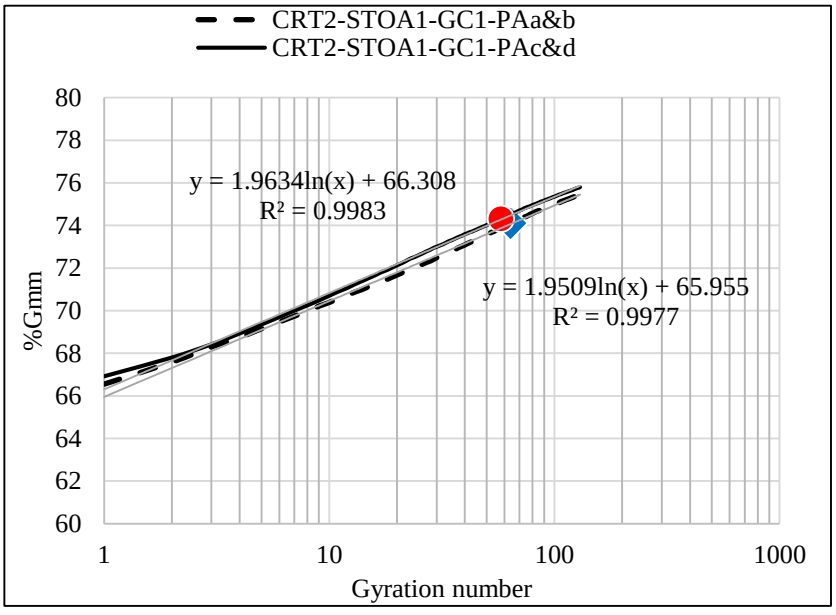

Figure 5.19: Graphical representation of compaction slope and locking point for CRT2-STOA1-GC1-PA.

It is possible to observe that:

- SMA10 mixes have higher compaction slopes than PA mixes. It can be seen that SMA10 mixtures resulted slopes in the range of 1.94-3.07 while PA mixtures ended with slopes in the range of 1.56-2.06.
- Mixes exposed to STOA1 tend to have lower compaction slope.
- Aging time variation have often the highest values of compaction slope.
- Rubberised mixes have higher compaction slope than mixes without rubber
- For rubberised mixtures, interrupted compaction tends to have not significant effects on compaction slope. Instead, in the cases of control mixtures (without rubber) there is a significant increase of compaction slope (from 1.56 to 1.85 for PA and from 1.94 to 2.53 for SMA10).

In Table 5.13, a quantitative trend of slope variation is represented. The symbol + means that there is an increase of compaction slope variation less than 10%; the symbol ++ means that there is an increase of compaction slope variation more than 10%; the symbol - means that there is a decrease of compaction slope variation less than 10%; the symbol -- means that there is a decrease of compaction slope variation more than 10% and; the symbol = means that the compaction slope variation is not significant (less than 2% in absolute value).

Table 5.13: Compaction slope trend

Compaction slope	Interrupted compaction	Aging time (from 60 min to 240 min)	Aging temperature (from 135°C to 180°C)
PA – control	++	++	=
PA – CRT2	=	+	+
PA – CRT1	N.A.	=	++
PA – CRN	+	++	-
SMA10 – control	++	++	++
SMA10 – CRT2	=	=	-
SMA10 – CRT1	N.A.	++	+
SMA10 – CRN	=	+	-

Symbols. PA: Porous Asphalt; SMA10: Stone Mastic Asphalt with an upper sieve size of the aggregate of 10 mm; control: sample without rubber; CRT1: sample with CRT1 rubber; CRT2: sample with CRT2 rubber; CRN: sample with CRN rubber; +: increase < 10%; ++: increase ≥ 10%; -: decrease < 10%; - -: decrease ≥ 10%; =: unvaried (variations less than 2% in absolute value); N.A.: not available.

5.6.5 N (92%Gmm)

The Number of gyrations corresponding to 92% of G_{mm} is one of the parameters suggested by Leiva and West (2008) to understand the compactability of mixtures.

It is clear that the hardest mixes to compact have higher values of N (92% G_{mm}). In other words, higher number of gyrations correspond to higher compaction energy.

In Table 5.14 the number of gyrations corresponding to 92% of G_{mm} is reported.

The study of N (92% G_{mm}) has been developed for SMA10 mixtures (AV<8%). It shows that:

- Mixes exposed to STOA2 have the highest number of gyrations to obtain 92% of G_{mm} (from 109 to 141 gyrations).
- Rubberised mixtures have lower N(92%G_{mm}) than mixtures without rubber (from 35 to 113 for rubberised mixtures and from 91 to 141 for un-rubberised mixtures).
- Referring to N(92%G_{mm}) variations, rubberised mixtures have higher values than un-rubberised mixtures (from -1% to 223% and from -13% to 55% respectively).
- Referring to rubberised mixtures, CRN-samples have the highest N(92%G_{mm}) and CRT2-samples have the lowest N(92%G_{mm}).
- Interrupted compaction process entails variations of N(92%G_{mm}) from -13% to 20%.
- Aging time entails variations of N(92%G_{mm}) from 10% to 223%.
- Aging temperature entails variations of N(92%G_{mm}) from -1% to 169%.

Table 5.14: N (92% G_{mm})

	N (92%Gmm)				ΔN (92%Gmm)		
	STOA1-GC1	STOA1-GC2	STOA2-GC1	STOA3-GC1	Interrupted compaction effect	Aging time effect	Aging temperature effect
PA-control	-	-	-	-	-	-	-
PA-CRT2	-	-	-	-	-	-	-
PA-CRT1	-	-	-	-	-	-	-
PA-CRN	-	-	-	-	-	-	-
SMA10-control	128	112	141	91	-13%	10%	55%
SMA10-CRT2	35	42	113	42	20%	223%	169%
SMA10-CRT1	65	-	114	67	-	75%	70%
SMA10-CRN	69	73	109	110	6%	58%	-1%

Symbols. N (92%Gmm): number of gyrations corresponding to 92% of G_{mm}; ΔN (92%Gmm): variation of number of gyrations corresponding to 92% of G_{mm}; STOA1: short-time oven aged (@180°C for 60 minutes); STOA2: short-time oven aged (@180°C for 240 minutes); STOA3: short-time oven aged (@135°C for 240 minutes); GC1: Gyratory compaction with standard procedure; GC2: Gyratory compaction with interrupted procedure (stops of 60 seconds); PA: Porous Asphalt; SMA10: Stone Mastic Asphalt with an upper sieve size of the aggregate of 10 mm; control: sample without rubber; CRT1: sample with CRT1 rubber; CRT2: sample with CRT2 rubber; CRN: sample with CRN rubber.

In Table 5.15, a quantitative trend of N(92%G_{mm}) variation is represented. The symbol + means that there is an increase of N(92%G_{mm}) variation less than 10%; the symbol ++ means that there is an increase of N(92%G_{mm}) variation more than 10%; the symbol - means that there is a decrease of N(92%G_{mm}) variation less than 10%; the symbol -- means that there is a decrease of N(92%G_{mm}) variation more than 10% and; the symbol = means that the N(92%G_{mm}) variation is not significant (less than 2% in absolute value).

Table 5.15: N (92% G_{mm}) trend

N (92% G_{mm})	Interrupted compaction	Aging time (from 60 min to 240 min)	Aging temperature (from 135°C to 180°C)
PA – control	N.A.	N.A.	N.A.
PA – CRT2	N.A.	N.A.	N.A.
PA – CRT1	N.A.	N.A.	N.A.
PA – CRN	N.A.	N.A.	N.A.
SMA10 – control	--	++	++
SMA10 – CRT2	++	++	++
SMA10 – CRT1	N.A.	++	++
SMA10 – CRN	+	++	=

Symbols. PA: Porous Asphalt; SMA10: Stone Mastic Asphalt with an upper sieve size of the aggregate of 10 mm; control: sample without rubber; CRT1: sample with CRT1 rubber; CRT2: sample with CRT2 rubber; CRN: sample with CRN rubber; +: increase < 10%; ++: increase ≥ 10%; -: decrease < 10%; - -: decrease ≥ 10%; =: unvaried (variations less than 2% in absolute value); N.A.: not available.

5.6.6 %G_{mm} (N_{ini})

Another way to indicate the compactability of mixes is to analyse the percentage of maximum theoretical specific gravity at N_{ini} (Superpave mix procedure, The Asphalt Institute, 2000).

Mixes that compact too quickly (air voids at N_{ini} are too low) may be tender during construction and unstable when subjected to traffic (Leiva-Villacorta 2007).

In Table 5.16 the percentage of maximum theoretical specific gravity at N_{ini} is reported.

Table 5.16 and Table 5.17 show the effects of short-term oven aging on percentage of the maximum theoretical specific gravity at the initial number of gyrations.

In Table 5.17, the symbol + means that there is an increase of $\%G_{mm}(N_{ini})$ variation less than 10%; the symbol ++ means that there is an increase of $\%G_{mm}(N_{ini})$ variation more than 10%; the symbol - means that there is a decrease of $\%G_{mm}(N_{ini})$ variation less than 10%; the symbol -- means that there is a decrease of $\%G_{mm}(N_{ini})$ variation more than 10% and; the symbol = means that the $\%G_{mm}(N_{ini})$ variation is not significant (less than 2% in absolute value).

Table 5.16: $\%G_{mm}$ (N_{ini})

	$\%G_{mm}$ (N_{ini})				$\Delta\%G_{mm}$ (N_{ini})		
	STOA1-GC1	STOA1-GC2	STOA2-GC1	STOA3-GC1	interrupted compaction effect	Aging time effect	Aging temperature effect
PA-control	70.0	70.8	67.1	69.3	1%	-4%	-3%
PA-CRT2	70.5	70.2	66.1	69.7	0%	-6%	-5%
PA-CRT1	69.6	-	71.5	70.2	-	3%	2%
PA-CRN	71.3	71.8	70.8	70.7	1%	-1%	0%
SMA10-control	82.7	84.0	82.1	83.4	2%	-1%	-2%
SMA10-CRT2	88.2	87.5	85.2	87.4	-1%	-3%	-3%
SMA10-CRT1	84.5	-	83.9	84.1	-	-1%	0%
SMA10-CRN	86.5	85.9	85.1	84.3	-1%	-2%	1%

Symbols. $\%G_{mm}$ (N_{ini}): percentage of maximum theoretical specific gravity at N_{ini}; $\Delta\%G_{mm}$ (N_{ini}): variation of percentage of maximum theoretical specific gravity at N_{ini}; STOA1: short-time oven aged (@180°C for 60 minutes); STOA2: short-time oven aged (@180°C for 240 minutes); STOA3: short-time oven aged (@135°C for 240 minutes); GC1: Gyratory compaction with standard procedure; GC2: Gyratory compaction with interrupted procedure (stops of 60 seconds); PA: Porous Asphalt; SMA10: Stone Mastic Asphalt with an upper sieve size of the aggregate of 10 mm; control: sample without rubber; CRT1: sample with CRT1 rubber; CRT2: sample with CRT2 rubber; CRN: sample with CRN rubber.

It is possible to note that:

- All the variations of $\%G_{mm}$ (N_{ini}) are lesser than 6% in absolute value. This is due to the fact that the relative density at N_{ini} is an early point in the gyratory compaction process.
- After the first 10 gyrations, it is impossible to note the effects of interrupted compaction. This is attributed to the interrupted compaction hypothesis, used in this study, which imposes the first stop after 10 gyrations. Therefore, there are not differences between GC1 (standard compaction process) and GC2 (interrupted compaction process) from the starting point to 10 gyrations.
- Referring to aging time and aging temperature, there are small differences between SMA10 and PA mixes. This is due to the fact that N_{ini} is equal to 8 and 10 gyrations for SMA10 and PA respectively.

Table 5.17: $\%G_{mm}@N_{ini}$ trend

$\%G_{mm}$ (N_{ini})	Interrupted compaction	Aging time (from 60 min to 240 min)	Aging temperature (from 135°C to 180°C)
PA – control	=	=	=
PA – CRT2	=	=	=
PA – CRT1	N.A.	+	=
PA – CRN	=	=	=
SMA10 – control	=	=	=
SMA10 – CRT2	=	=	=
SMA10 – CRT1	N.A.	=	=
SMA10 – CRN	=	=	=

Symbols. PA: Porous Asphalt; SMA10: Stone Mastic Asphalt with an upper sieve size of the aggregate of 10 mm; control: sample without rubber; CRT1: sample with CRT1 rubber; CRT2: sample with CRT2 rubber; CRN: sample with CRN rubber; +: increase < 10%; ++: increase ≥ 10%; -: decrease < 10%; - -: decrease ≥ 10%; =: unvaried (variations less than 2% in absolute value); N.A.: not available.

5.7 Conclusions

To define the effects of different laboratory short-term oven aging and compaction process on compactability and workability, the following parameters have been analysed: i) air void content (AV); ii) locking point; iii) compaction slope; iv) percentage of the maximum theoretical specific gravity at the initial number of gyrations ($\%G_{mm}@N_{ini}$); v) number of gyrations corresponding to 92% of G_{mm} ($N@92\%G_{mm}$).

It is possible to observe that:

- In all cases investigated, effects of short-term oven aging are more evident than interrupted compaction effects in terms of compactability and workability.
- Short-time oven aging (STOA) entails a worse compaction of mixes. In more detail:
    - Mixes exposed to STOA1-GC1 usually tend to have:
        - The lowest air void content (from 23.50% to 25.12% for PA and from 3.50% to 6.50% for SMA10).
        - The lowest locking point (from 41 to 61 for PA and from 52 to 59 for SMA10).

        - The lowest compaction slope (from 1.56 to 2.06 for PA and from 1.94 to 2.66 for SMA10).
        - The lowest number of gyrations need to obtain 92% of G_{mm} (from 35 to 128 for SMA10).
    - Mixes exposed to STOA2-GC1 usually tend to have:
        - The highest air void content (from 23.69% to 28.30% for PA and from 5.50% to 7.80% for SMA10).
        - The highest locking point (from 55 to 61 for PA and from 64 to 78 for SMA10).
        - The higher compaction slope (from 1.80 to 2.01 for PA and from 2.60 to 3.07 for SMA10).
        - The highest number of gyrations need to obtain 92% of G_{mm} (from 109 to 141 for SMA10).
- Aging time effects are more evident than aging temperature effects.
- Interrupted compaction process (GC) entails a worse compaction of mixes. In more detail:
    - Higher air void variations when SMA10 samples are considered (from 3% to 11%). Unusually behaviour is showed by rubberised PA mixes (from -6% to -4%). Instead, PA mixes without rubber have un air void variation of +15%.
    - Usually, higher locking point variations (+26% for PA-control and +6% for SMA10-control)
    - Higher number of gyrations needed to obtain 92% of G_{mm} (from 6% to 20%) when SMA10-rubberised samples are considered.
    - Not significant effects in terms of $\%G_{mm}@N_{ini}$ (less than 1% for PA and in the range of -1% to 2% for SMA10).
- With some exceptions, un-rubberised mixes (control samples) are more difficult to compact than rubberised mixes when STOA 2 (higher time of aging) or STOA 3 (higher temperature of aging) are applied. In these cases, the presence of crumb rubber seems to play a positive role in aging process.
- After the first 10 gyrations, it is impossible to note the effects of interrupted compaction process. This is attributed to the interrupted compaction hypothesis used in this study, which imposes the first stop after 10 gyrations. Therefore, there are not differences between GC1 (standard compaction) and GC2 (interrupted compaction) from the starting point to 10 gyrations.
- Rubberised mixes have:
    - Lower air void content (from 23.00% to 25.41% for PA and from 3.10% to 7.11% for SMA10). This aspect needs further investigation.
    - Higher compaction slope (from 1.59 to 2.06 for PA and from 2.52 to 3.07 for SMA10).
    - The lowest number of gyrations need to obtain 92% of G_{mm} (from 35 to 114 for SMA10)

  - Higher percentage of maximum theoretical specific gravity at N_{ini} (from 66.1% to 71.8% PA and from 83.9% to 88.2% for SMA10).
  - Higher air void variations when SMA10 samples are considered (from 8% to 77%).
  - Lower air void variations when PA samples are considered (from -6% to 6%).
  - Lower locking point variations when SMA10 samples are considered (from -4% to 25%).
  - the highest variations related to number of gyrations needed to obtain 92% of G_{mm} (from - 1% to 223%).
  - Not significant effects in terms of $\%G_{mm}@N_{ini}$ (from -6% to 3% for PA and from -3% to 1% for SMA10).
- Un-rubberised mixes have:
  - Higher air void content (from 23.50% to 28.30% for PA and from 6.50% to 7.80% for SMA10). This aspect needs further investigation.
  - Lower compaction slope (from 1.56 to 1.85 for PA and from 1.94 to 3.06 for SMA10).
  - The highest number of gyrations need to obtain 92% of G_{mm} (from 91 to 141 for SMA10).
  - Lower percentage of maximum theoretical specific gravity at N_{ini} (from 67.10% to 70.80% PA and from 82.10% to 84.00% for SMA10).
  - Lower air void variations when SMA10 samples are considered (from 3% to 20%).
  - Higher air void variations when PA samples are considered (from 7% to 20%).
  - Higher locking point variations when SMA10 samples are considered (from 6% to 50%).
  - The lowest variations related to number of gyrations needed to obtain 92% of G_{mm} (from - 13% to 55%).
  - Not significant effects in terms of $\%G_{mm}@N_{ini}$ (from -3% to 1% for PA and from -2% to 2% for SMA10).

- SMA10 mixes have:
  - Higher air void variations than PA mixes (from 3% to 77% for SMA10 and from -6% to 20% for a PA).
  - Higher Locking point than PA mixes. It can be seen that SMA10 mixtures resulted Locking point in the range of 52 to 78 while PA mixtures ended with locking point in the range of 41 to 62.
  - Higher locking point variations than PA mixes (from -4% to 50% for SMA10 and from -10 to 34% for a PA).
  - Higher compaction slopes than PA mixes. It can be seen that SMA10 mixtures resulted slopes in the range of 1.94 to 3.07 while PA mixtures ended with slopes in the range of 1.56 to 2.06.

- A similar trend in terms of $\%G_{mm}$ (N_{ini}) with PA mixes (-3% to 2% for SMA10 and from -6% to 3% for PA).

- The variations of $\%G_{mm}$ (N_{ini}) are lesser than 6% in absolute value. This is due to the fact that the relative density at N_{ini} is an early point in the gyratory compaction process.

Referring to the different crumb rubber used, it is possible to observe that:

- CRT2-samples generally have the lowest air void content.
- CRT1-samples generally have the highest air void content.
- CRN-samples generally have the lowest locking point.
- CRT2-samples generally have the highest locking point.
- CRT2-samples generally have the lowest compaction slope (SMA10-cases).
- CRN-samples generally have the lowest compaction slope (PA-cases).
- CRT1-samples generally have the highest compaction slope.
- CRT2-samples have the lowest N(92%Gmm).
- CRN-samples have the highest N(92%Gmm).

This means that CRT2-mixes are essentially the best to compact.

6 CR-added bituminous mixtures - Mixture performance: experiments and analyses

6.1 Introduction

The most important mechanical properties related to the materials used for bound material layers are (Brown and Foo 1994):

- Stiffness - is required to ensure good load spreading ability;
- Fatigue strength - it will prevent cracking due to traffic loading;
- Resistance to permanent deformation - it eliminates rutting.

In laboratory scale, the stiffness can be measured using Indirect Tensile Stiffness Modulus (ITSM), the fatigue strength can be measured using Indirect Tensile Fatigue Test (ITFT) and, the resistance to permanent deformation of road materials can be measured using Repeated Load Axial Test (RLAT).
This section deals with the study of macro-component affinity and performance related test.
It represents the last step of the experimental programme showed in section before ("Rutting and Stiffness test").
The aim is to study the effect of different laboratory short-term oven aging (STOA) and interrupted compaction on stiffness and rutting of dry rubberised asphalt mixture.
In the pursuit of this, ITSM and RLAT test were carried out.
Specimens used in this section are the same of those used in Section 5. After compaction study they have been subjected to mechanic performance study.

6.2 Stiffness

Stiffness modulus is one of the most fundamental parameters used to evaluate pavement mixes. It is an important input for pavement design and evaluation of asphalt materials.

HMA mixes are defined as non-linear viscoelastic materials. At relatively low stress levels, asphalt materials may be defined as approximately linear viscoelastic material.

In Figure 6.1 the typical domains of behaviour observed on bituminous mixtures (ϵ, strain – N, number of loading) is reported.

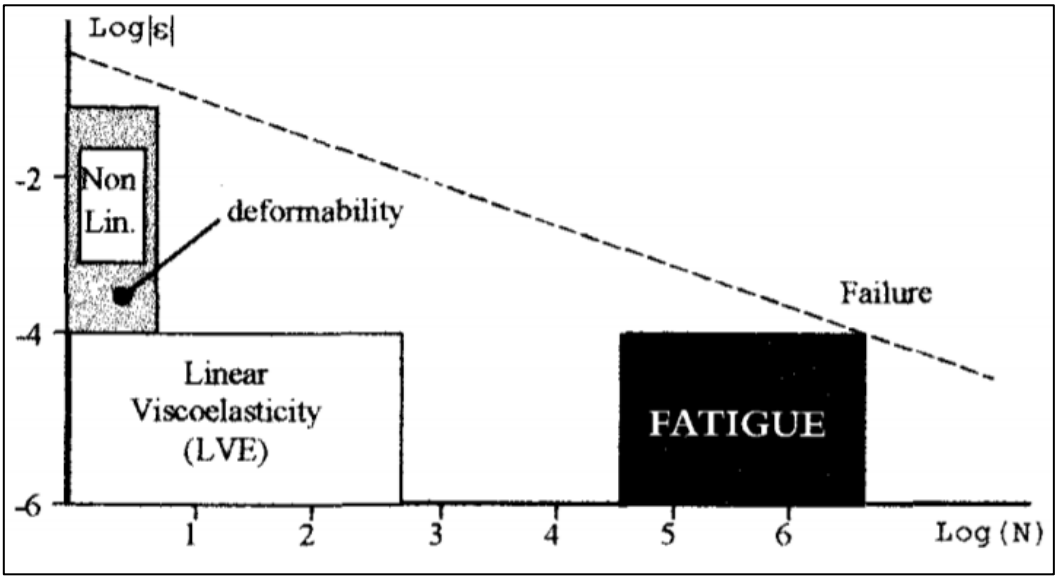

Figure 6.1: Typical domains of behaviour observed on bituminous mixtures (Di Benedetto 1990; Di Benedetto et al. 2001).

Whether in laboratory or the field, stiffnessis usually regarded as an indicator of the quality of mixtures and is required in the design to evaluate cumulative damage and also to assess age-hardening trends of bituminous mixtures (Epps et al. 2000).

The mix stiffness is generally estimated throught the master curves. It represents the relationship between mix stiffness, loading time (or frequency) and, temperature. This relationship is determined through indirect tensile test or the four-point bending test.

Typically, the stiffness modulus of asphalt mixes increases with decreasing temperature and increasing loading frequency (Jahromi and Khodaii 2009).

The stiffness modulus of bituminous mixes follows the frequency-temperature superposition principle. This means that a master curve of the complex modulus can be constructed for a reference temperature from

experimental data over a limited range of frequencies and temperatures, provided that a shift factor is used to calculate the reference frequency (EN-12697:26 2012).

The aim of the master curve is to determine the stiffness modulus at any arbitrary combination of loading frequency and test temperature. For this purpose, the stiffness has to be measured at various frequencies and temperatures. These results are used to determine the parameters in an Arrhenius equation, which is used often in this case (EN-12697:26 2012).

Strain can be based on the total deformation (maximum deformation during one loading cycle) or just on the elastic (resilient) deformation or an average of the two (Hakim et al. 2012).

In this study, all specimens have been tested in stiffness and resistance to permanent deformation.

As has been widely reported in literature, there are different test methods to study or test the cyclic behaviour in the small strain domain (of about 10^{-6} m/m to 10^{-4} m/m) of a compacted bituminous mix (Partl and Francken 1997; Francken 1998).

To determine the stiffness of the HMA samples, the indirect tensile stiffness modulus test (ITSM, EN-12697:26 2012) using a Cooper NU 14 tester was conducted (see Figure 6.2).

The specimen during the test is loaded vertically by means of loading strips.

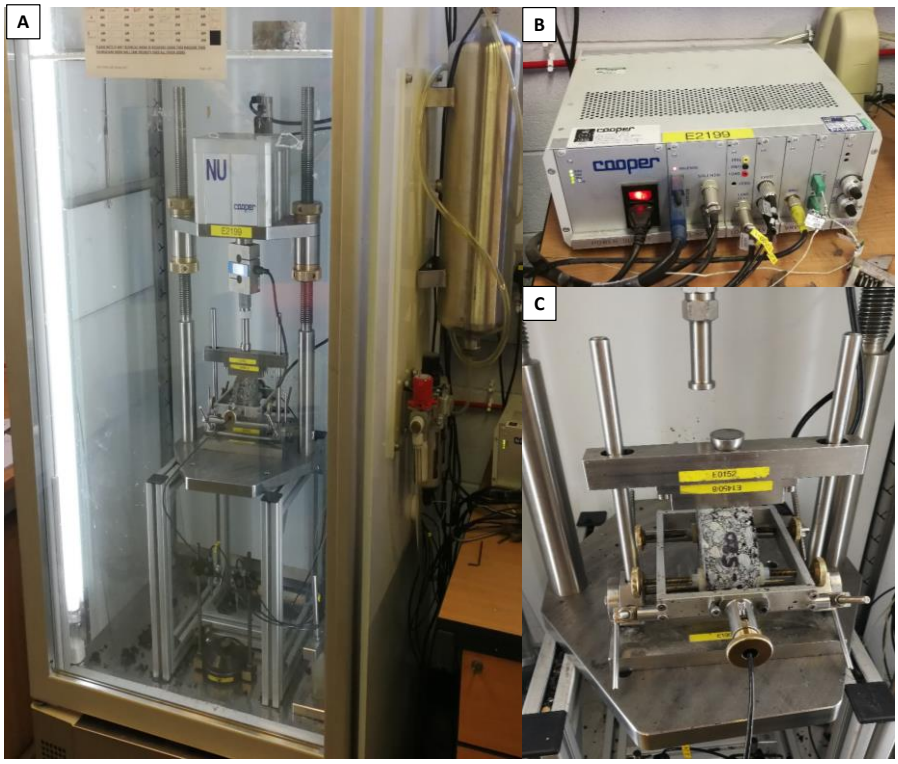

Figure 6.2: Component of Cooper NU 14 tester

Symbols. A: Temperature controlled cabinet and Servo-Pneumatic Universal Testing Machine (Cooper NU 14 tester); B: Data acquisition system; C: Indirect tensile stiffness modulus measurement system to perform.

The load results in a uniform tensile stress in the horizontal direction perpendicular to the plane of loading (Kennedy and Anagnos 1983; Hondros 1959).

The stress-strain ratio of asphalt materials is primarily dependent on loading time, the stress magnitude and temperature (Hakim et al. 2012).

In Table 6.1 the main parameters of ITSM test are reported and in Figure 6.3 a typical result of ITSM test is shows.

Table 6.1: Main parameters of ITSM test (EN-12697:26 2012).

Parameter	Value
Test temperature [°C]	20
Poisson's ratio	0.35
Target rise-time [ms]	124
Target horizontal deformation [microns]	5
Number of conditioning pulses	10

Stiffness (E) has been calculated using the following equation (EN-12697:26 2012):

$$E = \frac{\sigma}{\varepsilon} \qquad \text{(Eq. 20)}$$

Where, E is the stiffness modulus [MPa]; σ is the applied stress [MPa] and ε is the applied strain in microstrain.

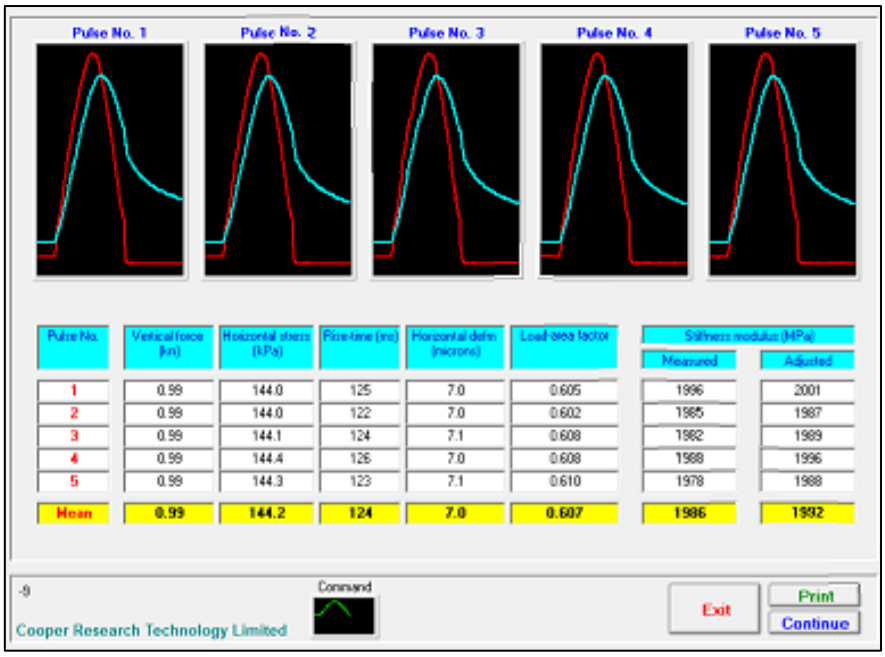

Figure 6.3: Typical result of ITSM test.

Prior of the starting of testing, all the samples have been subjected to a particular preparation protocol (EN-12697:26 2012). It consisted of:

- Store the specimens on a flat surface at a temperature of 20°C after the time of cutting (cutting was performed no more than 8 days after compaction of the mixes).
- Measure the dimensions of the specimens according to EN-12697:29 (2002).
- Determine the bulk density of the specimens according to EN-12697:6 (2012) or EN-12697:7 (2014).

After that, all samples have been removed from storage and place it at the test temperature (20 ± 0.5 °C) for at least four hours to reach the uniform temperature.

6.3 Fatigue

Fatigue cracking, also known as crocodile cracking or alligator cracking, is a type of damage that can endanger the health of large sections of the pavement in a relatively short time. It is a sign that the pavement and its supporting foundation are unable to bear the weight of traffic.

Then, fatigue property of asphalt mixture is closely related to the service life of asphalt pavement.

In order to predict the fatigue failure of a pavement system needs to be known both the strain-fatigue cycles relationship and the strain that the mixes will undergo in the roadway under a design loading (Maupin 1971).

The strain-fatigue cycles relationship is influenced by many things (e.g., load magnitudes, temperature, ect.).

For this reason, the best estimate is obtained by testing fatigue specimens in the laboratory, at various strain levels, and at a temperature that represents a field temperature.

The fatigue life of bituminous mixes determined from laboratory tests depends on the definition of initial strain/stress and the definition of failure. The results normally are presented in plots of initial strain vs. number of cycles (Said 1998).

All fatigue tests include repetitive deformations, with both elastic and plastic deformations.

Indirect tensile fatigue test (ITFT) is an effective method which has been used in many researches (Read, Collop, and Singleton 1997; Tabaković et al. 2010; Modarres 2013).

This test describes a method to estimate the resistance to fatigue failure of bituminous mixtures.

The mixtures are investigated under repeated load applications with a constant load mode using the NAT machine (A. T. Subhy 2016).

In Table 6.2 the main parameters of ITFT test are reported.

The fatigue life is determined as the total number of load applications that cause a complete fracture of the specimen.

Table 6.2: Main parameters of ITFT test (EN-12697:24 2012)

Parameter	Value
Test temperature [°C]	20
Poisson's ratio	0.35
Loading condition	Controlled-stress
Loading rise-time [s]	0.1 loading time and 0.4 rest time

The results should only be considered as indicating the fatigue characteristics of bituminuos mixtures.

The specimens are conditioned at the test temperature before being placed in the test frame, centred on and with the flat faces of the specimen perpendicular to the bottom loading strip.

The top loading strip is then being placed on the frame so that it is located centrally on the specimen. The loading is then applied via the test apparatus.

Each specimen is tested at different target level of the maximum tensile stress at the centre of the specimen.

For each specimen, the maximum tensile horizontal strain at the centre of the specimen is calculated from Poisson's ratio, the maximum tensile stress at the centre of the specimen and the indirect tensile stiffness modulus at the maximum tensile stress at the centre of specimen.

For a full test, shall be carried out determinations on not less than ten specimens for mixture with a maximum nominal aggregate size of 20 mm and below and on not less twelve specimens for mixture with a maximum nominal aggregate size greater than 20 mm.

Air void content is controlled by the compaction effort and is one of the most important variables affecting the fatigue resistance of compacted bituminous mixtures (J. Harvey et al. 1994).

Infact, as shown earlier, the compaction process affects the residual air void. This aspect has direct consequences on master curve and fatigue cracking (Fordyce 1997).

Hight air void values entail lower values of moduli and lower fatigue life (John Harvey and Tsai 2007).

Good compaction provides increased resistance to deformation, higher durability under traffic for the wearing course, reduced risk to water penetration (frost damage), fretting and embrittlement of the binder, and an even riding surface (Hartman, Gilchrist, and Walsh 2001).

Lower air void content creates a more homogeneous aggregateasphalt structure with fewer, smaller, and better-distributed voids, resulting in less stress concentration at large voids (John Harvey and Tsai 2007).

Previous investigations (Finn 1967) of this problem indicate that there is a correlation between mix stiffness and fatigue life.

This correlation indicates that a simple stiffness test might possibly be used to predict fatigue failure (Maupin 1971).

6.4 Rutting

Permanent deformation or rutting is one of the most common forms of load-associated distress in flexible pavements (A. T. Subhy 2016). It is a failure of the flexible pavements in which material under the wheel path flows and densifies to form a depression or rut (Sunarjono 2013).

Rutting occurs due to various mechanisms such as (Irfan et al. 2017; Eisenmann and Hilmer 1987):

- densification (compaction) due to the repeated loading;
- plastic shear deformation due to the repeated action of shear and tensile stress, and/or;
- loss of materials under wheel path due to repeated heavy traffic loads.

Densification (decrease in volume and increase in density) of the asphalt concrete occurs in first few years of service life (initial rutting) while the shear deformation is manifested due to the material movement beneath the wheel path and causes upheaval on the sides of the path/roadway (secondary rutting).

If a pavement has been well compacted during construction, further densification during rutting is unlikely, and permanent deformation is principally due to shear flow (Eisenmann and Hilmer 1987).

Rutting phenomenon is illustrated in Figure 6.4. It is possible to observe the relationships of strain-time and stress-time when a wheel load is applied to a road pavement. Wheel load entails a deformation or strain of the material. Most of this is recoverable when the load goes away, but a small part may remain.

Over time, with a large number of load applications, these small irrecoverable strains accumulate to form permanent deformation, which manifests as rutting in the pavement (Sunarjono 2013). For this reason, it is possible to affirm that rutting is influenced by mixture properties (i.e. volumetric composition, material properties, aggregate skeleton interlocking).

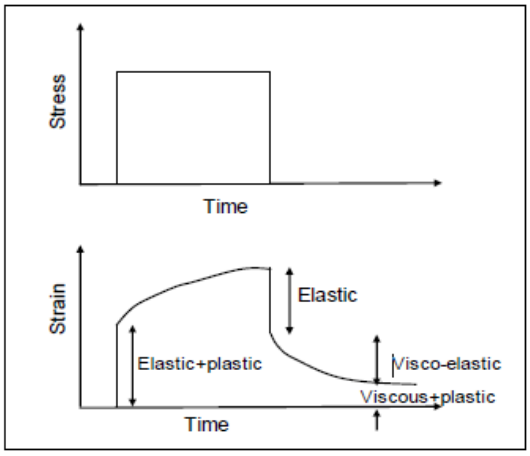

Figure 6.4: Idealised response of a bituminous mixture (Sunarjono 2013).

The RLAT test measures the permanent deformation that occurs in a sample after applying a certain stress and frequency (Al-Mosawe 2016). It was carried out with the Nottingham Asphalt Tester (NAT) procedure.

All the samples have been subjected to a particular preparation protocol (DD-226 1996). It consisted of:

- Coat the ends of the specimen (top and bottom surface) with a thin layer of silicone grease.
- Coat the ends of the specimen (top and bottom surface) with graphite flakes or powder.
- Store the samples in a dry atmosphere (< 65 % relative humidity) at a temperature of 20 °C ± 5 °C. Specimens shall not be stacked.

Before the test, all samples have been removed from storage and place it at the test temperature (30 ± 0.5 °C) for at least four hours to reach the uniform temperature. After that, each sample has been subject to RLAT test.

During the test, the specimen is positioned vertically between the upper and lower steel loading platens. The repeated load is applied axially, while the vertical deformation of the specimen is measured by two sensor (LVDTs) mounted on the upper loading platen (Abdulmajeed and Muniandy 2017; Sunarjono 2013). The pulsating load consists of a square wave form with a frequency of 0.5 Hz (i.e. a pulse of one second duration followed by a rest period of one second duration). This simulates the slow moving traffic that leads to the most deformation in a real road (Sunarjono 2013).

The test consists of applying a number of load pulses to the flat faces of the specimen and recording the resulting deformation (Abdulmajeed and Muniandy 2017). It is composed by two main steps: i) a precondition step and; ii) a measurement step.

The measure of the specimen's resistance to permanent deformation corresponds to the axial strain obtained at the end of the test. In Table 6.3 the main parameters of RLAT test are reported.

Table 6.3: Main parameters of RLAT test (DD-226 1996).

Parameter	Value
Temperature [°C]	30 ± 0.5
Axial stress [kPa]	100 ± 2
Load application period [s]	1
Rest period [s]	1
Conditioning stress [kPa]	10
Conditioning period [s]	600 ± 6
Number of load applications [pulse]	1800
Test duration [s]	3600

The axial strain (ε_d) has been calculated using the following equation (DD-226 1996):

$$\varepsilon_{d,(n,T)} = \frac{\Delta h}{h_0} \qquad \text{(Eq. 21)}$$

Where, $\varepsilon_{d,(n,T)}$ is the axial strain caused to the specimen after *n* applications of load at temperature *T* (°C); h_0 is the original distance between the specimen loading surfaces (mm); *h* is the axial deformation (change in distance between the specimen loading surfaces, mm).

According to Pasandin and Perez (2014) studies, there are no requirements for the acceptance of conventional mixtures in terms of RLAT results.

However, this test is useful to compare the performance of the different mixtures analysed.

The benefit of using the RLAT test is that it is simple, available, and it represent the frequent passage of vehicles in the road by applying repeated load (Al-Mosawe 2016).

An example of RLAT results (accumulated permanent deformation values versus the number of loading cycles) is reported in Figure 6.5. The axial strain increase with load cycles during the test.

Each curve represents the average of at least four curves. It was obtained by the average of the percent strain values at 10, 100, 1000, 1400 and 1800 pulses.

Maximum axial strain value is one of parameters used to evaluate the permanent deformation.

It is the value of axial strain at 1800 pulses. Lower values of this parameter correspond to mixes with higher resistance to permanent deformations.

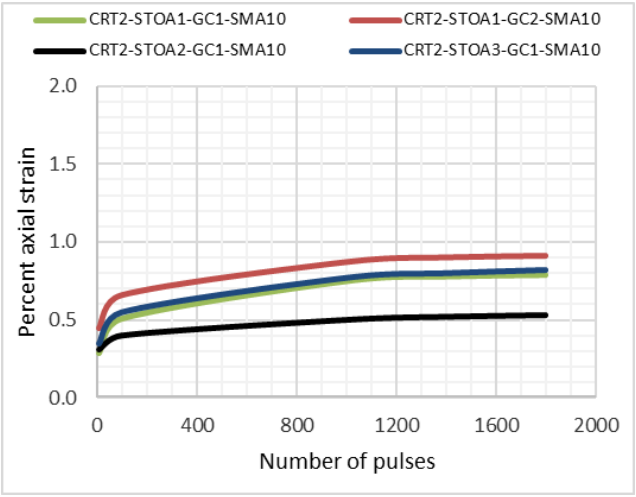

Figure 6.5: Accumulated permanent deformation vs. number of loading cycles (RLAT test).

Symbols. STOA1: short-time oven aged (@180°C for 60 minutes); STOA2: short-time oven aged (@180°C for 240 minutes); STOA3: short-time oven aged (@135°C for 240 minutes); GC1: Gyratory compaction with standard procedure; GC2: Gyratory compaction with interrupted procedure (stops of 60 seconds); SMA10: Stone Mastic Asphalt with an upper sieve size of the aggregate of 10 mm; CRT2: sample with CRT2 rubber.

Another typical test result is the relationship between total cumulative permanent strain and number of cycles (Al-Mosawe 2016). It consists of three stages (see Figure 6.6): primary stage, secondary stage, and tertiary stage.

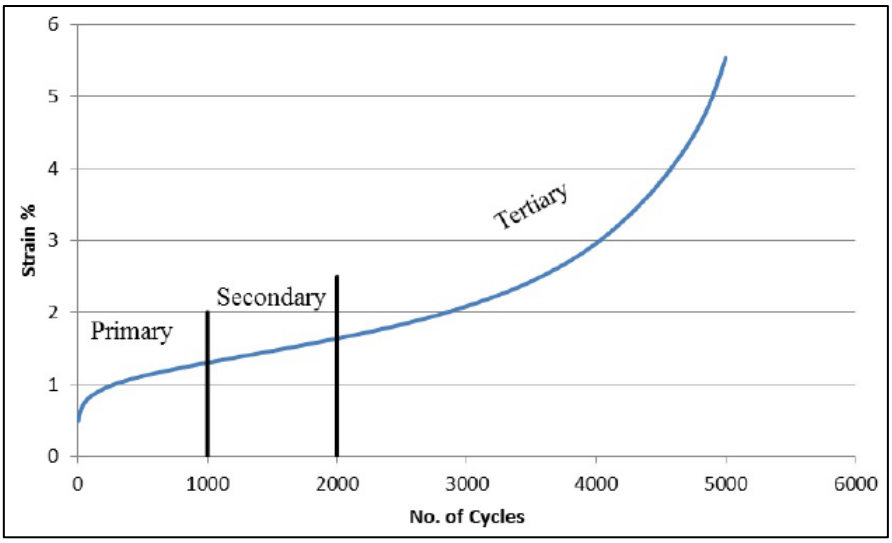

Figure 6.6: The three Stages of RLAT Test (source: Al-Mosawe 2016)

In the primary stage, the permanent strain accumulates rapidly and then the rate of increase in permanent strain per cycle starts to decrease until it reaches a constant value; this will be the starting point of the secondary stage. After that, the sample begins to gain strain again and the rate of strain accumulation starts to increase rapidly; this is considered to be the onset of the tertiary stage (Zhou, Scullion, and Sun 2004).

6.5 Results

Accumulated permanent deformation values versus the number of loading cycles was recorded during the RLAT test. Each curve represents the average of at least four curves. They are classified based on mix disign (PA or SMA10) and type of rubber used (CRT1, CRT2, CRN or control). All diagrams had been reported in ANNEX 2.

6.5.1 Stiffness

Related to stiffness analysis, Table 6.4 summarise the following parameters:

- Stiffness value of each case investigated.
- Stiffness variation related to:
  - Interrupted compaction effect: stiffness variations between STOA1-GC1 and STOA1-GC2.
  - Aging time effect: stiffness variations between STOA1-GC1 and STOA2-GC1.
  - Aging temperature effect: stiffness variations between STOA3-GC1 and STOA2-GC1.

In Table 6.5, a quantitative trend of stiffness is represented. The symbol + means that there is an increase of stiffness variation less than 10%; the symbol ++ means that there is an increase of stiffness variation more than 10%; the symbol - means that there is a decrease of stiffness variation less than 10%; the symbol -- means that there is a decrease of stiffness variation more than 10% and; the symbol = means that the stiffness variation is not significant (less than 2% in absolute value).

Table 6.4: Stiffness [MPa]

	Stiffness				Stiffness variation		
	STOA1-GC1	STOA1-GC2	STOA2-GC1	STOA3-GC1	Interrupted compaction effect	Aging time effect	Aging temperature effect
PA-CRT1	915	-	1904	1670	-	108%	14%
PA-CRT2	1233	1516	1913	1662	23%	55%	15%
PA-CRN	1229	1524	1860	1576	24%	51%	18%
PA-control	1155	1339	1713	1232	16%	48%	39%
SMA10-CRT1	3844	-	5750	4186	-	50%	37%
SMA10-CRT2	3348	3170	5222	4666	-5%	56%	12%
SMA10-CRN	3591	4432	6644	5558	23%	85%	20%
SMA10-control	2480	3196	5940	4017	29%	140%	48%

Symbols. STOA1: short-time oven aged (@180°C for 60 minutes); STOA2: short-time oven aged (@180°C for 240 minutes); STOA3: short-time oven aged (@135°C for 240 minutes); GC1: Gyratory compaction with standard procedure; GC2: Gyratory compaction with interrupted procedure (stops of 60 seconds); PA: Porous Asphalt; SMA10: Stone Mastic Asphalt with an upper sieve size of the aggregate of 10 mm; control: sample without rubber; CRT1: sample with CRT1 rubber; CRT2: sample with CRT2 rubber; CRN: sample with CRN rubber.

In the light of the results obtained, the stiffness analysis has shown that:

- Effects of different laboratory short-term oven aging (STOA), in terms of stiffness variation, are more evident in SMA10 samples than in PA samples.
- The stiffness variations of SMA10 mixes are higher than PA mixes (from -5% to 140% for SMA10 and from 14% to 108% for a PA).
- Effects of short-term oven aging (aging time and aging temperature effects) are more evident than interrupted compaction effects. In the first case the stiffness variations vary in the range of 12%-140%; in the second case it varies in the range of -5% to +29%.
- Mixes exposed to STOA1 have the lowest stiffness values. Instead, mixes exposed to STOA2 have the highest stiffness value.
- Aging time is the main parameter that influence the stiffness variations.
- Higher aging temperatures are associated with higher stiffness values. The corresponding increase varies from 14% to 39% for PA and from 12% to 48% for SMA10.
- Higher stiffness values correspond to rubberised mixtures.

Table 6.5: Stiffness trend

Stiffness	Interrupted compaction	Aging time (from 60 min to 240 min)	Aging temperature (from 135°C to 180°C)
PA – control	++	++	++
PA – CRT2	++	++	++
PA – CRT1	N.A.	++	++
PA – CRN	++	++	++
SMA10 – control	++	++	++
SMA10 – CRT2	=	++	++
SMA10 – CRT1	N.A.	++	++
SMA10 – CRN	++	++	++

Symbols. PA: Porous Asphalt; SMA10: Stone Mastic Asphalt with an upper sieve size of the aggregate of 10 mm; control: sample without rubber; CRT1: sample with CRT1 rubber; CRT2: sample with CRT2 rubber; CRN: sample with CRN rubber; +: increase < 10%; ++: increase ≥ 10%; -: decrease < 10%; - -: decrease ≥ 10%; =: unvaried (variations less than 2% in absolute value); N.A.: not available.

Figure 6.7 and Figure 6.8 highlight the stiffness of PA and SMA10 samples. It is possible to observe that:

- Stiffness of un-rubberised samples is usually lower than the stiffness of rubberised samples.
- For PA samples, un-rubberised mixes vary in the range of 1155-1713 MPa, instead rubberised mixes vary in the range of 915-1913 MPa.
- For SMA10 samples, un-rubberised mixes vary in the range of 2480-5940 MPa, instead rubberised mixes vary in the range of 3170-6640 MPa.

Figure 6.9 and Figure 6.10 are focused on interrupted compaction effects. In this case, it is possible to note that:

- Samples made with interrupted compaction process (STOA1-GC2) present an increase of stiffness.
- For PA samples, stiffness variation is equal to +16% for control-mix, +23% for CRT2-mix and, +24% for CRN-mix (see Figure 6.9).
- For SMA10 samples (Figure 6.10), stiffness variation is equal to +29% for control-mix and, +23% for CRN-mix. Unexpectedly, CRT2-mix seems to have a decrease of stiffness (-5%).

Figure 6.11 and Figure 6.12 are referred to aging time effects.

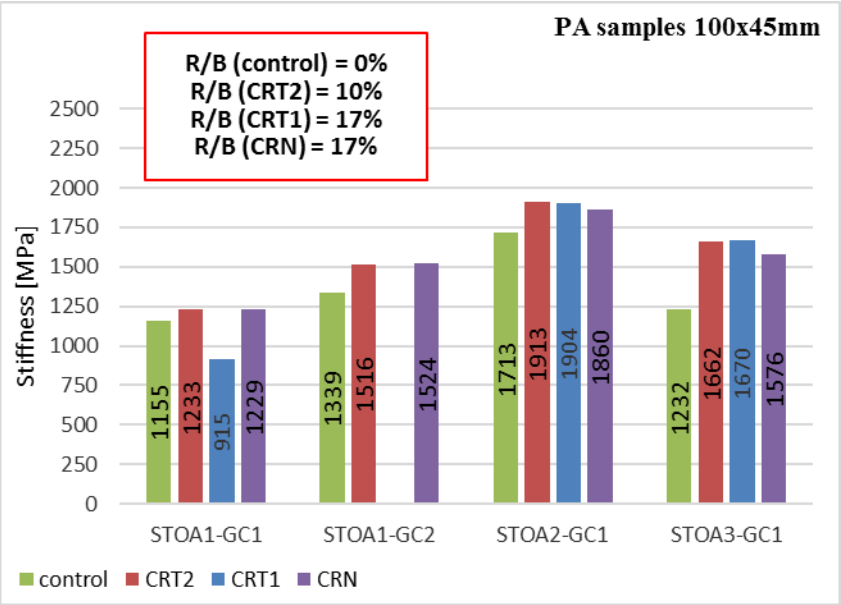

Figure 6.7: Stiffness [MPa] for PA.

Symbols. R: rubber; B: bitumen; R/B: rubber-bitumen ratio; PA: Porous Asphalt; control: sample without rubber; CRT1: sample with CRT1 rubber; CRT2: sample with CRT2 rubber; CRN: sample with CRN rubber; STOA1: short-time oven aged (@180°C for 60 minutes); STOA2: short-time oven aged (@180°C for 240 minutes); STOA3: short-time oven aged (@135°C for 240 minutes); GC1: Gyratory compaction with standard procedure; GC2: Gyratory compaction with interrupted procedure (stops of 60 seconds).

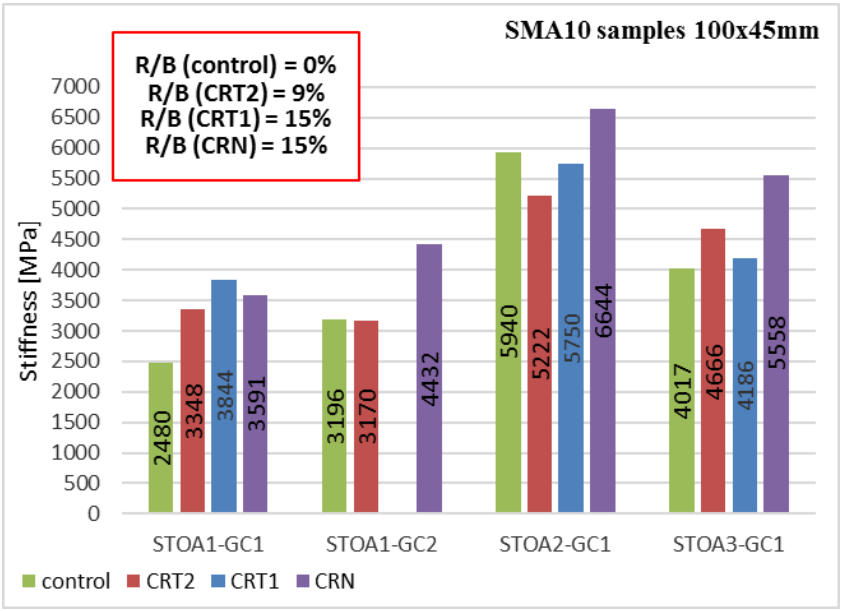

Figure 6.8: Stiffness [MPa] for SMA10.

Symbols. R: rubber; B: bitumen; R/B: rubber-bitumen ratio; SMA10: Stone Mastic Asphalt with an upper sieve size of the aggregate of 10 mm; control: sample without rubber; CRT1: sample with CRT1 rubber; CRT2: sample with CRT2 rubber; CRN: sample with CRN rubber; STOA1: short-time oven aged (@180°C for 60 minutes); STOA2: short-time oven aged (@180°C for 240 minutes); STOA3: short-time oven aged (@135°C for 240 minutes); GC1: Gyratory compaction with standard procedure; GC2: Gyratory compaction with interrupted procedure (stops of 60 seconds).

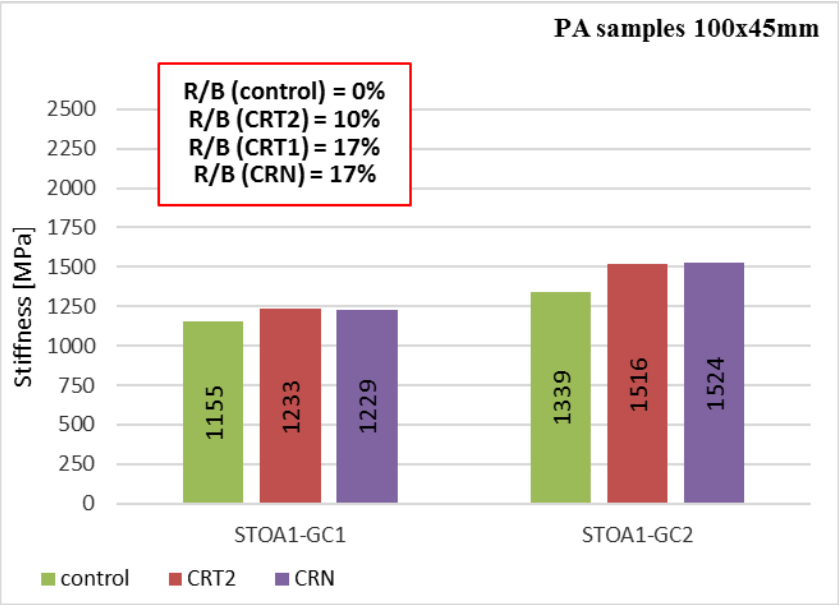

Figure 6.9: Interrupted compaction effect on stiffness [MPa], for PA.

Symbols. R: rubber; B: bitumen; R/B: rubber-bitumen ratio; PA: Porous Asphalt; control: sample without rubber; CRT2: sample with CRT2 rubber; CRN: sample with CRN rubber; STOA1: short-time oven aged (@180°C for 60 minutes); GC1: Gyratory compaction with standard procedure; GC2: Gyratory compaction with interrupted procedure (stops of 60 seconds).

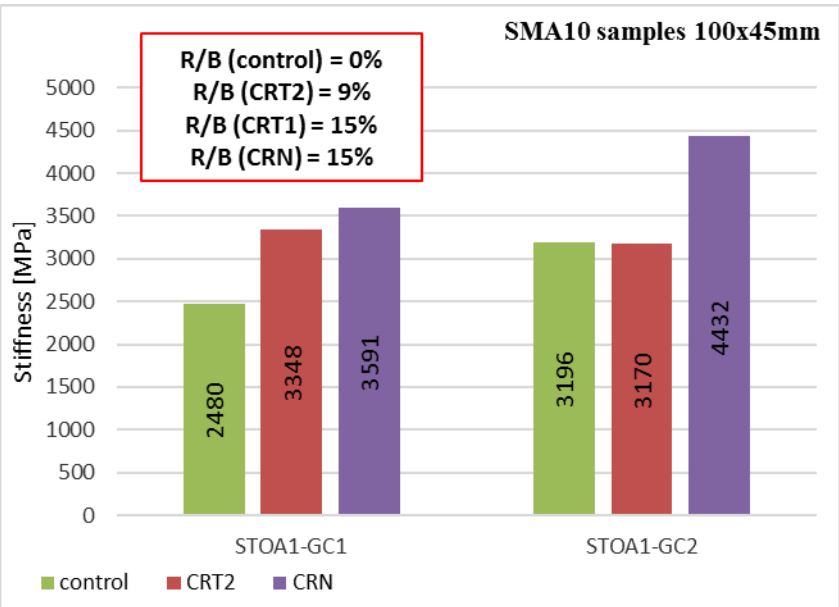

Figure 6.10: Interrupted compaction effect on stiffness [MPa], for SMA10.

Symbols. R: rubber; B: bitumen; R/B: rubber-bitumen ratio; SMA10: Stone Mastic Asphalt with an upper sieve size of the aggregate of 10 mm; control: sample without rubber; CRT2: sample with CRT2 rubber; CRN: sample with CRN rubber; STOA1: short-time oven aged (@180°C for 60 minutes); GC1: Gyratory compaction with standard procedure; GC2: Gyratory compaction with interrupted procedure (stops of 60 seconds).

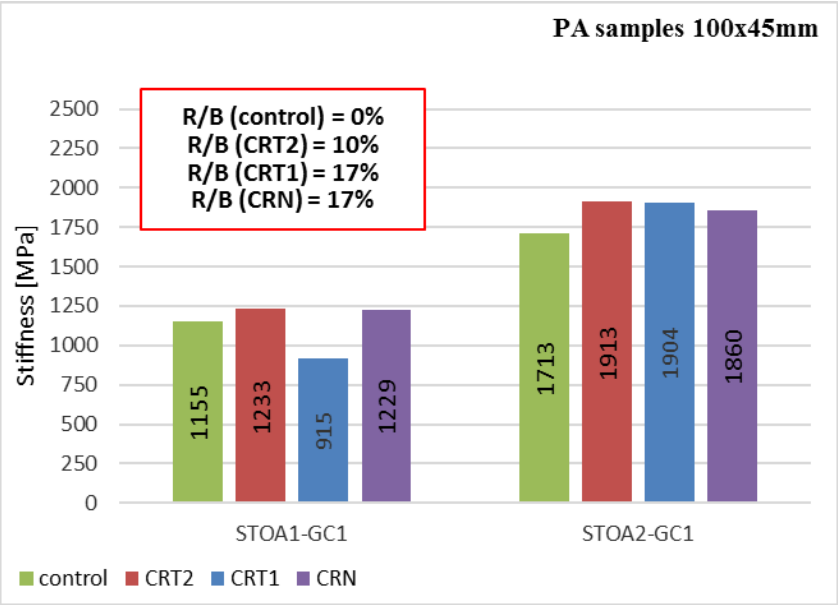

Figure 6.11: Aging time effect on stiffness [MPa], for PA.

Symbols. R: rubber; B: bitumen; R/B: rubber-bitumen ratio; PA: Porous Asphalt; control: sample without rubber; CRT1: sample with CRT1 rubber; CRT2: sample with CRT2 rubber; CRN: sample with CRN rubber; STOA1: short-time oven aged (@180°C for 60 minutes); STOA2: short-time oven aged (@180°C for 240 minutes); GC1: Gyratory compaction with standard procedure.

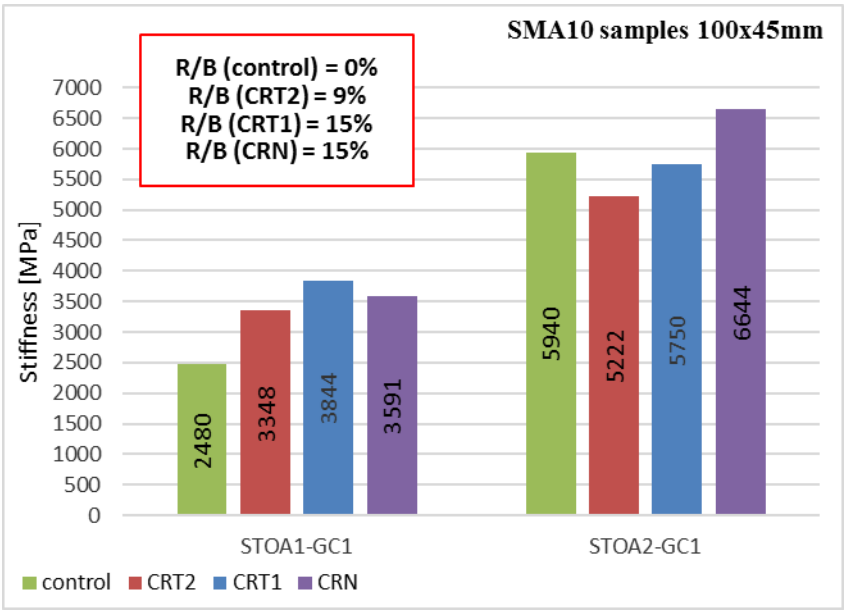

Figure 6.12: Aging time effect on stiffness [MPa], for SMA10.

Symbols. R: rubber; B: bitumen; R/B: rubber-bitumen ratio; SMA10: Stone Mastic Asphalt with an upper sieve size of the aggregate of 10 mm; control: sample without rubber; CRT1: sample with CRT1 rubber; CRT2: sample with CRT2 rubber; CRN: sample with CRN rubber; STOA1: short-time oven aged (@180°C for 60 minutes); STOA2: short-time oven aged (@180°C for 240 minutes); GC1: Gyratory compaction with standard procedure.

The increase of aging time (from 60 minutes to 240 minutes) causes a general increase of the stiffness.

For PA samples, the increase of stiffness is equal to +48% for control-mix, +55% for CRT2-mix, +112% for CRT1-mix and, +51% for CRN-mix.

For SMA10, instead, it is equal to +140% for control-mix, +56% for CRT2-mix, +50% for CRT1-mix and, +85% for CRN-mix.

In Figure 6.12, moreover, it is possible to note that:

- Stiffness variation of rubberized samples is lower than the stiffness variation of samples made without rubber (from +50% to 85% for samples with rubber and +140% for samples without rubber).
- Stiffness variation of samples made with CRN rubber is higher than the stiffness variation of samples made with treated rubber (85% for CRN and from 50% to 56% for CRT1 and CRT2 respectively).

Finally, Figure 6.13 and Figure 6.14 are referred to aging temperature effects.

In Figure 6.13, it is possible to note that:

- The increase of aging temperature (from 135°C to 180°C) entails a general increase of the stiffness (+39% for control, +15% for CRT2, +14% for CRT1 and, +18% for CRN).
- Stiffness variation of samples made with rubber is lower than the stiffness variation of samples made without rubber (from +14% to +18% for samples with rubber and +39% for samples without rubber).

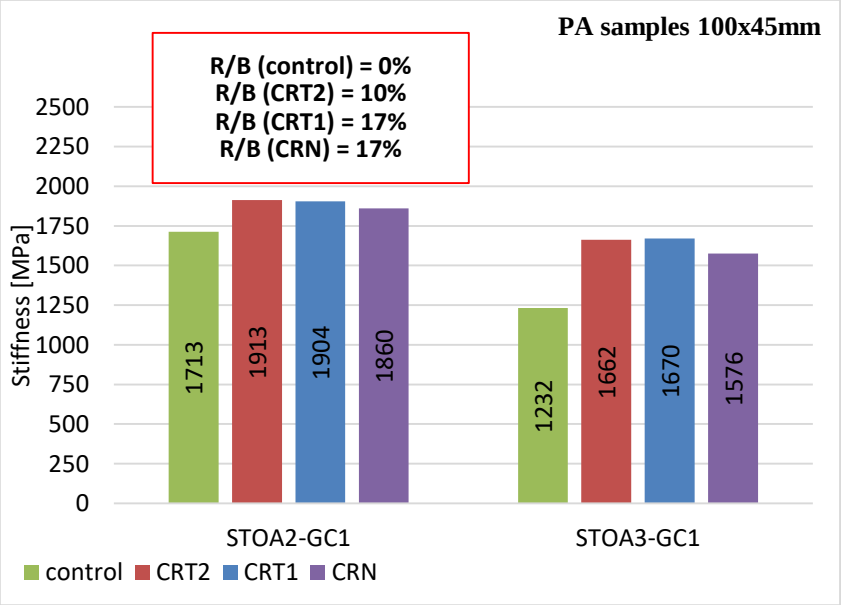

Figure 6.13: Aging temperature effect on stiffness [MPa], for PA.

Symbols. R: rubber; B: bitumen; R/B: rubber-bitumen ratio; PA: Porous Asphalt; control: sample without rubber; CRT1: sample with CRT1 rubber; CRT2: sample with CRT2 rubber; CRN: sample with CRN rubber; STOA1: short-time oven aged (@180°C for 60 minutes); STOA2: short-time oven aged (@180°C for 240 minutes); STOA3: short-time oven aged (@135°C for 240 minutes); GC1: Gyratory compaction with standard procedure; GC2: Gyratory compaction with interrupted procedure (stops of 60 seconds).

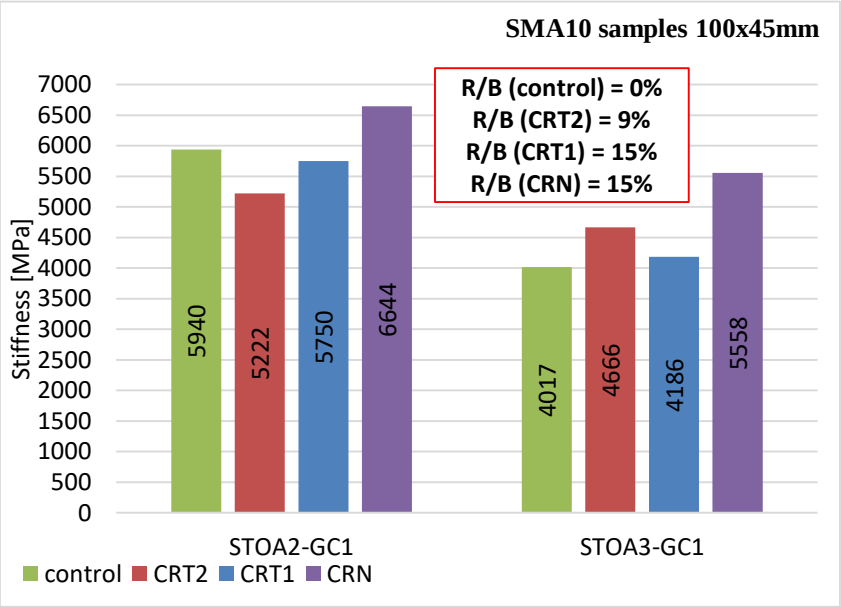

Figure 6.14: Aging temperature effect on stiffness [MPa], for SMA10.

Symbols. R: rubber; B: bitumen; R/B: rubber-bitumen ratio; SMA10: Stone Mastic Asphalt with an upper sieve size of the aggregate of 10 mm; control: sample without rubber; CRT1: sample with CRT1 rubber; CRT2: sample with CRT2 rubber; CRN: sample with CRN rubber; STOA2: short-time oven aged (@180°C for 240 minutes); STOA3: short-time oven aged (@135°C for 240 minutes); GC1: Gyratory compaction with standard procedure.

At the same time, in Figure 6.14:

- The increase of aging temperature (from 135°C to 180°C) entails a general increase of the stiffness (+48% for control, +12% for CRT2, +37% for CRT1 and, +20% for CRN).
- Stiffness variation of samples made with rubber is lower than the stiffness variation of samples made without rubber (from +12% to 37% for samples with rubber and +48% for samples without rubber)

6.5.2 Rutting

Related to rutting analysis, Table 6.6 summarise the following parameters:

- Maximum axial strain value of each case investigated.
- Maximum axial strain variation related to:
  - Interrupted compaction effect: axial strain variations between STOA1-GC1 and STOA1-GC2.
  - Aging time effect: axial strain variations between STOA1-GC1 and STOA2-GC1.
  - Aging temperature effect: axial strain variations between STOA3-GC1 and STOA2-GC1.

Table 6.6: Percent strain at 1800 pulses [%]

	Percent strain at 1800 pulses				Variation of percent strain at 1800 pulses		
	STOA1-GC1	STOA1-GC2	STOA2-GC1	STOA3-GC1	Interrupted compaction effect	Aging time effect	Aging temperature effect
PA-control	1.75	1.76	1.13	1.52	1%	-35%	-26%
PA-CRT2	1.37	1.53	0.81	1.25	12%	-41%	-35%
PA-CRT1	1.64	-	1.71	1.35	-	4%	27%
PA-CRN	1.58	1.40	0.85	1.36	-11%	-46%	-38%
SMA10-control	1.00	1.04	0.70	1.11	4%	-30%	-37%
SMA10-CRT2	0.79	0.91	0.53	0.82	15%	-33%	-35%
SMA10-CRT1	1.38	-	0.96	1.06	-	-30%	-9%
SMA10-CRN	0.98	1.01	0.77	0.88	3%	-21%	-13%

Symbols. STOA1: short-time oven aged (@180°C for 60 minutes); STOA2: short-time oven aged (@180°C for 240 minutes); STOA3: short-time oven aged (@135°C for 240 minutes); GC1: Gyratory compaction with standard procedure; GC2: Gyratory compaction with interrupted procedure (stops of 60 seconds); PA: Porous Asphalt; SMA10: Stone Mastic Asphalt with an upper sieve size of the aggregate of 10 mm; control: sample without rubber; CRT1: sample with CRT1 rubber; CRT2: sample with CRT2 rubber; CRN: sample with CRN rubber.

Figure 6.15 shows the percent strain at 1800 pulses of PA and SMA10 samples.

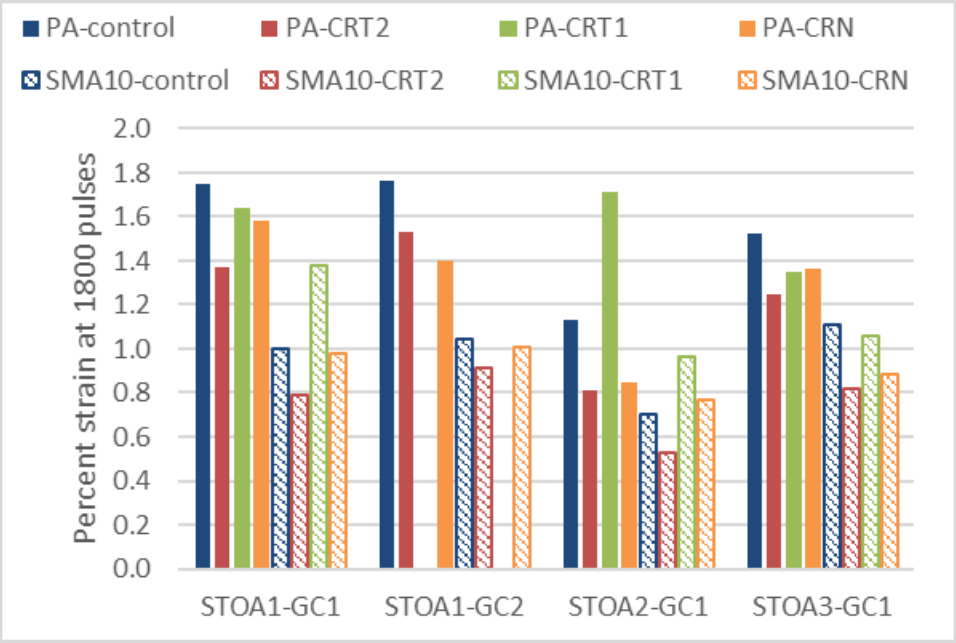

Figure 6.15: Percent strain of PA and SMA10 samples

Symbols. PA: Porous Asphalt; SMA10: Stone Mastic Asphalt with an upper sieve size of the aggregate of 10 mm; control: sample without rubber; CRT1: sample with CRT1 rubber; CRT2: sample with CRT2 rubber; CRN: sample with CRN rubber; STOA1: short-time oven aged (@180°C for 60 minutes); STOA2: short-time oven aged (@180°C for 240 minutes); STOA3: short-time oven aged (@135°C for 240 minutes); GC1: Gyratory compaction with standard procedure; GC2: Gyratory compaction with interrupted procedure (stops of 60 seconds).

It is possible to note that:

- Axial strain values of SMA-samples are lower than axial strain values of PA-samples. They vary in the range of 0.53-1.38% for SMA-cases and in the range of 0.81-1.76% for PA-cases.
- Lower values of axial strain correspond to mixes with higher resistance to permanent deformations.
- CRT2-mixes always have the lower values of axial strain (from 0.53% to 0.91% for SMA10 and from 0.81% to 1.52% for PA). This make them the best mixes in terms of resistance to permanent deformations.
- Control-mixes usually have the higher values of axial strain (from 0.70% to 1.11% for SMA and from 1.13% to 1.76% for PA). This make them the worst mixes in terms of resistance to permanent deformations.
- Referring only to rubberised mixes, CRT1-cases have the highest values of axial strain.
- The presence of rubber into the mixes seems to play a positive role and improves the rutting resistance. In fact, the use of CRT2 rubber may increase the resistance to permanent deformations up to 28% (max variation between control-cases and CRT2-cases).
- Interrupted compaction process tends to worsen the rutting resistance of mixes. The variation of axial strain is in the range of 3-15% for SMA and less of 12% for PA.
- STOA effects are more evident than interrupted compaction effects in terms of rutting. In the first case the maximum axial strain varies in the range of -46% to +27%. Instead, in the second case, it varies in the range of -11% to 15%.
- STOA process tends to improve the rutting resistance of mixes. In more detail, samples exposed to STOA2 or STOA3 have a lower axial strain than samples exposed to STOA1. A negative variation of axial strain causes an improvement of resistance to permanent deformations.
- Aging time effect is more evident than aging temperature effect.
- Aging time effect entails a variation of axial strain in the range of -46% to 4% for PA-cases and in the range of -33% to -21% for SMA-cases.
- Aging temperature effect entails a variation of axial strain in the range of -38% to 27% for PA-cases and in the range of -37% to -9% for SMA-cases.
- An unusually behaviour, in the PA-cases, is shown by CRT1-mixes. In this case, the axial strain seems to increase when mixes are exposed to STOA2 or STOA3 (+4% and +27% respectively).
- Rubberised mixes have a better rutting resistance than un-rubberised mixes, when STOA 2 (higher time of aging) or STOA 3 (higher temperature of aging) are applied.

6.6 Conclusions

Short-term oven aging and compaction process effects on stiffness and rutting have been analysed in this section. All test was carried out with the Nottingham Asphalt Tester (NAT).

Referring to stiffness, it can be concluded that:

- In all cases investigated, effects of short-term oven aging are more evident than interrupted compaction effects in terms of stiffness.
- Short-time oven aging (STOA) entails a general increase of stiffness. Mixes exposed to STOA1 (light aging) tend to have the lowest stiffness. Instead, mixes exposed to STOA2 (massive aging) have the highest stiffness and stiffness variation.
- Increase of aging time (from 60 minutes to 240 minutes) entails a general increase of the stiffness (from 48% to 108% for PA and from 50% to 140% for SMA10).
- Increase of aging temperature (from 135°C to 180°C) entails a general increase of the stiffness (from 14% to 39% for PA and from 12% to 48% for SMA10).
- Rubberised mixes always have a higher stiffness value than mixes without rubber.
- The stiffness variation of rubberised SMA10 samples is lower than un-rubberised SMA10 samples when differents short-term oven aging are compared.

Referring to rutting, the main conclusions are:

- In all cases investigated, effects of short-term oven aging are more evident than interrupted compaction effects in terms of rutting.
- STOA process tends to improve the rutting resistance of mixes. Samples exposed to STOA2 or STOA3 have a lower axial strain than samples exposed to STOA1. A negative variation of axial strain causes an improvement of resistance to permanent deformations.
- Usually, the interrupted compaction process entails a worse resistance to permanent deformations.
- Rubberised mixes have a better resistance to rutting when STOA 2 (higher time of aging) or STOA 3 (higher temperature of aging) are applied.
- SMA mixes are more resistant to permanent deformation than PA mixes.
- CRT2-mixes are the most resistant to permanent deformation.

7 Expected life & Pay adjustment of flexible pavements: analyses and simulations[3]

7.1 Introduction

As-built pavements may present nonconformities (e.g., insufficient thickness, high air voids content, lack of asphalt binder). In these situations, data analysis, derivation of pay adjustment, and/or maintenance/rehabilitation options are needed.

Life cycle cost analysis (LCCA) can help derive the real consequences of nonconformities over pavement life (Symons and Monte 2010; Dilip, Ravi, and Sivakumar Babu 2013; N. J. Santero et al. 2008; N. Santero et al. 2011). Life cycle costs analysis (LCCA) is an economic evaluation tool that can provide valuable guidance to transportation officials in management decision process.

The application of LCCA to pavement management is vital because it permits the selection of the best alternative, based on the analysis of agency costs and user costs, taking into account, after selecting pavement type, different maintenance and rehabilitation (M&R) strategies within the same pavement type. Additionally, environmental costs can be considered.

Different methods can be used to assess the expected life of pavements in terms of rehabilitation and/or maintenance (see Table 7.1).

The AASHTO Guide 93 (AASHTO 1993) is the first tool used to design new and rehabilitated highway pavements in the United States. All versions of the AASHTO Design Guide are empirical design methods based on field performance data measured at the AASHO Road Test in 1958-60.

The overall approach of the 1993 AASHTO procedure for both flexible and rigid pavements is to design for a specified serviceability loss at the end of the design life of the pavement.

[3] This section mainly refers to the papers Praticò F.G., Noto S., Astolfi A., 2016 (see references).

Serviceability is defined in terms of the Present Serviceability Index (PSI) which varies between the limits of 5 (best) and 0 (worst). Serviceability loss at end of design life, ΔPSI, is partitioned between traffic and environmental effects.

The mechanistic approach, instead, seeks to explain phenomena only by reference to physical causes.

In pavement design, the phenomena are the stresses, strains and deflections within a pavement structure, and the physical causes are the loads and material properties of the pavement structure.

The relationship between these phenomena and their physical causes is typically described using a mathematical model. Various mathematical models can be used; the most common is a layered elastic model.

Along with this mechanistic approach, empirical elements are used when defining what value of the calculated stresses, strains and deflections result in pavement failure.

The relationship between physical phenomena and pavement failure is described by empirically derived equations that compute the number of loading cycles to failure.

So, basically, the mechanistic-empirical approach (Q. Li et al. 2011) uses both mathematical models and experimental results to estimate the future pavement distress under a defined pavement condition of climate, traffic patterns, materials properties and pavement structure (ARA 2004). However, the accuracy of the model estimation is dependent on calibration.

The mechanistic-empirical approaches used in this study are described below.

KenPave (Y. H. Huang 2003) analyzes pavements based on multi-layer elastic theory under a circular loaded area. This method can be applied to layered systems with different behaviours (i.e., linear elastic, nonlinear elastic, or viscoelastic).

For KenPave it is noted that modulus (derived through the Witczak formula, Asphalt Institute 1979), Poisson ratio, and thickness for the different layers (PEM/DGFC, BIC, BAC, CTB, SBA, SGR) are the main inputs.

The main output are stresses, deflections, and design life. Damage analysis can be made by dividing each year into a maximum of 12 periods, each with a different set of material properties.

MnPAVE method (MnPAVE 2012), instead, combines empirical relationships with a representation of the physics and mechanics behind flexible pavement behavior.

The software relies on finding: i) tensile strain at the bottom of the asphalt layer; ii) compressive strain at the top of the subgrade and; iii) maximum principal stress in the middle of the aggregate base layer.

MnPAVE simulates traffic loads on a pavement using a Layered Elastic Analysis (LEA) called WESLEA.

All layers are assumed to be isotropic in all directions and infinite in the horizontal direction, whereas the last layer is assumed to be semi-infinite in the vertical direction.

The software calculates normal and shear stress, normal strain, and displacement at specified locations.

It consists of three inputs: climate, structure, and traffic; and three design levels: basic, intermediate, and advanced.

For bituminous layers the following parameters have to be specified: asphalt binder type (e.g., PG 70-28), asphalt binder content (w/w), air voids content, modulus, thickness.

Output includes the expected life of the pavement, which is calculated using a damage factor based on Miner's Hypothesis. Reliability is estimated using Monte Carlo simulation.

The M-EPDG (Mechanistic-Empirical Pavement Design Guide) have been proposed as an advanced pavement design tool. With its basis in empirical field or laboratory observed performance and mechanistic principles, resulting designs are assumed to produce improved thickness estimates over traditional empirical designs (ARA 2004).

The MEPDG procedure offers several improvements over the AASHTO Guide 1993 and presents a new paradigm in the way pavement design is performed.

However, MEPDG is substantially more complex than the AASHTO Guide 1993 and it requires significantly more inputs from the designer.

While use of the empirical method (AASHTO Guide 1993) has been successful for different years, it was recognized that it presents several limitations including being based on a limited number of pavement sections at one location, one climate, limited traffic, and one limited set of materials (AASHTO 1993).

However, this design procedure is insufficient for the traffic, materials and construction techniques of today.

One of the main parameters of AASHTO Guide 1993 is the Structural Number (SN).

It is indicative of the total pavement thicknesses required and it is based on: i) layer coefficient; ii) layer thickness and; iii) layer drainage coefficient.

The structural number expresses the structural strenght of a pavement required for given combination of soil support (Resilient Modulus, MR), total traffic expressed in equivalent 18-kip single axle loads, terminal serviceability and, environment.

The SN must be converted to actual thickness of surfacing, base and subbase, by means of appropriate layer coefficients representing the relative strength of the construction materials.

Layer coefficients are based on the elastic moduli and have been determined based on stress and strain calculations in a multilayered pavement system (Van Til et al. 1972).

Using these concepts, the layer coefficient may be adjusted (increased or decreased) in order to maintain a constant value of stress or strain required to improve comparable performance.

The resilient modulus is a measure of the elastic property of soil recognizing certain nonlinear characteristics. It can be used directly for the design of flexible pavements but must be converted to a modulus of subgrade reaction (k-value) for the design of rigid or composite pavement.

Resilient modulus refers to the material's stress-strain behavior under normal pavement loading conditions. The procedure for estimating the resilient modulus depends on material type.

Although the elastic (resilient) modulus has been adopted as the standard material quality measure, it is necessary to identify (corresponding) layer coefficients because of their treatment in the structural number design approach.

These aspects represent the main limits of the AASHTO 1993 when unconventional materials are used.

Materials used in pavement constructions play a fundamental role. It is known that properties of materials change with time and these changes may be advantageous or disadvantageous to performance. However, in most cases, time is a net negative factor and works to reduce serviceability.

In light of this, the basic advantages of a mechanistic-empirical pavement design method (e.g., MEPDG) over a purely empirical one (e.g., AASHTO 1993) are:

- It can be used for both existing pavement rehabilitation and new pavement construction.
- It accommodates changing load types.
- It can better characterize materials allowing for:
    - Better utilization of available materials.
    - Accommodation of new materials.
    - An improved definition of existing layer properties.
- It uses material properties that relate better to actual pavement performance.
- It provides more reliable perform.
- It better defines the role of construction.
- It accommodates environmental and aging effects on materials.

Table 7.1: Characteristics of design methods applaied.

Method	AASHTO 93	KenPave (*)	MnPAVE	M-EPDG
Inputs	t_i, M_R, a_i and m_i	t_i, E_i, v_i	t_i, m.c., E_i	t_i, m.c., E_i
Traffic	ESALs	TNLR	ESALs	AADTT
Design Period Length [years]	20	20	20	20

Symbols. t_i: layer thickness; M_R: subgrade resilient modulus; a_i: structural coefficient; m_i: drainage coefficients; E_i: stiffness modulus of bituminous mixtures; v_i: Poisson's ratio; m.c.: materials characteristics; (*): (Y. H. Huang 2003; Tarefder, Ahmed, and Rahman 2013; Dilip, Ravi, and Sivakumar Babu 2013)*; ESALs: equivalent single axle load; TNLR: total number of load repetitions for each load group during each period; AADTT: average annual daily truck traffic.*

Moduli and fatigue/rutting properties estimate is crucial in this process. The characterization of the subgrade and base materials (used as unbound) can be carried out based on soil classification, based on soil properties

which correlate whit the resilient modulus (e.g., unconfined compression test, California bearing ratio, ect.), or based on actual laboratory testing (resilient modulus, AASHTO-T294 1994; AASHTO-T274 1982; AASHTO-T307 1999; NCHRP 1-28A 2003; Hossain 2010).

The same applies to the resilient modulus of Hot Mix Asphalt (HMA) which can be estimated (Table 7.2), back calculated (starting from other properties/tests), or obtained through laboratory tests (see Tjan and Napitupulu 2013).

Table 7.2: Evaluation of the resilient modulus of HMA.

Method	Reference	Main inputs
Van Der Poel equation	(Van Der Poel 1954)	T_W, T_{RB}, T, PI
Shell nomograph	(Bonnaure et al. 1977)	S_B, V_G, V_B
Bonnaure et al. equation	(Bonnaure et al. 1977)	S_B, V_G, V_B
Heukelom and Klomp equation	(Heukelom, W. and Klomp 1964)	S_B, C^1_V, C_V
Asphalt Institute equations	(Asphalt Institute 1979)	β_1, β_5, f, T, P_{200}, AV, η, V_B,
Witczak Predictive equation	(Andrei, Witczak, and Mirza 1999)	η, f, AV, V_{Beff}, $P_{3/4}$, $P_{3/8}$, P_4, P_{200}
Tjan and Napitupulu equation	(Tjan and Napitupulu 2013)	P_{max}, ν_i, L, H

Symbols. T_W: time of loading; T_{RB}: softening point; T: temperature [°F]; PI: penetration index; S_B: stiffness modulus of bitumen; V_G: percent volume of aggregate [%]; V_B: percent volume of bitumen [%]; C^1_V: aggregate volume concentration; C_V: $V_G / (V_G + V_B)$; β_1 and β_5: temporary constants; f: load frequency [Hz]; P_{200}: percentage by weight of aggregate passing through a No. 200 sieve (0.075 mm) [%]; AV: volume of air voids [%]; η: bitumen viscosity [106 poise]; V_{Beff}: percent effective bitumen content by volume [%]; $P_{3/4}$: percent retained on 3/4 in. (19 mm) sieve by total aggregate weight (cumulative) [%]; $P_{3/8}$: percent retained on 3/8 in. (9.5 mm) sieve by total aggregate weight (cumulative) [%]; P_4: percent retained on #4 (4.75 mm) sieve by total aggregate weight (cumulative) [%]; P_{max}: peak load; ν_i: Poisson's ratio; L: thickness of cyclindrical specimen [mm]; H: recoverable horizontal deformation [mm]; HMA: Hot Mix Asphalt.

Air voids content, asphalt binder percentage and type, aggregate properties greatly affect moduli (see Table 7.2), fatigue (Micaelo et al. 2015), rutting laws and expected life (Anderson and Kennedy 1993; Mannan, Islam, and Tarefder 2015), and surface performance (Mensching et al. 2013; Pratico' and Moro 2011).

Consequently, pay adjustment depends on nonconformities relating to the above HMA characteristics (Burati et al. 2003; Banerjee, De Fortier Smit, and Prozzi 2012; Pratico' and Casciano 2015).

Additional issues arise when dealing with bridge pavements, where deck-pavement interaction makes the derivation of pay adjustments well-grounded in logic even more complex (Pratico 2007; Park et al. 2009; Bridge Engineering Section Alberta Transportation 2013; EAPA 2013; T. D. Larson, Seavey, and Lange 1998).

All the above issues make more complex acceptance procedures and pay adjustment derivation.

7.2 Methodology

Figure 7.1 summarises main tasks and methodology used in the following.

Task 1 deals with data gathering, for both as-design pavement and as-built pavement. Two types of as-design pavements are given, based on their surface course.

Task 2 focuses on the derivation of the expected life for each solution. 40 case-studies are considered (13 cases with PEM and 27 cases with DGFC).

Each pavement-case under investigation is analysed in detail and model inputs are assessed. Through the different algorithms expected life is derived.

Task 3 focuses on the derivation of the pay adjustment in percentage, PA_{ji}/C, where positive values represent a bonus, while negative values are penalties, *i* refers to the *i*-th pavement solution, *j* to the *j*-th method /e.g., AASHTO 1993), *C* is the construction cost.

The following algorithm was used (F.G. Praticò 2015):

$$\frac{PA_{ji}}{C} = \frac{\left(R^{D} - R^{E_{ji}}\right)}{1 - R^{D}} \qquad \text{(Eq. 22)}$$

where *D* is the expected life of the as-design pavement, E_{ij} is the expected life of the *i*-th pavement solution, estimated through the *j*-the method.

In task 4, once obtained the technical and financial indicators, analyses were carried out and average and the analysis of variance was carried out.

In Figure 7.1 the relation between relative modulus (E_i/E) and air voids content (as an effect of a different compaction) is reported.

Three linear regressions are depicted: DGFC, PEM and (Austroads and AAPA 1999). Note that, as expected, DGFC and Austroads and AAPA (1999) have a similar behaviour.

Importantly, first derivatives are quite similar (-0.06 ± 0.01). It may be observed that AV can vary due to many factors (asphalt binder percentage, aggregate grading, degree of compaction). Consequently, the above plots represent just one out of many possible curves AV vs. E_i/E.

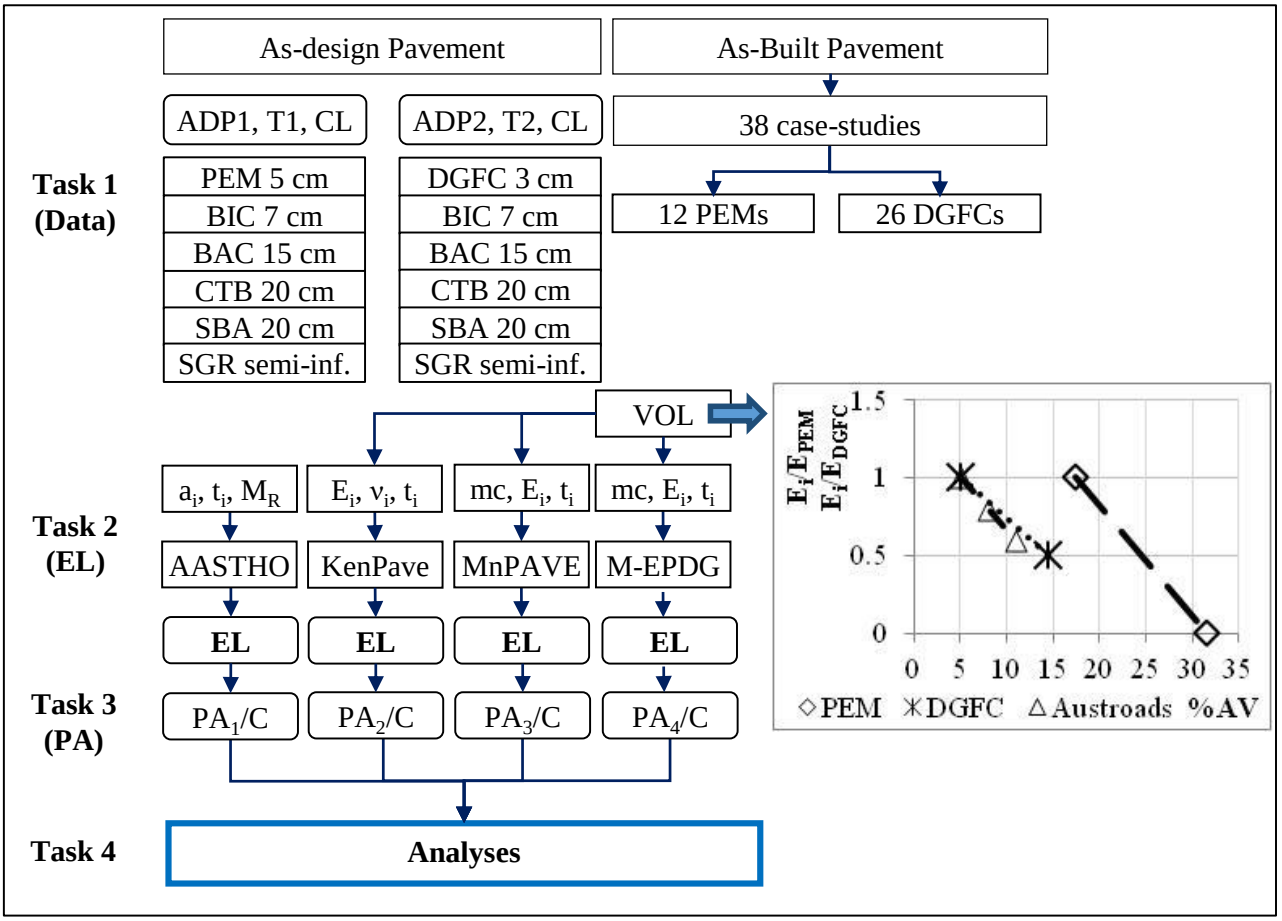

Figure 7.1: Graphical diagram of the experimental design (Praticò, Noto and Astolfi, 2016)

Symbols. ADP1: as-design pavement with PEM; ADP2: as-design pavement with DGFC; PEM: Porous European Mixture; DGFC: Dense Graded Friction Course; BIC: binder course; BAC: base course; CTB: cement-treated base; SBA: subbase; SGR: subgrade; ai: coefficients that represent the relative strength of the material (Structural Number); ti: layer thickness; MR: subgrade resilient modulus; Ei: stiffness modulus of bituminous mixtures of the i-th simulation; vi: Poisson's ratio; mc: materials characteristics (grading, air voids content, bitumen percentage and type); EL: expected life; PA/C: pay adjustments; VOL: volumetrics; AASHTO: AASHTO 1993; T1, T2: design traffic con ADP1, ADP2, respectively; CL: climate; %AV: air voids percentage; EPEM: modulus @ %AV=17.5; EDGFC: modulus @ %AV=5; Austroads: Austroads and AAPA 1999.

7.3 Analyses and results

Table 7.3 - Table 7.4 and Figure 7.2 Figure 7.3 Figure 7.4 Figure 7.5 summarise results and analyses.

Table 7.3 and Figure 7.2 illustrate contract specifications and the main nonconformities of as-built pavement. In Figure 7.2, x-axes represent the given section (1-14 and 1-26, respectively, see Figure 7.1), while y-axes report air voids content (AV, %), asphalt binder percentage (b, %), and the thickness of the surface layer (tPEM, tDGFC, tBIC, tBAC). Note that all the cores with a DGFC show percentage of air voids higher than the optimal one.

Table 7.3: Contract specifications (ANAS, 2010).

Layer	t [cm]			AV [%]			b [%]		
	min	opt	max	min	opt	max	min	opt	max
DGFC	-	3	-	3	5	6	4.5	5.5	6.1
PEM	-	5	-	16	17.5	27	4.8	5.7	5.8
BIC	4	7	8	3	6.5	8	4.1	5.0	5.5
BAC	8	15	18	3	6.5	9	3.8	4.5	5.2

Symbols. t: layer thickness; AV: air voids; b: asphalt binder by weight of aggregate; min: minimum; opt: optimum; max: maximum; PEM: Porous European Mixture; DGFC: Dense Graded Friction Course; BIC: binder course; BAC: base course.

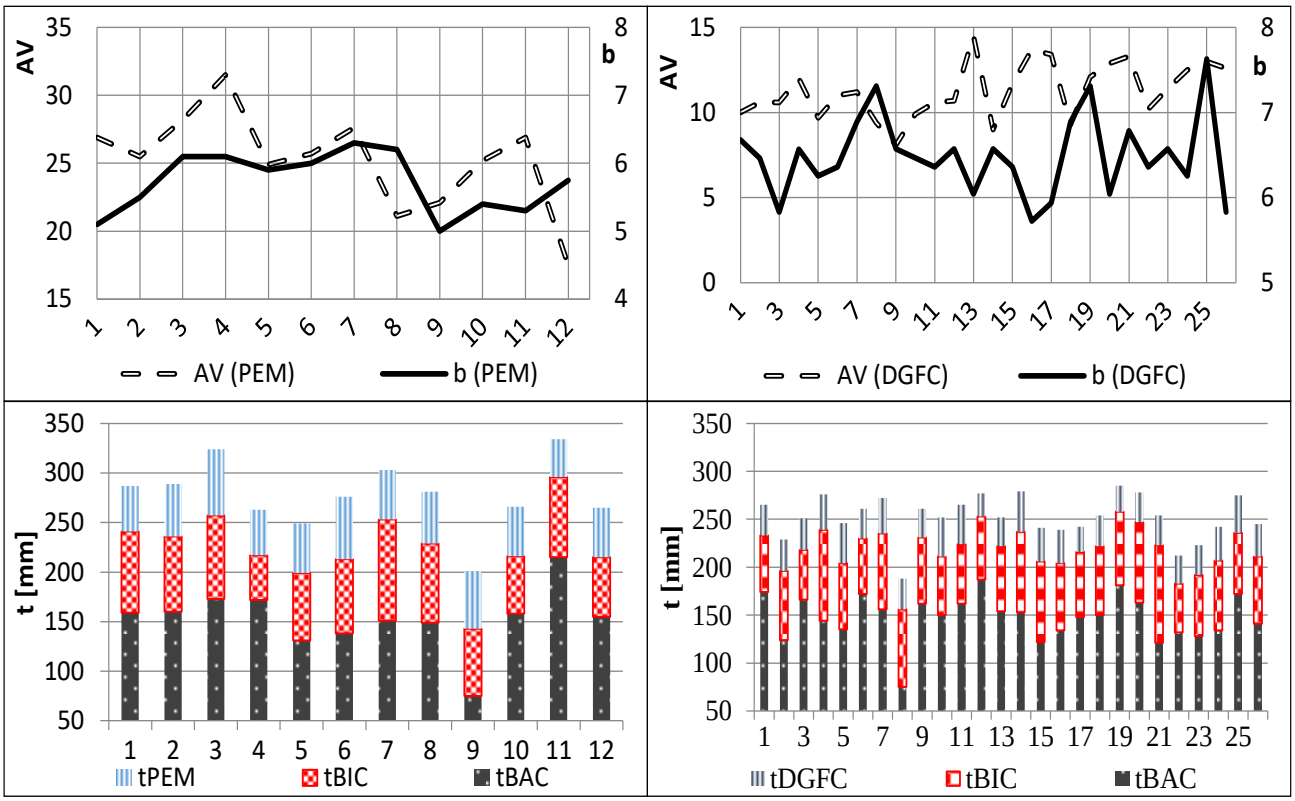

Figure 7.2: Summary of nonconformities (HMA layers; Praticò, Noto and Astolfi, 2016).

Symbols. b: bitumen [%]; AV: air voids [%]; PEM: Porous European Mixture; DGFC: Dense Graded Friction Course; tPEM: PEM thickness [mm]; tDGFC: DGFC thickness [mm]; tBIC: BIC thickness [mm]; tBAC: BAC thickness [mm]; PEM: Porous European Mixture; DGFC: Dense Graded Friction Course.

Figure 7.3 - Figure 7.4 - Figure 7.5 illustrates the expected life obtained for each method, where EL_K is the expected life obtained through the KenPave method (Y. H. Huang 2003), EL_M is the expected life obtained by using the MnPAVE method (MnPAVE 2012), EL_{ME} is the expected life according to the M-EPDG (ARA 2004) and EL_A is the expected life obtained through the well-known AASHTO Guide (AASHTO 1993).

Forty case-studies (12+26: as-built; 2: as-design, ADP1, ADP2, see Figure 7.1) are summarized.

Apart from the equality line (solid line), note that two types of interpolating straight lines are reported: with zero intercept (double line), and best (linear) fit (dotted line).

The linear regression passing for (20,20) is not depicted because it mainly overlaps the best linear fit.

The expected life estimated through the KenPave method usually yields values which are higher (for both low and high expected lives).

The expected life estimated through the MnPAVE method is higher when EL_A is lower than about 20, and *vice versa*.

Note that the same applies to EL_M. The second row of pictures refers to the pay adjustment in percentage (PA/C) for the three methods (all the mixes considered). (PA/C) is obtained through the application of equation (22).

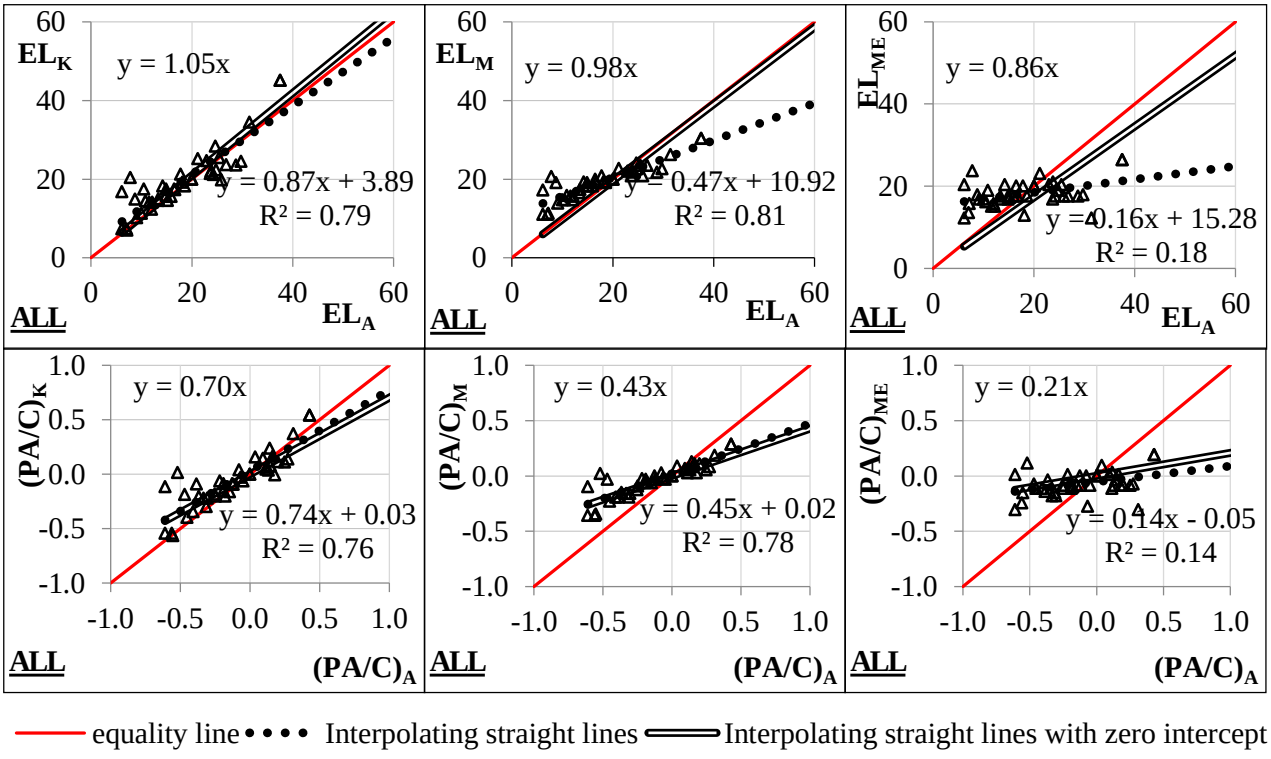

Figure 7.3: Expected life, percentage pay adjustment for the four methods (ALL cases; Praticò, Noto and Astolfi, 2016).

Symbols. EL: expected life obtained through the indicated method; PA/C: pay adjustment; K: KenPave method; M: MnPAVE method; ME: M-EPDG method; A: AASHTO 93 method; ALL: 40 cases.

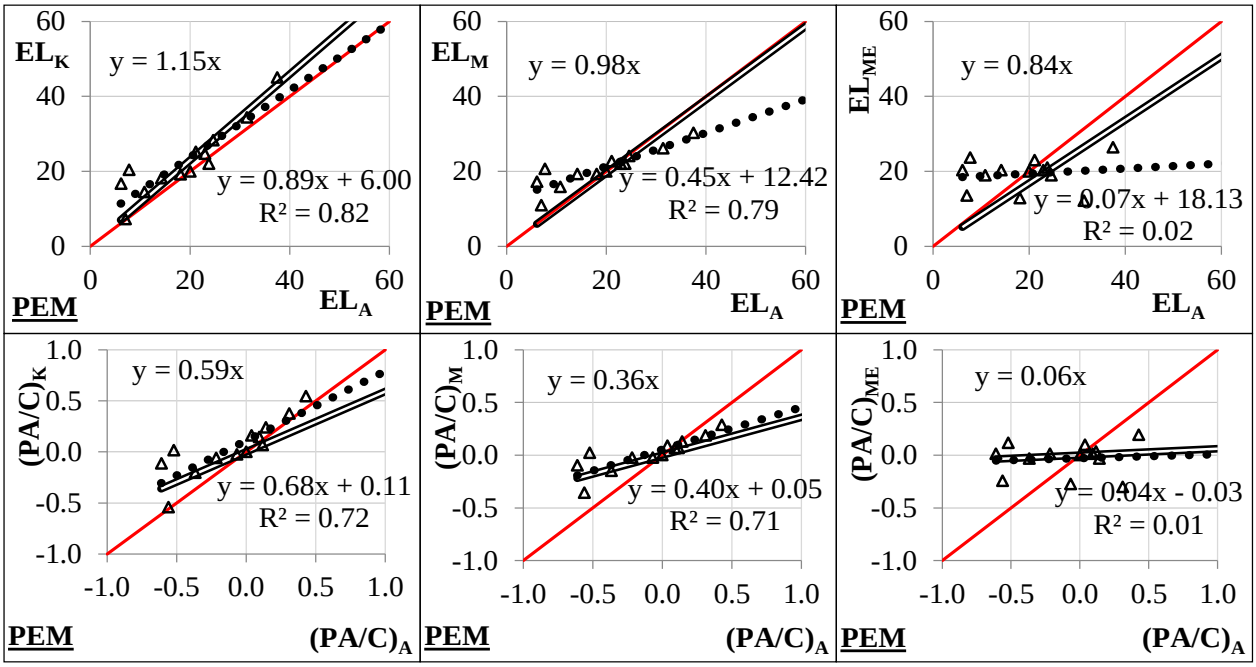

Figure 7.4: Expected life, percentage pay adjustment for the four methods (PEM cases; Praticò, Noto and Astolfi, 2016).

Symbols. EL: expected life obtained through the indicated method; PA/C: pay adjustment; K: KenPave method; M: MnPAVE method; ME: M-EPDG method; A: AASHTO 93 method; PEM: only PEM-surfaces pavements (12+1 cases).

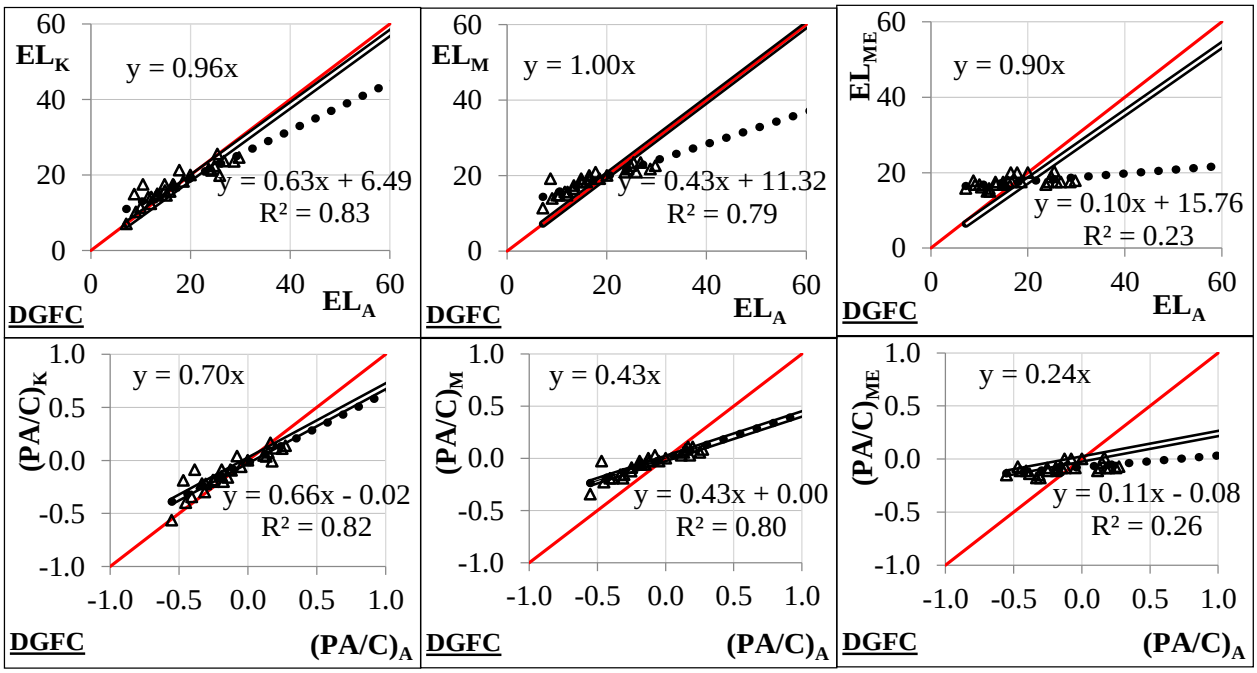

Figure 7.5: Expected life, percentage pay adjustment for the four methods (DGFC cases; Praticò, Noto and Astolfi, 2016).

Symbols. EL: expected life obtained through the indicated method; PA/C: pay adjustment; K: KenPave method; M: MnPAVE method; ME: M-EPDG method; A: AASHTO 93 method; DGFC: only DGFC-surfaces pavement (26+1 cases).

Estimates carried out through the KenPave method yield lower penalties (PA/C negative) and lower bonuses (PA/C positive), with respect to the AASHTO method. Estimates carried out through the MnPAVE method (plot in the middle) yield lower penalties and lower bonuses, with respect to the AASHTO method. The same applies to M-EPDG.

The third and fourth rows of pictures refer to the results obtained by considering only the Porous European Mixes (PEMs). For the different methods under analysis (K, A, M), expected life outcomes perform as in the general case. KenPave method yields higher values than AASHTO one. MnPAVE method yields higher values only when close to the origin of the axes.

Note that AASHTO method yields higher penalties and bonuses, which is consistent with the behaviour outlined before in the general case. The last two rows refer to the results obtained by considering only the dense-graded friction courses (DGFC). AASHTO yields a lower expected life (close to the origin) and higher EL for higher values. Consequently, AASHTO overestimates penalties and underestimate bonuses. Overall M-EPDG vs. AASHTO correlation is weak and calls for further research.

As above mentioned, slopes (m, m_{20}, m_0) and y-intercepts (q, q_{20}, q_0) of the linear regressions were derived, where q and m refer to the *best fit*, q_{20} and m_{20} refer to the straight line passing for (20,20), and m_0 corresponds to q_0=0. Note that EL-related y-intercepts are very different from zero: about 4-6 for the KenPave method, about 11-12 for the MnPAVE method, and 15-19 for the M-EPDG.

These high values point out that the methods under investigation diverge when far from the equilibrium point (EL=20). Table below summarises results in terms of expected life and consequences on pay adjustment.

Assumed an expected life of 20 years (AASHTO method), the following applies:

- the corresponding values of EL_K, EL_M and EL_{ME} are 20 (derived through regression parameters m_{20}, q_{20});
- the corresponding values of $(PA/C)_K$ and $(PA/C)_M$ are zero (derived through equation 22).

In the pursuit of examining the risk of deriving different pay adjustments, note that a given reject quality level (RQL) is usually set up (Burati et al., 2003). When the quality measure is PWL (percent within limits) this value is about 50%. In turn, it corresponds to a (PA/C) of 20%, based, for example, on the empirical law *PF=100-PA=55+0.5*PWL*. Furthermore, the highest value of bonus (PA/C positive) is usually 5-10% (Buddhavarapu et al. 2014).

Now, based on the above, the average σ of EL (in 15-30) is about 1.2-2, while for (PA/C) it is about 0.04.

On average, the coefficient of variation results 6% for EL and 40% for (PA/C). It turns out that just on the boundary between penalty and rejection, (PA/C) values are about twice the standard deviation. This fact

implies that taking into consideration the average among four values (i.e., AASHTO, KenPave, MnPAVE, M-EPDG) can halve standard deviation and can allow better estimates.

Table 7.4: EL, PA/C: main statistics.

	EL_A	0	5	10	15	20	25	30	35	40
	$(PA/C)_A$	-1.00	-0.68	-0.41	-0.18	0.00	0.15	0.28	0.38	0.47
EL-ALL	σ	7.39	5.54	3.69	1.85	0.00	1.85	3.69	5.54	7.39
	Av.	8.31	11.23	14.15	17.08	20.00	22.92	25.85	28.77	31.69
	CV	89%	49%	26%	11%	0%	8%	14%	19%	23%
PA/C-ALL	σ	0.39	0.26	0.15	0.07	0.00	0.06	0.10	0.14	0.16
	Av.	-0.53	-0.37	-0.23	-0.11	0.00	0.09	0.17	0.24	0.30
	CV	73%	71%	68%	66%	-	61%	59%	57%	54%
EL-PEM	σ	8.36	6.27	4.18	2.09	0.00	2.09	4.18	6.27	8.36
	Av.	8.29	11.22	14.14	17.07	20.00	22.93	25.86	28.78	31.71
	CV	101%	56%	30%	12%	0%	9%	16%	22%	26%
PA/C-PEM	σ	0.43	0.29	0.17	0.08	0.00	0.06	0.11	0.16	0.19
	Av.	-0.54	-0.37	-0.23	-0.11	0.00	0.09	0.17	0.24	0.29
	CV	79%	77%	75%	73%	-	70%	68%	66%	65%
EL-DGFC	σ	6.70	5.02	3.35	1.67	0.00	1.67	3.35	5.02	6.70
	Av.	8.33	11.25	14.16	17.08	20.00	22.92	25.84	28.75	31.67
	CV	80%	45%	24%	10%	0%	7%	13%	17%	21%
PA/C-DGFC	σ	0.36	0.24	0.14	0.06	0.00	0.05	0.09	0.12	0.14
	Av.	-0.52	-0.36	-0.23	-0.10	0.00	0.09	0.17	0.24	0.30
	CV	69%	66%	63%	60%	-	55%	52%	50%	47%

Symbols. EL: expected life [years]; A: AASHTO method; PA/C: pay adjustments; σ: standard deviation; Av.: average; CV: coefficient of variation; ALL: all pavement types (PEMs+DGFCs), 40 cases; PEM: Porous European Mixture; DGFC: Dense Graded Friction Course.

7.4 Conclusions

After the analysis carried out in the section, there is the awareness that a number of parameters may affect results and inferences under analysis and further research is needed.

The design methods used are: i) AASHTO 93; ii) KenPave; iii) MnPAVE and; iv) M-EPDG.

Based on the above facts, the following conclusions can be drawn:

1. The methods herein analysed have a similar trend with regard to the independent variables under investigation (e.g., AV). However, there are some exceptions. Specifically, KenPave provides expected lives comparable to the value obtained through AASHTO. Instead, MnPAVE and M-EPDG largely overrate expected lives when $EL<EL_{ADP}$ and underrate when $EL>EL_{ADP}$. The trend appears similar also by referring to PA/C.

2. The standard deviation of the percentage pay adjustment increases when nonconformities are more severe and decreases when close to the situation in which neither penalty nor bonus is requested;
3. The coefficient of variation of (PA/C) shows higher values when EL decreases;
4. Methods can provide outputs very far from the AASHTO93 solution;
5. High levels of nonconformity, which refer to the limit condition between penalty and rejection of the pavement, yield a very high variance of outputs.
6. In terms of expected life with respect to the AASHTO 93 Guide, all the methods perform in a range of slope from 0.15 up to 1, which correspond to angles from 10 degrees up to 45 degrees (AASHTO);
7. Outcomes of this study can be refit researchers and practitioners in acceptance plan development and pay adjustment derivation. Based on the above, it is recommended what follows:
    i. to use the same pavement design methodology used in the project;
    ii. when needed, to reduce output variance through the use of more than one pavement design methodology.

8 Interrupted compaction

8.1 Introduction

Compaction is the process by which the volume of air, in an HMA, mixture is reduced by using external forces to reorient the constituent aggregate particles into a more closely spaced arrangement.

This reduction of air volume produces a corresponding increase in HMA density (Roberts, Kandhal, et al. 1996).

It is well known that laydown and compaction phases, in the field, are longher than the compaction in the lab. Infact, in accordance with the SGC (Superpave Gyratory Compactor) procedure, a lab compaction is about 4-5 minutes for a porous asphalt mix and about 5-6 minutes for a dense graded mix. Obviously, this time is not realistic for a field compaction.

On site compaction is conceptually different from that in lab. This is due to the fact that it occurs along a segment of pavement of variable length and width.

Then, the time estimate for paving is extremely complex and depends of many factors, such as equipment used, lenght of the segment of work, standby time for equipment and operators, ect. In this case is better to refer to hourly or daily production rate.

Many studies on construction productivity have been conducted. However, most of them focus on cost management rather than construction time estimation. Little information is available on production rates for construction time estimation (Kuo 2004).

Compaction is the most important factor in dense graded pavement performance (Bell, Hicks, and Wilson 1984; Hughes 1984, 1989; Brown and Foo 1994). An inadequate compaction results in a pavement with decreased stiffness, reduced fatigue life, accelerated aging/decreased durability, rutting, raveling, and moisture susceptibility (Hughes 1984, 1989).

Asphalt technologist agree that the density of an asphalt mixture is one of the most prominent measurements for road quality (Miller, Hartmann, and Doreè 2011; Huerne 2004; Abd El Halim, Phang, and

Haas 1993; Vasenev, Hartmann, and Dorée 2012). The desired density and quality are reached by the adequate compaction.

During a typical compaction sequence, for a dense graded mix in the field, it is possible to obtain (Corps Army of Engineers and Federal Aviation Administration 2000):

- approximately 75 to 85 percent of TMD (Theoretical Maximum Density) when the mix passes out from under the screed (part of a paving machine that spreads, smoothes and provides initial compaction);
- approximately 92 to 95 percent TMD when all rollers are finished compacting the mat;
- an additional 2 to 4 percent of TDM due to the traffic loading.

The problem behind this study is the difference between in-field and in-lab compaction process for a hot mix asphalt (HMA).

This difference has serious implications for the performances of road pavement, especially when crumb rubber is used.

The main in-lab methods (or device) for HMA compaction are (Chen et al. 2014): i) marshall impact hummer; ii) Superpave Gyratory Compactor (SGC); iii) linear Kneading compactor; iv) vibratory-Kneading compactor and; v) mobile steel wheel simulator.

The SGC method is preferable to Marshall method because faithfully reproduces material compression that occurs during the in-field compaction. It is important to note that these methods allow to transfer all compaction energy in a continuous way. This aspect is in contrast with the typical rolling pattern followed in field (see Figure 8.1).

Rollers have to travel a much greater distance that the paver within a given time. Travel speed is dependent on the rolling speed and number of passes needed to cover the paving width. In this logic short breaks, joint compaction, change direction and more should not be overlooked.

Figure 8.1 shows the roller passes sequence needed to compact all width of line paved. As it is possible to note, roller follows the path from pass 1 to pass 6 for one complete coverage (3 laps with two passes per lap, 6 passes in total).

Two coverage of the mat will require 12 passes and so on. In addition, an extra lap (2 passes) for the longitudinal joint and onother one pass for the next coverage (see pass 7 in Figure 8.1) are necessary.

This typical scheme, that can change as a function of drum width, paver width and, number of passes, implies that the different parts of mat get compaction energy discontinuously. Infact, to repeat the procedure (second coverage) roller must first complete all laps.

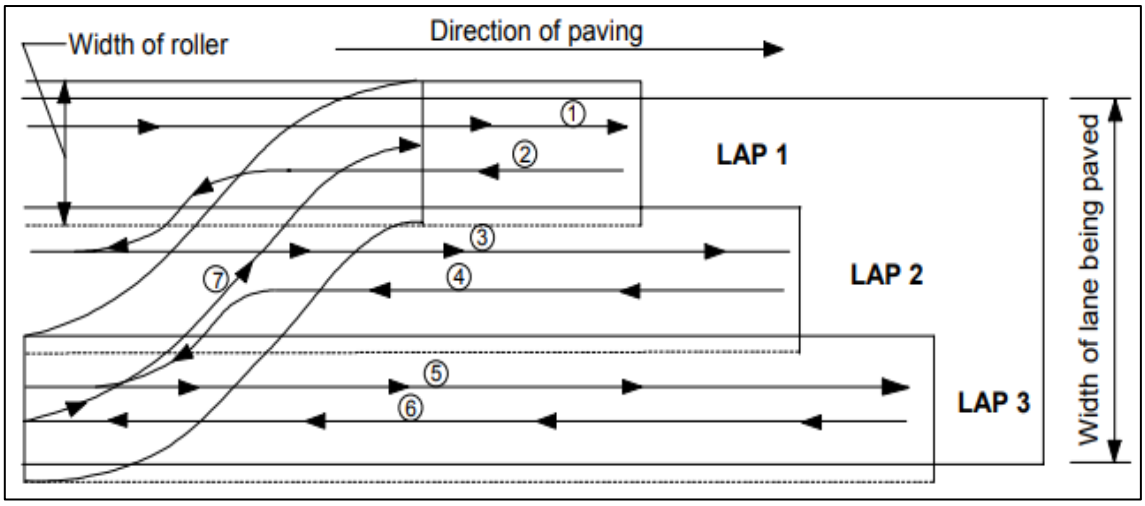

Figure 8.1: Typical rolling pattern (Austroads 2001).

Then, the idea of the interrupted compaction was introduced in order to study in-depth the consequences deriving from having CR in the mixture and to take due account the technical aspects abovementioned. Figure 8.2 shows the logical scheme of the study. It explains how this section is organised.

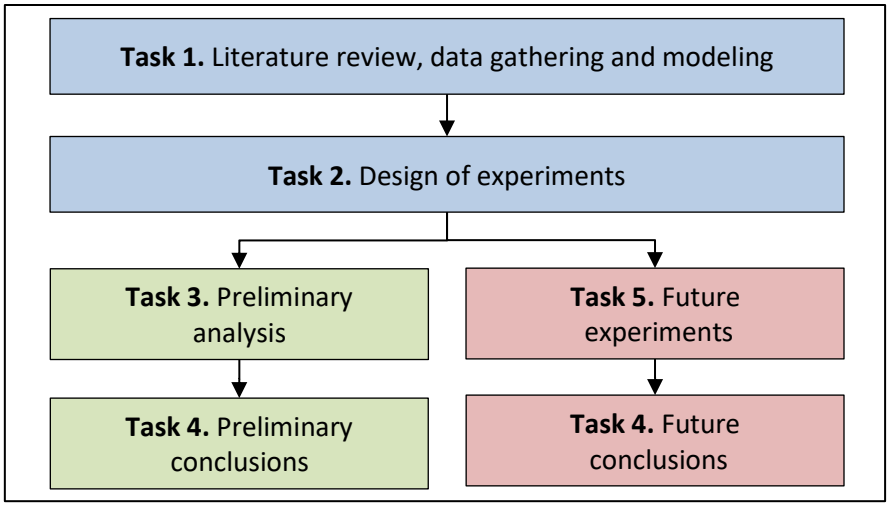

Figure 8.2: Logical scheme of the study.

8.2 Objectives

In light of the problem highlighted before, the objectives of this section are:

- To set up an innovative method, by using SGC, able to better simulate in-field compcation.
- To analyse the effect of crumb rubber on mixtures during the compaction step. This aspect could turn out of remarkable importance for a greater use of rubber in road pavements.

8.3 Main causes that affect compaction process

HMA compaction is influenced by a myriad of factors; some related to the environment (e.g., ground temperature, air temperature, wind speed, solar flux), some determined by mix and structural design (e.g., aggregate gradation, asphalt binder, etc.) and some under contractor and agency control during construction (e.g., number of passes, speed and timing, lift thickness, distance and time haul, etc.).

Environmental factors are determined by when and where paving occurs. Mix and structural design factors are determined before construction. Finally, construction factors are the most controllable and adaptable of all the factors affecting compaction.

HMA temperature is one of the greatest factors that directly affects asphalt binder viscosity and thus compaction (Timm et al. 2001; Floss 2001).

As HMA temperature decreases, the asphalt binder becomes more viscous and resistant to deformation. When the mix cools, the asphalt binder becomes stiff enough to effectively prevent any further reduction in air voids regardless of the applied compactive effort.

For this reason, during the paving process, cooling of HMA needs to be well monitored to ensure that there is adequate time to carry out the compaction process.

Dickson and Corlew (1970), in their studies, analised the thermal environment that controls the transfer of heat from the hot-mix asphalt concrete to its surroundings.

Their attention was focalised on: i) atmospheric temperature; ii) wind velocity, iii) solar radiant flux; iv) initial temperature of the mix; v) initial base temperature distribution and; vi) thickness of lift.

They have showed that the heat loss to the base exceeds that to the atmosphere. This implies that the temperature distribution of the entire mat with time is of importance when considering compaction. Base temperature, laydown temperature, air temperature, and mat thickness are the four most important factors affecting cooling rate.

8.3.1 Cessation temperature concept

It is generally agreed that with a normally behaving mix, the ability to reduce air voids during construction becomes appreciably more difficult at about 79°C (Hughes 1989).

This temperature, called cessation temperature, is a function of the mix properties and is used as a rule of thumb and is dependent on the viscosity of the mix (Scherocman 1984).

It is generally agreed that below this temperature very little, if any, additional compaction can be obtained after the initial reduction in air voids.

Below cessation temperature rollers can still be operated on the mat to improve smoothness and surface texture but further compaction will generally not occur.

Conversely, if the binder is too fluid and the aggregate structure is weak (e.g., at high temperatures), roller loads will simply displace, or “shove” the mat rather than compact it. In general, the combination of asphalt cement binder and aggregate needs to be viscous enough to allow compaction but stiff enough to prevent excessive shoving.

This implies that, mat temperature is crucial to both the actual amount of air void reduction for a given compactive effort, and the overall time available for compaction.

The cessation limit approach determines the length of time available for rolling before the mat temperature reaches a predetermined cessation temperature.

It has been demonstrated that the base temperature is more important than the atmospheric temperature (Dickson and Corlew 1972).

An alternative to compensate for cold base temperatures is to increase the lift thickness to meet the temperature-time limitations.

Then, according to Roberts, Prithvi, et al. (1996), the major factors affecting the time available for compaction are:

- **Initial mat temperature -** Higher initial mat temperatures require more time to cool down to cessation temperature, thus increasing the time available for compaction. However, overheating the HMA will damage the asphalt binder and cause emissions.
- **Mat or lift thickness** - Thicker lifts have a smaller surface-to-volume ratio and thus lose heat more slowly, which increases the time available for compaction.
- **Temperature of the surface on which the mat is placed** - Hotter surfaces will remove heat from the mat at a slower rate, increasing the time available for compaction.
- **Ambient temperature -** Hotter air temperatures will remove heat from the mat at a slower rate, increasing the time available for compaction.
- **Wind speed** - Lower wind speeds will decrease mat heat loss by convection, which will increase the time available for compaction.

8.4 Data gathering

In pursuit of the objectives referred to in this section, a collection of experimental data has been carried out with the aim of seeing and understandig the in-field compaction procedure. Data gathering has interested

an urban road with a hight-traffic level in the South of Italy. The main characteristics of the laydown and compaction phase are summarised in Table 8.1.

Table 8.1: Main characteristics of the laydown and compaction phase (in-field data gathering).

	Characteristics	Value
Pavement	Total length of section [m]	420
	Width of lane [m]	5
	Layer thickness (at the end of compaction) [m]	0.03
	Air temperature [°C]	20
	Type of Hot Mix Asphalt	traditional
Roller	Weight [kg]	8000
	Drum width [m]	1.5
	Drum temperature [°C]	ambient
Paver	Paver width [m]	2.5
	Layer thickness after paver (before roller passes) [m]	0.04

The main factors observed during data gathering have been: i) number of roller passes; ii) total time of compaction (from the paver passage to the last roller passage) and; ii) time between two consecutive passes of roller. The plan of data collection has interested nine different point, distributed along the length of section, in an appropriate way.

Each point consists in one square meter of HMA surface. The results of the in-site investigation are reported in Table 8.2. It it possible to note that the number of passes and the total time of compaction vary widely point-to-point.

Referring to number of roller passes there is a range of values that varies from 3 to 10 passes with an average of 6 passes for point.

Table 8.2: Results of in-site investigation.

Points	Total number of passes	Time of compaction [hh:mm:ss]
1	4	00:17:08
2	5	00:25:01
3	10	00:07:45
4	3	00:10:42
5	7	00:31:12
6	7	00:33:00
7	5	00:23:49
8	9	00:11:25
9	6	00:33:41
Average	6	00:21:31

Note that the same thing happens for the total time of compaction (from the paver passage to the last roller passage). It varies between 7 to 33 minutes and it is far from considerations made before on in-lab compaction (4-6 minute, Superpave Gyratory Compactor).

Another very important aspect is the variability of the time between two consecutive passes of roller.

Figure 8.3 shows the wide variety of values measured during a real in-field compaction. For each point, the partial times of two consecutive passes of roller have been reported. In the same time, the total number of passes can be derived.

In the specific case, the compaction process varies significantly both in terms of total number and in terms of temporal distribution of passes. In some cases, the time between two consecutive passes is much higher than 10 minutes. Most of these, instead, are lesser than 5 minutes.

These aspects are very common during a real compaction phase. Often, many considerations about the compaction procedure are remitted to the experience of operators and are closely linked to the other factors that affect the compaction (i.e., place, temperature, etc.).

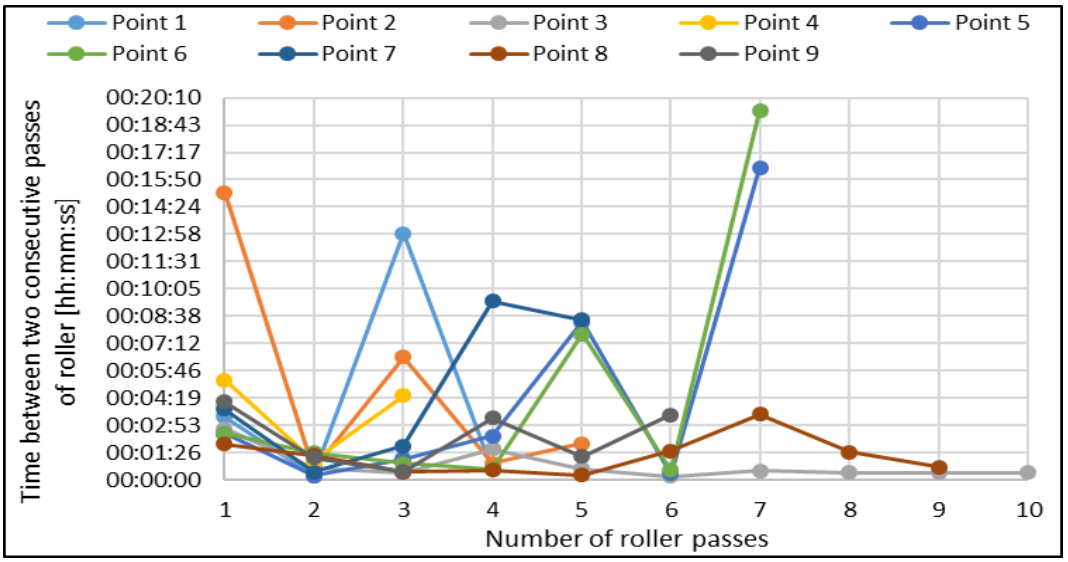

Figure 8.3: Time between two consecutive passes of roller

8.5 Experimental design

In Table 8.3 and Figure 8.4 the main parameters and the experimental plan of this section are summarised. In Figure 8.4, the “preliminary analysis” has been carried out in order to identify the best interrupted compaction process to be used for sample manufacturing.

Table 8.3: Main parameters of the study.

Parameter	Type/Quantity
Rubber type	CRT2 / CRT1 / CRN
Rubber content [%, by weight referred to total mix]	0 or 2
Mix design	PA / SMA10
T_{mix} [°C]	180
t_{mix} [s]	210
N_{ini}	10 *for PA* / 8 *for SMA10*
N_{des}	50 *for PA* / 100 *for SMA10*
N_{max}	130 *for PA (a, b)* / 160 *for SMA10 (c, d, e)*
Compaction process	GC1 (standard) / GC2 / GC3 / GC4
v [rpm] and ϕ [°]	30 and 1.25 *(a, b)*
T_{GC} [°C]	160±5
d [mm] and compaction pressure [kPa]	100 and 600 *(f)*

Symbols. T_{mix}: mixing temperature [°C]; t_{mix}: mixing time [s]; PA: Porous Asphalt; SMA10: Stone Mastic Asphalt with an upper sieve size of the aggregate of 10 mm; CRT2: CRT2 rubber; CRT1: Asphalt plus rubber; CRN: CRN rubber; N_{max}: maximum number of gyrations; GC1: Gyratory compaction with standard procedure; GC2: Gyratory compaction with interrupted procedure (stop of 60 seconds each 10 gyrations); GC3: Gyratory compaction with interrupted procedure (stop of 300 seconds each 10 gyrations); GC4: Gyratory compaction with interrupted procedure (stop of 300 seconds each 5 gyrations); v: speed of rotation [rpm]; φ: angle of gyration [°]; T_{GC}: gyratory compactor temperature [°C]; d: specimen diameter [mm]; a: (ANAS 2008); b: (ANAS 2009); c: (AASHTO 2001); d: (Cominsky et al. 1994); e: (EN-12697:10 2017); f: (EN-12697:31 2014).

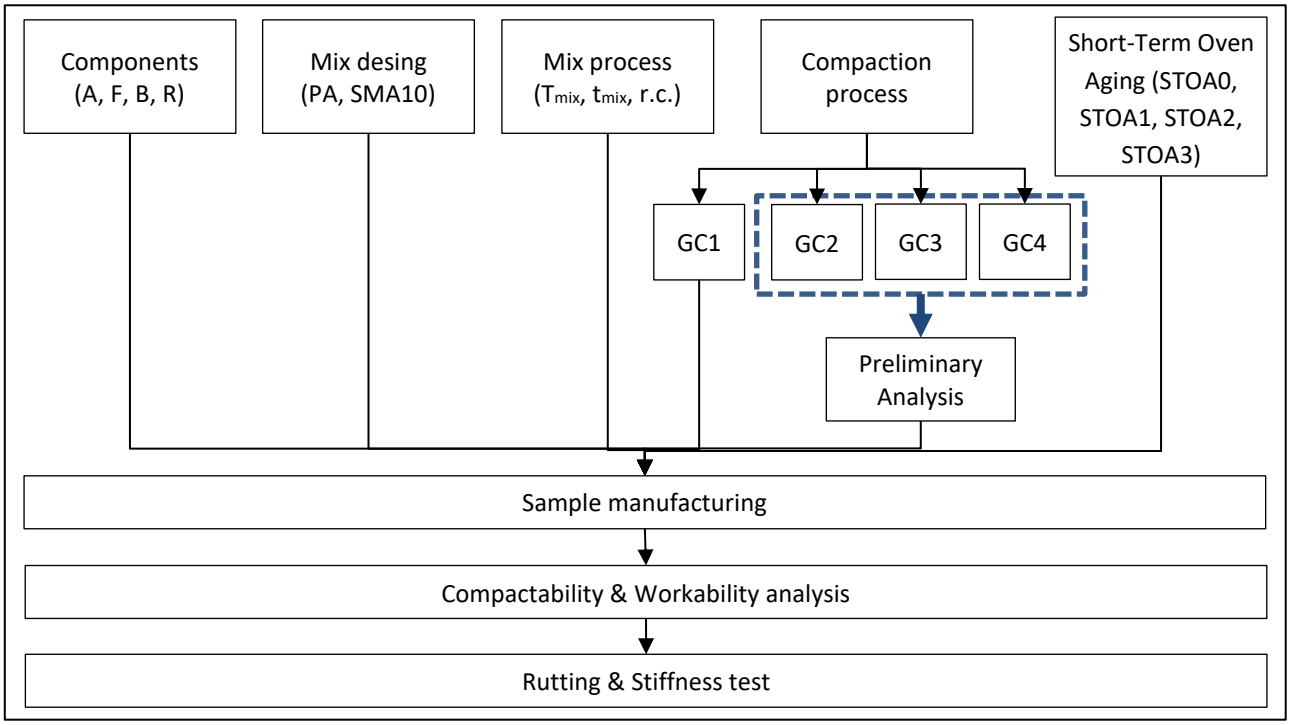

Figure 8.4: Experimental plan

Symbols. A: aggregate; F: filler; B: bitumen 50-70; R: rubber; PA: Porous Asphalt; SMA10: Stone Mastic Asphalt with an upper sieve size of the aggregate of 10 mm; T_{mix}: mixing temperature [°C]; t_{mix}: mixing time [s]; r.c.: rubber content; GC1: Gyratory compaction with standard procedure; GC2: Gyratory compaction with interrupted procedure (stop of 60 seconds each 10 gyrations); GC3: Gyratory compaction with interrupted procedure (stop of 300 seconds each 10 gyrations); GC4: Gyratory compaction with interrupted procedure (stop of 300 seconds each 5 gyrations); STOA0: without short-time oven aged; STOA1: short-time oven aged (@180°C for 60 minutes); STOA2: short-time oven aged (@180°C for 240 minutes); STOA3: short-time oven aged (@135°C for 240 minutes).

8.6 Preliminary analysis

In order to try to simulate the real in-field compaction process with the SGC (Superpave Gyratory Compactor), different compaction procedures have been introduced.

A preliminary analysis has been carried out to define the best interupted compaction process to apply for the "sample manufacturing" step.

In Figure 8.5 the logical scheme followed is summarised.

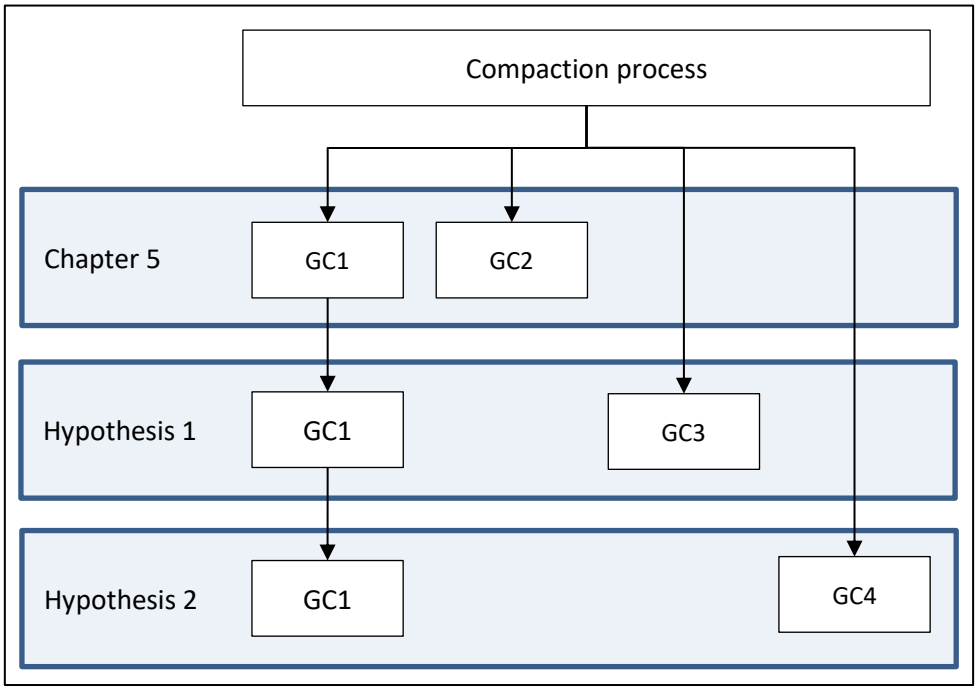

Figure 8.5: Experimental plan of preliminary analysis related to compaction process.

Symbols. GC1: Gyratory compaction with standard procedure; GC2: Gyratory compaction with interrupted procedure (stop of 60 seconds each 10 gyrations); GC3: Gyratory compaction with interrupted procedure (stop of 300 seconds each 10 gyrations); GC4: Gyratory compaction with interrupted procedure (stop of 300 seconds each 5 gyrations).

The “interrupted compaction” is a compaction process, carried out throght the giratory compactor (SGC), in which after a certain number of girations, a given stop is given for a certain time.

Starting from the compaction procedures introduced in Chapter 5 (GC1 and GC2), others two hypothesis have been considered (GC3 and GC4).

In Table 8.4 a summary of the characteristics of interrupted processes applied in this section is reported.

Table 8.4: Summary of main characteristics of compaction processes.

	Characteristics of interruption processes			
Compaction process	Time of interruption [s]	Frequency of interruption [gyrations]	Time of compaction for PA [min]	Time of compaction for dense-graded [min]
GC1	0	-	4-5	5-6
GC2	60	10	≈18	≈22
GC3	300	10	≈65	≈80
GC4	300	5	≈130	≈160

Symbols. GC1: Gyratory compaction with standard procedure; GC2: Gyratory compaction with interrupted procedure (stop of 60 seconds each 10 gyrations); GC3: Gyratory compaction with interrupted procedure (stop of 300 seconds each 10 gyrations); GC4: Gyratory compaction with interrupted procedure (stop of 300 seconds each 5 gyrations); PA: porous Asphalt.

Results of Chapter 5 have show that the effects of interrupted compaction (GC2), in terms of compactability and workability, need further studies and investigations.

In particular, the effects of interrupted compaction have been overshadowed by the effects of short-time oven aging.

Often, samples made with interrupted compaction (GC2) have presented different behaviour in terms of air void content.

In the light of this, the attention of this study has been focalised on GC3 and GC4 processes.

Starting to GC2 process, the logic behind of GC3 was to modify the length of the stops imposed to the compaction process. In this case, the compaction was stopped for 300 seconds after each 10 gyrations.

In order to obtain a heavier compaction process, the second hypothesis introduced (GC4) consists of the change of interruption frequency of GC3. In this second case the compaction was stopped for 300 seconds after each 5 gyrations.

The preliminary analysis has affected ten different mixes and was conducted without short-term oven aging. In this case, real and lab-mixes have been used.

Mixes differs to mix type (real Porous Asphalt, real Dense-Graded Friction Course and lab Porous Asphalt), compaction process (GC1, GC3 and GC4), height of sample (about 50 mm for case a, about 100 mm for case b) or presence of CRT2 rubber.

Figure 8.6 shows the densification curves obtained by applying GC3. In the same figure, a comparison of GC1 and GC3 process has been reported.

Figure 8.6-A refers to a real mix (dense grade friction course); Figure 8.6-B, instead, refers to real and lab mixes (porous asphalt, PA).

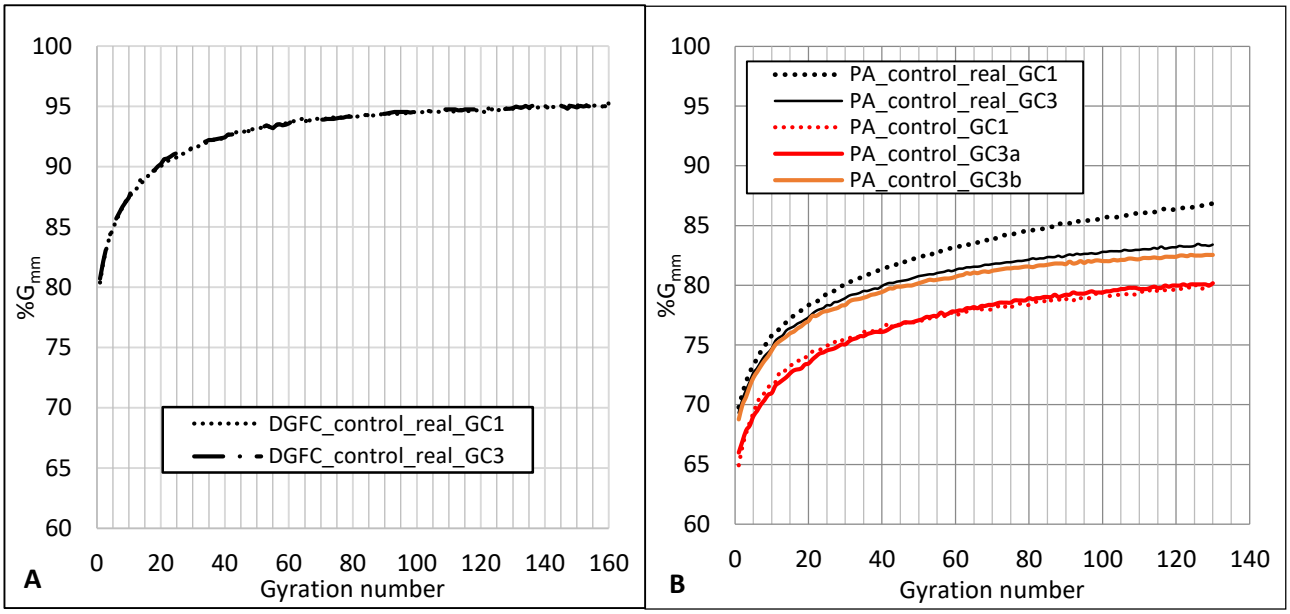

Figure 8.6: Densification curves related to GC1 and GC3.

As it is possible to observe in Figure 8.6, in many cases, the densification curves follow the same trend. It is important to note that, differently from Chapter 5, in these cases short-time oven aging was not applied. This means that, notwithstanding the fact that different stops were applied, GC3 does not entail any effect on compaction. Figure 8.7, instead, shows the densification curves obtained by applying GC4. In the same figure, a comparison of GC1 and GC4 process has been reported. Figure 8.7-A refers to a real mix (dense grade friction course); Figure 8.7-B, instead, refers to a lab mix (porous asphalt, CRT2).

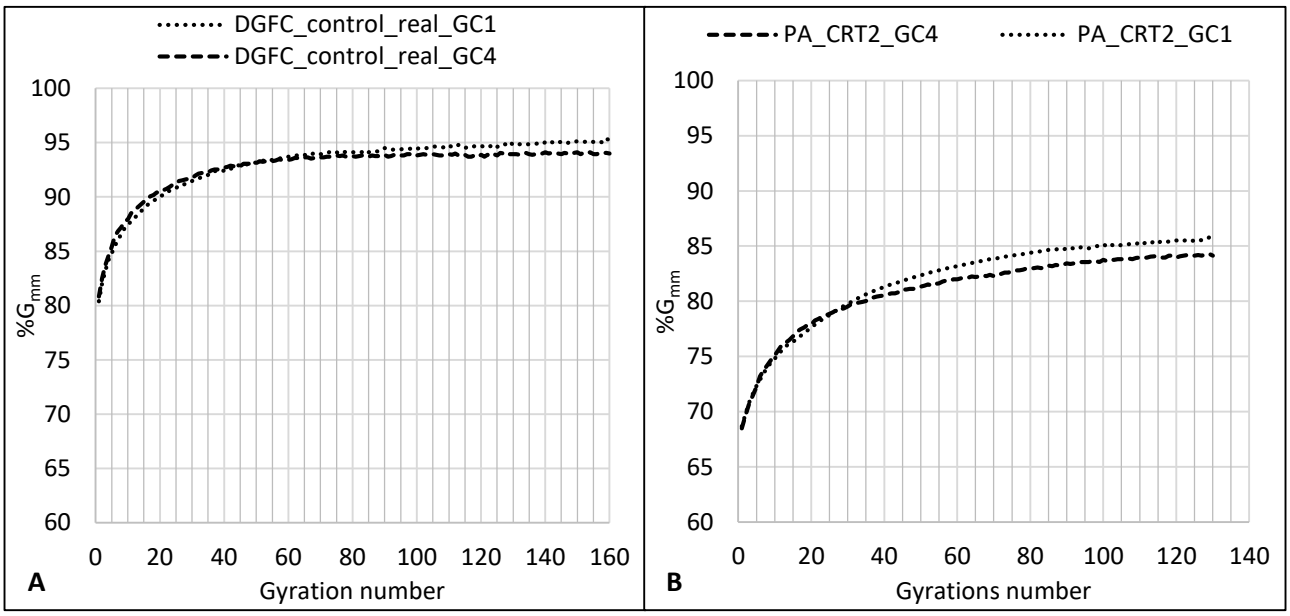

Figure 8.7: Densification curves related to GC1 and GC4.

It is possible to note that the two densification curves are the same in the first part of the graph and they vary in the second part. This implies that there is a moment, during the compaction process, after that the trend of compaction curve varies. This behaviour seems not occurring in Figure 8.6, where GC1 and GC3 processes are comparated.

One of the reasons is based on the different properties between GC3 and GC4 process. They vary in frequency of interruption and this reflects on the temperature of compaction process. In more detail, the properties of GC4 make the compaction process extremely long (more than two hours, see Table 8.4).

During this time, a very important role is played by mix temperature that, how seen before, is influenced by different factors.

The trend of densification curves, obtained in Figure 8.6 and Figure 8.7, is strongly agree with what was said by the Corps Army of Engineers and Federal Aviation Administration (2000) and better explained before.

In Table 8.5 and Figure 8.6 and Figure 8.7 it is possible to note how $\%G_{mm}$ varies as a function of number of gyrations N. For dense graded mix, $\%G_{mm}$(@N=1) is approximately 80 percent. It corresponds, in lab, to the preparation of loose mix in the mould and, in field, to the passage of loose mix under the screed. For porous mix, instead, the $\%G_{mm}$(@N=1) varies in the renge 65 to 70 percent.

The $\%G_{mm}$(@N_{des}) is about 94 percent for dense graded mix and in the range of 76 to 81 for a porous mix. In this case, it corresponds to the end of compaction in the field.

Finally, the additional compaction between N_{des} and N_{max}, corresponding to the compaction needed to produce a laboratory density that should never be exceeded in the field, is about 1% for dense graded mix and it varies in the range 2-4 percent for porous asphat mix.

Table 8.5: Percentage of maximum theoretical specific gravity at different steps of compaction.

Mix	Main characteristics	$\%G_{mm}$ (N=1)	$\%G_{mm}$ (N_{des})	$\%G_{mm}$ (N_{max})	$\%G_{mm}(N_{max})$ - $\%G_{mm}(N_{des})$
PA_control_real_GC1	PA without rubber	69.78	82.30	86.83	4.53
PA_control_real_GC3		69.31	80.76	83.40	2.64
PA_control_ GC1		64.92	76.97	79.87	2.90
PA_control_ GC3a		66.00	77.08	80.18	3.10
PA_control_ GC3b		68.78	80.18	82.55	2.37
DGFC_control_real_GC1	DGFC without rubber	80.38	94.43	95.23	0.80
DGFC_control_real_GC3		80.69	94.55	95.10	0.56
DGFC_control_real_GC4		80.82	93.83	94.01	0.18
PA_CRT2_GC1	PA with rubber	68.65	81.02	85.45	4.43
PA_CRT2_GC4		68.47	81.32	84.14	2.82

Symbols. GC1: Gyratory compaction with standard procedure; GC3: Gyratory compaction with interrupted procedure (stop of 300 seconds each 10 gyrations); GC4: Gyratory compaction with interrupted procedure (stop of 300 seconds each 5 gyrations; $\%G_{mm}$: percentage of maximum theoretical specific gravity; PA: Porous Asphalt; DGFC: dense-graded friction courses; N: number of gyrations; N_{des}: design number of gyrations; N_{max}: maximum number of gyrations.

To determine the time available for compaction (TAC) of the samples produced, the temperature of mould has often been monitoring. This choice was motivated by the difficulty/impossibility to check the temperature of mix during the compaction process.

Mould temperature was considered equal to the mix temperature and was used for the next considerations. This allowed to determine the cessation limit, corresponding to the time that the mould temperature was equal to cessation temperature (79°C). The temperature cooling curve is schematically represented in Figure 8.8.

Figure 8.8-A refers to a general form presents in literature (Wardati et al. 2016). It describes the relationship between temperature and cooling time (Jendia and Jarada 2005) and it is represented from the moment of mix laydown (T=0 min) to the traffic opening time. Figure 8.8-B, instead, refers to investigated cases where interrupted process was applied. Each trend has been derived by the monitoring of mould temperature.

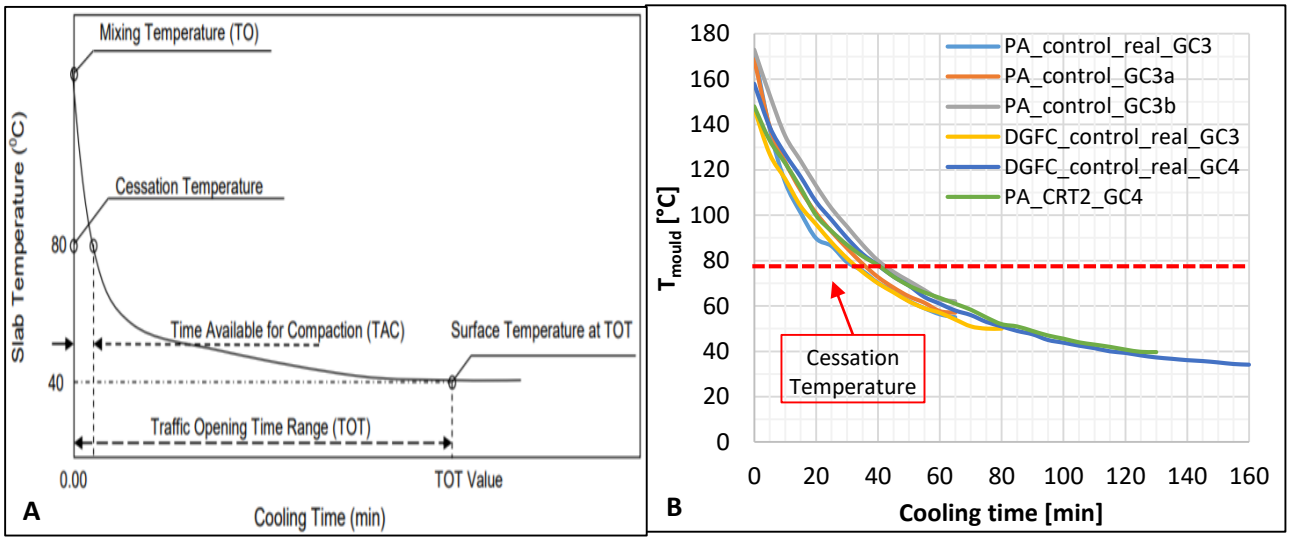

Figure 8.8: Temperature cooling curve of asphalt mixture (A, Wardati et al. 2016; B, investigated cases)

Symbols. T_{mould}: mould temperature.

In Figure 8.8-A, it is possible to observe that there is a gradual reduction in HMA temperature according to time until it becames stable.

Moreover, three main temperatures can be identified: i) mixing temperature; ii) cessation temperature and; surface temperature.

They are important because allow to define two intervals: i) the time available for compaction (TAC) and; ii) an additional time needed to achive the surface temperature for traffing opening.

The concept of time available to compact (TAC) plays a very important role for the achievement of proper densification in the field.

160

It highlights the relationship between mix temperature, base temperature, mat thickness, and the time available for the densification process to occur (Decker 2006).

A similar behaviour has been obtained in Figure 8.8-B. In this study, it is important to pointed out that all compactions have been carried out in lab, then:

- ambient temperature was about 20°C;
- wind speed can be considered negligible;
- initial mixture temperature was about 150-180°C;
- thickness of samples was often about 100 millimiters;
- temperature of the surface on which the mixture is placed is in the range 150-180°C.

All these factors have contributed to a very slow heat loss. This implies that the time available for compaction (TAC) greatly increases and, although the presence of interruptions, it is possible to transfer all the compaction energy to the mixture.

With reference to the temperature of the bearing surface, is better to observe that, during a compaction in field, it is very close to ambient temperature and the bearing surface, generally, is made of HMA or cement concrete or soil.

This contrast with the procedure of SGC followed in lab, where the bearing surface was made of metal (bottom of mould) and its temperature was imposed equal to mix temperature.

For a more realistic simulation, between in-lab and in-field procedure, the mould should have two different temperatures:

- ambient temperature for the bottom of mould (it corresponds to bearing surface);
- mixture temperature for the side wall of mould (it corresponds to adjoining material).

In Table 8.6, for each case investigated, the time available for compaction (TAC) and the number of gyrations corresponding to the cessation temperature ($N@T_{ces}$) are reported.

Obviously, all considerations here reported are only about the interrupted compaction process (GC3- and/or GC4-cases).

GC1-cases are not considered because the duration of standard compaction process is very short, and consequently mix and mould temperature don't meet the cessation temperature (T_{ces}= 79°C) before the end of compaction.

In Table 8.6 is possible to note that TAC varies as a function of initial temperature (T_{ini}) and thickness.

Table 8.6: Summary of relevant parameters for the analysis of cessation limit.

Mix	($@T_{ces}$) N ($@T_{ces}$)	($@T_{ces}$) TAC [h:m:s]	($@t=0$) T_{ini} mix [°C]	($@t=0$) T_{ini} mould [°C]	($@t_{end}$) Thickness [mm]
PA_control_real_GC3	61	00:29:31	167	172	90
PA_control_GC3a	71	00:37:52	164	169	49
PA_control_GC3b	82	00:42:49	179	173	96
DGFC_control_real_GC3	65	00:31:50	153	147	94
DGFC_control_real _GC4	41	00:41:18	153	158	95
PA_CRT2_ GC4	41	00:41:05	157	148	94

Symbols. N: number of gyrations; T_{ces}: cessation temperature (79°C); TAC: time available for compaction, is the time from start to T_{ces}; T_{ini}: initial temperature [°C]; t_{end}: end of compaction; t: time.

In Figure 8.9 and Table 8.7 it is possible to note how %Gmm varies during the compaction process. For this reason, Δ%Gmm has been derived. It has been obtained by the following equation:

$$\Delta\%G_{mm,i} = \frac{\%G_{mm}(N_i) - \%G_{mm}(N_{i-5})}{\%G_{mm}(N_{\max}) - \%G_{mm}(N=1)} \qquad \text{(Eq. 23)}$$

In detail it consists of the variation of $\%G_{mm}$. It has been derived every 5 compaction gyrations.

In Figure 8.9, for each curve, the point corresponding to cessation temperature is indicated. Note that, after this point (over the TAC), the variation of $\%G_{mm}$ is less than 2%.

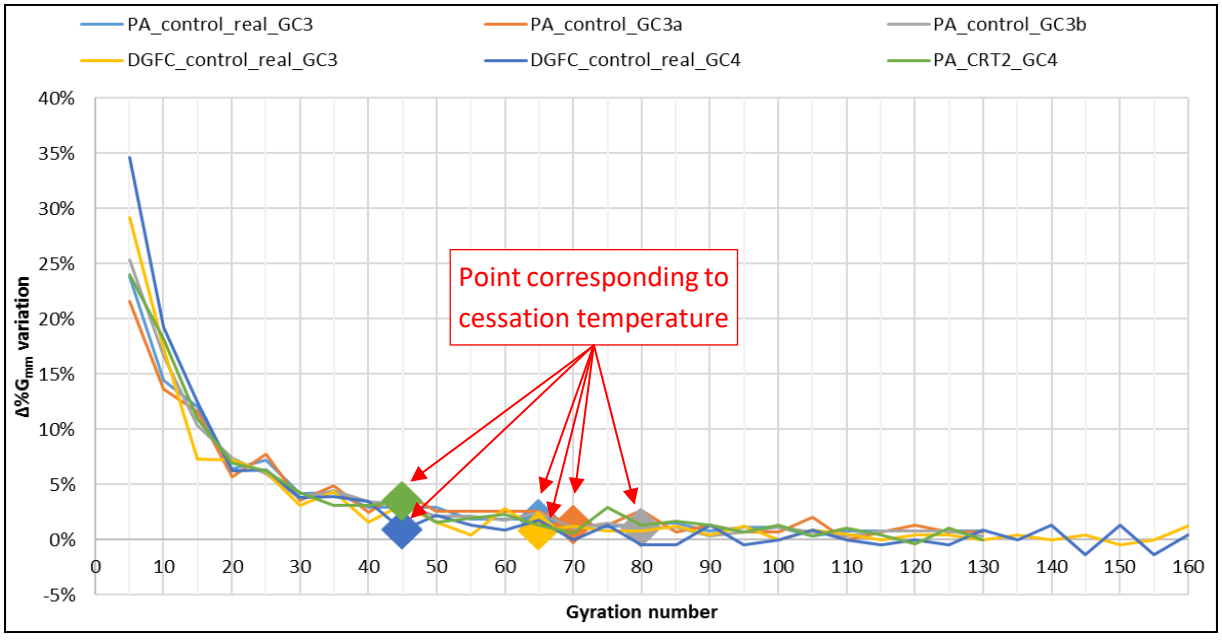

Figure 8.9: $\Delta\%G_{mm}$ trend during compaction process.

Symbols. $\Delta\%G_{mm}$: variation of percentage of maximum theoretical specific gravity.

Referring to Table 8.7 it is possible to note that:

- In cases 1, 3 and 9, 130 gyrations out of 130 have occurred within the time available for compaction (TAC); while in the case 6, 160 gyrations out of 160. Then, in these cases, all compaction energy, corresponding to N_{des}, has been transferred to mixture.
- In case 2, where GC3 has been applied, only 65 gyrations out of 130 have occurred within TAC. Note that the corresponding N_{des} is equal to 50 gyrations. Then, it is possible to affirm that all compaction energy has been transferred to mixture.
- In case 4, it was determined that 70 gyrations out of 130 have occurred within TAC, with a N_{des} of 50 gyrations. Then, here too, it is possible to affirm that all compaction energy has been transferred to mixture. This implies that (as reported in Figure 8.6) there are not substantial differences between case 3 and case 4. Essentially, the lengh of TAC has compensated the effect of GC3.
- Case 5 is another example where all compaction energy has been transferred. Infact about 80 gyrations out of 130 have occurred within TAC (for a corresponding N_{des} of 50 gyrations). Case 5 differs to case 4 only for the height of samples (96 mm in the first case and 49 mm in the second case).
- Cases 7 and 8 are about DGFC and consist on GC3 and GC4 respectively. In this case N_{des} was 100 gyrations (dense grade mix). In both cases not all compaction energy has been transferred before of the cessation temperature. Infact, it was determined that only 65 gyrations out of 160 and 45 gyrations out of 160 have occurred within TAC respectively. This aspect implies consequances in terms of densification curve (see Figure 8.7-A).
- The same behaviour is found in the cases 9 and 10, where rubberised PA-mixes are analised. In case 10, 45 gyrations out of 130 have occurred within TAC (for a corresponding N_{des} of 50 gyrations). This is another case where not all compaction energy has been transferred. This effect (between GC1- and GC4 case) is shown in Figure 8.7-B.

Table 8.8 reports different parameters (e.g., AV and locking point), different materials used (e.g., PA_control_real), three alternative compaction types (GC1, GC3, and GC4) and, the consequent effects. Note that all cases are made without short-time oven aging (STOA0).

Table 8.7: Δ%G_{mm} values (derived every 5 compaction gyrations).

Cases	1	2	3	4	5	6	7	8	9	10
Gyrations (N_i)	PA_control_real_GC1	PA_control_real_GC3	PA_control_GC1	PA_control_GC3a	PA_control_GC3b	DGFC_control_real_GC1	DGFC_control_real_GC3	DGFC_control_real_GC4	PA_CRT2_GC1	PA_CRT2_GC4
5	20.7%	23.8%	29.4%	21.6%	25.4%	29.8%	29.2%	34.6%	21.9%	24.0%
10	14.6%	14.5%	16.7%	13.7%	16.7%	17.2%	17.4%	19.3%	14.7%	18.2%
15	8.2%	12.1%	9.6%	11.6%	10.4%	10.2%	7.4%	12.5%	9.1%	11.0%
20	6.5%	6.4%	5.6%	5.7%	7.4%	8.1%	7.2%	6.3%	7.8%	7.0%
25	5.8%	7.2%	5.7%	7.7%	6.0%	4.8%	6.2%	6.3%	6.8%	6.3%
30	3.9%	4.2%	4.0%	3.6%	3.7%	4.5%	3.1%	3.9%	6.0%	4.3%
35	3.9%	4.3%	3.5%	4.9%	4.4%	3.8%	4.3%	3.9%	5.1%	3.1%
40	4.0%	2.9%	1.8%	2.5%	3.5%	2.7%	1.6%	3.5%	3.9%	3.1%
45	3.8%	2.9%	1.8%	4.4%	3.2%	3.1%	3.2%	**0.9%**	3.2%	**3.5%**
50	1.9%	2.9%	2.4%	2.5%	2.1%	2.0%	1.6%	2.2%	3.1%	1.6%
55	1.9%	1.9%	2.4%	2.6%	2.1%	1.6%	0.4%	1.3%	2.6%	1.9%
60	2.9%	1.9%	0.6%	2.6%	1.8%	2.0%	2.9%	0.9%	2.2%	2.3%
65	2.3%	**1.9%**	4.3%	2.6%	2.5%	1.2%	**0.8%**	1.8%	2.2%	1.3%
70	2.6%	1.5%	-0.6%	**1.3%**	1.1%	0.4%	1.2%	0.0%	1.9%	0.7%
75	1.3%	1.1%	1.2%	1.3%	1.5%	1.2%	0.8%	1.3%	1.6%	3.0%
80	1.7%	1.5%	1.2%	2.7%	**1.1%**	0.0%	0.8%	-0.4%	1.5%	1.3%
85	1.7%	1.5%	3.8%	0.7%	1.1%	0.0%	1.2%	-0.4%	1.5%	1.7%
90	1.7%	0.8%	-0.6%	1.3%	0.4%	2.4%	0.4%	1.3%	0.9%	1.3%
95	2.0%	1.2%	1.3%	0.7%	0.7%	-0.8%	1.3%	-0.5%	0.0%	0.7%
100	1.4%	1.2%	2.6%	0.7%	1.1%	0.4%	0.0%	0.0%	2.3%	1.4%
105	1.0%	0.4%	-1.3%	2.0%	0.7%	1.6%	0.8%	0.9%	-0.3%	0.3%
110	0.7%	0.8%	0.6%	0.0%	0.4%	0.9%	0.5%	0.0%	1.6%	1.0%
115	1.4%	0.8%	1.9%	0.7%	0.7%	-2.1%	0.0%	-0.5%	-0.7%	0.4%
120	1.4%	0.8%	1.3%	1.4%	0.7%	1.7%	0.4%	0.0%	1.3%	-0.4%
125	1.1%	0.8%	2.0%	0.7%	0.8%	-0.9%	0.4%	-0.5%	-0.3%	1.1%
130	1.4%	0.8%	-1.3%	0.7%	0.4%	1.3%	0.0%	0.9%	0.0%	0.0%
135	-	-	-	-	-	0.4%	0.4%	0.0%	-	-
140	-	-	-	-	-	1.2%	0.0%	1.4%	-	-
145	-	-	-	-	-	0.0%	0.4%	-1.4%	-	-
150	-	-	-	-	-	0.4%	-0.4%	1.4%	-	-
155	-	-	-	-	-	-0.4%	0.0%	-1.4%	-	-
160	-	-	-	-	-	1.2%	1.3%	0.5%	-	-
N_{des}	50	50	50	50	50	100	100	100	50	50
Gyrations within TAC	130/130	65/130	130/130	70/130	80/130	160/160	65/160	45/160	130/130	45/130
Final Sample Thickness [mm]	86	90	49	49	96	93	94	95	92	94

Symbols. GC1: Gyratory compaction with standard procedure; GC3: Gyratory compaction with interrupted procedure (stop of 300 seconds each 10 gyrations); GC4: Gyratory compaction with interrupted procedure (stop of 300 seconds each 5 gyrations; TAC: time available for compaction, is the time from start to T_{ces}; N_{des}: design number of gyrations.

Table 8.8: Compaction parameters

		STOA0-GC1	STOA0-GC3	STOA0-GC4	(GC3-GC1)/GC1	(GC4-GC1)/GC1
AV (Nmax)	PA_control_real	13.17%	16.60%	-	26.0%	-
	PA_control	20.13%	19.82%	-	-1.5%	-
	PA_CRT2	14.55%	-	15.86%	-	9.0%
	DGFC_control_real	4.77%	4.90%	5.99%	2.6%	25.5%
Locking point	PA_control_real	over 130	103	-	-	-
	PA_control	68	73	-	7.4%	-
	PA_CRT2	over 130	-	over 130	-	-
	DGFC_control_real	over 130	82	over 130	-	-
CS	PA_control_real	4.06	3.26	-	-19.7%	-
	PA_control	3.18	3.40	-	7.2%	-
	PA_CRT2	4.08	-	3.56	-	-12.7%
	DGFC_control_real	2.87	2.81	2.35	-2.1%	-18.4%
CS (from N_{ini} to N_{des})	PA_control_real	4.25	3.62	-	-14.8%	-
	PA_control	3.23	3.72	-	15.4%	-
	PA_CRT2	3.98	-	3.74	-	-6.2%
	DGFC_control_real	3.08	2.97	2.48	-3.5%	-19.3%
N ($92\%G_{mm}$)	PA_control_real	n.a.	n.a.	-	-	-
	PA_control	n.a.	n.a.	-	-	-
	PA_CRT2	n.a.	-	n.a.	-	-
	DGFC_control_real	35	32	31	-8.6%	-11.4%
$\%G_{mm}(N_{ini})$	PA_control_real	75.80	74.71	-	-1.4%	-
	PA_control	71.82	70.99	-	-1.2%	-
	PA_CRT2	74.79	-	75.09	-	0.4%
	DGFC_control_real	86.59	86.64	87.20	0.1%	0.7%

Symbols. GC1: Gyratory compaction with standard procedure; GC3: Gyratory compaction with interrupted procedure (stop of 300 seconds each 10 gyrations); GC4: Gyratory compaction with interrupted procedure (stop of 300 seconds each 5 gyrations; AV: Air void content (refers to N_{max}, maximum number of gyrations); CS: compaction slope; N ($92\%G_{mm}$): number of gyrations corresponding to 92% of G_{mm}; $\%G_{mm}(N_{ini})$: percentage of maximum theoretical specific gravity at N_{ini}; STOA0: without short-time oven aged; n.a.: not available.

The approach followed in this section is of the type step-by-step. This has resulted in the variation of the characteristics of samples during their manufacturing. For this reason, not all parts of the Table 8.8 are complete. In DGFC case, where GC3 and GC4 are present, it is possible to note that the effects of GC4 are higher than GC3. Infact, it is possible to affirm that:

- The air void variation is 2.6% for GC3 and 25.5% for GC4.
- The compaction slope variation is -2.1% for GC3 and -18.4% for GC4. Similar consideration can be made if CS is calculated between N_{ini} and N_{des}. In this last case the compaction slope variation is -3.5% for GC3 and -19.3% for GC4.
- The variation of number of gyrations corresponding to 92% of G_{mm} is -8.6% for GC3 and -11.4% for GC4.
- The variation of $\%G_{mm}$ (N_{ini}) is 0.1% for GC3 and 0.7% for GC4.

This has meant that the variation of interruption frequency has played a consistent and determining role in the compactability and workability of mixes.

In Table 8.9 an analysis of compaction slope variation as a function of cessation limit is reported. The slope of the densification curve before and after the cessation limit has been determined.

It is possible to note that the compaction slope before the cessation limit (CS_{bef}) is very similar to the compaction slope of full curve (CS_{full}).

Indeed, the corresponding variations are less than 4.4% with some exceptions (20.7 % and 45.1% for DGFC mixes).

On the contrary, the compaction slope after the cessation limit (CS_{aft}) presents important variations with the compaction slope of full curve (CS_{full}). The latter vary in the range of -18.0% to -69.0%.

One more interesting aspect is the variation between compaction slope before the cessation limit (CS_{bef}) and the compaction slope after the cessation limit (CS_{aft}).

This difference (ΔCS) is very acute for DGFC mixes (Dense Graded Friction Course) where the difference is about 2.02 for GC3 and 2.67 for GC4. The corresponding variations are -59% and -78%, respectively.

Instead, for PA-mixes, ΔCS is less than 0.64 with a corresponding variation of -19%.

One exception is represented by PA_control_GC3a where ΔCS is equal 1.30 and the corresponding variation is -40%.

It is still possible to note that ΔCS of a lab mix (PA_control_GC3b) is generally higher than the ΔCS of a real mix (PA_control_real_GC3). In the first case ΔCS is about 1.30 and in the second case it corresponds to 0.64.

When lab rubberised mix is considered, it is possible to observe that ΔCS decreases from 1.30 to 0.45.

The presence of rubber lessens the differences of CS before and after the cessation limit significantly.

The variation between CS_{bef} and CS_{aft} varies from -40% for mixes without rubber to -12% for mixes with rubber.

Table 8.9: Effects of cessation limit on compaction slope (CS).

Mix	CS_{full}	CS_{bef}	CS_{aft}	$(CS_{aft} - CS_{bef})/CS_{bef}$	$(CS_{aft} - CS)/CS$	$(CS_{bef} - CS)/CS$	ΔCS
PA_control_real_GC3	3.26	3.32	2.68	-19%	-18%	1.9%	0.64
PA_control_ GC3a	3.40	3.35	2.77	-17%	-19%	-1.5%	0.58
PA_control_GC3b	3.14	3.27	1.98	-40%	-37%	4.4%	1.30
DGFC_control_real_GC3	2.81	3.40	1.38	-59%	-51%	20.7%	2.02
DGFC_control_real_GC4	2.35	3.40	0.74	-78%	-69%	45.1%	2.67
PA_CRT2_ GC4	3.56	3.66	3.21	-12%	-10%	2.9%	0.45

Symbols. CS: compaction slope; CS_{full}: compaction slope of full curve; ΔCS= CS_{bef} - CS_{aft}: difference between CS_{bef} and CS_{aft}; CS_{bef}: compaction slope (slope of the densification curve) before the cessation limit; CS_{aft}: compaction slope (slope of the densification curve) after the cessation limit; cessation limit: moment when the mould temperature is equal to cessation temperature (79°C).

8.7 Preliminary conclusions

In the light of the observations and results present in this section, it is possible to conclude that:

- For a good compaction process is important to know the time available for compaction (TAC). Staying in the proper temperature zone for rolling is very important in order to obtain a good mixture densification.
- TAC is maily affected by environmental factors, for example ground temperature, air temperature, wind speed, solar flux. For this reason, it varies on a case-by-case.
- All the compaction energy, needed to compact the mix, must be given before the mixture reaches the cessation temperature (79°C). The compaction energy supplied after that the mixture has exceeded the cessation temperature does not contribute to compaction process.
- Field compaction is a process that is generally longher than the lab compaction.
- For a realistics simulation in lab of the in-field compaction process, different hypoteses have been introduced to modify the procedure of Superpave Gyratory Compactor (SGC). The hypoteses introduced (GC2, GC3 and GC4) have been based on time and frequency of interruption of the SGC.
- As long as all gyrations, corresponding to N_{des}, occur within the TAC, there are not significant effects in terms of densification curves. In the contrary, when some gyrations occur after TAC (i.e. when mix temperature is under the cessation temperature, 79°C), consequence on densification curves can be seen. This is due to the fact that not all compaction energy has been transferred to the mixes.
- Referring to the interrupted compaction procedures here introduced, GC4 seems to be the best way to simulate the in-field compaction.
- For a better in-lab simulation of the in-field compaction, the mould should have two different temperatures:
    - ambient temperature for the bottom of mould (it corresponds to bearing surface);
    - mixture temperature for the side wall of mould (it corresponds to adjoining material).

An important element in achieving smooth riding asphalt pavements is maintaining steady continuous paving.

It is important to ensure a proper coordination among operating asphalt plant production, operating paver speed and operating roller speed.

In this way, it is possible to ensure that:

- Asphalt plant production rates reach to average paver speed so that the paver can be kept moving steadily forward.

- Paving speed reachs to roller capacity so that the paver forward speed (and rate of supply) does not exceed the capacity of rollers to provide effective compaction, or alternatively to determine the number of rollers required to achieve compaction for a give output.

The following reccommendations are suggested to lead to better control of TAC:

- Compaction to be done immediately after the laying process;
- The roller/compactor should be right behind the paver for better compaction.

In light of the preliminary conclusions derived above, future steps of the study consist of the sample manufacturing with and without rubber using GC1 and GC4 compaction process. All samples will be tested for the stiffness and rutting tests.

9 Conclusions

This study aimed at investigating the main aspects of road pavement design in order to improve the performance of innovative mixes.
In more detail, in this thesis the superficial and mechanical properties of conventional and innovative road pavements have been investigated.
It contains a collection of experiments related to: i) laboratory-based study of the surface properties of road pavement; ii) laboratory-based study of the mechanical properties of road pavement and; iii) determination of expected life and pay adjustment.

The study related to the set-up of models for the prediction of surface characteristics of road pavements makes several contributions to the literature (Section 3).
It adds to the relatively small amount of research that examines whether macrotexture and pendulum test can be explained and predicted based on simple physical and geometric models.
Furthermore, the results of this research help provide a better understanding of the importance and the criticalities of assessing macro- and micro-texture at an early stage and on small samples.
It has been shown that macro- and microtexture test can be explained and predicted based on simple physical and geometric models.
Macro- and microtexture measures on laboratory samples can be related to the corresponding measures on real pavements.
Due to the small quantity of sand and to the complexity of surface texture, modelling explains that MTD measurements are affected by the volume of sand used.

As shown in Section 4, a quality-control procedure for rubberised asphalt mastic was defined.
The interaction between several CRs and bitumen during mixing, hauling and paving operations has been investigated.
The study was carried out adapting a Brookfield rotational viscometer as a low shear mixer.

A new set of impellers (DHR), developed at the Nottingham Transportation Engineering Centre (NTEC), was adopted.

Based on results, it follows that the order of components in the asphalt plant (bitumen-filler-rubber sequence versus bitumen-rubber-filler sequence) does not have significant effects on viscosity.

The variation of viscosity over time is linked to the swelling process of the rubber.

The SMA mastics have a behaviour to the one of PA mastics, but higher viscosity values. This is due to a higher filler content. In both cases, the lowest viscosity was obtained using CRT2 rubber and the highest viscosity is obtained using CRN rubber, $\eta(CRT2) < \eta(CRT1) < \eta(CRN)$.

Constant swelling of the ambient CR (CRN rubber) was recorded over the 5 hours, while the specifically pre-treated rubber particles allows a significant mitigation of the mastic swelling phenomena which in all cases ceased slightly after the mixing operations (below 30 mins).

To define the effects of different laboratory short-term oven aging and compaction processes on compactability and workability (Section 5), the following parameters have been analysed: i) air void content (AV); ii) locking point; iii) compaction slope; iv) percentage of the maximum theoretical specific gravity at the initial number of gyrations ($\%G_{mm}@N_{ini}$); v) number of gyrations corresponding to 92% of G_{mm} ($N@92\%G_{mm}$).

It can be concluded that:

- Short-time oven aging (STOA) entails a worse compaction of mixes. Aging time effects are more evident than aging temperature effects.
- Usually, interrupted compaction process entails a worse compaction of mixes.
- STOA effects are more evident than interrupted compaction effects in terms of compactability and workability.
- Usually, CRT2 mixes are easier to compact than other rubberised mixes.
- With some exceptions, un-rubberised mixes (control samples) are more difficult to compact than rubberised mixes when STOA 2 (higher time of aging) or STOA 3 (higher temperature of aging) are applied. In these cases, the presence of crumb rubber seems to play a positive role in aging process.

Furthermore, short-term oven aging and compaction process effects on stiffness and rutting have been analysed (Section 6). Tests were carried out through the Nottingham Asphalt Tester (NAT).

Referring to stiffness, it can be concluded that:

- Short-time oven aging (STOA) entails a general increase of stiffness. Mixes exposed to STOA1 (light aging) tend to have the lowest stiffness. Instead, mixes exposed to STOA2 (massive aging) have the highest stiffness and stiffness variation.

- Samples made through the interrupted compaction process present an unusual increase of stiffness. They need further consideration.
- Rubberised mixes always have a stiffness that is higher than mixes without rubber.
- The stiffness variation of rubberised SMA10 samples is lower than un-rubberised SMA10 samples when differents short-term oven aging are compared.

Referring to rutting, the main conclusions are:

- STOA process tends to improve the rutting resistance of mixes. Samples exposed to STOA2 or STOA3 have a lower axial strain than samples exposed to STOA1. A negative variation of axial strain causes an improvement of resistance to permanent deformations.
- Usually, the interrupted compaction process entails a worse resistance to permanent deformations.
- STOA effects are more evident than interrupted compaction effects in terms of rutting.
- Rubberised mixes have a better resistance to rutting when STOA 2 (higher time of aging) or STOA 3 (higher temperature of aging) are applied.
- Aging time effects are more evident than aging temperature effects in terms of rutting.
- SMA mixes are more resistant to permanent deformation than PA mixes.
- CRT2-mixes are the most resistant to permanent deformation.

Finally, the design methods used in Section 7 were: i) AASHTO 93; ii) KenPave; iii) MnPAVE and; iv) M-EPDG. Based on the analysis carried out, the following conclusions can be drawn:

- The methods analysed have a similar trend with regard to the independent variables under investigation (e.g., AV).
- KenPave provides expected lives comparable to the value obtained through AASHTO. Instead, MnPAVE and M-EPDG largely overrate expected lives when EL<ELADP and underrate when EL>ELADP. The trend appears similar also by referring to PA/C.
- High levels of nonconformity, which refer to the limit condition between penalty and rejection of the pavement, yield a very high variance of outputs.
- The standard deviation of the percentage pay adjustment increases when nonconformities are more severe and decreases when close to the situation in which neither penalty nor bonus is requested.
- The coefficient of variation of (PA/C) shows higher values when EL decreases.

10 References

AASHTO-R30. 2002. “Standard Practice for Mixture Conditioning of Hot Mix Asphalt.”

AASHTO-T274. 1982. “The Standard Method of Testing for Resilient Modulus of Subgrade Soils.” Washington, D.C.: American Association of State Highway and Transportation Officials (AASHTO).

AASHTO-T294. 1994. “Standard Method of Test for Resilient Modulus of Unbound Granular Base/Subbase Materials and Subgrade Soils - SHRP Protocol P46.” Washington, D.C.: American Association of State Highway and Transportation Officials (AASHTO).

AASHTO-T307. 1999. “Standard Method of Test for Determining the Resilient Modulus of Soils and Aggregate Materials.” Washington, D.C.: American Association of State Highway and Transportation Officials (AASHTO).

AASHTO-T312. 2015. “Standard Method for Preparing and Determining the Density of Hot Mix Asphalt (HMA) Specimens by Means of the SHRP Gyratory Compactor.”

AASHTO. 1993. “Guide for Design of Pavement Structures, FHWA-RD-97-077.”

AASHTO, P.S. 2001. “AASHTO Provisional Standards.” Washington, D.C.: American Association of State Highway and Transportation Officials.

AASHTO T316. 2013. “Standard Method of Test for Viscosity Determination of Asphalt Binder Using Rotational Viscometer.” American Association of State Highway and Transportation Officials (AASHTO).

Abd El Halim, A. O., W. A. Phang, and R. C. Haas. 1993. “No Title.” *Journal of Transportation Engineering* 119 (6): 914–32. https://doi.org/doi.org/10.1061/(ASCE)0733-947X(1993)119:6(914).

Abdelrahman, M., and S. Carpenter. 1999. “Mechanism of Interaction of Asphalt Cement with Crumb Rubber Modifier.” *Transportation Research Record: Journal of the Transportation Research Board*, 106–13. https://doi.org/10.3141/1661-15.

Abdullah, Mohd Ezree, Kemas Ahmad Zamhari, Rosnawati Buhari, Mohd Nafarizal Nayan, and Mohd Rosli Hainin. 2013. “Short Term and Long Term Aging Effects of Asphalt Binder Modified with Montmorillonite.” *Key Engineering Materials* 594–595: 996–1002. https://doi.org/10.4028/www.scientific.net/KEM.594-595.996.

Abdulmajeed, S.G., and R. Muniandy. 2017. “The Effect of Binder Type and Temperature Differential on The Rutting Performance of Hot Mix Asphalt.” *International Journal of Applied Engineering Research* 12 (17):

6841–52. http://www.ripublication.com.

Al-Mosawe, H. 2016. “Prediction of Permanent Deformation in Asphalt Mixtures.” University of Nottingham, UK.

Al-shamsi, Khalid, and Mohammad Louary. 2006. “Laboratory Optimization of Asphalt Concrete Mixtures Design.” In *Third Gulf Conference on Roads (TGR06)*, 82–91.

Altieb, Z.A., M.M.A. Aziz, K.A.B. Kassim, and H.B. Jibrin. 2016. “A Short Review on Usib Rubber as Modification of Bitumr.” *Jurnal Teknologi*. https://doi.org/10.11113/jt.v78.9479.

ANAS. 2008. “Gestione Delle Pavimentazioni Stradali – Linee Guida Di Progetto e Norme Tecniche Prestazionali.” Ricerca & Innovazione, Centro Sperimentale Stradale.

ANAS, Capitolato. 2009. “Capitolato Speciale d’Appalto – Parte 2a Norme Tecniche Pavimentazioni Stradali/Autostradali.” Ministero delle Infrastrutture e dei Trasporti – Ispettorato per la Circolazione e la Sicurezza Stradale.

Andersen, Lasse G., Jesper K. Larsen, Elsje S. Fraser, Bjarne Schmidt, and Jeppe C. Dyre. 2015. “Rolling Resistance Measurement and Model Development.” *Journal of Transportation Engineering*. https://doi.org/10.1061/(ASCE)TE.1943-5436.0000673.

Anderson, D.A., and T.W. Kennedy. 1993. “Development of SHRP Binder Specification.” *Journal of the Association of Asphalt Paving Technologists* 62: 481–507.

Anderson R.M., Turner P.A., Peterson R.L., Mallick R.B. 2002. “Relationship of Superpave Gyratory Compaction Properties to HMA Rutting Behavior.” *Transportation Research Board*.

Andrei, D., M.W. Witczak, and M.W. Mirza. 1999. “Development of a Revised Predictive Model for the Dynamic (Complex) Modulus of Asphalt Mixtures.”

Antunes, I., F. Giuliani, J.B. Sousa, and G. Way. 2005. “Asphalt Rubber: Bitume Modificato Con Polverino Di Gomma Di Pneumatico Riciclata.” *Applied Mechanics and Materials* 466–467: 157–60.

ARA. 2004. “Guide for Mechanistic-Empirical Design of New and Rehabilitated Pavement Structures, NCHRP Project 1-37A.” *Transportation Research Board of the National Academies*.

Araujo, Victor M.C., Iuri S. Bessa, and Verônica T.F. Castelo Branco. 2015. “Measuring Skid Resistance of Hot Mix Asphalt Using the Aggregate Image Measurement System (AIMS).” *Construction and Building Materials* 98: 476–81. https://doi.org/10.1016/j.conbuildmat.2015.08.117.

Asphalt Institute. 1979. *A Basic Asphalt Emulsion Manual Volume 1 – Understanding and Using Emulsion*.

Asphalt Plus, LLC. 2017. “Mix Design Guidance for Dry Process Elastiko Crumb Rubber-Modified Asphalt Mixes.”

ASTM-D4402/D4402M. 2015. “Standard Test Method for Viscosity Determination of Asphalt at Elevated Temperatures Using a Rotational Viscometer.” ASTM International. www.astm.org.

ASTM-D6925. 2015. “Standard Test Method for Preparation and Determination of the Relative Density of Asphalt Mix Specimens by Means of the Superpave Gyratory Compactor.”

ASTM-E1845. 2015. “Standard Practice for Calculating Pavement Macrotexture Mean Profile Depth.” West Conshohocken PA: ASTM International.

ASTM-E2157. 2015. “Standard Test Method for Measuring Pavement Macrotexture Properties Using the Circular Track Meter.” West Conshohocken, PA: ASTM International.

ASTM-E2380/E2380M. 2015. “Standard Test Method for Measuring Pavement Texture Drainage Using an Outflow Meter.” West Conshohocken PA: ASTM International.

ASTM-E965. 2006. “Standard Test Method for Measuring Pavement Macrotexture Depth Using a Volumetric Technique.” West Conshohocken PA: ASTM International.

Austroads. 2001. “Asphalt Paving Speed.” Austroads and AAPA (Australian Asphalt Pavement Association).

Austroads, and AAPA. 1999. “Air Voids in Asphalt, Pavement Work Tips – No.17.” Austroads and AAPA (Australian Asphalt Pavement Association).

Babalghaith, A.M., H.A. Alsoliman, and A.S. Al-Suhaibani. 2016. “Comparison of Rheological Properties for Polymer Mofified Asphalt Produced in Riyadh.” *International Journal of Civil, Environmental, Structural, Construction and Architectural Engineering* 10 (2).

Bahia, Husein, Timothy P Friemel, Pehr A Peterson, Jeffrey S Russel, and Brian Poehnelt. 1998. “Optimization of Constructibility and Resistance to Traffic: A New Design Approach for HMA Using the Superpave Compactor.” *Journal of the Association of Asphalt Paving Technologists* 67: 189–232.

Bai, Fan, Xinhua Yang, and Guowei Zeng. 2016. “A Stochastic Viscoelastic-Viscoplastic Constitutive Model and Its Application to Crumb Rubber Modified Asphalt Mixtures.” *Materials and Design* 89: 802–9. https://doi.org/10.1016/j.matdes.2015.10.040.

Balmer, G.G. 1979. “Pavement Texture: Its Significance and Development.” *Transportation Research Board Research Record 666*.

Banerjee, Ambarish, Andre De Fortier Smit, and Jorge A. Prozzi. 2012. “Influence of Operational Tolerances on HMA Performance.” *Construction and Building Materials* 27 (1): 15–23. https://doi.org/10.1016/j.conbuildmat.2011.08.003.

Basueny, A., A. Carter, D. Perraton, and M. Vaillancourt. 2016. “Laboratory Evaluation of Complex Modulus and Fatigue Resistance of Asphalt Mixtures with RAP.” In *RILEM Bookseries*, 521–32.

Behl, Ambika, Gajendra Kumar, and Girish Sharma. 2013. “Performance of Low Energy Crumb Rubber Modified Bituminous Mixes.” *Procedia - Social and Behavioral Sciences*. https://doi.org/10.1016/j.sbspro.2013.11.097.

Bell, C.A., Y. AbWahab, M.E. Cristi, and D. Sosnovske. 1994. “Selection of Laboratory Aging Procedures for Asphalt-Aggregate Mixtures.” *SHRP-A-383 Report*. Washington, DC., USA.

Bell, C.A., R.G. Hicks, and J.E. Wilson. 1984. “Effect of Percent Compaction on Asphalt Mixture Life.” *Placement and Compaction of Asphalt Mixtures, F.T. Wagner, Ed.*, 107–30.

Benedetto, H. Di. 1990. “Nouvelle Approche Du Comportement Des Enrobes Bitumineux: Resultats Experimentaux et Formulation Rheologique.” In *Proceedings of the Fourth International RILEM Symposium*, 385–401. Budapest: Ed Chapman and Hall.

Benedetto, H. Di, M. N. Partl, L. Francken, and C. De La Roche Saint Andrè. 2001. “Stiffness Testing for Bituminous Mixtures.” *Materials and Structures/Mat&iaux et Construction*. RILEM TC 182-PEB PERFORMANCE TESTING AND EVALUATION OF BITUMINOUS MATERIALS.

Bianchi, M. 2009. “Criteri Di Calcolo Delle Pavimentazioni Stradali Flessibili: I Metodi Particellari.” Alma Mater

Studiorum - Università degli Studi di Bologna.

Biligiri, K.P. 2016. “Tyre/Road Noise Damping Characteristics Using Nomographs and Fundamental Vibroacoustical Relationships.”

Bocci, E., G. Cerni, and S. Colagrande. 2016. “Mechanical Behaviour of Asphalt Concrete Containing C&D Recycled Materials.” In , 557–68. RILEM Bookseries.

Bonnaure, F., G. Gest, A. Gravois, and P. Uge. 1977. “A New Method of Predicting the Stiffness of Asphalt Paving Mittures.” In *AAPT Proceedings*, 64–104.

Boscaino, Gabriele, Bernardo Celauro, Clara Celauro, and Antonio Amadore. 2009. “Evaluation of the Laboratory Prediction of Surface Properties of Bituminous Mixtures.” *Construction and Building Materials* 23 (2): 943–52. https://doi.org/10.1016/j.conbuildmat.2008.05.006.

Bridge Engineering Section Alberta Transportation. 2013. “Specifications for Bridge Construction – Section 17 Asphalt Concrete Pavement.” In , 15th ed. Edmonton, Alberta.

Brown, E., and K.Y. Foo. 1994. “Comparison of Uncon_ned-and Con_ned-Creep Tests for Hot Mix Asphalt.” *Journal of Materials in Civil Engineering* 6 (2): 307–26.

Buddhavarapu, P., A. Smit, J. Prozzi, W. Fan, and Z. Gurmu. 2014. “Revised Pay Adjustment Factors for HMA and Concrete Pavements.” *FHWA/TX-14/0-6675-1*. Austin.

Burati, J.L., R.M. Weed, C.S. Hughes, and H.S. Hill. 2003. “Optimal Procedures for Quality Assurance Specifications.” *FHWA-RD-02-095*.

Cantisani, Giuseppe, Antonio D’Andrea, Paola Di Mascio, and Giuseppe Loprencipe. 2016. “Reliance of Pavement Texture Characteristics on Mix-Design and Compaction Process.” In *RILEM Bookseries*, 271–81. https://doi.org/10.1007/978-94-017-7342-3_22.

Cao, Weidong. 2007. “Study on Properties of Recycled Tire Rubber Modified Asphalt Mixtures Using Dry Process.” *Construction and Building Materials* 21 (5): 1011–15. https://doi.org/10.1016/j.conbuildmat.2006.02.004.

Chang, S.Y., and F. Gronwald. 2016. “A Multi-Criteria Evaluation of the Methods for Recycling Scrap Tires.” *Journal of Solid Waste Technology and Management* 42 (2): 145–56.

Chen, Jingsong, Baoshan Huang, Xiang Shu, and Chichun Hu. 2014. “DEM Simulation of Laboratory Compaction of Asphalt Mixtures Using an Open Source Code.” *Journal of Materials in Civil Engineering*. https://doi.org/10.1061/(asce)mt.1943-5533.0001069.

Chiu, Chui Te, and Li Cheng Lu. 2007. “A Laboratory Study on Stone Matrix Asphalt Using Ground Tire Rubber.” *Construction and Building Materials* 21 (5): 1027–33. https://doi.org/10.1016/j.conbuildmat.2006.02.005.

Chu, L.J., T.F. Fwa, and K.H. Tan. 2016. “Considering Aggregate Polishing Effect in Prediction of Pavement Skid Resistance.” In *8th International Conference on Maintenance and Rehabilitation of Pavements, MAIREPAV 2016*. https://doi.org/10.3850/978-981-11-0449-7-238-cd.

Clauzade, C. 2010. “LIFE CYCLE ASSESSMENT OF 9 RECOVERY METHODS FOR END-OF-LIFE TYRES.”

Clyne, T. R., X. Li, M.O. Marasteanu, and E.L. Skok. 2003. “Dynamic and Resilient Modulus on Mn/Dot Asphalt Mixtures.” *Final Report*.

CNR-B.U.-105. 1985. “Norme per La Misura Delle Caratteristiche Superficiali Delle Pavimentazioni - Metodo Di Prova per La Misura Della Resistenza Di Attrito Radente Con l’apparecchio Portatile a Pendolo.”

CNR-B.U.-94. 1983. “Norme per La Misura Delle Caratteristiche Superficiali Delle Pavimentazioni – Metodo Di Prova per La Misura Della Macro-Rugosità Superficiale Con Il Sistema Della Altezza Di Sabbia.” Consiglio Nazionale delle Ricerche.

Colorado-Procedure:77-09. 2009. “Determination of Macro-Texture of Planed Hot Mix Asphalt Pavement.”

Colorado-Procedure:77-14. 2014. “Determination of Macro-Texture of a Pavement Surface.”

Cominsky, Ronald, Gerald a Huber, Thomas W Kennedy, and Michael Anderson. 1994. “The Superpave Mix Design Manual for New Construction and Overlays.” *Publication NO SHRP-S-407 Strategic Highway Research Program, U.S.*

Coni, M. 2010. “Sovrastrutture Di Strade, Ferrovie Ed Aeroport.” Università degli Studi di Cagliari. http://web.tiscali.it/mauroconi/.

Corps Army of Engineers, ., and . Federal Aviation Administration. 2000. “Hot-Mix Asphalt Paving Handbook 2000.” *Transportation Research Board*.

CTI project. 2017. “Innovative Manufacturing of Crumb Rubber Modified Asphalt Concrete.”

DD-226. 1996. “Method for Determining Resistance to Permanent Deformation of Bituminous Mixtures Subject to Unconfined Dynamic Loading.” London, UK: British Standard (BSI).

Decker, Dale S. 2006. “State-of-the-Practice for Cold-Weather Compaction of Hot-Mix Asphalt Pavements.” *Transportation Research Circular E-C105: Factors Affecting Compaction of Asphalt Pavements*, Transportation Research Board, .

Dessouky, S., and M. Diaz. 2015. “Evaluation of Asphalt Mixes Workability and Compactability Using Laboratory and Accelerated Field Testing.” In *TMS Middle East - Mediterranean Materials Congress on Energy and Infrastructure Systems (MEMA 2015)*. TMS (The Minerals, Metals & Materials Society).

Dickson, P.F., and J.S. Corlew. 1970. “Thermal Computations Related to the Study of Pavement Compaction Cessation Requirement.” In *Proceedings, Association of Asphalt Paving Technologist*. Vol. 39.

———. 1972. “Cooling of Hot-Mix Asphalt Laid on Frozen Subgrade.” In *Proceedings, Association of Asphalt Paving Technologist*.

Dilip, D., P. Ravi, and G.L. Sivakumar Babu. 2013. “Life-Cycle Cost Analysis of Long Lasting Pavements.” *Indian Highways* 41 (4): 5–14.

Do, M.T., L.P. Kerzreho, J.M. Balay, and M. Gothie. 2013. “Full Scale Tests for the Assessment of Wear of Pavement Surfaces.” In *TRB 82nd Annual Meeting (Transportation Research Board)*.

Dondi, Giulio, Piergiorgio Tataranni, Matteo Pettinari, Cesare Sangiorgi, Andrea Simone, and Valeria Vignali. 2014. “Crumb Rubber in Cold Recycled Bituminous Mixes: Comparison between Traditional Crumb Rubber and Cryogenic Crumb Rubber.” *Construction and Building Materials* 68: 370–75. https://doi.org/10.1016/j.conbuildmat.2014.06.093.

Douries, W.L. 2004. “Factors Influencing Asphalt Compactibility and Its Relation to Asphalt Rutting Performance.” University of Stellenbosh.

Dunford, Alan. 2013. “Friction and the Texture of Aggregate Particles Used in the Road Surface Course.”

University of Nottingham.

EAPA. 2013. “Asphalt Pavements on Bridge Decks.” www.eapa.org.

Ecopneus. 2012. “Dagli Pneumatici Fuori Uso All’Asphalt Rubber: Lo Stato Dell’arte.”

Ecopneus, a. 2013. “L’impiego Di Prodotti Da Pneumatici Fuori Uso Nelle Pavimentazioni Stradali.”

Ecopneus, b. 2016. “Il Recupero Di Materiale.” http://www.ecopneus.it/it/il-pneumatico-fuori-uso-pfu/il-recupero-di-materiale.html.

Eisenmann, J., and A. Hilmer. 1987. “Influence of Wheel Load and Inflation Pressure on The Rutting Effect at Theoretical Investigations.” In *Proc. 6th International Conference on the Structural Design of Asphalt Pavements*. Ann Arbor, Michigan, USA.

EN-12593. 2015. “Bitumen and Bituminous Binders - Determination of the Fraass Breaking Point.” European Committee for Standardization.

EN-12697:10. 2017. “Bituminous Mixtures - Test Methods - Part 10: Compactability.”

EN-12697:24. 2012. “Bituminous Mixtures - Test Methods for Hot Mix Asphalt - Part 24: Resistence to Fatigue.”

EN-12697:26. 2012. “Bituminous Mixtures – Test Methods for Hot Mix Asphalt. Part 26: Stiffness.”

EN-12697:29. 2002. “Bituminous Mixtures - Test Method for Hot Mix Asphalt - Part 29: Determination of the Dimensions of a Bituminous Specimen.”

EN-12697:30. 2012. “Bituminous Mixtures - Test Methods for Hot Mix Asphalt - Part 30: Specimen Preparation by Impact Compactor.”

EN-12697:31. 2014. “Bituminous Mixtures - Test Methods for Hot Mix Asphalt - Part 31: Specimen Preparation by Gyratory Compactor.”

EN-12697:6. 2012. “Bituminous Mixtures - Test Methods for Hot Mix Asphalt - Part 6: Determination of Bulk Density of Bituminous Specimens.”

EN-12697:7. 2014. “Bituminous Mixtures - Test Methods for Hot Mix Asphalt - Part 7: Determination of Bulk Density of Bituminous Specimens by Gamma Rays.”

EN-13036:1. 2010. “Road and Airfield Surface Characteristics – Test Methods – Part 1: Measurement of Pavement Surface Macrotexture Depth Using a Volumetric Patch Technique.”

EN-13036:4. 2011. “Road and Airfield Surface Characteristics - Test Methods - Part 4: Method for Measurement of Slip/Skid Resistance of a Surface: The Pendulum Test.”

EN-13108:5. 2016. “Bituminous Mixtures - Material Specifications - Part 5: Stone Mastic Asphalt.” European Committee for Standardization.

EN-13302. 2003. “Bitumen and Bituminous Binders - Determination of Dynamic Viscosity of Bituminous Binder Using a Rotating Spindle Apparatus.” European Committee for Standardization.

EN-13398. 2017. “Bitumen and Bituminous Binders - Determination of the Elastic Recovery of Modified Bitumen.” European Committee for Standardization.

EN-1426. 2015. “Bitumen and Bituminous Binders - Determination of Needle Penetration.” European

Committee for Standardization.

EN-1427. 2015. “Bitumen and Bituminous Binders - Determination of the Softening Point - Ring and Ball Method.” European Committee for Standardization.

EN-ISO-3838. 2004. “Crude Petroleum and Liquid or Solid Petroleum Products - Determination of Density or Relative Density - Capillary-Stoppered Pyknometer and Graduated Bicapillary Pyknometer Methods.”

Epps, A., J.T. Harvey, Y.R. Kim, and R. Roque. 2000. “Structural Requirements of Bituminous Paving Mixtures.” Washington DC, USA: Millennium papers, Transportation Research Records.

Ergun, Murat, S Iyinam, and A F Iyinam. 2005. “Prediction of Road Surface Friction Coefficient Using Only Macro-and Microtexture Measurements.” *Journal of Transportation Engineering* 131 (4): 311–19. https://doi.org/10.1061/(ASCE)0733-947X(2005)131:4(311).

ETRMA. 2014. “Statistics – Edition 2014.” European Tyre & Rubber Manufacturers Association. www.ertma.org.

Farina, A., M.C. Zanetti, E. Santagata, and G.A. Blengini. 2017. “Life Cycle Assessment Applied to Bituminous Mixtures Containing Recycled Materials: Crumb Rubber and Reclaimed Asphalt Pavement.” *Resources, Conservation and Recycling* 117: 204–212. https://doi.org/10.1016/j.resconrec.2016.10.015.

Farouk, A.I.B., N.A. Hassan, M.Z.H. Mahmud, J. Mirza, R.P. Jaya, M.R. Hainin, H. Yaacob, and N.I.M. Yusoff. 2017. “Effects of Mixture Design Variables on Rubber–bitumen Interaction: Properties of Dry Mixed Rubberized Asphalt Mixture.” *Materials and Structures/Materiaux et Constructions* 50 (1). https://doi.org/10.1617/s11527-016-0932-3.

Feraldi, R., S. Cashman, M. Huff, and L. Raahauge. 2013. “Comparative LCA of Treatment Options for US Scrap Tires: Material Recycling and Tire-Derived Fuel Combustion.” *International Journal of Life Cycle Assessment* 18 (3): 613–625. https://doi.org/10.1007/s11367-012-0514-8.

Finn, F. N. 1967. “Factors Involved in the Design of Asphaltic Pavement Surfaces.” *National Cooperative Highway Research Program Report N. 39*. Washington, D.C.

Fisco, N.R. 2009. “Comparison of Macrotexture Measurement Methods.”

Flintsch, Gerardo, Edgar de León, Kevin McGhee, and Imad AI-Qadi. 2007. “Pavement Surface Macrotexture Measurement and Applications.” *Transportation Research Record*. https://doi.org/10.3141/1860-19.

Floss, R. 2001. *Compaction Technology in Earthwork and Highway and Transportation Engineering*. Edited by BOMAG GmbH&Company OHG. Munich.

Fordyce, D. 1997. “The Compaction of Asphaltic Mixtures.” Dublin, Ireland.

Francken, L. 1998. “Bituminous Binders and Mixtures, State-of-Theart and Laboratory Tests on Mechanical Behaviour and Mix Design.”

Georgiou, Panos, and Andreas Loizos. 2014. “A Laboratory Compaction Approach to Characterize Asphalt Pavement Surface Friction Performance.” *Wear* 311: 114–22. https://doi.org/10.1016/j.wear.2013.12.028.

Ghabchi, Rouzbeh, Manik Barman, Dharamveer Singh, Musharraf Zaman, and Muhammad Ali Mubaraki. 2016. “Comparison of Laboratory Performance of Asphalt Mixes Containing Different Proportions of RAS and RAP.” *Construction and Building Materials* 124: 343–51. https://doi.org/10.1016/j.conbuildmat.2016.07.029.

Gibreil, Hussein A.A., and Cheng Pei Feng. 2017. “Effects of High-Density Polyethylene and Crumb Rubber Powder as Modifiers on Properties of Hot Mix Asphalt.” *Construction and Building Materials* 142: 101–108. https://doi.org/10.1016/j.conbuildmat.2017.03.062.

González, V., F. J. Martínez-Boza, F. J. Navarro, C. Gallegos, A. Pérez-Lepe, and A. Páez. 2010. “Thermomechanical Properties of Bitumen Modified with Crumb Tire Rubber and Polymeric Additives.” *Fuel Processing Technology* 91: 1033–1039. https://doi.org/10.1016/j.fuproc.2010.03.009.

González, V, F J Martínez-Boza, C Gallegos, A Pérez-Lepe, and A Páez. 2012. “A Study into the Processing of Bitumen Modified with Tire Crumb Rubber and Polymeric Additives.” *Fuel Processing Technology* 95: 137–143. https://doi.org/10.1016/j.fuproc.2011.11.018.

Goodman, S.N., Y. Hassan, and A.O. AbdElHalim. 2006. “Preliminary Estimation of Asphalt Pavement Frictional Properties from Superpave Gyratory Specimen and Mix Parameters.” *Transportation Research Records*, 173–80.

Government of South Australia, G. 2016. “Road Surface Texture Measurement Recommended Inves-Tigatory Levels.” *Tech Note 25*. Revision 2.

Gudimettla, J.M, A.L. Cooley, and R Brown. 2003. “Workability of Hot Mix Asphalt.” *National Center for Asphalt Technology at Auburn University. Report No 03-3*.

Hakim, H., R. Nilsson, L.M. Vieira, and S. Said. 2012. “Round Robin Test of Stiffness Modulus by Indirect Tensile Method According to EN 12697-26:2004 Annex C.” In *5th Eurasphalt & Eurobitume Congress*. Istanbul.

Hallas, K., and G. Hunwin. 2009. “A Study of Pendulum Slider Dimensions for Use on Profiled Surfaces.” *RR726 Research Report*.

Hartman, A. M., M. D. Gilchrist, and G. Walsh. 2001. “EFFECT OF MIXTURE COMPACTION ON INDIRECT TENSILE STIFFNESS AND FATIGUE.” *Journal of Transportation Engineering* 127 (5).

Harvey, J., K. Eriksen, S. Sousa, and C.L. Monismith. 1994. “Effects of Laboratory Specimen Preparation on Aggregate-Asphalt Structure, Airvoid Content Measurement, and Repetitive Simple Shear Test Results.” *Transp. Res. Rec. 1454*, 113–22.

Harvey, John, and Bor-Wen Tsai. 2007. “Effects of Asphalt Content and Air Void Content on Mix Fatigue and Stiffness.” *Transportation Research Record: Journal of the Transportation Research Board*. https://doi.org/10.3141/1543-05.

Heitzman, M. 1992. “Design and Construction of Asphalt Paving Materials with Crumb Rubber Modifier.” *Transportation Research Record: Journal of the Transportation Research Board*.

Hesami, Saeid, Iman Salehi Hikouei, and Seyed Amir Ali Emadi. 2016. “Mechanical Behavior of Self-Compacting Concrete Pavements Incorporating Recycled Tire Rubber Crumb and Reinforced with Polypropylene Fiber.” *Journal of Cleaner Production* 133: 228–34. https://doi.org/10.1016/j.jclepro.2016.04.079.

Heukelom, W. and Klomp, A.J.G. 1964. “Road Design and Dynamic Loading.” *Road Design and Dynamic Loading* 33.

Hondros, G. 1959. “Evaluation of Poisson’s Ratio and Modulus of Materials of Low Tensile Resistance by Brazilian (Indirect Tensile) Test with Particular Reference to Concrete.” *Australian Journal of Applied Science* 10 (3).

Hossain, M.S. 2010. “Characterization of Unbound Pavement Materials From Virginia Sources for Use in the New Mechanistic-Empirical Pavement Design Procedure.” *FHWA/VTRC 11-R6*.

Huang, Chengyi, and Shunqi Mei. 2011. “Investigation of Road Surface Texture Wavelengths.” *New Tribological Ways*.

Huang, Yang Hsien. 2003. *Pavement Analysis and Design*. *Pearson*. 2nd Editio. Prentice-Hall. https://doi.org/10.1186/s12940-016-0203-3.

Huang, Yue, Roger N. Bird, and Oliver Heidrich. 2007. “A Review of the Use of Recycled Solid Waste Materials in Asphalt Pavements.” *Resources, Conservation and Recycling* 52 (1): 58–73. https://doi.org/10.1016/j.resconrec.2007.02.002.

Huerne, H.L. 2004. “Compaction of Asphalt Road Pavements Using Finite Elements and Critical State Theory.” University of Twente.

Hughes, C.S. 1989. “National Cooperative Highway Research Program Synthesis of Highway Practice 152: Compaction of Asphalt Pavement.” *Transportation Research Board*.

Hughes, C.S. 1984. “Importance of Asphalt Compaction.” *Better Roads* 54 (10): 22–24.

Hung, S.S., F. Farshidi, D. Jones, M.Z. Alavi, J.T. Harvey, and H. Sadraie. 2014. “Investigation of Wet-Process Asphalt Rubber Binder Testing with Modified Dynamic Shear Rheometer Equipment: Intermi Report on Screening Tests.”

Hurley, Graham C., and Brian D. Prowell. 2005. “Evaluation of Sasobit for Use in Warm Mix Asphalt.” *National Center for Asphalt Technology - Report 05-06*.

Ibrahim, M.R., H.Y. Katman, M.R. Karim, S. Koting, and N.S. Mashaan. 2013. “A Review on the Effect of Crumb Rubber Addition to the Rheology of Crumb Rubber Modified Bitumen.” *Advances in Materials Science and Engineering*. https://doi.org/10.1155/2013/415246.

Inturri, G. 2012. “Cenni Di Meccanica Della Locomozione: Aderenza e Resistenza Al Moto.” Catania: University of Catania.

Irfan, M., Y. Ali, S. Iqbal, S. Ahmed, and I. Hafeez. 2017. “Rutting Evaluation of Asphalt Mixtures Using Static, Dynamic and Repeated Creep Load Tests.” *Arabian Journal for Science and Engineering*. https://doi.org/10.1007/s13369-017-2982-4.

ISO-13473:1. 2013. “Characterization of Pavement Texture by Use of Sur-Face Profiles. Part 1: De-Termination of Mean Profile Depth.”

ISO-13473:2. 2002. “Characterization of Pavement Texture by Use of Sur-Face Profiles – Part 2: Terminology and Basic Requirements Related to Pavement Texture Profile Analysis.”

ISO-13473:3. 2002. “Characterization of Pavement Texture by Use of Sur-Face Profiles. Part3: Specifications and Classification of Profilometers.”

ISPRA. 2018. “Rapporto Rifiuti Speciali 2018 – Dati Di Sintesi.” *Edizione 2018*. Istituto Superiore per la Protezione e la Ricerca Ambientale.

Iuele, T. 2016. “Road Surface Micro - and Macrotexture Evolution in Relation to Asphalt Mix Composition.” *Advanced Materials and Structural Engineering – Hu (Ed.)*.

Jackson, N.M., B. Choubane, and C.R. Holzschuher. 2007. “Measuring Pavement Friction Characteristics at

Variable Speeds for Added Safety Pavement Surface Condition/Performance Asscessment: Reliability and Relevancy of Procedures and Technoloies, STP 1486." West Conshohocken, PA: ASTM International.

Jahromi, S. G., and A. Khodaii. 2009. "Master Curves for Stiffness Asphalt Concrete." *International Journal of Pavement Research and Technology* 2 (4): 148–53.

Jendia, S., and A. Jarada. 2005. "Traffic Opening Time and Time Available for Compaction for Fresh Asphalt Layer Using Slab Specimens Model." *The Islamic University Journal - Series of Natural Studies and Engineering* 14 (1): 11–35.

Jung, J.S., K.E. Kaloush, and J.B. Way. 2002. "Life Cycle Cost Analysis: Conventional Versus Asphalt-Rubber Pavements." Rubber Pavements Association.

Kennedy, T.W., and J.N. Anagnos. 1983. "Procedures for the Static and Repeated Load Indirect Tensile Tests." Austin.

Khasawneh, M.A., and R.Y. Liang. 2008. "Correlation Study between Locked-Wheel Skid Trailer and Dynamic Friction Tester." In *TRB 87th Annual Meeting*. Washington DC.

Khosla, N. Paul, and Dinesh Ayyala. 2013. "A Performance-Based Evaluation of Superpave Design Gyrations for High Traffic Surface Mixes." *Procedia - Social and Behavioral Sciences*. https://doi.org/10.1016/j.sbspro.2013.11.103.

Kim, Sung Gi, and Kyung Woong Kim. 2008. "Influence of Pad-Pivot Friction on Tilting Pad Journal Bearing." *Tribology International* 41: 694–703. https://doi.org/10.1016/j.triboint.2007.12.003.

Kliewer, J.E., C.A. Bell, and D.A. Sosnovske. 1995. "Investigation of the Relationship between Field Performance and Laboratory Aging Properties of Asphalt Mixtures."

Koba, H., L. Skotnicki, and A. Szydlo. 2012. "Laboratory Evaluation of Asphalt-Rubber Mastic Prepared Using Mixed (Wet+dry) Method."

Kogbara, Reginald B., Eyad A. Masad, Emad Kassem, A. Scarpas, and Kumar Anupam. 2016. "A State-of-the-Art Review of Parameters Influencing Measurement and Modeling of Skid Resistance of Asphalt Pavements." *Construction and Building Materials*. https://doi.org/10.1016/j.conbuildmat.2016.04.002.

Kubo, K. 2011. "Present Status of Porous Elastic Rubber Surface (PERS) in Japan."

Kumbargeria, Y.S., and K.P. Biligiri. 2016. "Understanding Aging Behaviour of Conventional Asphalt Binders Used in India." *Transportation Research Procedia* 17: 282 – 290.

Kuo, Yao-Chen. 2004. "Highway Earthwork and Pavement Production Rates for Construction Time Estimation." University of Texas at Austin.

L'Italia del riciclo. 2015. "Rapporto 2015 – Parte 2: Approfondimenti Settoriali Dedicati Alle Singole Filiere Del Riciclo e Recupero – Gomme e Pneumatici Fuori Uso."

Larson, R.M., T.E. Hoerner, K.D. Smith, and A.S. Wolters. 2008. "Relationship between Skid Resistance Numbers Measured with Ribbed and Smooth Tire and Wet Accident Locations." *Final Report - State Job Number 134323*.

Larson, T.D., R. Seavey, and D.A. Lange. 1998. "Relationship Between Timber Bridge Characteristics and Asphalt Pavement Wear Surface Performance." *1996-1997*.

Lee, S.J., S.N. Amirkhanian, B.J. Putman, and K.W. Kim. 2007. "Laboratory Study of the Effects of Compaction

on the Volumetric and Rutting Properties of CRM Asphalt Mixtures." *Journal of Materials in Civil Engineering* 19 (12): 1079–89.

Lee, Soon Jae, Serji N. Amirkhanian, and Kwang W. Kim. 2009. "Laboratory Evaluation of the Effects of Short-Term Oven Aging on Asphalt Binders in Asphalt Mixtures Using HP-GPC." *Construction and Building Materials* 23: 3087–3093. https://doi.org/10.1016/j.conbuildmat.2009.03.012.

Leiva-Villacorta, F. 2007. "Relationships between Laboratory Measured Characteristics of HMA and Field Compactability." Auburn University.

Leiva, Fabricio, and Randy West. 2008. "Analysis of Hot-Mix Asphalt Lab Compactability Using Lab Compaction Parameters and Mix Characteristics." *Transportation Research Record: Journal of the Transportation Research Board* 2057: 89–98. https://doi.org/10.3141/2057-11.

Lesueur, Didier. 2009. "The Colloidal Structure of Bitumen: Consequences on the Rheology and on the Mechanisms of Bitumen Modification." *Advances in Colloid and Interface Science*. https://doi.org/10.1016/j.cis.2008.08.011.

Li, Qiang, Danny X. Xiao, Kelvin C. P. Wang, Kevin D. Hall, and Yanjun Qiu. 2011. "Mechanistic-Empirical Pavement Design Guide (MEPDG): A Bird's-Eye View." *Journal of Modern Transportation* 19 (2): 114–33. https://doi.org/10.1007/BF03325749.

Li, Shuo, Dwayne Harris, and Tim Wells. 2016. "Surface Texture and Friction Characteristics of Diamond-Ground Concrete and Asphalt Pavements." *Journal of Traffic and Transportation Engineering (English Edition)* 3 (5): 475–82. https://doi.org/10.1016/j.jtte.2016.08.001.

López-Moro, Francisco Javier, María Candelas Moro, Francisco Hernández-Olivares, Bernabé Witoszek-Schultz, and Manuel Alonso-Fernández. 2013. "Microscopic Analysis of the Interaction between Crumb Rubber and Bitumen in Asphalt Mixtures Using the Dry Process." *Construction and Building Materials* 48: 691–699. https://doi.org/10.1016/j.conbuildmat.2013.07.041.

M. A. Yazdi, J. Yang, L. Yihui, H. Su. 2015. "A Review on Application of Waste Tire in Concrete." *World Academy of Science, Engineering and Technology International Journal of Civil and Environmental Engineering* 9 (12).

Maghool, Farshid, Arul Arulrajah, Yan Jun Du, Suksun Horpibulsuk, and Avirut Chinkulkijniwat. 2017. "Environmental Impacts of Utilizing Waste Steel Slag Aggregates as Recycled Road Construction Materials." *Clean Technologies and Environmental Policy*, 1–10. https://doi.org/10.1007/s10098-016-1289-6.

Mallick, Rajib. 1999. "Use of Superpave Gyratory Compactor To Characterize Hot-Mix Asphalt." *Transportation Research Record: Journal of the Transportation Research Board*. https://doi.org/10.3141/1681-11.

Mannan, U.A., M.R. Islam, and R.A. Tarefder. 2015. "Effects of Recycled Asphalt Pavements on the Fatigue Life of Asphalt under Different Strain Levels and Loading Frequencies." *International Journal of Fatigue* 78: 72–80.

Marvillet, J., and P. Bougalt. 1979. "Workability of Bituminous Mixes. Development of a Workability Meter." In *Proceedings, Association of Asphalt Paving Technologists*. Vol. 48. Denver, Colorado.

Maupin, G.W. 1971. "Relationship of Fatigue to the Tensile Stiffness of Asphaltic Concrete." *Final Report on Phase 1: Laboratory Investigation*. Charlottesville, Virginia.

Meegoda, Jay N., and Shengyan Gao. 2015. “Evaluation of Pavement Skid Resistance Using High Speed Texture Measurement.” *Journal of Traffic and Transportation Engineering (English Edition)* 2 (6): 382–90. https://doi.org/10.1016/j.jtte.2015.09.001.

Mensching, David J., Leslie Myers McCarthy, Yusuf Mehta, and Michael Byrne. 2013. “Modeling Flexible Pavement Overlay Performance for Use with Quality-Related Specifications.” *Construction and Building Materials* 48: 1072–1080. https://doi.org/10.1016/j.conbuildmat.2013.07.058.

Micaelo, R., A. Pereira, L. Quaresma, and M. T. Cidade. 2015. “Fatigue Resistance of Asphalt Binders: Assessment of the Analysis Methods in Strain-Controlled Tests.” *Construction and Building Materials*. https://doi.org/10.1016/j.conbuildmat.2015.08.070.

Miller, S.R., T. Hartmann, and A.G. Doreè. 2011. “Measuring and Visualizing Hot Mix Asphalt Concrete Paving Operations.” *Automation in Construction* 20 (4): 474–81. https://doi.org/10.1016/j.autcon.2010.11.015.

MnPAVE. 2012. *User’s Guide*. Minnesota Department of Transportation.

Modarres, Amir. 2013. “Investigating the Toughness and Fatigue Behavior of Conventional and SBS Modified Asphalt Mixes.” *Construction and Building Materials*. https://doi.org/10.1016/j.conbuildmat.2013.05.044.

Nataadmadja, A. D., M. T. Do, D. J. Wilson, and S. B. Costello. 2015. “Quantifying Aggregate Microtexture with Respect to Wear-Case of New Zealand Aggregates.” *Wear* 332–333: 907–17. https://doi.org/10.1016/j.wear.2014.11.028.

NCHRP 1-28A. 2003. “Harmonized Test Methods for Laboratory Determination of Resilient Modulus for Flexible Pavement Design.” *Transportation Research Board*.

Noyce, David A., Hussain U. Bahia, Josué M. Yambó, and Guisk Kim. 2005. “Incorporating Road Safety into Pavement Management: Maximizing Asphalt Pavement Surface Friction for Road Safety Improvements.” *Midwest Regional University Transportation Center*.

Ossa, A., J. L. García, and E. Botero. 2016. “Use of Recycled Construction and Demolition Waste (CDW) Aggregates: A Sustainable Alternative for the Pavement Construction Industry.” *Journal of Cleaner Production* 135: 379–86. https://doi.org/10.1016/j.jclepro.2016.06.088.

Otsuki, Michio, and Hiroshi Matsukawa. 2013. “Systematic Breakdown of Amontons’ Law of Friction for an Elastic Object Locally Obeying Amontons’ Law.” *Scientific Reports*, Scientific Report 3, . https://doi.org/10.1038/srep01586.

Paje, S. E., M. Bueno, F. Terán, R. Miró, F. Pérez-Jiménez, and A. H. Martínez. 2010. “Acoustic Field Evaluation of Asphalt Mixtures with Crumb Rubber.” *Applied Acoustics* 71 (6): 578–82. https://doi.org/10.1016/j.apacoust.2009.12.003.

Park, Hee Mun, Ji Young Choi, Hyun Jong Lee, and Eui Yoon Hwang. 2009. “Performance Evaluation of a High Durability Asphalt Binder and a High Durability Asphalt Mixture for Bridge Deck Pavements.” *Construction and Building Materials* 23: 219–225. https://doi.org/10.1016/j.conbuildmat.2008.01.001.

Partl, M. N., and L. Francken. 1997. “RILEM Interlaboratory Tests on Stiffness Properties of Bituminous Mixtures.” In *Proceedings of the Fifth International RILEM Symposium MTBM*, 15–26. Lyon, France.

Pasandin, A R, and I Perez. 2014. “Mechanical Properties of Hot-Mix Asphalt Made with Recycled Concrete Aggregates Coated with Bitumen Emulsion.” *Construction and Building Materials*.

https://doi.org/10.1016/j.conbuildmat.2014.01.053.

Pavement-Interactive. 2018. “Superpave Mix Design.” 2018. http://www.pavementinteractive.org/superpave-mix-design/.

Pereira, P., and J. Oliveira. 2010. “Sustainability Issues of Asphalt Rubber Pavements.” In *39th International Congress on Noise Control Engineering 2010, INTER-NOISE 2010*, 7369–78.

Petersen, J.C. 2009. “A Review of the Fundamentals of Asphalt Oxidation: Chemical, Physicochemical, Physical Property and Durability Relationships.” *Transportation Research Board*.

Pettinari, M, G Dondi, C Sangiorgi, and F Petretto. 2013. “The Use of Cryogenic Crumb Rubber in the Cold Recycling Technique.” In *Airfield and Highway Pavement 2013*. https://doi.org/10.1061/9780784413005.091.

Poel, C Van Der. 1954. “A General System Describing the Visco-elastic Properties of Bitumens and Its Relation to Routine Test Data.” *Journal of Applied Chemistry* 4: 221–36. https://doi.org/10.1002/jctb.5010040501.

Postorino, Maria Nadia, and Filippo Giammaria Praticò. 2012. “An Application of the Multi-Criteria Decision-Making Analysis to a Regional Multi-Airport System.” *Research in Transportation Business and Management* 4: 44–52. https://doi.org/10.1016/j.rtbm.2012.06.015.

Pradyumna, T.Anil, Abhishek Mittal, and P.K. Jain. 2013. “Characterization of Reclaimed Asphalt Pavement (RAP) for Use in Bituminous Road Construction.” *Procedia - Social and Behavioral Sciences*. https://doi.org/10.1016/j.sbspro.2013.11.211.

Pratico’, F. G., R. Ammendola, and A. Moro. 2010. “Factors Affecting the Environmental Impact of Pavement Wear.” *Transportation Research Part D: Transport and Environment* 15 (3): 127–33. https://doi.org/10.1016/j.trd.2009.12.002.

Pratico’, F.G. 2017. “Metrics for Management of Asphalt Plant Sustainability.” *Journal of Constr. Engineering and Management*. https://doi.org/http://dx.doi.org/10.1061/(ASCE)CO.1943-7862. 00012.

Pratico’, F.G., and A. Casciano. 2015. “Variability of HMA Characteristics and Its Influence on Pay Adjustment.” *Journal of Civil Engineering and Management* 21 (1): 119–30. https://doi.org/10.3846/13923730.2013.802713.

Pratico’, F.G., and A. Moro. 2011. “In-Lab and on-Site Measurements of Hot Mix Asphalt Density: Convergence and Divergence Hypotheses.” *Construction and Building Materials* 25 (2): 1065–71. https://doi.org/10.1016/j.conbuildmat.2010.06.071.

Pratico’, F.G., and R. Vaiana. 2012. “Improving Infrastructure Sustainability in Suburban and Urban Areas: Is Porous Asphalt the Right Answer? And How?” In *WIT Transactions on the Built Environment*, edited by C.A. Brebbia and J. W. S. Longhurst, 673–84. Urban Transport: Urban Transport and the Environment in the 21st Century. https://doi.org/10.2495/UT120571.

Pratico’, F.G., Rosolino Vaiana, and Teresa Iuele. 2015. “Macrotexture Modeling and Experimental Validation for Pavement Surface Treatments.” *Construction and Building Materials* 95: 658–66. https://doi.org/10.1016/j.conbuildmat.2015.07.061.

Praticò, F.G. 2015. “Simple Equations for Cost of Premature Failure of Flexible Pavements in Low-Volume Roads.” *Transportation Research Record: Journal of the Transportation Research Board* 2474: 73–81. https://doi.org/10.3141/2474-09.

Praticò, F.G., A. Moro, S. Noto, and G. Colicchio. 2016. “Three-Year Investigation on Hot and Cold Mixes with Rubber.” In *8th International Conference on Maintenance and Rehabilitation of Pavements, MAIREPAV 2016*. https://doi.org/10.3850/978-981-11-0449-7-085-cd.

Praticò, F.G., S. Noto, and A. Astolfi. 2017. “In-Lab versus on-Site Measurement of Surface Performance of Flexible Pavements.” In *Tenth International Conference on the Bearing Capacity of Roads, Railways and Airfields*.

Praticò, F.G., and R. Vaiana. 2013. “A Study on Volumetric versus Surface Properties of Wearing Courses.” *Construction and Building Materials* 38: 766–75. https://doi.org/10.1016/j.conbuildmat.2012.09.021.

Pratico, F G. 2007. “Non-Conformities in Flexible Pavements: A Theoretical and Experimental Study on Pay Adjustment.” In *25th Inaugural Construction Management and Economics: “Past, Present and Future” Conference, CME 2007*.

Praticò, Filippo G., and R. Vaiana. 2015. “A Study on the Relationship between Mean Texture Depth and Mean Profile Depth of Asphalt Pavements.” *Construction and Building Materials* 101: 72–79. https://doi.org/10.1016/j.conbuildmat.2015.10.021.

Presti, D. Lo. 2011. “Rheology and Curing of Tyre Rubber Modified Bitumens.” Università degli Studi di Palermo. https://doi.org/DOI: 10.13140/RG.2.1.2815.2720.

Presti, D. Lo, G. Giancontieri, and D. M. Hargreaves. 2017. “Improving the Rheometry of Rubberized Bitumen: Experimental and Computation Fluid Dynamics Studies.” *Construction and Building Materials* 136: 286–97. https://doi.org/10.1016/j.conbuildmat.2016.12.200.

Presti, Davide Lo. 2013. “Recycled Tyre Rubber Modified Bitumens for Road Asphalt Mixtures: A Literature Review.” *Construction and Building Materials*. https://doi.org/10.1016/j.conbuildmat.2013.09.007.

Rahman, M. 2004. “Characterisation of Dry Process Crumb Rubber Modified Asphalt Mixtures.” University of Nottingham.

Ramírez, Antonio, Juan Gallego, José R. Marcobal, and Carlos Blázquez. 2015. “Development of New Laboratory Equipment for Measuring the Accelerated Polishing of Asphalt Mixes.” *Wear*. https://doi.org/10.1016/j.wear.2014.11.006.

Read, J.M., A.C. Collop, and T. Singleton. 1997. “Practical Fatigue Characterisation of Bituminous Paving Mixtures.” *Asphalt Paving Technology*, 74–108.

Roberts, F. L., S. Prithvi, E. Kandhal, R. Brown, L. Dah-Yinn, and T. W. Kennedy. 1996. *Hot Mix Asphalt Materials, Mixture Design, and Constrution*. *Hot Mix Asphalt Materials, Mixture Design, and Constrution*.

Roberts, F.L., P.S. Kandhal, E.R. Brown, D.Y. Lee, and W. Kennedy. 1996. *Hot Mix Asphalt Materials, Mixture Design and Construction*. Second Edi. NAPA Education Foundation.

Roque, R., A. Ravanshad, and G. Lopp. 2013. “Use of Aggregate Image Measurement System (AIMS) to Evaluate Aggregate Polishing in Friction Surfaces.” *Final Report*.

Ruth, B.E., and R. Roque. 1995. “Crumb Rubber Modifier (CRM) in Asphalt Pavements.” *Transportation Congress*.

Said, S. F. 1998. “Validation of Indirect Tensile Test for Fatigue Testing of Bituminous Mixes.”

Sandberg, U. 1998. “Influence of Road Surface Texture on Traffic Characteristics Related to Environment,

Economy and Safety: A State-of-the-Art Study Regarding Measures and Measuring Methods." Measuremen. Swedish.

Sangiorgi, Cesare, Shahin Eskandarsefat, Piergiorgio Tataranni, Andrea Simone, Valeria Vignali, Claudio Lantieri, and Giulio Dondi. 2017. "A Complete Laboratory Assessment of Crumb Rubber Porous Asphalt." *Construction and Building Materials* 132: 500–507. https://doi.org/10.1016/j.conbuildmat.2016.12.016.

Santagata, E., D. Dalmazzo, M. Lanotte, M.C. Zanetti, and B. Ruffino. 2012. "Relationship between Crumb Rubber Morphology and Asphalt Rubber Viscosity."

Santagata, E, S Fiore, M Zanetti, and B Ruffino. 2013. "Use of Crumb Rubber in Road Paving Applications: Workers' Health Risk Assessment." *Proceedings Sardinia 2013, Fourteenth International Waste Management and Landfill Symposium*.

Santero, N. J., J. T. Harvey, E. Kohler, and B. Farnbach. 2008. "Life Cycle Cost Analysis of Dowel Bar Retrofit."

Santero, Nicholas, Alexander Loijos, Mehdi Akbarian, and John Ochsendorf. 2011. "Methods, Impacts, and Opportunities in the Concrete Pavement Life Cycle." *Concrete and Sustainability Hub, Department of Civil and Environmental Engineering, Massachusetts Institute of Technology*. https://doi.org/10.1371/journal.pone.0079038 PONE-D-13-17623 [pii].

Sarsam, S.I., and H.N. Al Shareef. 2015. "Assessment of Texture and Skid Variables at Pavement Sur-Face." *Applied Research Journal* 1 (8): 422–32.

Scherocman, J.A. 1984. "Guidelines for Compacting Asphalt Concrete Pavement." *Better Roads* 54 (3): 12–17.

Segre, N., and I. Joekes. 2000. "Use of Tire Rubber Particles as Addition to Cement Paste." *Cement and Concrete Research* 30: 1421–25. https://doi.org/10.1016/S0008-8846(00)00373-2.

Shen, J., Z. Xie, and Bo Li. 2014. "Comprehensive Evaluation of the Long-Term Performance of Rubberized Pavement: Phase II: The Influence of Rubber and Asphalt Interaction on Mixture Durability." *Report No.: FHWA-GA-12-1229*.

Shen, Junan, Serji Amirkhanian, Feipeng Xiao, and Boming Tang. 2009. "Surface Area of Crumb Rubber Modifier and Its Influence on High-Temperature Viscosity of CRM Binders." *International Journal of Pavement Engineering* 10 (5): 375–381. https://doi.org/10.1080/10298430802342757.

Shu, Xiang, and Baoshan Huang. 2014. "Recycling of Waste Tire Rubber in Asphalt and Portland Cement Concrete: An Overview." *Construction and Building Materials* 67: 217–224. https://doi.org/10.1016/j.conbuildmat.2013.11.027.

SILENT RUBBER PAVE. 2017. "Accelerate the Commercialization of RARX Technology Process in the Global Markets of ECOLOGICALLY FRIENDLY SILENT RUBBER PAVEMENTS." https://cordis.europa.eu/project/rcn/209860_en.html.

Snyder, M.D. 2007. "Current Perspectives on Pavement Surface Characteristics, ACPA Publication EB235P Pavement Surface Characteristics: A Synthesis and Guide." *R&T Update, Concreten Pavement Research & Technology* 8.02.

Sodupe-Ortega, E., E. Fraile-Garcia, J. Ferreiro-Cabello, and A. Sanz-Garcia. 2016. "Evaluation of Crumb Rubber as Aggregate for Automated Manufacturing of Rubberized Long Hollow Blocks and Bricks." *Construction and Building Materials* 106: 305–316.

https://doi.org/10.1016/j.conbuildmat.2015.12.131.

Sousa, J., G. Way, and D.D. Carlson. 2001. “Cost Benefit Analysis and Energy Consumption of Scrap Tire Management Options.” Rubber Pavements Association.

Sousa, J.S. 2015. “Reacted and Activated Rubber - The New Frontier in Improved Pavements.” http://www.consulpav.com/shrp/.

Speight, James G. 2016. “Asphalt Paving.” In *Asphalt Materials Science and Technology*, 409–35. Elsevier. https://doi.org/https://doi.org/10.1016/C2013-0-15469-4.

Su, Haolin, Jian Yang, Gurmel S. Ghataora, and Samir Dirar. 2015. “Surface Modified Used Rubber Tyre Aggregates: Effect on Recycled Concrete Performance.” *Magazine of Concrete Research* 67 (12): 680–91. https://doi.org/10.1680/macr.14.00255.

Subhy, A.T. 2016. “Characterisation and Development of Rubberised Bitumen and Asphalt Mixture Based on Performance-Related Requirements.” University of Nottingham.

Subhy, Ayad, Davide Lo Presti, and Gordon Airey. 2015. “An Investigation on Using Pre-Treated Tyre Rubber as a Replacement of Synthetic Polymers for Bitumen Modification.” *Road Materials and Pavement Design* 16: 245–64. https://doi.org/10.1080/14680629.2015.1030826.

Sunarjono, Sri. 2013. “Performance of Foamed Asphalt under Repeated Load Axial Test.” In *Procedia Engineering*, 698 – 710. The 2nd International Conference on Rehabilitation and Maintenance in Civil Engineering. https://doi.org/10.1016/j.proeng.2013.03.064.

Symons, and Monte. 2010. “Life-Cycle Cost Analysis for Airport Pavements.” Edited by Airfield Asphalt Pavement Technology Program. *AAPTP 06-06*. Auburn, AL.

Tabaković, Amir, Amanda Gibney, Ciaran McNally, and Michael D. Gilchrist. 2010. “Influence of Recycled Asphalt Pavement on Fatigue Performance of Asphalt Concrete Base Courses.” *Journal of Materials in Civil Engineering*. https://doi.org/10.1061/(asce)mt.1943-5533.0000093.

Tarefder, R., M.U. Ahmed, and M.M. Rahman. 2013. “Evaluating Functional and Structural Condition Based Maintenances of Airfield Pavements.” *Civil Engineering Dimension* 15 (2): 71–80. https://doi.org/10.9744/ced.15.2.71-80.

TEKNECO. 2015. “Un Milione Di Tonnellate Di Pneumatici Fuori Uso Raccolti e Recuperati.” 2015. http://www.tekneco.it/ambiente/1-milione-di-tonnellate-di-pneumatici-fuori-uso-raccolti-e-recuperati/.

Tex-241-F. 2015. “Test Procedure for COMPACTING BITUMINOUS SPECIMENS USING THE SUPERPAVE GYRATORY COMPACTOR (SGC).” Texas Department of Transportation.

Til, C.J. Van, B.F. Mc Cullough, B.A. Vallerga, and R.G. Hicks. 1972. *Evaluation of AASHTO Interim Guides for Design of Pavement Structures*. National C. OAKLAND, CALIFORNIA: MATERIALS RESEARCH & DEVELOPMENT, INC.

Timm, D. H., V. R. Voller, E. Lee, and J. Harvey. 2001. “Calcool: A Multi-Layer Asphalt Pavement Cooling Tool for Temperature Prediction During Construction.” *International Journal of Pavement Engineering* 2 (3): 169–85. https://doi.org/doi.org/10.1080/10298430108901725.

Tjan, A, and R. Napitupulu. 2013. “Verification of Resilient Modulus Prediction of Asphalt Mixtures.” In *Proceedings of the Eastern Asia Society for Transportation Studies*.

Tuononen, Ari J. 2016. “Onset of Frictional Sliding of Rubber-Glass Contact under Dry and Lubricated Conditions.” *Scientific Reports*. https://doi.org/10.1038/srep27951.

Vaiana, R., G.F. Capiluppi, V. Gallelli, T. Iuele, and V. Minani. 2012. “Pavement Surface Performances Evolution: An Experimental Application.” *Procedia - Social and Behavioral Sciences* 53: 1151–62. https://doi.org/10.1016/j.sbspro.2012.09.964.

Vallerga, B.A. 1981. “Pavement Deficiencies Related to Asphalt Durability.” In *Proceedings of the Association of Asphalt Paving Technologists*, 481–491.

Vasenev, Alexandr, Timo Hartmann, and André Dorée. 2012. “A Real-Time System for Prediction Cooling within the Asphalt Layer to Support Rolling Operations.” In *5th Eurasphalt & Eurobitume Congress*. Istanbul.

Vavrik, W.R., and S.H. Carpenter. 1998. “Calculating Air Voids at Specified Number of Gyrations in Superpave Gyratory Compactor.” *Transportation Research Record 1630*, 117–125.

Wambold, J.C., and J.J. Henry. 1995. “International PIARC Experiment to Compare and Harmonize Texture and Skid Resistance Measurements.” *Nordic Road & Transport Research* 6 (2): 28–31.

Wang, Hainian, Zhanping You, Julian Mills-Beale, and Peiwen Hao. 2012. “Laboratory Evaluation on High Temperature Viscosity and Low Temperature Stiffness of Asphalt Binder with High Percent Scrap Tire Rubber.” *Construction and Building Materials* 26 (1): 583–90. https://doi.org/10.1016/j.conbuildmat.2011.06.061.

Wardati, Hashima, Haininb Mohd Rosli, Nadia Ismailc Norfarah, Md. Yusoffc Nur Izzi, Abdullahd Mohd Ezree, and Abdul Hassan Norhidayah. 2016. “EVALUATING THE COOLING RATE OF HOT MIX ASPHALT IN TROPICAL CLIMATE.” *Jurnal Teknologi (Sciences & Engineering)* 78 (4): 97–104. https://doi.org/DOI: 10.11113/jt.v78.8004.

Wellner, F., G. Canon Falla, R. Millow, A. Blasl, G. Di Mino, C.M. Di Liberto, S. Noto, D. Lo Presti, A. Jimenez Del Barco Carrion, and G. Airey. 2015. “High-Content RAP Warm Asphalt Mixture Design.”

Woodward, David, Philip Millar, Claudio Lantieri, Cesare Sangiorgi, and Valeria Vignali. 2016. “The Wear of Stone Mastic Asphalt Due to Slow Speed High Stress Simulated Laboratory Trafficking.” *Construction and Building Materials* 110: 270–77. https://doi.org/10.1016/j.conbuildmat.2016.02.031.

Xiaowei, Cheng, Huang Sheng, Guo Xiaoyang, and Duan Wenhui. 2017. “Crumb Waste Tire Rubber Surface Modification by Plasma Polymerization of Ethanol and Its Application on Oil-Well Cement.” *Applied Surface Science* 409: 325–342. https://doi.org/10.1016/j.apsusc.2017.03.072.

Xie, Zhaoxing, and Junan Shen. 2016. “Performance Properties of Rubberized Stone Matrix Asphalt Mixtures Produced through Different Processes.” *Construction and Building Materials* 104: 230–34. https://doi.org/10.1016/j.conbuildmat.2015.12.063.

Youssf, Osama, Julie E. Mills, and Reza Hassanli. 2016. “Assessment of the Mechanical Performance of Crumb Rubber Concrete.” *Construction and Building Materials* 125: 175–83. https://doi.org/10.1016/j.conbuildmat.2016.08.040.

Yu, G. X., Z. M. Li, X. L. Zhou, and C. L. Li. 2011. “Crumb Rubber-Modified Asphalt: Microwave Treatment Effects.” *Petroleum Science and Technology* 29 (4): 411–17. https://doi.org/10.1080/10916460903394102.

Zainudin, M. Zulfikri M., Faridah Hanim Khairuddin, Choy Peng Ng, Siti Khadijah Che Osmi, N. Aina Misnon,

and S. Murniati. 2016. “Effect of Sugarcane Bagasse Ash as Filler in Hot Mix Asphalt.” *Materials Science Forum* 846: 683–89. https://doi.org/10.4028/www.scientific.net/MSF.846.683.

Zanetti, M.C., S. Fiore, B. Ruffino, E. Santagata, D. Dalmazzo, and M. Lanotte. 2015. “Characterization of Crumb Rubber from End-of-Life Tyres for Paving Applications.” *Waste Management* 45: 161–170. https://doi.org/10.1016/j.wasman.2015.05.003.

Zanetti, M.C., S. Fiore, B. Ruffino, E. Santagata, and M. Lanotte. 2014. “Assessment of Gaseous Emissions Produced on Site by Bituminous Mixtures Containing Crumb Rubber.” *Construction and Building Materials* 67: 291–96. https://doi.org/10.1016/j.conbuildmat.2014.03.030.

Zanetti, M.C., E. Santagata, S. Fiore, B. Ruffino, D. Dalmazzo, and M. Lanotte. 2016. “Evaluation of Potential Gaseous Emissions of Asphalt Rubber Bituminous Mixtures. Proposal of a New Laboratory Test Procedure.” *Construction and Building Materials* 113: 870–79. https://doi.org/10.1016/j.conbuildmat.2016.03.101.

Zaumanis, M., L. D. Poulikakos, and M. N. Partl. 2018. “Performance-Based Design of Asphalt Mixtures and Review of Key Parameters.” *Materials and Design* 141: 185–201. https://doi.org/10.1016/j.matdes.2017.12.035.

Zhang, Z. 2012. “Influencing Factors Research on Compaction Effect of Coarse Rubber Granule Asphalt Mixture.”

Zhao, F.R., T.J. Qiu, and H. Zhang. 2016. “Effect of Macro-Texture Features on Anti-Sliding Characteristics of Cement Concrete Pavement.” *Zhongguo Gonglu Xuebao/China Journal of Highway and Transport* 29 (7): 15–21.

Zhou, F, T Scullion, and L Sun. 2004. “Verification and Modeling of Three-Stage Permanent Deformation Behavior of Asphalt Mixes.” *Journal of Transportation Engineering* 130 (4): 486–94. https://doi.org/10.1061/(ASCE)0733-947X(2004)130:4(486).

Zhu, J. 2016. “Storage Stability and Phase Separation Behaviour of Polymer-Modified Bitumen Characterization and Modelling.”

11 ANNEX 1 – Densification curves

This section reports in more detail the results discussed in section 5.

11.1 PA-control (Porous Asphalt mixes without rubber)

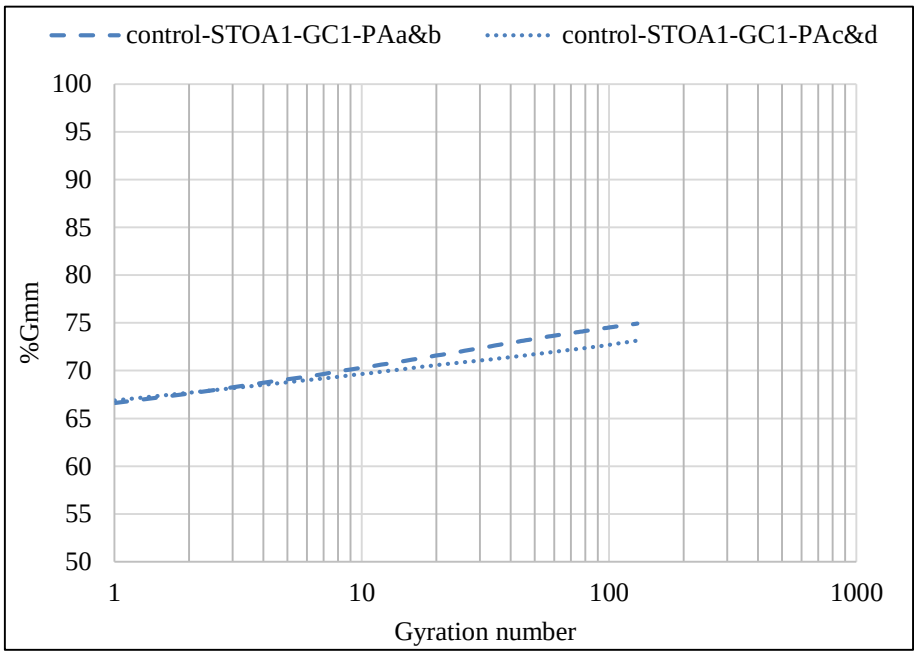

Figure 11.1: Densification curves of PA-control samples (Porous Asphalt mixes without rubber), STOA1-GC1.

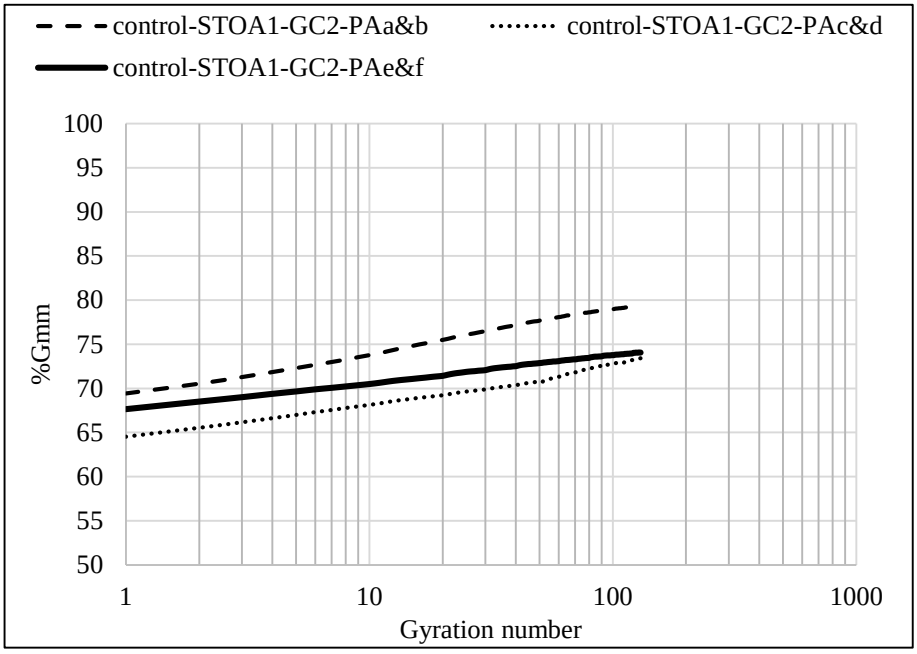

Figure 11.2: Densification curves of PA-control samples (Porous Asphalt mixes without rubber), STOA1-GC2.

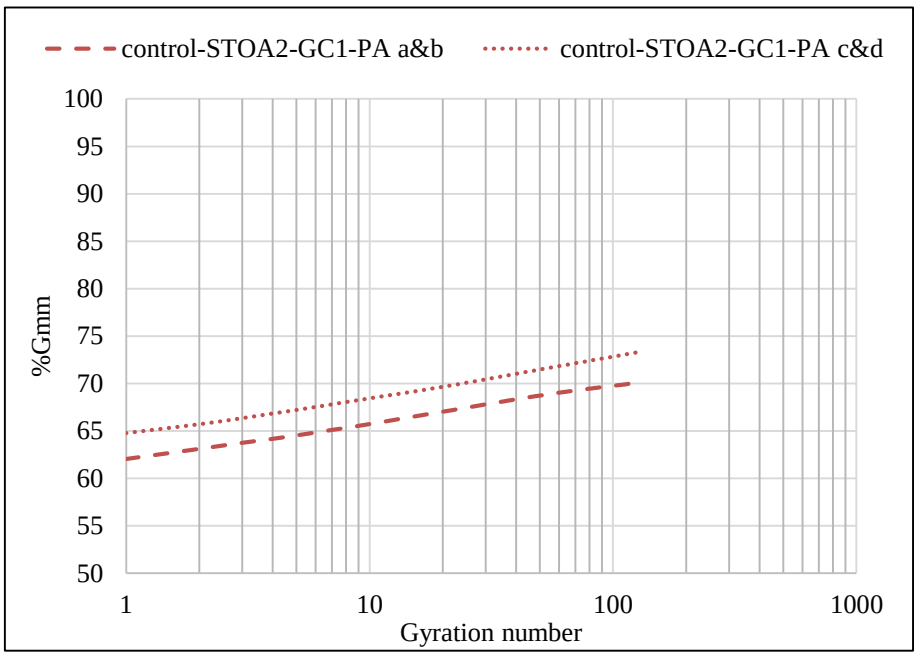

Figure 11.3: Densification curves of PA-control samples (Porous Asphalt mixes without rubber), STOA2-GC1.

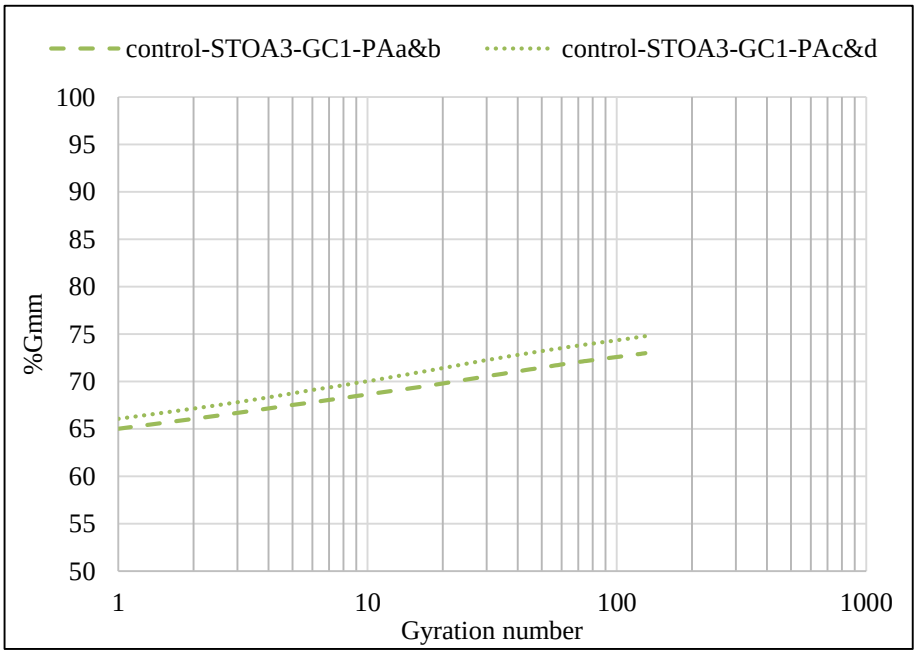

Figure 11.4: Densification curves of PA-control samples (Porous Asphalt mixes without rubber), STOA3-GC1.

11.2 PA-CRT1 (Porous Asphalt mixes with CRT1 rubber)

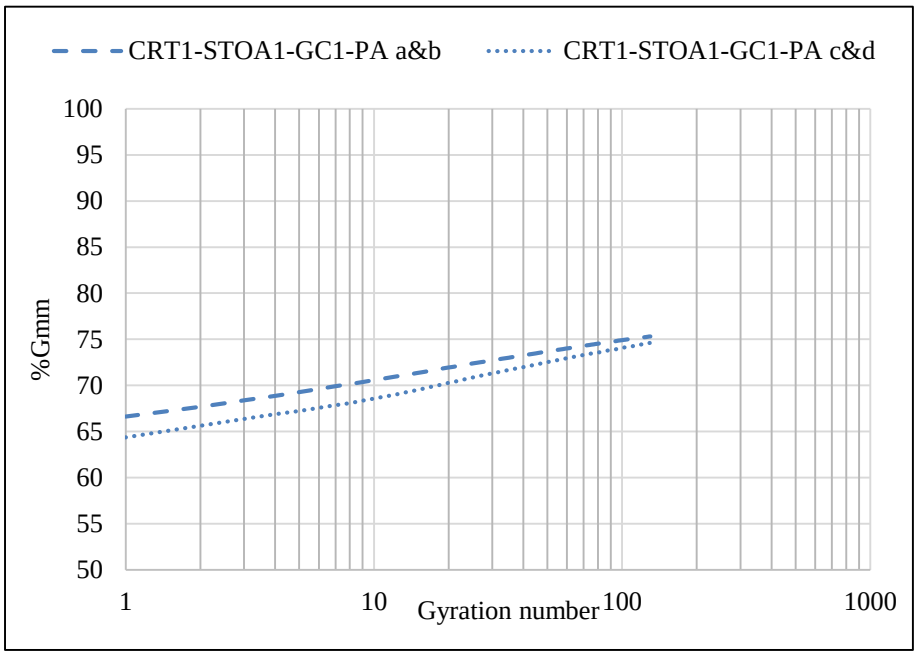

Figure 11.5: Densification curves of PA-CRT1 samples (Porous Asphalt mixes with CRT1 rubber), STOA1-GC1.

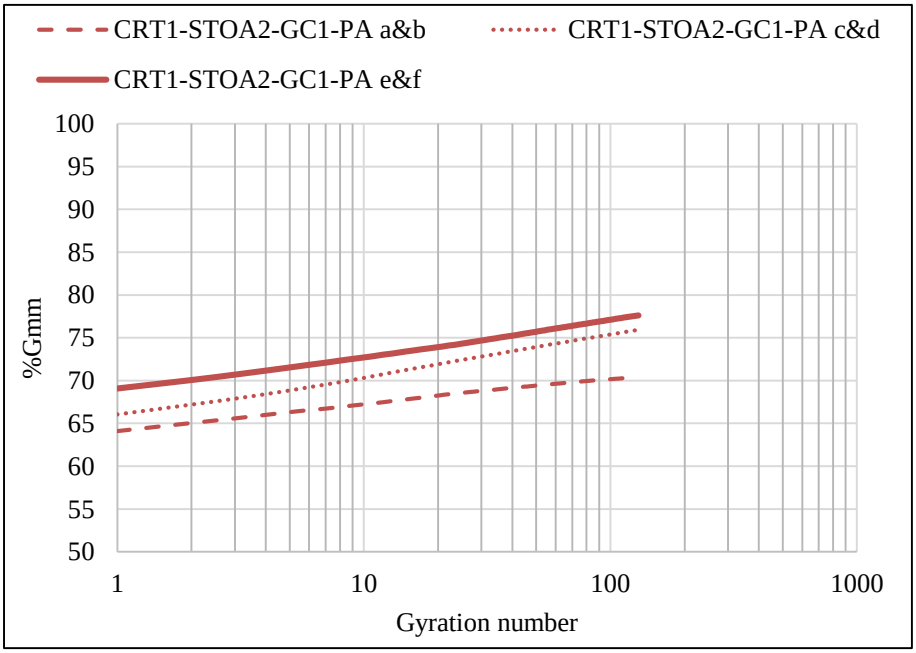

Figure 11.6: Densification curves of PA-CRT1 samples (Porous Asphalt mixes with CRT1 rubber), STOA2-GC1.

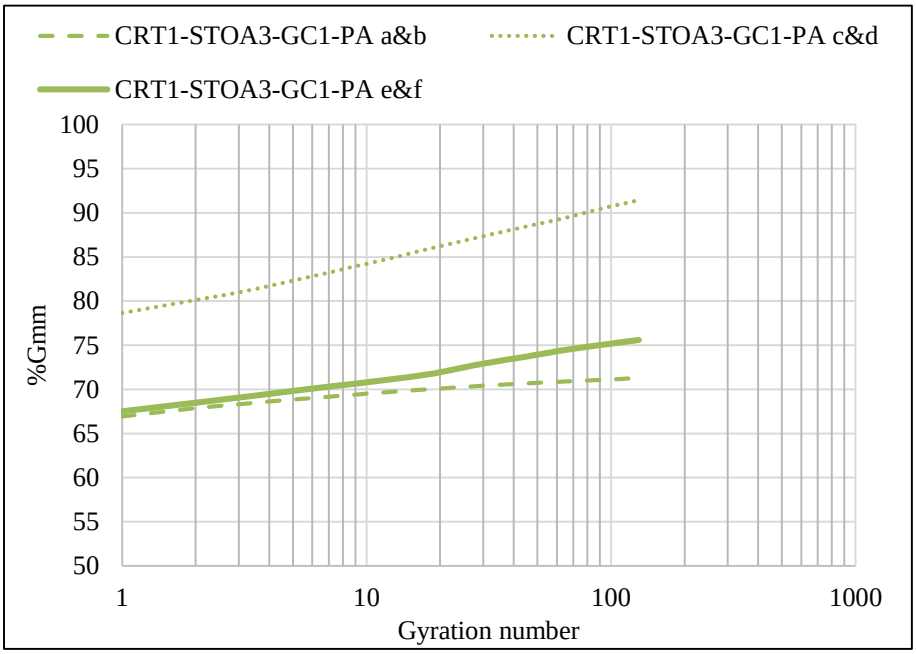

Figure 11.7: Densification curves of PA-CRT1 samples (Porous Asphalt mixes with CRT1 rubber), STOA3-GC1.

11.3 PA-CRT2 (Porous Asphalt mixes with CRT2 rubber)

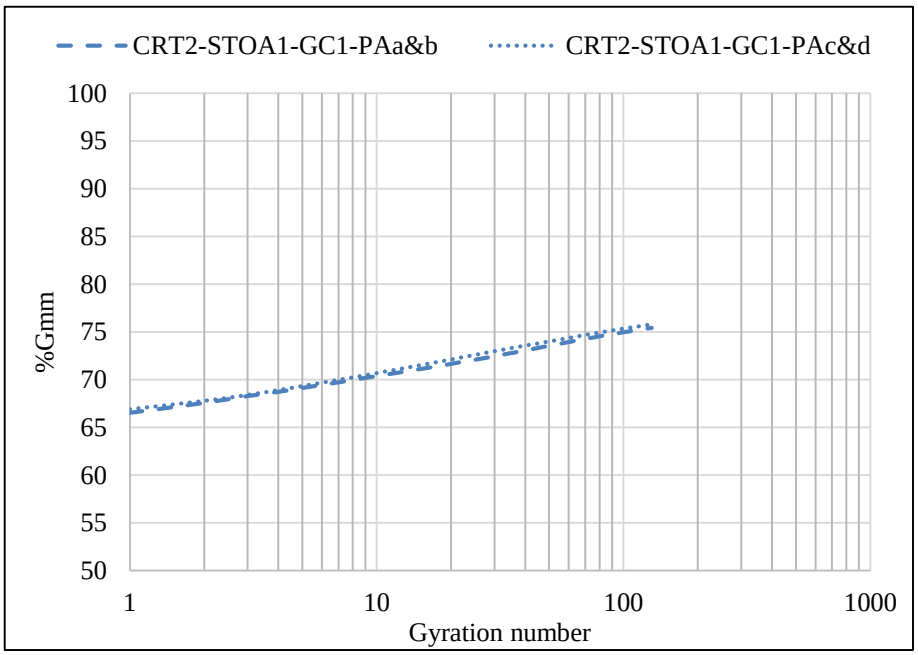

Figure 11.8: Densification curves of PA-CRT2 samples (Porous Asphalt mixes with CRT2 rubber), STOA1-GC1.

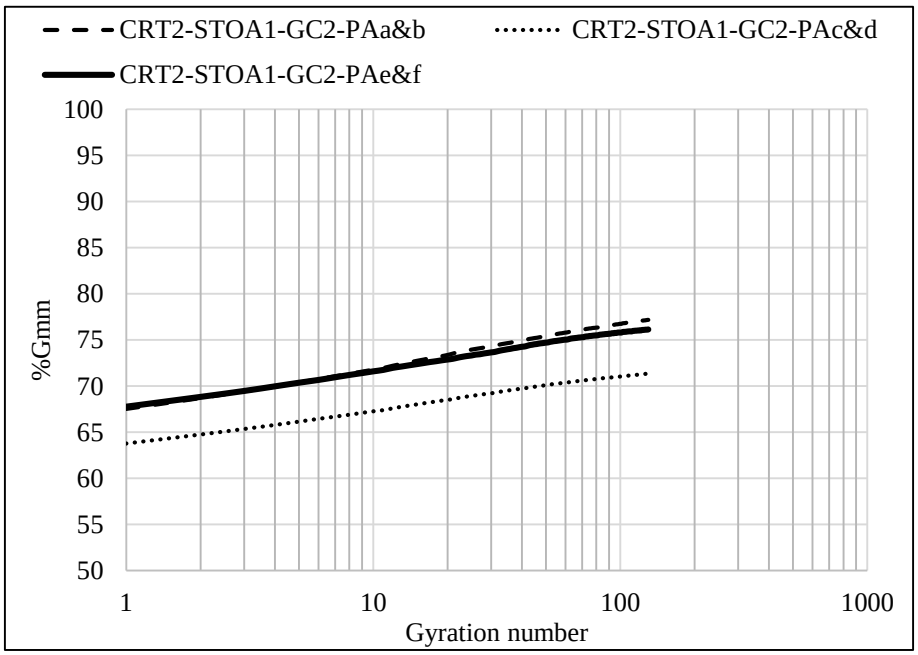

Figure 11.9: Densification curves of PA-CRT2 samples (Porous Asphalt mixes with CRT2 rubber), STOA1-GC2.

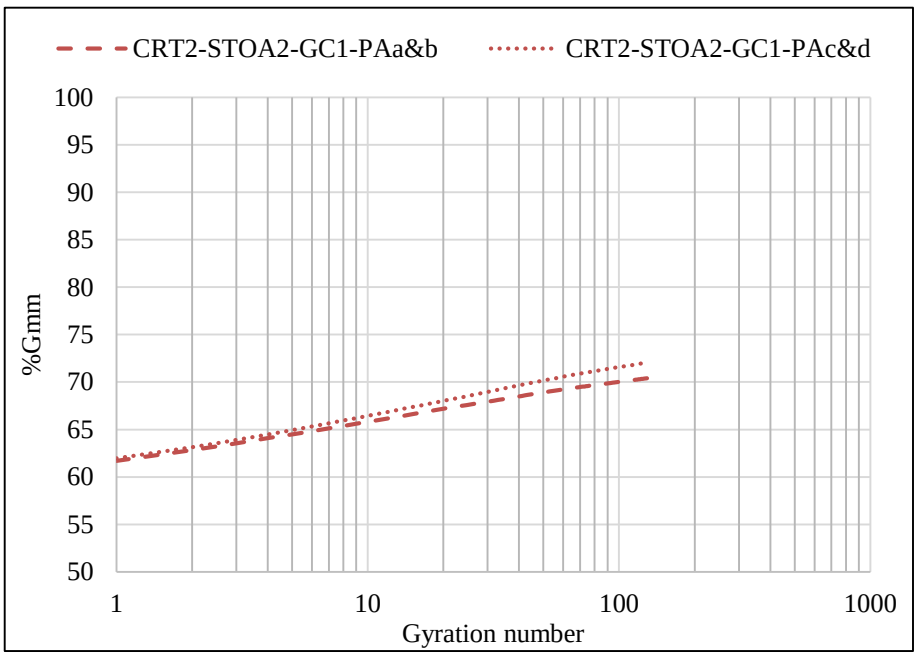

Figure 11.10: Densification curves of PA-CRT2 samples (Porous Asphalt mixes with CRT2 rubber), STOA2-GC1.

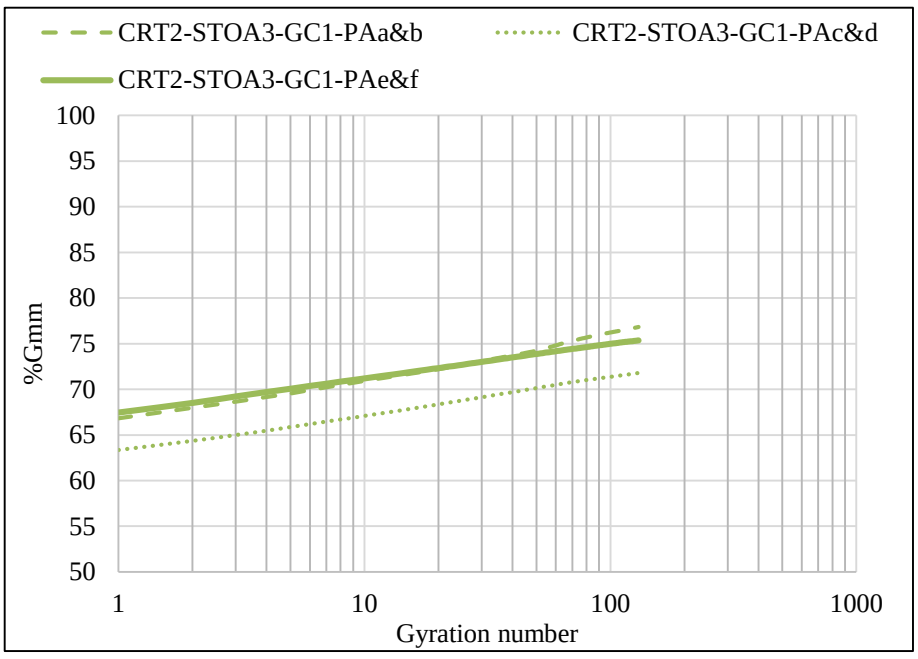

Figure 11.11: Densification curves of PA-CRT2 samples (Porous Asphalt mixes with CRT2 rubber), STOA3-GC1.

11.4 PA-CRN (Porous Asphalt mixes with CRN rubber)

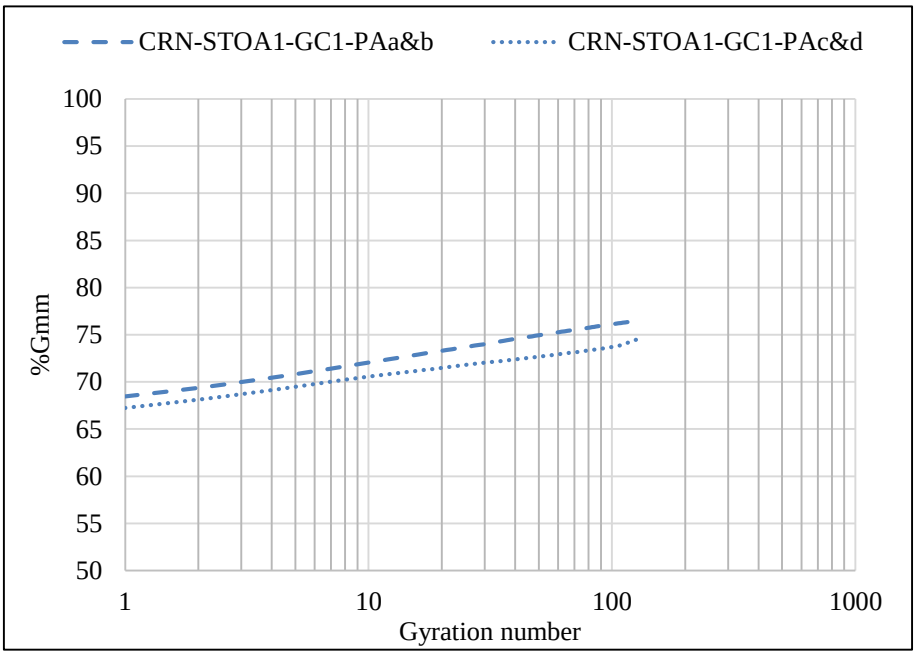

Figure 11.12: Densification curves of PA-CRN samples (Porous Asphalt mixes with CRN rubber), STOA1-GC1.

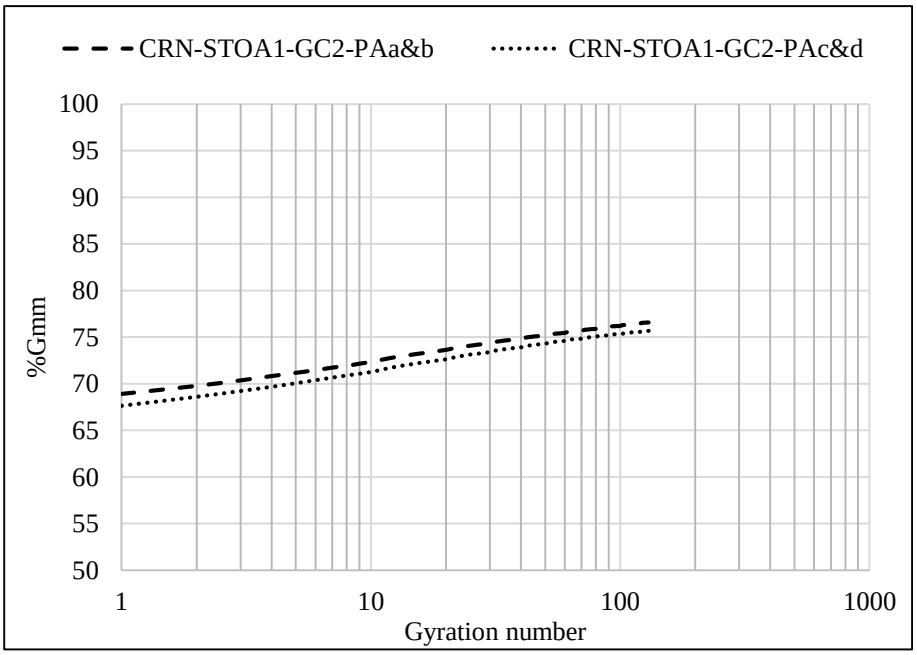

Figure 11.13: Densification curves of PA-CRN samples (Porous Asphalt mixes with CRN rubber), STOA1-GC2.

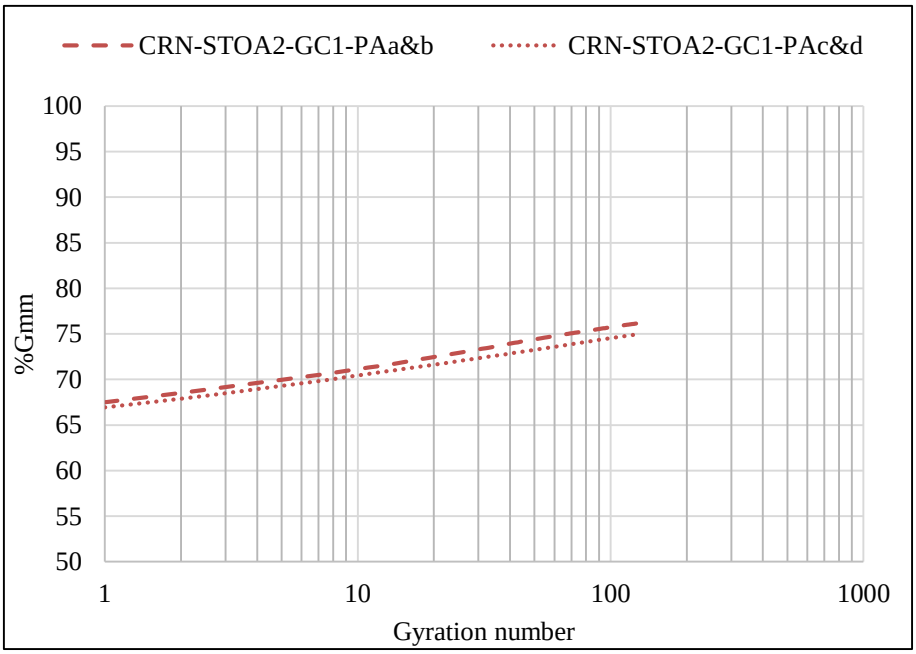

Figure 11.14: Densification curves of PA-CRN samples (Porous Asphalt mixes with CRN rubber), STOA2-GC1.

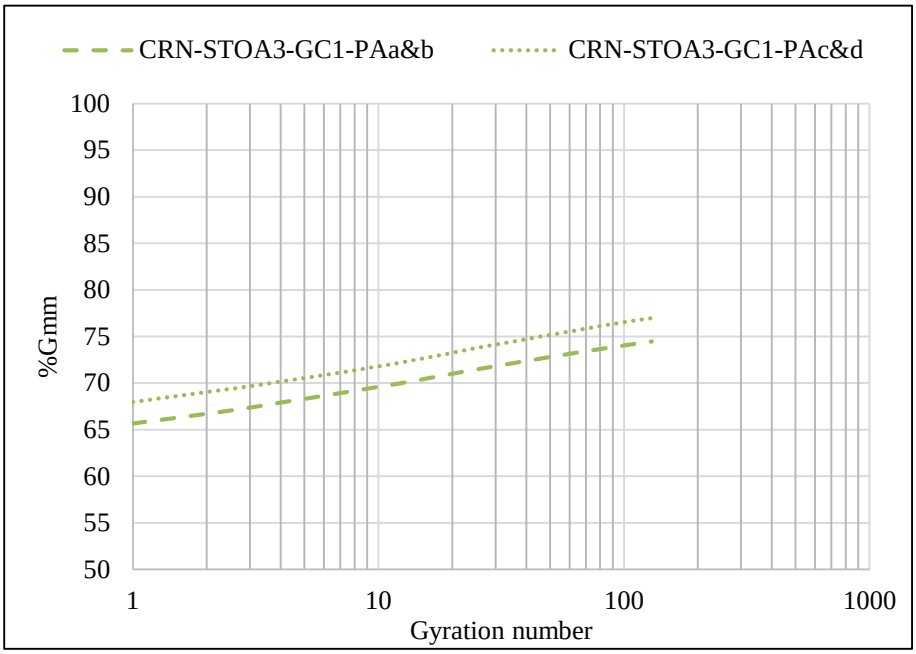

Figure 11.15: Densification curves of PA-CRN samples (Porous Asphalt mixes with CRN rubber), STOA3-GC1.

11.5 SMA10-control (Stone Mastic Asphalt mixes without rubber)

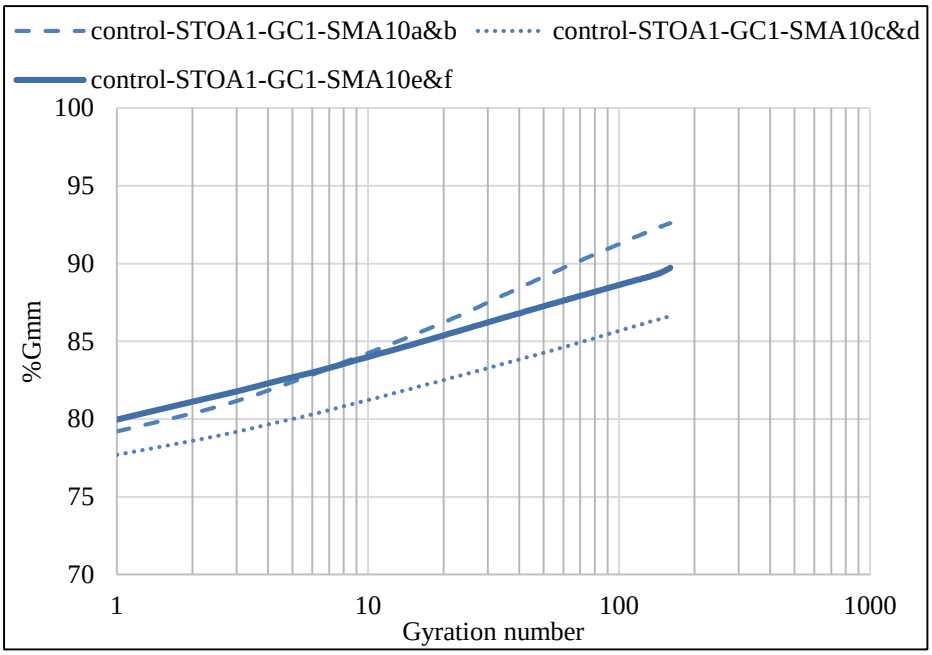

Figure 11.16: Densification curves of SMA10-control samples (SMA10 mixes without rubber), STOA1-GC1.

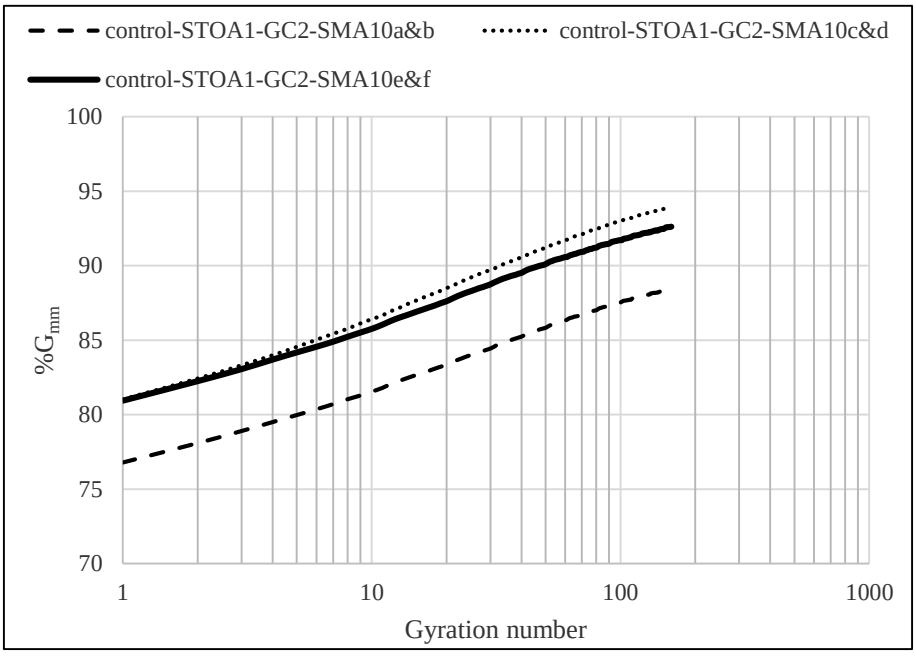

Figure 11.17: Densification curves of SMA10-control samples (SMA10 mixes without rubber), STOA1-GC2.

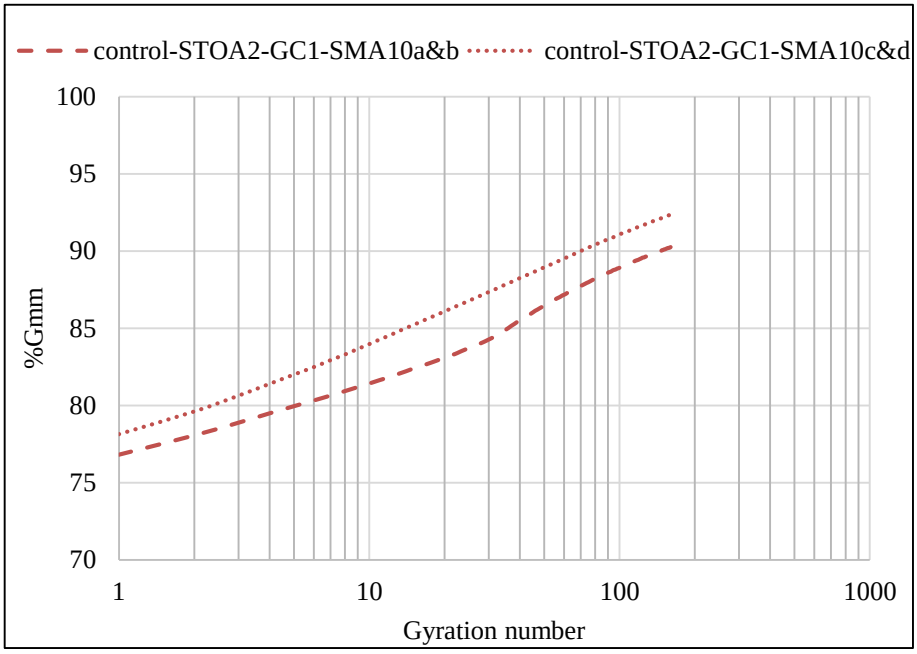

Figure 11.18: Densification curves of SMA10-control samples (SMA10 mixes without rubber), STOA2-GC1.

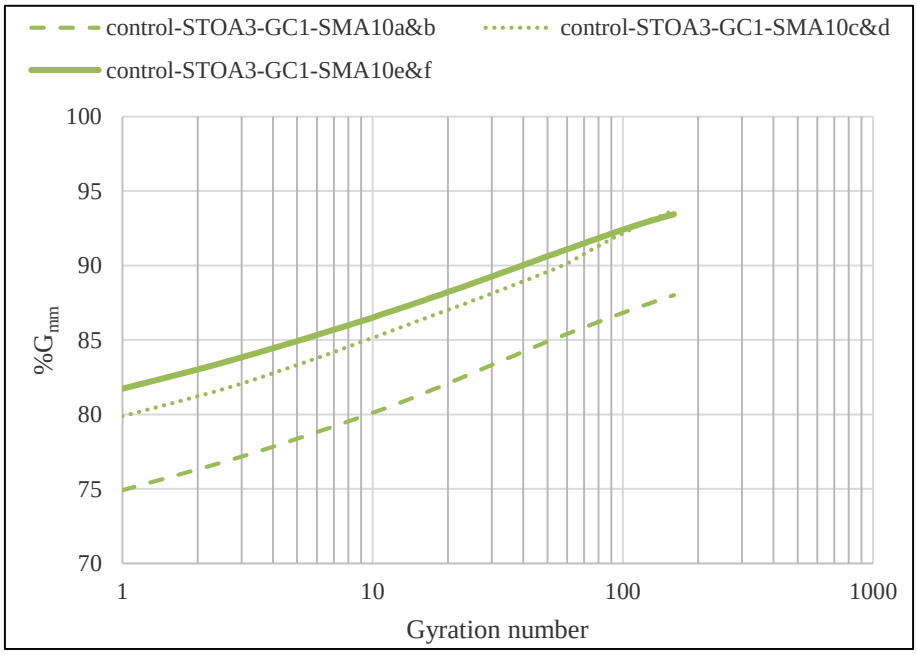

Figure 11.19: Densification curves of SMA10-control samples (SMA10 mixes without rubber), STOA3-GC1.

11.6 SMA10-CRT1 (Stone Mastic Asphalt mixes with CRT1 rubber)

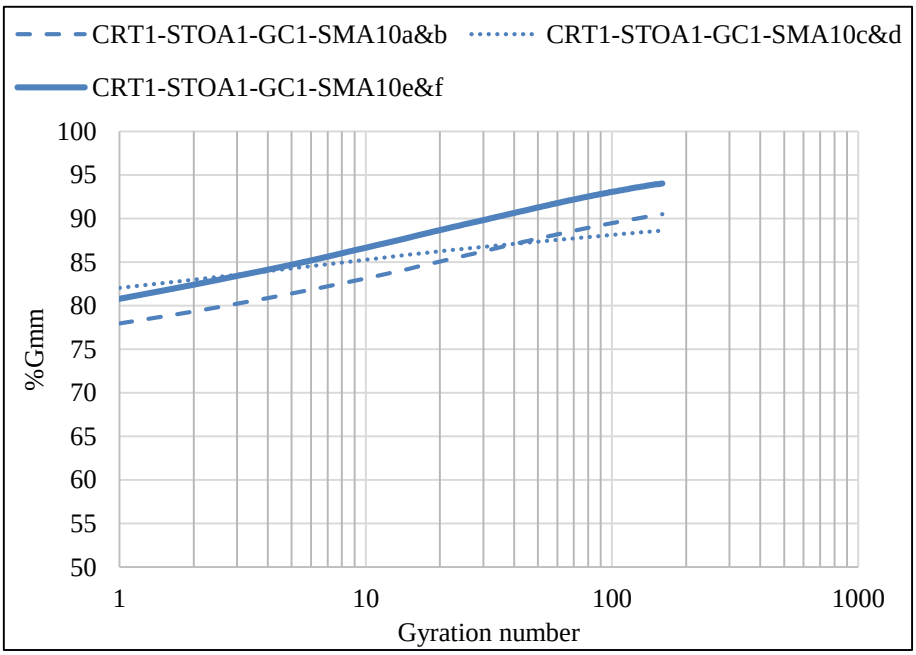

Figure 11.20: Densification curves of SMA10-CRT1 samples (SMA10 mixes with CRT1 rubber), STOA1-GC1.

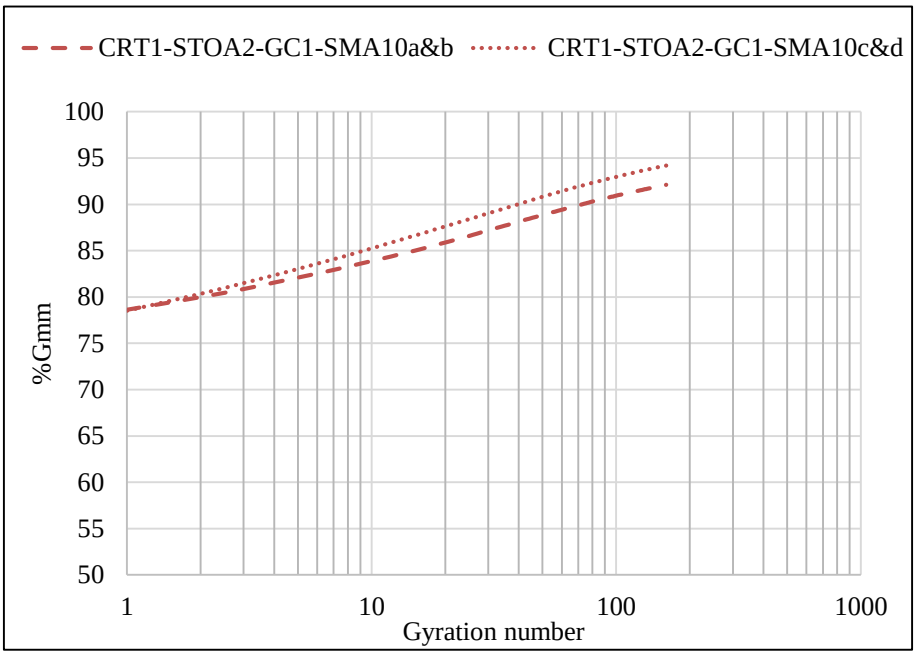

Figure 11.21: Densification curves of SMA10-CRT1 samples (SMA10 mixes with CRT1 rubber), STOA2-GC1.

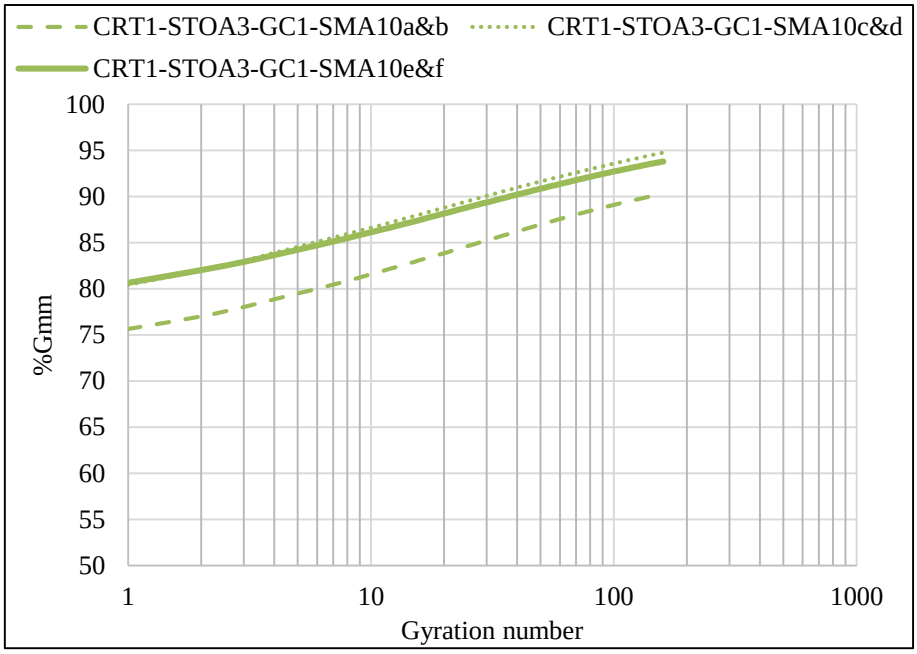

Figure 11.22: Densification curves of SMA10-CRT1 samples (SMA10 mixes with CRT1 rubber), STOA3-GC1.

11.7 SMA10-CRT2 (Stone Mastic Asphalt mixes with CRT2 rubber)

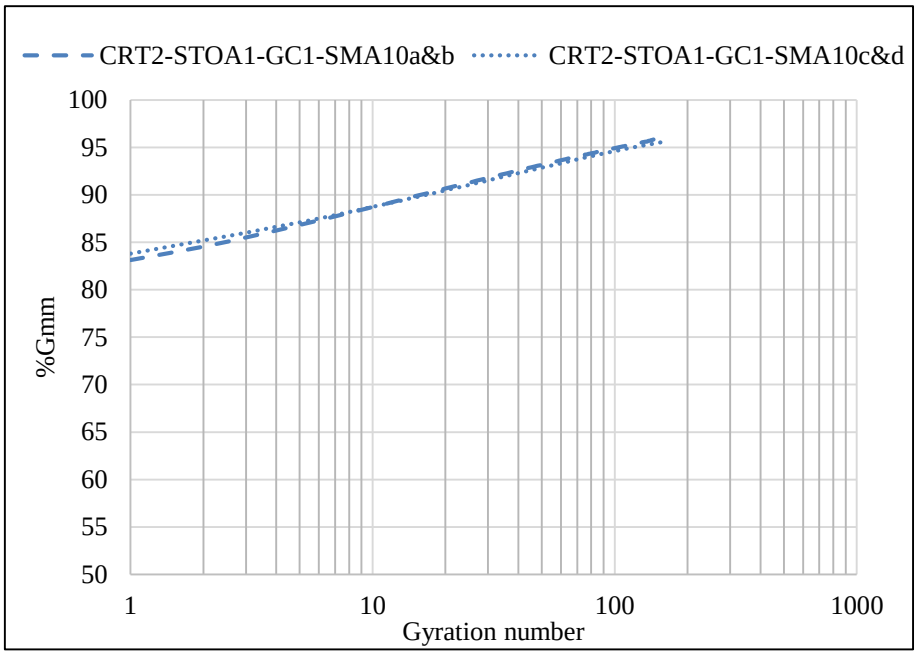

Figure 11.23: Densification curves of SMA10-CRT2 samples (SMA10 mixes with CRT2 rubber), STOA1-GC1.

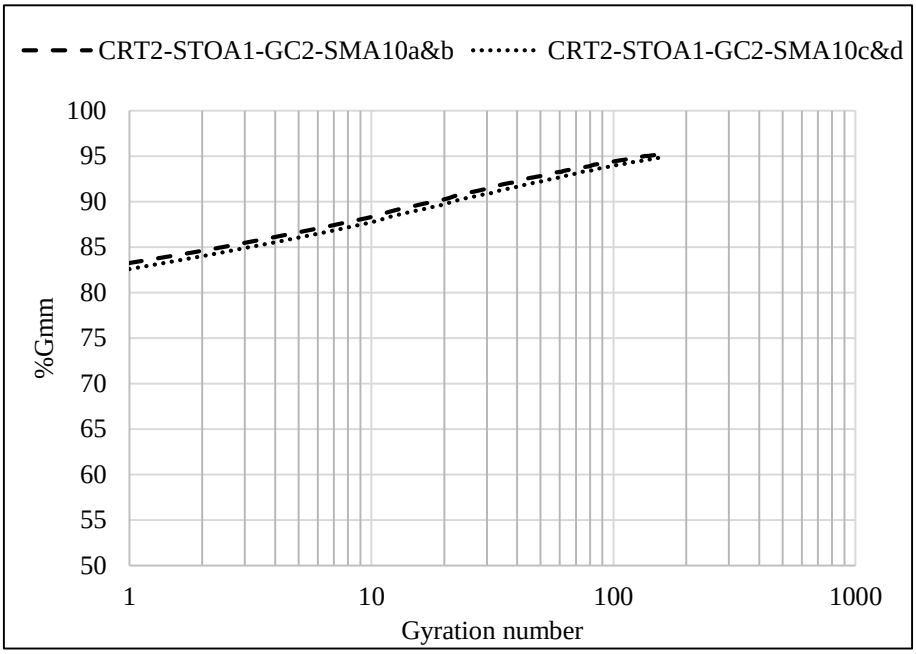

Figure 11.24: Densification curves of SMA10-CRT2 samples (SMA10 mixes with CRT2 rubber), STOA1-GC2.

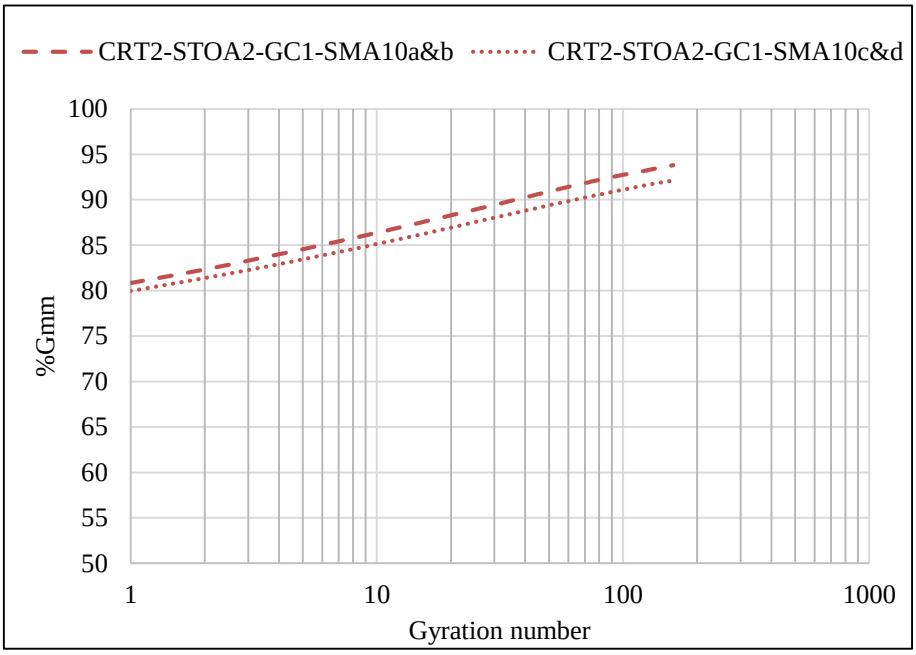

Figure 11.25: Densification curves of SMA10-CRT2 samples (SMA10 mixes with CRT2 rubber), STOA2-GC1.

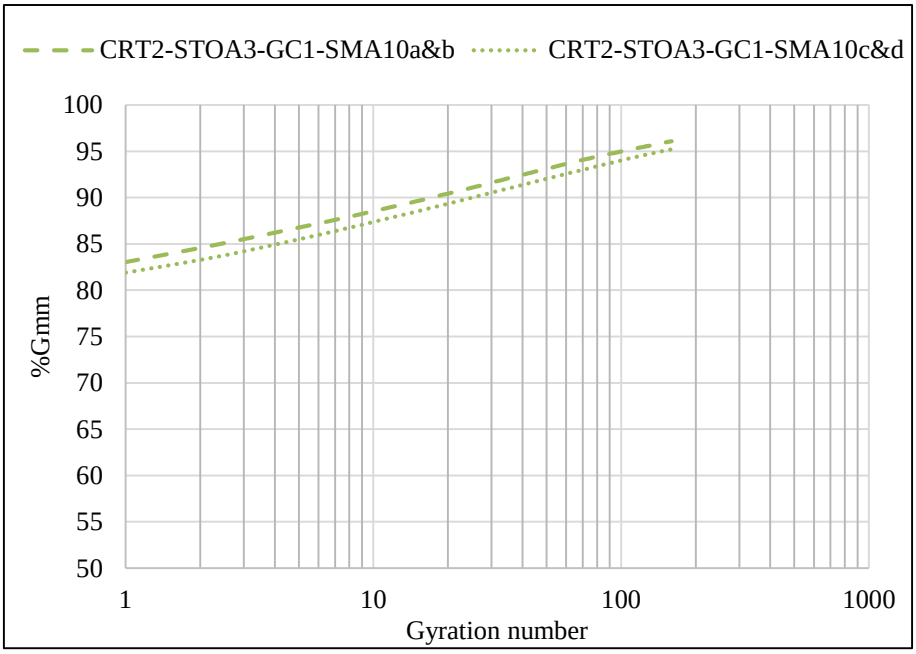

Figure 11.26: Densification curves of SMA10-CRT2 samples (SMA10 mixes with CRT2 rubber), STOA3-GC1.

11.8 SMA10-CRN (Stone Mastic Asphalt mixes with CRN rubber)

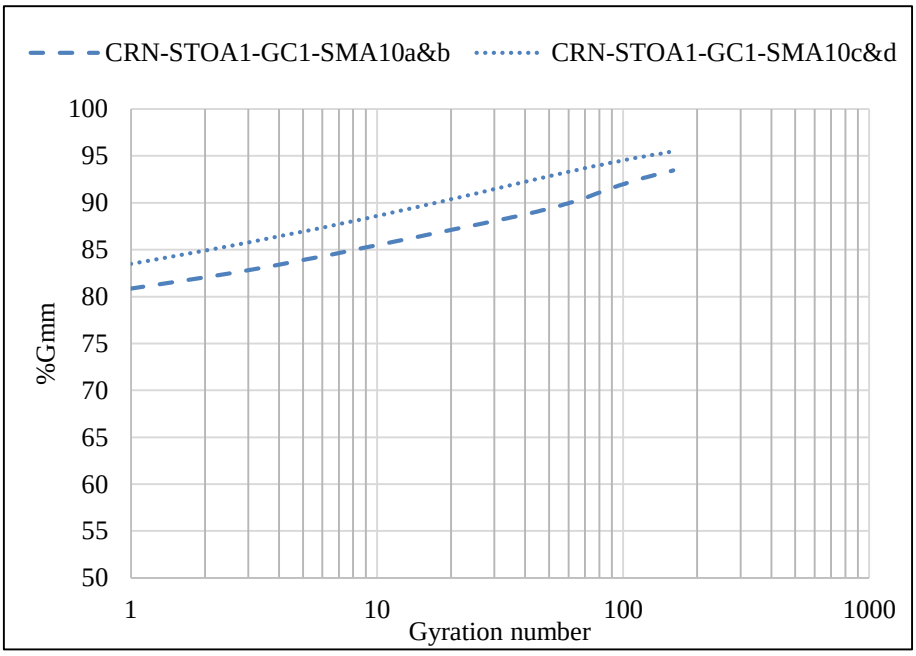

Figure 11.27: Densification curves of SMA10-CRN samples (SMA10 mixes with CRN rubber), STOA1-GC1.

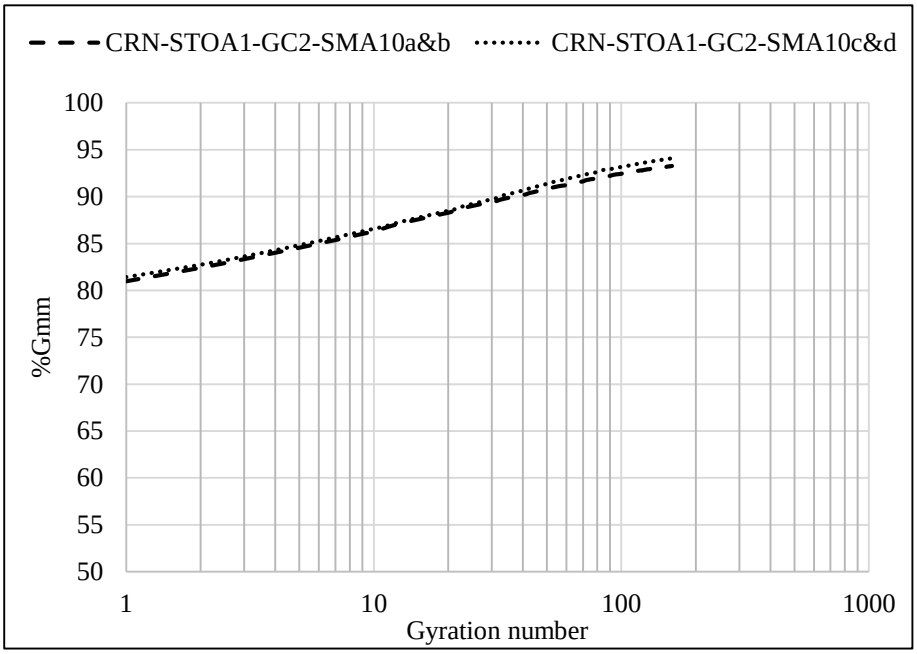

Figure 11.28: Densification curves of SMA10-CRN samples (SMA10 mixes with CRN rubber), STOA1-GC2.

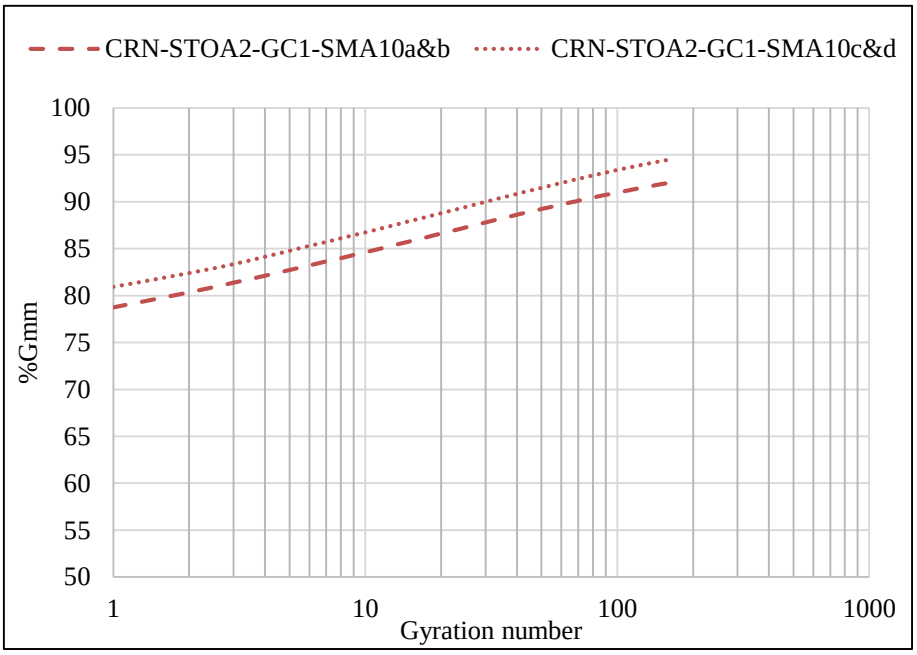

Figure 11.29: Densification curves of SMA10-CRN samples (SMA10 mixes with CRN rubber), STOA2-GC1.

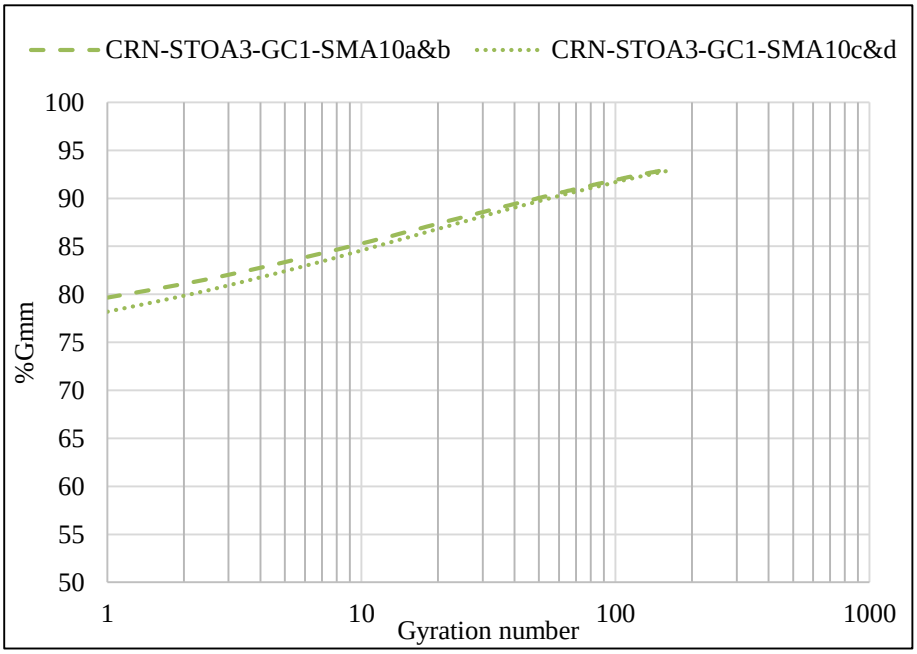

Figure 11.30: Densification curves of SMA10-CRN samples (SMA10 mixes with CRN rubber), STOA3-GC1.

12 ANNEX 2 – RLAT test results

This section reports in more detail the results discussed in section 6.

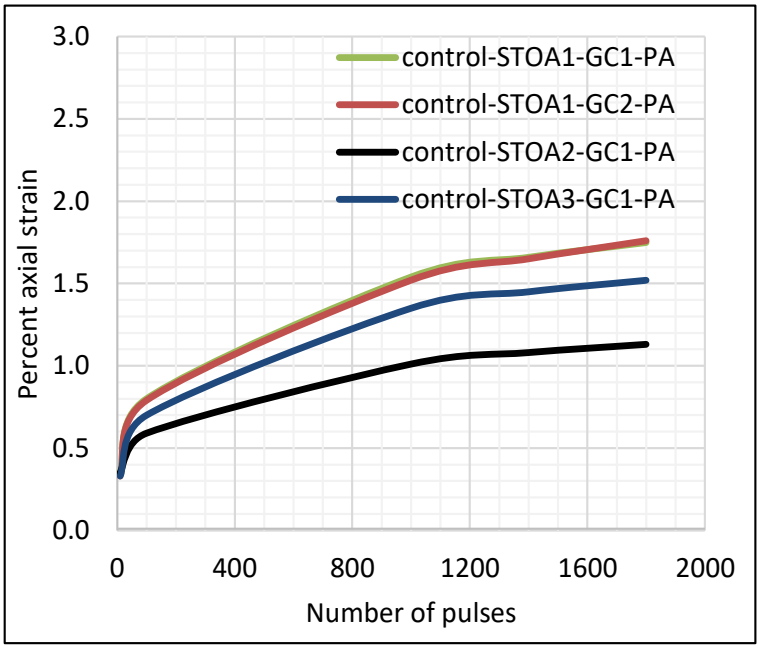

Figure 12.1: Accumulated permanent deformation vs. number of loading cycles (RLAT test, Porous Asphalt mixes without rubber).

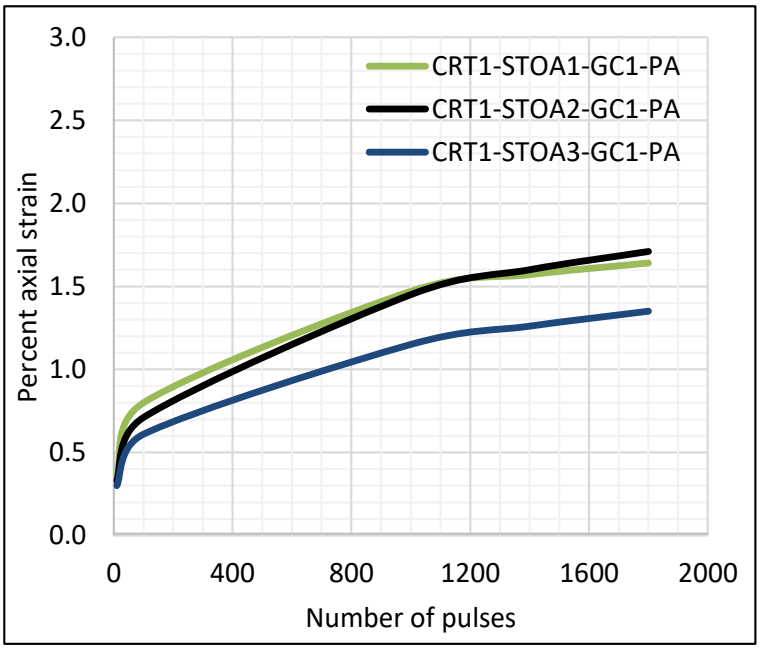

Figure 12.2: Accumulated permanent deformation vs. number of loading cycles (RLAT test, Porous Asphalt mixes with CRT1 rubber).

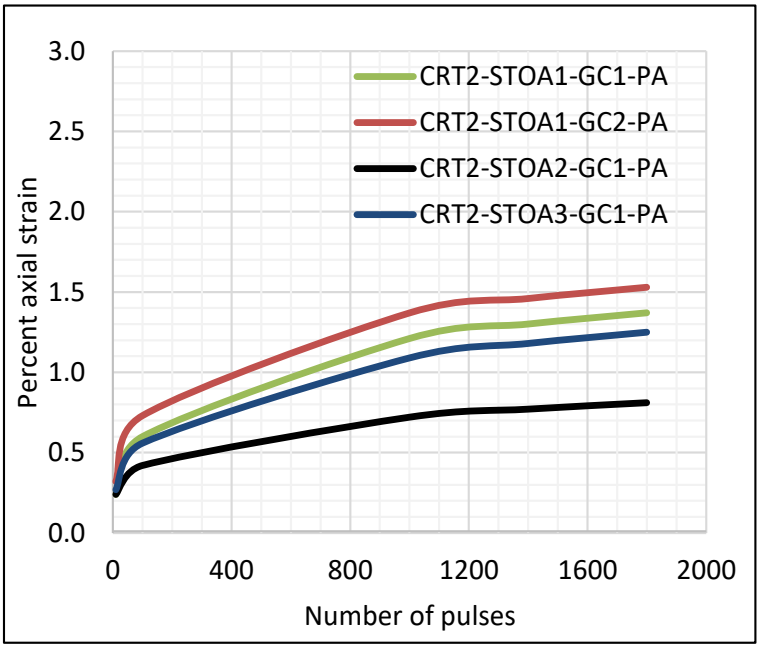

Figure 12.3: Accumulated permanent deformation vs. number of loading cycles (RLAT test, Porous Asphalt mixes with CRT2 rubber).

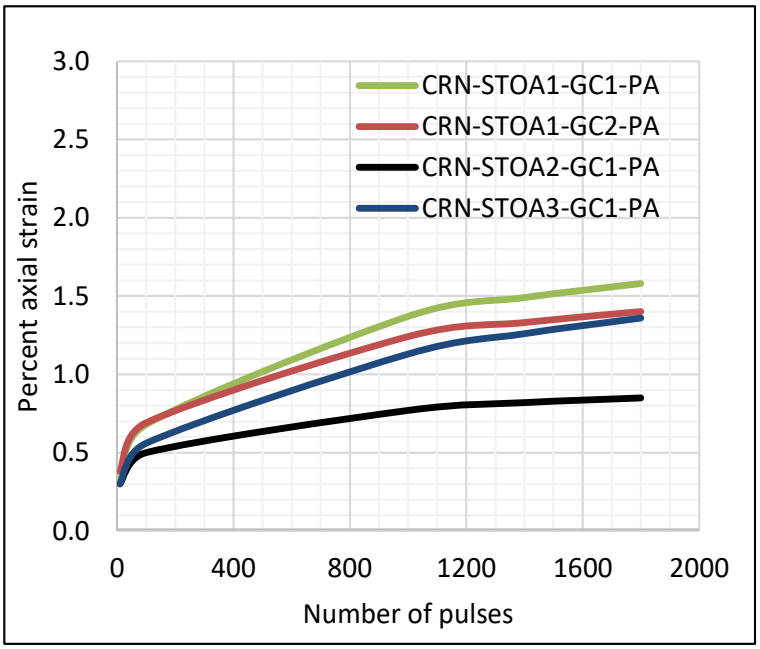

Figure 12.4: Accumulated permanent deformation vs. number of loading cycles (RLAT test, Porous Asphalt mixes with CRN rubber).

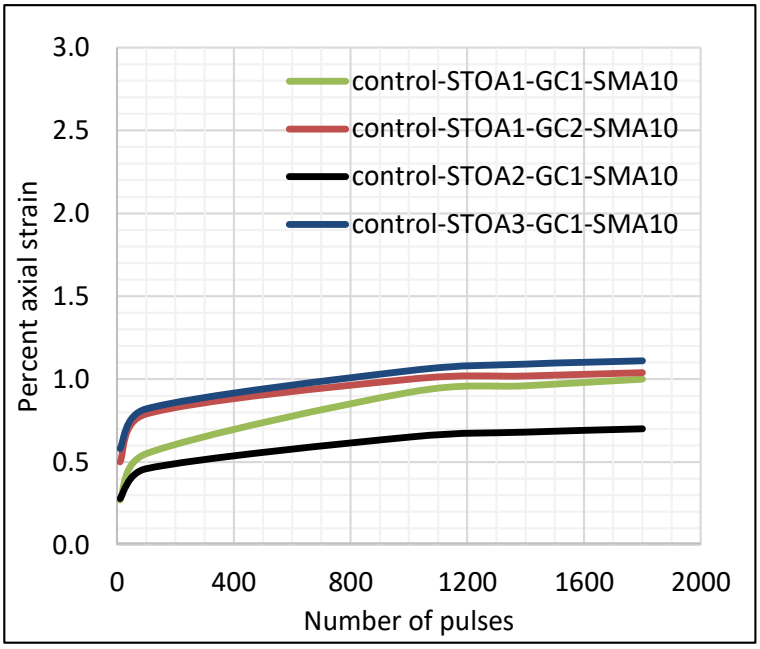

Figure 12.5: Accumulated permanent deformation vs. number of loading cycles (RLAT test, Stone Mastic Asphalt mixes without rubber).

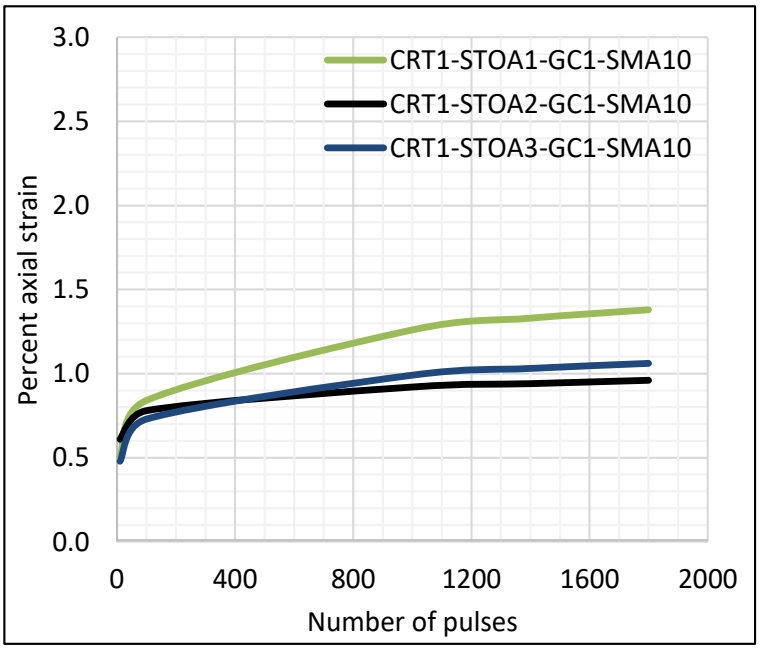

Figure 12.6: Accumulated permanent deformation vs. number of loading cycles (RLAT test, Stone Mastic Asphalt mixes with CRT1 rubber).

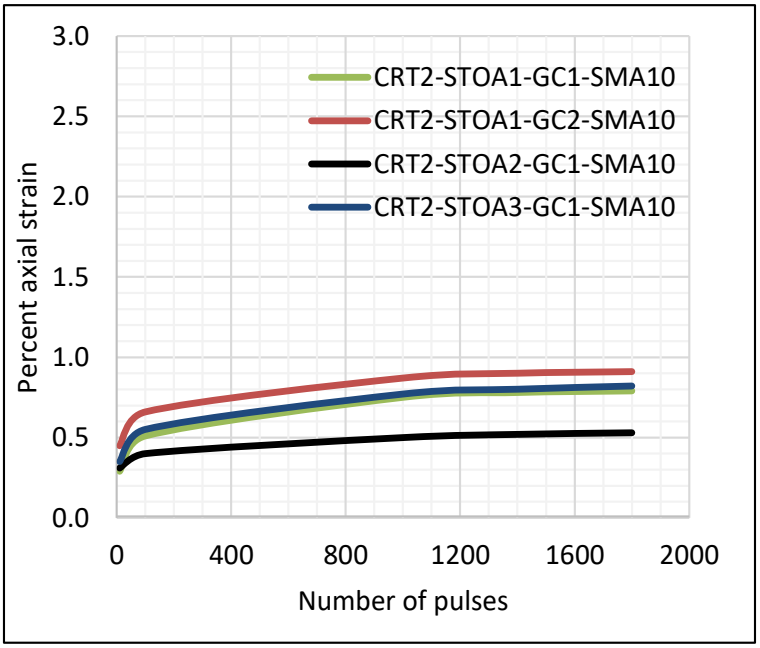

Figure 12.7: Accumulated permanent deformation vs. number of loading cycles (RLAT test, Stone Mastic Asphalt mixes with CRT2 rubber).

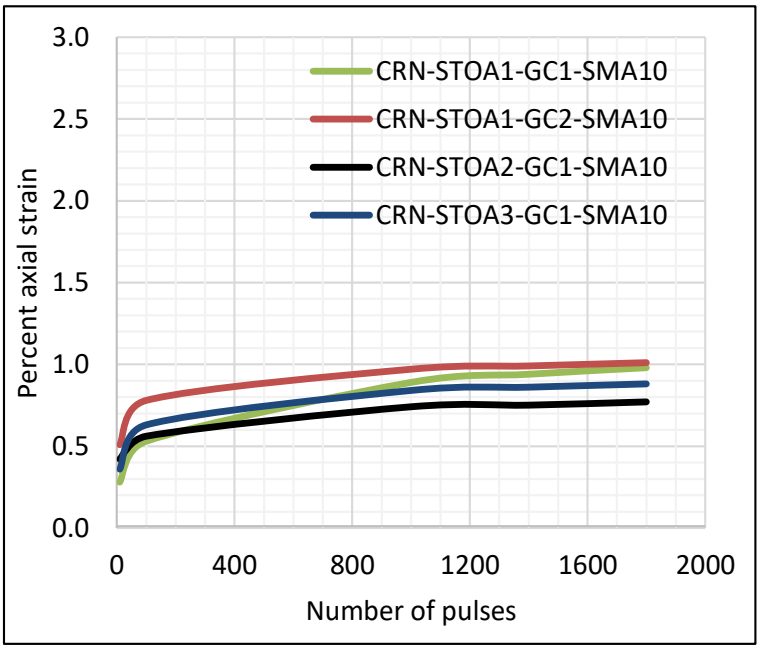

Figure 12.8: Accumulated permanent deformation vs. number of loading cycles (RLAT test, Stone Mastic Asphalt mixes with CRN rubber).

13 Scientific publications

13.1 Scientific publications – already on Scopus website (29/05/2019)

- Filippo G. Praticò, Silvia Noto, Armando Astolfi, 2018. "In-lab versus on-site measurement of surface performance of flexible pavements". Bearing Capacity of Roads, Railways and Airfields – Loizos et al. (Eds) © 2017 Taylor & Francis Group, London, ISBN 978-1-138-29595-7.
- Filippo G. Praticò, Armando Astolfi, 2017. "A new and simplified approach to assess the pavement surface micro- and macrotexture". Construction and Building Materials 148 (2017) 476–483. http://dx.doi.org/10.1016/j.conbuildmat.2017.05.050.0950-0618/© 2017 Elsevier Ltd.
- Filippo G. Praticò, Silvia Noto, Armando Astolfi, 2016. "ISSUES AND PERSPECTIVES IN THE APPLICATION OF DIFFERENT PAVEMENT DESIGN METHODS TO LIFE CYCLE COST ANALYSIS". Proc. of the Eighth Intl. Conf. on Maintenance and Rehabilitation of Pavements Copyright © 2016 by Mairepav8 2016 Organizers. Published by Research Publishing, Singapore ISBN: 978-981-11-0449-7: doi:10.3850/978-981-11-0449-7-083-cd.

13.2 Scientific publications – submitted to Journals and conferences (ISIS-Scopus Index)

- Armando Astolfi, Ayad T. Subhy, Filippo G. Praticò, Davide Lo Presti, 2019. "Quality-control procedure for dry-process rubberised asphalt mastics". 7th International conference Bituminous Mixtures and Pavements. 12-14 June 2019, Thessaloniki, Greece.

Others publications are going to be submitted to International Scientific Journals.